Rain induced attenuation studies for satellite communications in tropical regions

Ismail, Ahmad Fadzil

Award date:
2001

Awarding institution:
University of Bath

Rain Induced Attenuation Studies for Satellite Communications in Tropical Regions

Submitted by Ahmad Fadzil Ismail

for the degree of PhD

of the University of Bath

2001

ProQuest LLC
789 East Eisenhower Parkway
P.O. Box 1346
Ann Arbor, MI 48106-1346

Abstract

Commercial operations of K_u-band and higher frequencies in tropical and equatorial regions are constrained as a result of attenuation from rain. Statistics* for 20 consecutive months of rainfall intensity and K_u-band satellite signal attenuation measurements in Malaysia are presented in this thesis. Measured statistics are then compared with The ITU-R prediction models. Significant differences are evident between measured rainfall rates and attenuation with predicted values using the latest ITU-R models; which appear to underestimate the annual statistics. The statistics are then broken down to examine seasonal and diurnal variations. Characteristics of rain events such as fade duration, inter-fade interval and average duration are presented. It is essential to identify such characteristics for the design and implementation of fade countermeasure techniques on satellite links. The use of "time-diversity" as a fade mitigation technique to alleviate the effect of rain attenuation is investigated. The measured attenuation data were analysed in order to assess the diversity gain from the use of this technique.

The investigation also emphasises the determination of the vertical extent of rain and the closely related on-average vertical profile of attenuation. Major uncertainties of attenuation prediction in the tropics relates to the appropriate rain height and the path correction factor. As an insight to this problem, statistical distributions of tropical rain reflectivity gradients have been drawn from a zenith pointing radar system measurements operated for a period of 6 months in Papua New Guinea. The zenith path reduction factor is determined from the analyses of the variability of rain specific attenuation with height. New correction factors in stratiform and convective rain are deduced. In addition, theoretical models for equatorial rain drop size distribution is also derived using a co-located distrometer measurements.

* Reader should exercise caution in the interpretation of statistics at the low time exceedance levels since data present in this region is of dubious statistical significance.

Acknowledgements

Many people have contributed to the completion of this thesis. I am especially grateful and would like to express my sincere appreciation to Professor Peter A. Watson, my supervisor, for his support and guidance during the study and preparation of the thesis. Gratitude is also expressed to Dr. Robert J. Watson for his support and help especially in providing the numerical data of the total cross section.

Special thanks go to Mr. Affendi Tun Fuad Stephens, the Assistant General manager of Binariang Sdn Bhd and Mr. Poh Kee Seng, the transmission manager of MEASAT Broadcast Network Systems Sdn Bhd for making available the MEASAT databases. Thanks go to Mr. Hafi Kamaruddin and Mr. Yan Yap Ja, transmission engineers of MEASAT Network System Sdn Bhd for their technical assistance and help.

I would like to wish thank to Rutherford Appleton Laboratory for providing the distrometer and radar measurements from Papua New Guinea. My thanks also extended to those who have directly or indirectly given their support be in terms of advice, encouragement, moral or technical though minor they may seem to be.

Table of Contents

List of References

Appendixes

List of Tables

List of Figures

Acronyms

BER:	Bit Error Rate
DTH:	Direct To Home
IEEE:	Institute of Electrical and Electronics Engineers
ITU:	International Telecommunication Union
ITU-R:	International Telecommunication Union-Radiocommunication
LDR:	Linear Depolarisation Ratio
MEASAT:	Malaysia East Asia Satellite
MBNS:	MEASAT Broadcast Network Systems
SES:	Severely Errored Seconds
RAL:	Rutherford Appleton Laboratory
RCRU:	Radio Communications Research Unit
Unitech:	University of Technology
VSAT:	Very Small Aperture Terminal

Chapter 1

Introduction

1.1 Overview

The increasing demand for microwave and millimetre wave communications is already causing frequency spectrum congestion. Hence, existing and future satellite system operators are planning to employ frequency bands above 10 GHz [Wood, 1994; Prentiss, 1987]. The adversity in operating at such high frequencies for communication purposes is that there exists stronger interaction between the radio signals and atmospheric hydrometeors. Such interaction can substantially degrade the performance of communication systems. Hydrometeors are concentrations of water or ice particles that may exist in the atmosphere before being deposited on to the surface of the Earth [ITU-R PN.310-9, 1994].

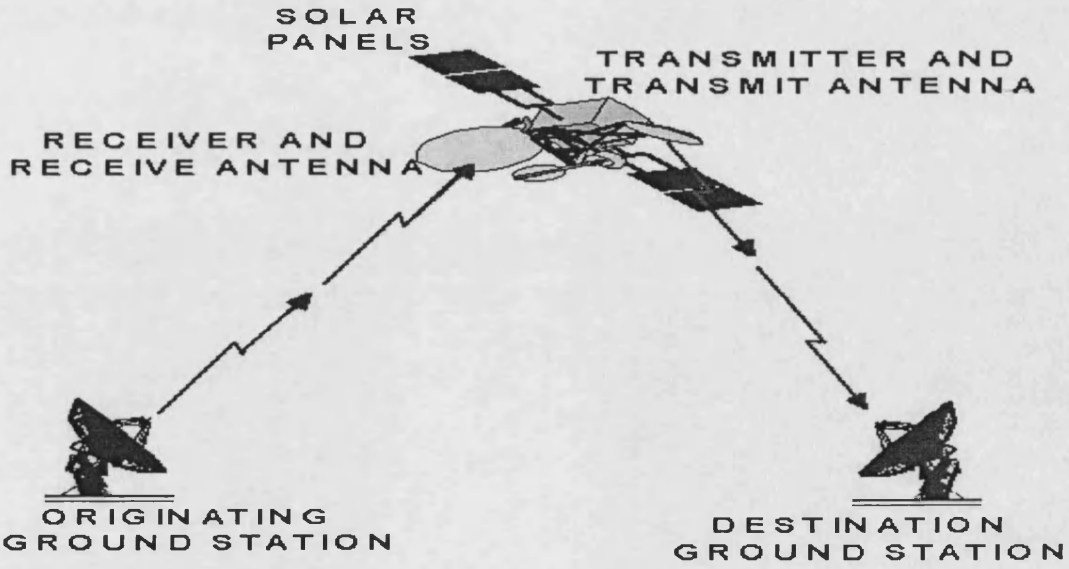

Figure 1.1: Basic segments of a satellite communications link

The hydrometeors commonly encountered along a radio path are in form of rain, snow, ice, hail and fog. The deterioration of signal strength or path loss caused by these particles will increase with the increase of frequency, particularly in the case of rain [Pratt and Bostian, 1986]. At 6/4 GHz (C-band) and lower, attenuation due to rain is generally negligible. At 14/11 GHz (K_u-band), attenuation can be significant in high rainfall rate regions of the world. At 30/20 GHz (K_a-band), 50/40 GHz (V-band) and higher, rain induced attenuation is the dominant link impairment nearly everywhere.

Satellite communications links have been introduced in the tropical countries since in many cases, these could be the most economical communications medium for the dissemination of information. Tropical countries are the nations located in regions with tropical climates lying geographically between the Tropics of Cancer and Capricorn, 23.5° N and 23.5° S, respectively [Riley and Spolton, 1974]. A tropical climate is classified as being warm all year around and having no winter. In the rainy tropics or the equatorial rain climate, between the 10° latitudes from Equator, precipitation is very heavy usually averaging more than 2000 mm per year and the humidity is very high [Hulbert, 1973; Barrett and Bailey, 1971]. There is no apparent dry season and thunderstorms occur almost every day. Every month has a mean temperature above 20° C.

There are conditions in some tropical and equatorial countries that pose certain difficulties for the installation of conventional telephony network and terrestrial microwave links. The complications are usually due to the geographical terrain, the distances involved and the sparse population. In most countries, dense tropical forests or similar inhospitable features usually separate the major towns and cities where populations are concentrated. Many tropical countries have geographical characteristics such as hills, mountains, valleys and ravines that obstruct the reception of microwave and television broadcast signals by line-of-sight means. There are nations where the citizens are fragmented by the geographical nature of the countries. Indonesia for example, is a fragmented archipelago of islands that stretch

over a distance of 2500 km in the South Pacific. The Filipinos are living on more than 7000 islands and islets that make up the Philippines.

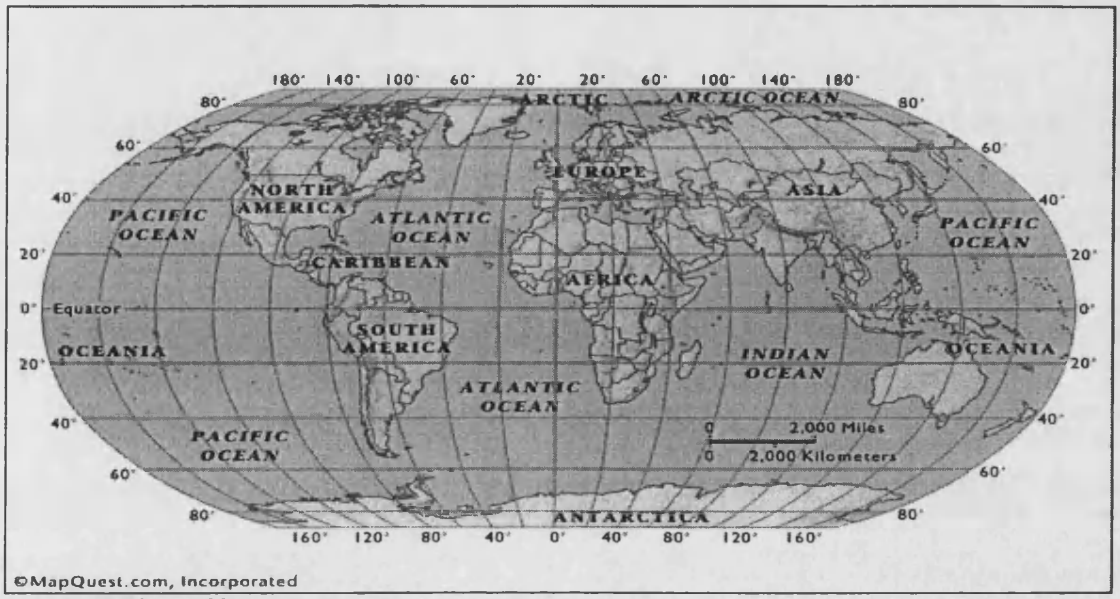

Figure 1.2: The world map

Nevertheless communications developments are crucial for any country regardless whether small or big if it is to grow economically. Key elements for economic growth for any nation are good national and international telecommunications [Read and Youtie, 1996]. The introduction of satellite services is one of the solutions that can provide the rapid break-through required by the developing countries. Proposals were made to set-up of satellite or radio systems services as providing cost effective solutions in the long term even though these might require very significant initial investments. The services to a large degree are distance and terrain independent. Unfortunately, the satellite-Earth links are not climate independent.

The explosive growth in demand has led to the incorporation of K_u-band services on a new series of satellites. With the advent of high-powered K_u-band and advanced new satellites design, television distribution, point-to-point communication, relay and live broadcasting of programs are now able to be received using small and inexpensive antennas [Williamson, 1990]. For instance, international (global) system such as the

INTELSAT VII satellites are built with 10 fully steerable K_u-band spot beam transponders. The INTELSAT VII-A fleet carries 14, and the future INTELSAT IX series will carry 12 K_u-band transponders. Paris-based EUTELSAT, another one of the world's leading satellite operators, owns a fleet of 18 geostationary K_u-band satellites delivering a full range of consumer and professional services to Europe, Asia, Africa and America. Nationally owned (regional) satellite systems that were launched in recent years, for example Mabuhay (Philippines), INSAT (India) and MEASAT (Malaysia) satellites are also carrying K_u-band transponders in addition to the lower frequency band transponders [Long, 1999].

These new K_u-band applications in satellite communications have now expanded into the areas where atmospheric propagation degradations particularly the effect of rain must be taken into consideration. Clouds and gasses also have effect on the signal level and they may be present during rain events. However, the attenuation introduced by these components is small compared to the attenuation caused by rain (0.5 to 1.5 dB for clouds and gasses for frequencies below 20 GHz [Dissanayake *et al.*, 1997).

1.2 System Requirements for Propagation Prediction

A decade ago, the operating frequencies of most available satellites in the tropics were C-band or S-band. The K_u-band satellite links were initially confined mainly to temperate regions [Pritchard and Sciulli, 1986]. Recently however, this new service has gradually been introduced worldwide including the tropical regions. In the future, new satellites in the tropical and equatorial will also have no alternative but to operate at K_u-band and higher frequencies due to spectrum limitations.

Performance predictions are an essential step in the design of all new satellite links. Performance is usually defined as the expected quality of the channel for a very high percentage of time (at least a month and usually a year). For satellite systems, it is usually that level achieved in what is called "clear sky" [Watson and Allnutt, 1998].

For analogue systems, the basic measure of systems performance is the signal-to-noise ratio in the base band channel. Meanwhile, the measure of quality of a digital communication system is the Bit Error Ratio (BER). BER is the ratio of number of bits received in error to the total number of bits transmitted [Dalgleish, 1989]. BER is either quoted as a percentage or more usually as a ratio. It is generally shown as a negative exponent. For example, 10^{-7} means that 1 out of 10^{7} bits are in error or 1 out of 10,000,000 bits are in error.

Typical BER for a satellite link today are on the order of 1 error per 10 million bits (1×10^{-7}) or less frequent [Allman *et al.*, 1999]. The lower the number of errors, the better quality the system. Severely Errored Seconds (SES) is the unit used to specify the error performance of more complex digital systems [Watson and Allnutt, 1998]. This indicates a second containing ten or more errors and usually expressed as SES per hour, day, or week. This method gives a better indication of the distribution of bit errors than a simple BER.

It is very critical to be able to predict accurately the likely impairment to be encountered on a given link in order to plan the services economically. The predicted value of signal loss and fading are used to determine the design parameters [Hughes, 1990]. Examples of design parameter are the power requirements of the equipment, the antenna characteristics and the service range or the hop length. These design parameters can be determined and from them the performance of a service is specified for a particular percentage of the time. The performance can be specified for example, at availability of 99% of time at a given receiving location or at a specified percentage of locations within a reception area. Availability is the ratio expressed as a percentage of the total time a service is capable of being used or is available to be used during a given interval to the length of the interval. In satellite communication terms, the link availability is usually expressed as a percentage of a year when the link will perform as per the required BER. As an example, 99% availability for a year, states that the link will be available for 867.24 hours and unavailable for 87.6 hours (8760 – 87.6

hours / 8760 hours x 100) or put another way; if the link was running at 64 kbps more than 20,183 million bits of data would be lost.

Equally important, other attribution such as the level of interfering signals exceeded for some small percentage of the time, for instance at 0.1%, also need to be predicted, again at the reception point or area of concern. Predictions are employed in order to know whether a satisfactory service will be provided at the required reception point or area and also for planning to avoid mutual interference with other systems sharing the same frequency band.

1.3 Development of ITU-R Propagation Prediction Models in the Tropics

Many researchers have worked in the studies of predicting the radiowave signal attenuation due to rain. The prediction of microwave and millimetre wave signal degradation is an iterative procedure. Several models were proposed by the scientists and have been adopted by the International Telecommunication Union (ITU). The ITU was formed in 1932 from the International Telegraph Union, which originated in 1865. The ITU is a specialised agency of United Nations, with over 150 current member nations. Initial theoretical models are then verified against measured data. The prediction models are improved to match the data and in the process they become semi-empirical models.

The ITU models seem to offer a good estimation for the signal attenuation caused by rain in temperate regions. However, inadequacies were discovered in the existing attenuation-prediction procedures where the models or recommendations failed to give good approximation of the rain induced attenuation in tropical regions [Yusof *et al.*, 1990; Zainal *et al.*, 1993; Ong and Zhu, 97]. In other words, proper representations for space-Earth microwave propagation now exist for temperate regions of the world and they were achieved through extensive measurements and modelling but that is not the case for the tropical regions. With progressive use of the K_u-band and higher

frequencies for space communications in this regions, combined with introduction of digital modulation techniques as well as multiple beam methodology for satellites; immediate research has been deemed necessary to review the effectiveness of prediction models currently in use

Studies have shown that the communication systems operating above 10 GHz are very vulnerable to attenuation due to rain, and the effects are more severe in the tropical regions which experience heavier rainfall intensity and contain relatively larger raindrops as compared to the temperate regions. Currently most of the data on rain induced attenuation and its effects on communication transmission are based on situations and conditions in the temperate regions, which cannot be reliably applied to the communication condition in tropical regions [Allnutt, 1989]. In addition to that, telecommunication engineers must be aware that the integrity of satellite equipment has been designed for use in countries with a temperate climate and may not be capable to adapt to conditions in countries with tropical climates [Thenakis, 1984].

With the development of satellite communications in the tropics, it has now become crucial to test the validity of published prediction techniques. Special focus should be granted to the current ITU methods or recommendations. It is apparent that available attenuation prediction methods are not generally applicable to tropical climates. Studies have been conducted to determine in what way should the models be refined to conform to tropical climates. Despite some advances in recent years, uncertainties, deficiencies and lack of universal applicability still exist in the proposed prediction models. This is largely due to insufficient or shortage of measurement data in high rainfall tropical areas. Successful development of prediction methods calls for thorough knowledge of the propagation characteristics along the path from the transmitter to the receiver. Such knowledge can be gained from theoretical studies of the relevant propagation phenomena and also from the long-term collection and analysis of measurement data. For example, measurements of received field strength

resulting from a transmission on the frequency of interest can provide statistics of the expected signal level.

The usefulness of such data may be increased significantly when collected simultaneously with measurements of the dominant characteristic influencing the propagation. For instance, simultaneous measurements of rainfall rate and a satellite beacon signal at gigahertz frequencies. Such sets of data can form the basis of a propagation prediction method that may then be employed in specific regions displaying similar propagation characteristics with similar rainfall rate distribution. The accuracy of such prediction methods thus relies on the extent and quality of the measurement data, and in many regions of the world, the development of satisfactory prediction methods awaits the acquisition of a suitably large collection of measurement data. It is against this background that a need for further propagation data for the tropical regions is examined in this thesis.

1.4 Objectives of the Thesis

The principal objective of this thesis is to quantify the propagation characteristics of a K_u-band satellite-Earth link operating in an equatorial climate, with particular reference to broadcast application. This will entail analysis of data, comparison with the existing prediction methods and where possible, development of models for improved predictions. A second objective will be to consider the opportunities for fade countermeasure, especially the use of "time diversity" [Schwartz, 1996] in broadcast and broadcast type applications.

Observations of attenuation during rainfall from a K_u-band satellite beacon measurement associated with the Malaysia East Asia Satellite (MEASAT) broadcasting satellite together with simultaneously gathered rain gauge data are used to meet these objectives. In addition, data from a radar system operated in Papua New Guinea (PNG) has been made available from the Rutherford Appleton Laboratory (RAL), UK as an aid

to investigate the structure of tropical rain with the objective of improving attenuation prediction models.

The scope of research initiated with such propagation data can be wide ranging. New experiments can be developed and analyses gathered from the investigation can be applied for the design of future satellite systems. In this thesis, attempts were made to compose the on average and time dependent statistical assessments of the degradation due to rain on a communication link established between MEASAT's satellite and the Earth terminal. With broadcast application in mind, the seasonal and diurnal variability of rain attenuation will be investigated in addition to the annual cumulative statistics. For instance, a satellite broadcast system may find greatest viewer demand during the late afternoon and evening hours, times that in some climates it is when the highest rainfalls occur.

This thesis is aimed to review the current status of available propagation data and information relating to the design of satellite telecommunication systems in tropical regions. The databases acquired from MEASAT offer exceptional opportunities to analyse available prediction models in detail where comparison can be made with predicted models for annual cumulative statistics.

In view of the extreme rainfall climates experienced in tropical regions, the analyses of possible use of time-diversity fade countermeasure techniques are investigated. This technique is particularly referenced to latest digital satellite broadcast applications. The techniques are relevant to time repeated video, multimedia messaging, data retrieval and distribution including broadcasting.

The thesis considers climatic effect with a particular emphasis on rain. Further evidences on the quantity and structure of rain in tropical regions are drawn from RAL zenith pointing radar system and a co-located distrometer that were operated in Papua New Guinea. The thesis presents derived statistical information on parameters related

to the prediction such as the melting layer heights. From the distrometer measurement data, the PNG rainfall drop size distribution models are established and presented in this thesis. In addition, the thesis also present several reflectivity related coefficients at K_u-band, K_a-band and V-band derived from the acquired data. The thesis inspected the extent of vertical variability of rain specific attenuation for both stratiform and convective as it is characterised by means of the gradient of the radar reflectivity. It is also the aim of this thesis to determine the appropriate vertical correction factor based on the radar measurement data which should help to improve the prediction of rain induced attenuation in tropical climates.

1.5 Organisation of the Thesis

The thesis is divided into eight main chapters. This chapter introduces the research motivations, objectives, and organisation of the thesis. Brief information concerning MEASAT and RAL data used in the research are introduced in this chapter. Chapter 2 presents theoretical concept study and background on propagation mechanisms, classification of world climates, classifications and characteristics of precipitation, and several related topics of the research. Chapter 3 offers findings acquired from processed data for Malaysia. Emphasis has been given to the presentations on the time dependent statistical assessments of the rainfall characteristics. Chapter 4 concentrates on the characteristics of signal degradation due to rainfall on communication links established between the satellite and Earth terminal. Building on these foundations, Chapter 5 describes subsequent research works and investigations carried out using the MEASAT databases. This chapter gives detail accounts of the procedure in predicting rain induced attenuation based on investigation findings. Measured attenuation distribution was compared with predicted attenuation distributions generated by different prediction models. The chapter also presents investigation results on the performance of 'time diversity.

Chapter 6 elaborates the attempt to model the rainfall drop size distribution in PNG from the data measured by the distrometer. The best model is determined out of several available solutions. Chapter 7 details the attempt to derive the parameter related with reflectivity and the investigation of vertical non-uniformity of the rain with height. The thesis ends with Chapter 8 where it gives conclusion and suggestion of future works.

1.6 Contributors of the Research Data

Figure 1.3: Map of Malaysia

MEASAT Broadcast Network Systems Sdn Bhd has acquired a beacon attenuation and rain measurement system. The system was installed at the MEASAT Earth station in Bukit Jalil, near Kuala Lumpur, Malaysia. The primary objective of this exercise is to obtain precipitation and signal degradation measurement databases for Malaysia. This is in a way useful for comparing the predicted values by available models with the local rain induced attenuation measured along the Earth-space path at centimetre and millimetre wavelengths of its transmission links. The measurement campaign was initiated and conducted under the responsibility of MEASAT Transmission Department of its engineering division. By obtaining local precipitation and signal

degradation measurements, the work also contributes new databases to help address the shortfall of satellite propagation data in tropical regions.

Data have been gathered for twenty consecutive months from August 1996 until March 1998, with a sampling rate of more than 1,500,000 seconds during rainfall. The databases include records of some very impressive downpours with rainfall rates that exceed 150 mm hr^{-1} for a notable period. Intense rainfall rates and thunderstorms have been detected and recorded. Rainfall intensity data are gathered concurrently to enable comparison with the beacon signal measurement. The databases were acquired with permission, were brought back to United Kingdom in September 1997 and February 1999 for analyses and detail investigation.

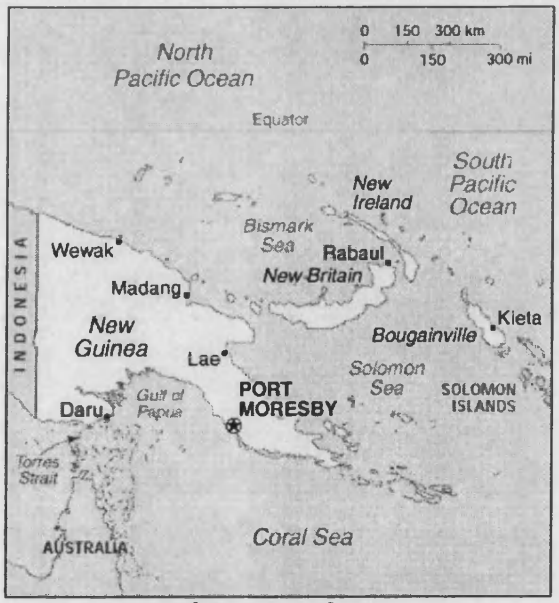

Figure 1.4: Map of Papua New Guinea

The Rutherford Appleton Laboratory, United Kingdom has developed an S-band vertically pointing Doppler radar in 1995 for monitoring precipitation in the tropical regions [Eastment *et al.*, 1995; Eastment *et al.*, 1998]. In November of that year, RAL has installed the radar and a Joss type distrometer at the University of Technology (Unitech) in Lae, Papua New Guinea. The experiments were carried out at an open space on the rooftop of Unitech's electronics laboratory. RAL started their continuous

campaign commencing from the following December for period of over six months. Measurements from both the radar and the distrometer have been collected, recorded and brought back to United Kingdom.

1.7 Conclusion

The available path attenuation data for tropical and equatorial regions of the world are still insufficient for a comprehensive evaluation of attenuation process in the tropical regions even on empirical basis. It is hoped that continuing efforts to collects the needed propagation data for this regions by more research organisations, and the analyses works such as presented in this thesis will soon satisfied the remaining requirements. Attempts were initiated to investigate the cause of inadequacies discovered in the existing attenuation prediction procedures particularly for tropical regions. Additional data would permit refinement of the prediction models. Therefore, there is an urgent need for continuous microwave propagation studies to be carried out in tropical regions where the effects of rainfall on microwave and millimetre wave transmission have not yet been fully quantified.

Chapter 2

Background on Propagation, Climates and Precipitation

2.1 Introduction

Before describing the measurement analyses and research findings, this chapter introduces the relevant theoretical background for which the investigation of the thesis has been carried out. Brief presentations of background on propagation mechanisms, climates and precipitation that considered most applicable to the area of the research are included in this chapter

2.2 Propagation Mechanisms

The general terms used to describe the propagation phenomena or mechanisms that can affect the characteristics of radiowaves, adapted from literatures [Allnutt, 1989; Ippolito, 1986] are reproduced below. These mechanisms are usually described in terms of variations in the signal characteristics of the wave, as compared to the natural or free space values, found in the absence of the mechanism. Most of the definitions are based on the Institute of Electrical and Electronics Engineers (IEEE) Standard Definitions of Terms for Radio Wave Propagation [IEEE standard, 1977]

1. **Absorption:** A reduction in the amplitude or field strength of a radiowave due to an irreversible conversion of energy from the radiowave to matter in the propagation path.
2. **Scattering:** A process in which the energy of a radiowave is dispersed in direction caused by interaction with inhomogeneities in the propagation medium
3. **Refraction:** A change in the direction of propagation of a radiowave resulting from the spatial variation of refractive index of the medium

4. **Diffraction:** A change in the direction of propagation of a radiowave resulting from the presence of an obstacle, a restricted aperture, or other object in the medium.
5. **Multipath:** The propagation condition that results in a transmitted radiowave reaching the receiving antenna by two or more propagation paths. Multipath can result from refractive index irregularities in the troposphere or ionosphere, or from structural and terrain scattering on the Earth's surface.
6. **Scintillation:** Rapid fluctuations of the amplitude and the phase of a radiowave caused by small-scale irregularities in the transmission path or paths with time.
7. **Fading.** The variation of the amplitude of a radiowave caused by changes in the transmission path or paths with time. The terms fading and scintillation are often used interchangeably; however, fading is usually used to describe slower time variations, on the order of seconds or minutes, while scintillation refers to more rapid variations, on the order of fractions of a second in duration.
8. **Frequency Dispersion.** A change in the frequency and phase components across the bandwidth of a radiowave, caused by a dispersive medium. A dispersive medium is one whose constitutive components (permittivity, permeability, and conductivity) depend on frequency (temporal dispersion) or wave direction (spatial dispersion)

Many of the mechanisms described above can be present on the transmission path at the same time and it is very difficult to distinguish the mechanism or mechanisms that produce a change in the characteristics of the transmitted signal. Propagation effects on communications links are usually defined in terms of variations in the signal parameters. The parameters that can be observed or measured on a typical link are amplitude, phase, polarisation, frequency, bandwidth, and angle of arrival. Each of the mechanisms above if present in the path, could affect one or more of the signal parameters. Figure 2.1 illustrates how the various mechanisms affect the measurable parameters of a signal on communications links.

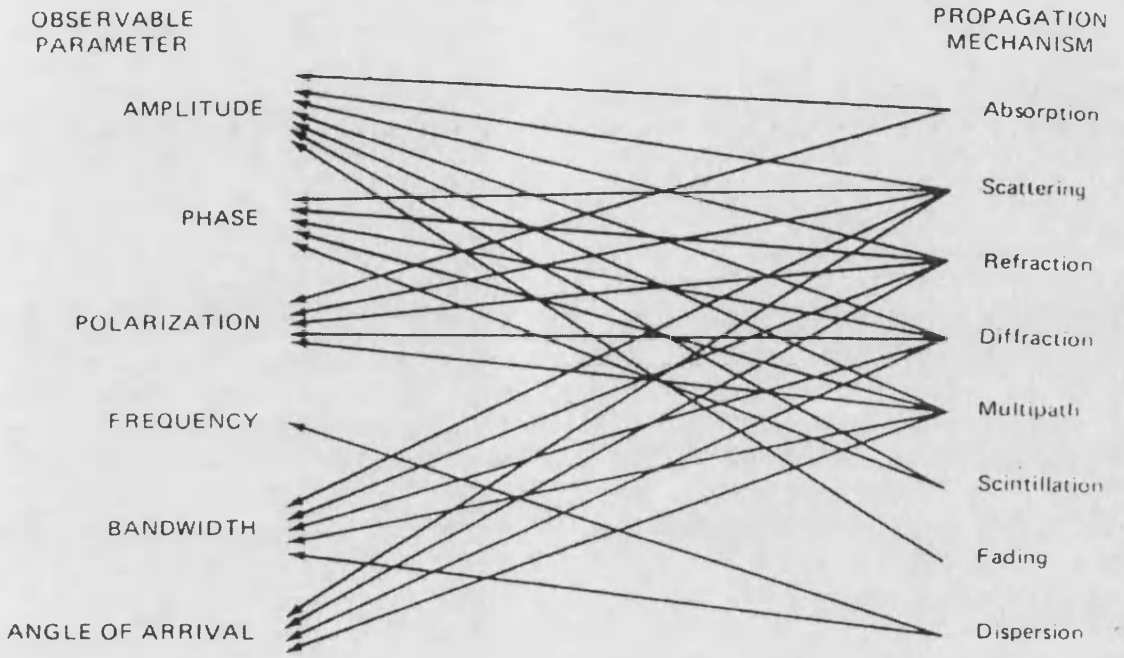

Figure 2.1 Radiowave propagation mechanisms and their impact on the parameters of communication signal [Ippolito, 1986]

2.2.1 Impairments Affecting Earth –space Communication Systems

For most modern satellite communication systems, they require accurate propagation information to support the design, implementation and operation. The propagation behaviour of radiowaves in ionospheric and tropospheric, near the Earth surface, or upon reflection of the surface, are of concern to telecommunication systems designer intending to use the atmospheric propagation medium for the transmission of electromagnetic energy between antennas in the system. Table 2. 1 below, adapted from ITU literature [Radiocommunication Bureau, 1996] identifies the relevant propagation effects along with those systems for which the effect is of significant importance.

Impairment	Physical causes	Affected systems	Frequency
Signal attenuation, sky Noise increases	Atmospheric gases, clouds, precipitation, sand and dust	All types of satellite systems	f> about 10 GHz
	Low ionospheric layers		f< 70 MHz
Signal depolarisation	Raindrops, ice crystals,	Dual-polar systems	at 6/4, 14/11 and 30/20 GHz
	Faraday rotation		below about 1 GHz
Signal scintillations (phase and amplitude)	Refractivity variations, especially at low elevation angles (below about 10°)	Low-margin systems, antenna tracking, uplink power control	f> about 10 GHz
	Ionospheric refractivity variations		10 MHz - 12 GHz
Refraction, atmospheric Multipath	Atmospheric gases Ionospheric electron Distribution	Systems operating at low elevation angles; antenna tracking	1 - 45 GHz
Reflection multipath, Shadowing, blockage	Objects, vegetation on Earth's surface	Mobile-satellite Services	
Propagation delays & Delay variations	Free-space, variations in Troposphere Total electron content	TDMA & position-location systems; closed-loop adaptive control systems	
Inter-system interference	Ducting, precipitation scatter, Diffraction	All types of satellite systems	6/4 GHz systems
	Ionospheric scattering and Reflection		f< 300 MHz
Dispersion	Total electron content Multipath	Wide bandwidth systems	

Table 2.1: Propagation impairments affecting satellite communication systems

2.3 Classification of World Climates

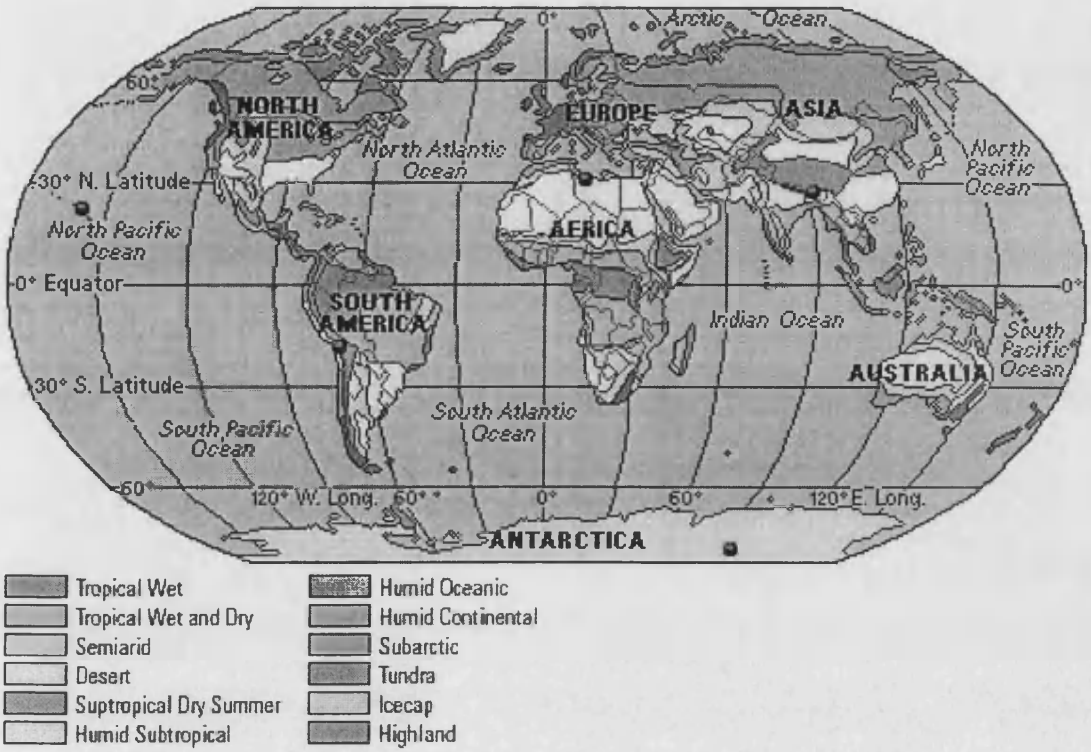

Figure 2.2: World climatic map [The World Book Encyclopaedia, 2000]

The Earth's surface is a patchwork of climate zones. Climatologists, the scientists who study the climate have organised similar types of climates into groups. One of the earliest classification was the division of earth into tropical, temperate and polar climates, using the tropics 23.5° N and S and the arctic 66.5° N and Antarctic 66.5° S circles as dividing lines, with temperature conditions being the only one considered having any importance [Riley and Spolton, 1974]. Wladimir Koppen, a German climatologist, introduced a modified version of a climate classification system in 1918. Koppen based his system on a region's vegetation, average monthly and annual temperature, and average monthly and annual precipitation. His modified version specifies 12 climate groups identified as: (1) tropical wet / equatorial, (2) tropical wet and dry, (3) semiarid, (4) desert, (5) subtropical dry summer, (6) humid subtropical, (7) humid oceanic, (8) humid continental, (9) sub arctic, (10) tundra, (11) icecap, and (12) highland. Descriptions and contours of each climate group as categorised by Koppen,

adapted from literatures [Sutcliffe, 1966; The World Book Encyclopaedia, 2000] are reproduced on the following subsection.

2.3.1 Tropical Wet / Equatorial Climate

Tropical wet or equatorial climates are hot and muggy the year around. Rainfall is heavy and occurs in frequent showers and thunderstorms throughout the year. Average annual rainfall varies from about 1750 to 2500 mm. The primary characteristic of the equatorial climate is its almost unchanging weather patterns. Unlike other climates, daily weather patterns dominate over seasonal weather. It is said that in this region, all seasons occur within a single day [Trewartha and Horn, 1980; Nieuwolt, 1981]. Temperatures are high, and they change little during the year. The coolest month has an average temperature no lower than 18° C. The temperature difference between day and night is greater than the temperature difference between summer and winter. Frost and freezing temperatures do not occur. These climates support dense tropical rain forests.

2.3.2 Tropical Wet and Dry Climate

Tropical wet and dry climates occur in areas next to regions that have tropical wet climates. Temperatures in tropical wet and dry climates are similar to those in tropical wet climates, where they remain high throughout the year. The main difference between the two climates lies in their rainfall. In tropical wet and dry climates, winters are dry, and summers are wet. In general, the length of the rainy season and the average rainfall decrease with increasing latitude. Not enough rain falls in tropical wet and dry climates to support rain forests. Instead, they support savannas the grasslands with scattered trees.

2.3.3 Semiarid Climate

Semiarid climates occur in regions with little precipitation. Semiarid climates also called steppe climates, usually border desert climates. The temperature change between day and night is considerable. One reason for the wide swings in temperature is that the skies are clear and the air is dry. Clouds would reflect much of the sun's intense radiation during the day, slowing the rate of heating of the air near the surface. At night, clouds and water vapour would absorb much of the earth's radiation, most of which consists of infrared rays, slowing the rate of cooling. Middle latitude semiarid climates are in the rain shadows of mountain ranges. Winds that descend the leeward slopes of these ranges are warm and dry.

2.3.4 Desert Climate

Desert climates are very similar to semiarid climates with exception that they are drier than semiarid climates. Desert climates occur over a greater land area than any other climate grouping. They occur in both tropical and middle latitudes. They cover broad east-west bands near 30° N and S latitude. Middle latitude deserts differ from their tropical counterparts mainly in their seasonal temperature changes. Winters are much colder in middle latitude deserts.

2.3.5 Subtropical Dry Summer Climate

Subtropical dry summer climates feature warm to hot, dry summers and mild, rainy winters. These climates, sometimes called Mediterranean climates, occur on the west side of continents roughly between 30° and 45° latitude. The closer to the coast the area is, the more moderate the temperatures and the less the contrast between summer and winter temperatures.

2.3.6 Humid Subtropical Climate

Humid subtropical climates are characterised by warm to hot summers and cool winters. Rainfall is distributed fairly evenly throughout the year. Winter rainfall and sometimes snowfall is associated with large storm systems that steer from west to east. Most summer rainfall occurs during thunderstorms and an occasional tropical storm or hurricane. Humid subtropical climates lie on the Southeast side of continents, roughly between 25° and 40° latitude.

2.3.7 Humid Oceanic Climate

Humid oceanic climates are found only on the western sides of continents where prevailing winds blow from sea to land. The moderating influence of the ocean reduces the seasonal temperature contrast so that winters are cool to mild and summers are warm. Moderate precipitation occurs throughout the year. Low clouds, fog, and drizzle are common. Thunderstorms, cold waves, heat waves, and droughts are rare.

2.3.8 Humid Continental Climate

Humid continental climates feature mild to warm summers and cold winters. The temperature difference between the warmest and coldest months of the year in-creases inland. The difference is as great 25° to 35° C. Precipitation is distributed fairly evenly throughout the year, though many locations well inland have more precipitation in the summer. Snow is a major element in humid continental climates. Winter temperatures are so low that snowfall can be substantial and snow cover persistent. Snow cover has a chilling effect on climate. Snow strongly reflects solar radiation back into space, lowering daytime temperatures. Snow also efficiently sends out infrared radiation, lowering nighttime temperatures.

2.3.9 Sub arctic Climate

Sub arctic climates have short, cool summers and long, bitterly cold winters. Freezes can occur even in midsummer. Most precipitation falls in the summer. Snow comes early in the fall and lasts on the ground into early summer.

2.3.10 Tundra Climate

Tundra climates are dry, with a brief, chilly summer and a bitterly cold winter. Continuous permafrost (permanently frozen ground) lies under much of the treeless tundra regions.

2.3.11 Icecap Climate

Icecap climates are the coldest on earth. Summer temperatures rarely rise above the freezing point. Temperatures are extremely low during the long, dark winter. Precipitation is meagre and is almost always in the form of snow.

2.3.12 Highland Climate

Highland climates occur in mountainous regions. A highland climate zone is composed of several areas whose climates are like those found in flat terrain. Because air temperature decreases with increasing elevation in the mountains, each climate area is restricted to a certain range of altitude. For example, the climate at the base of a mountain might be humid subtropical, and the climate at the summit might be tundra.

2.4 Classification of Precipitation

Initial understanding of precipitation types has revealed two broad classes of precipitation event. One involves a very intense and relatively short-lived convective precipitation with variable rain heights that might go up to height of more than 10 km. Convective rain is being characterised by intense rainfall that occurs for a short period and covers a small or localised area. The stratiform rain on the other hand can be characterised by medium and low rate events that occurs for a longer period of time. This type of rain comprises a long period of stratiform precipitation with a very well developed melting layer at a constant height.

Further studies are now being carried out by organisation such as Rutherford Appleton Laboratory, United Kingdom with radar data on precipitation events. Attempts are being made to characterise the vertical distribution of ice and water regions, and to determine the precipitation drop size distribution from measurements of fall velocity. Both parameters are considered important for improved radiowave propagation modelling. According to the ITU Handbook on Radiometeorology [Radiocommunication Bureau, 1996] and Houze [Houze, 1981], precipitation that occurs all over the world may be grouped into four different types. The fifth type of precipitation identified as 'warm rain' excerpted from literatures [Huffman and Norman, 1988; List *et al.*, 1988; Murakami *et al.*, 1994] is also included below.

2.4.1 Stratiform or Widespread

The first precipitation type can be identified as stratiform or widespread. It consists of a widespread region with low precipitation rates and small-embedded showers with possible intensity up to 25 mm hr^{-1}. This type of precipitation dominates the high percentage of rainfall rate statistics time in most climates. As can be observed in Figure 2.3, for a typical stratiform event produced from RAL measurement data during their campaign in the tropic [Eastment *et al.*, 1995; Eastment *et al.*, 1998], the melting

layer is a noticeable feature appearing in the bright band of the radar reflectivity display. The precipitation can be said as almost horizontally stratified and originated from the height of the melting layer.

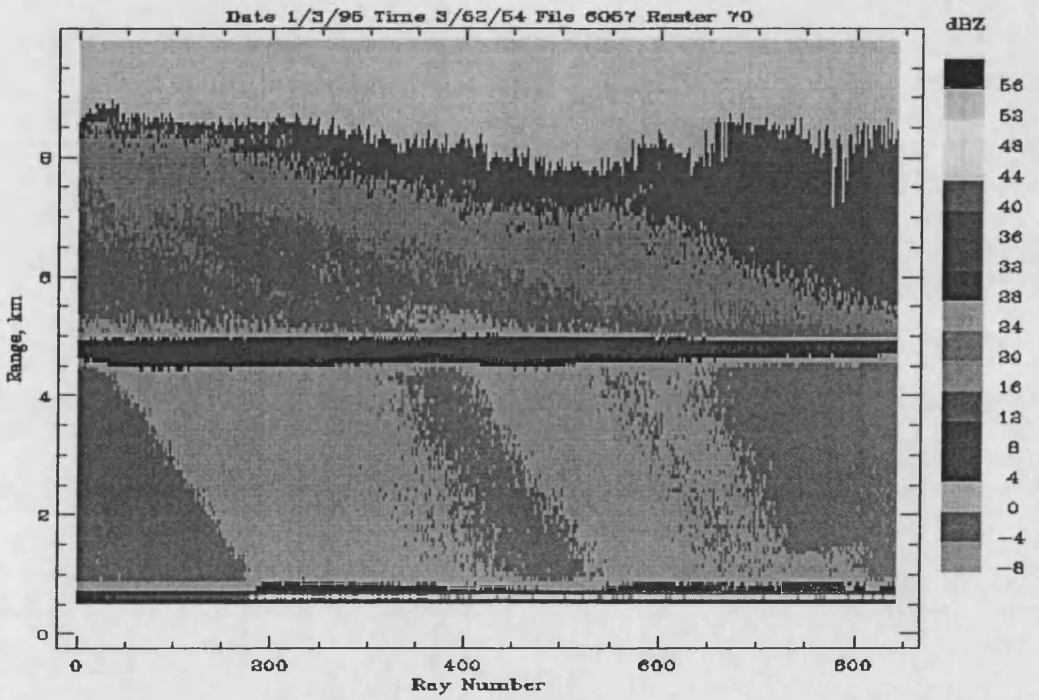

Figure 2.3: Reflectivity radar scan of a stratiform event

2.4.2 Convective or Showery

The second type of precipitation can be classified as convective or showery. It has a localised area of relatively concentrated precipitation characterised by strong up and down draft extending through deep vicinity of the troposphere. Figure 2.4, another radar scan produced from RAL data; exhibits forms of very well defined vertical cores of maximum reflectivity. The localised areas may be sometimes columnar in nature and even extend into the tropopause. This type of precipitation usually determines the low percentage of rainfall rate statistics time in most climates around the world. The large scales mixing of different type of precipitation particles observed are the result of strong vertical air motion.

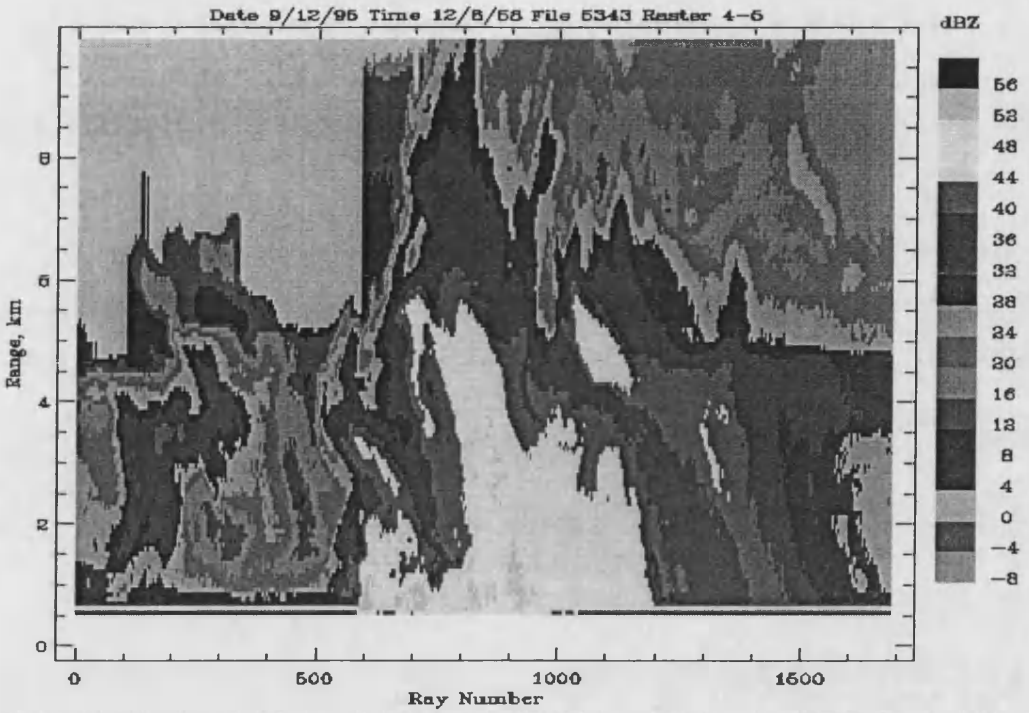

Figure 2.4: Reflectivity radar scan of a convective event

2.4.3 Monsoon

The third type of precipitation is the monsoon. It usually embodies a sequence of bands of strong convection followed by interval of stratiform precipitation. The band can be up to 50 km across, hundreds of kilometres in length, and produce heavy precipitation lasting for several hours.

2.4.4 Tropical Storm

The fourth precipitation and final classification by references [Radiocommunication Bureau, 1996; Houze, 1981] is the tropical storms that can be identified as hurricane or typhoon. As suggested by the name, it is very unlikely to occur in Europe. Tropical storms contain a large organised region of precipitation extending over hundreds of kilometres. The typhoons are described by several spiral bands terminating in area of intense precipitation surrounding the central region or 'eye' of the storm.

2.4.5 Warm Rain

The fifth type is the warm rain. It has been observed that there is possibility for precipitation to develop in clouds that contain no ice. The term 'warm rain' was derived after scientists noticed occurrences of precipitation in tropical regions that fell from clouds even when the temperatures never colder than 0°C. In warm rain processes, cloud droplets collide with each other and then coalesce (stick together) to form larger droplets [Huffman and Norman, 1988]. Eventually the droplets grow large enough that they become precipitation droplets.

2.5 Characteristics of Precipitation

The specific attenuation of precipitation relies on its microstructures such as drop size distribution, terminal velocity, orientation and shape, and temperature. All these structures have to be established in each point of the radiowave path. However, precipitation deviates notably in space and time and thus complicates the calculation of precipitation attenuation. Brief description of each microstructure is presented in the following subsections.

2.5.1 Drop Size Distribution

The Laws and Parson [Laws and Parson, 1943] drop size distribution has been found effective for most estimation of the attenuation and scattering properties of rain at frequencies up to about 40 GHz. The rain drop size distribution changes mainly with the rainfall rates and therefore the distribution may deviate within a storm. The use of a single distribution model may not be adequate for all locations in the world. This is because relative concentration of small drops can be highly variable. Different rain drop size distributions have been reported for tropical and temperate climates. It is also reported that relative densities of small drops having diameters less than 0.5 mm could not be well modelled by Laws and Parsons. Therefore, the use of the Marshall-

Palmer [Marshall and Palmer, 1976] drop size distribution is sometimes employed to aid the drawback.

The Laws and Parson and Marshall-Palmer distributions represent on-average distribution reflecting in the stratiform or widespread rain. In climates where showery convection is evident, other distributions are sometimes used. The other most often referenced distribution is the Joss and Waldvogel [Joss and Waldvogel, 1968]. The Joss distributions are classified into three rain types (drizzle, widespread rain and thunderstorm), while the Laws and Parson and Marshall-Palmer distributions include all the measurements in a single distribution. In Japan, a group of researchers [Jiang *et al.*, 1997] has proposed the use of Weibull distribution to represent the drop size distribution for rain measured in Tokyo. The measurements is obtained in the year 1993 and they also reported that the rain induced attenuation coefficients from the Weibull drop size distribution have given a very good agreement with experimental data obtained at Nagoya back in 1990. Another investigator [Gloaguen and Lavergnat, 1995] also suggested that the rain drop size distribution near Paris, France could be modelled by the Weibull distribution. Ajayi and Olsen [Ajayi and Olsen, 1985] on the other hand, by employing the 'method of moment regression', have described a single lognormal function to be accurately fitted over the entire range of rain rates measured in Ile-ife, Nigeria.

2.5.2 Terminal Velocity

Measurements to determine the terminal velocity were made in quiet conditions in a laboratory but had been assumed to apply in the atmosphere was conducted by previous researchers [Gunn and Kinzer, 1949]. They reported that the terminal velocity of a raindrop is a function of drops' sizes. Radar observations (which most of them are usually stratiform events) generally show only small differences in reflectivity values are detected for the region below the rain height. Therefore it is generally assumed that the number of raindrops, the size of raindrops and the liquid water

content of a volume of raindrops deviate only slightly with height. Based on such assumption, the specific attenuation can also be postulated to have very small deviation with height below the rain height because it depends primarily on liquid water content.

2.5.3 Orientation and Shape

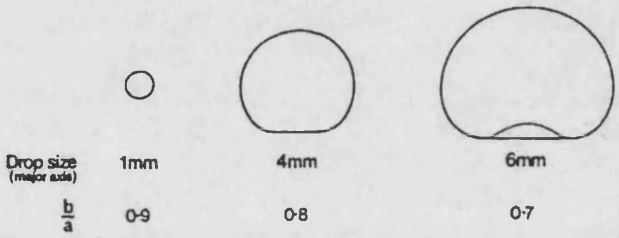

Figure 2.5: Typical raindrop shapes [Watson, 1997]

The raindrop shape depends upon a number of various factors. The shape is a function of their falling terminal velocity, sizes, and internal-and-external pressure at their surfaces. The force of gravity is a major orientation force on the raindrops. Falling drops assume nearly spheroidal shape when affected by gravity and surface tension of the water. While falling, drops may vibrate and oscillate but the net shape is oblate spheroidal with the symmetry axis close to vertical. Investigators [Pruppacher and Pitter, 1971] have modelled the drop shape of rain as a function of drop size. Observations made in a laboratory reported earlier [Pruppacher and Beard, 1970] agreed with the shape predictions by Pruppacher and Pitter. Raindrops could exist in size varying from very small to fairly large ones. The smallest drop may be equivalent to those found in the cloud, whereas the largest drop does not usually exceed 4-mm radius. This is because drop with the radii bigger than 4 mm is hydrodynamically unstable and will break up. Measurements show that water drops larger than 1 mm in-radius are oblate in spheroidal shape with a flattened base. Such condition can be observed in Figure 2.5

2.5.4 Temperature

Falling raindrops have a temperature that approximates the wet bulb temperature for the temperature, pressure and humidity of the surrounding air [Radiocommunication Bureau, 1996]. In the tropical regions, rainfall is predominantly convective, and researchers [Pan and Bryant, 1994] reported that it has been confirmed by radar observations that supercooled water drops can rise on the strong updraft to area well above the 0°C isotherm. This proves that small liquid droplets can exist at temperature below 0°C (especially in the updraft region of a convective storm). Nevertheless, attenuation by rain is generally contributed by significant numbers of large liquid water drops that exist between the height of the 0°C isotherm and the surface.

2.6 Measuring Precipitation Rate

Precipitation rate or rainfall rate is defined as 'a measure of the intensity of precipitation expressed by the increase in the height of water reaching the ground per unit time' [ITU-R PN.310-9, 1994]. Precipitation rate is generally expressed in millimetres per hour and commonly presented in units of mm hr^{-1}. There are several equipments that can be employed to obtained precipitation intensity measurements.

Comparison studies between the rainfall rates recorded by precipitation measuring devices have been conducted. It has been indicated in literature that collection techniques play an important part in making accurate precipitation intensity measurement. Different types of co-located equipment appear to give different rainfall rates [Brand, 2000]. Further research seems to be required. In recent work, corrective coefficients have been proposed to relate between the measurements on different types of equipment [Catalan, 1999]. Descriptions of several precipitations measuring equipment also commonly known as rain gauges that are commercially available are describe briefly below.

2.6.1 Optical Rain Gauge

The device is an optical sensor that measures precipitation rate and provides an analogue voltage equivalent to the measured precipitation intensity. The equipment employs the focusing and defocusing of an optical beam principle to estimate precipitation rate. It measures the precipitation rate by detecting the optical irregularities induced within the sample volume by precipitation particles falling through the beam of partially coherent infrared light. These irregularities are known as scintillation, and by detecting the intensity of scintillation, which are characteristics to precipitation; the actual rainfall rate can be determined [TWI System Inc., 1996].

2.6.2 Impact Distrometer

A distrometer is a device that able to convert the raindrop impact momentum into rain drop size and rainfall rate. The instrument operates base on the principle of transforming the vertical momentum of impacting drops into electric pulses, the amplitude of which is a function of the drop diameter. The equipment obtains additional information about the number of drop, and from such knowledge the drop size distribution and rainfall intensity can be derived.

2.6.3 Rain Sensor

The device uses the principle of a precision volume drop passing through an optical beam. The sensor is moulded plastic and aerodynamically shaped to lessen the effect of wind on the reading. The rain gauge operates on the principal of counting known volume drops as they pass an optical sensor. The sensor measures the amount of rain passing through it by an infrared optical system with no moving parts.

2.6.4 Tipping Bucket Rain Gauge

The rain gauge comprises a divided bucket assembly that is pivoted at the centre. Rain collects in one side of the bucket that then tips when a predetermined volume of water has been collected. The tipping action discharges the collected water and repositions the opposite side of the bucket under the discharge nozzle. a switch is activated when the bucket tips on its pivot. The number of times the switch is closed in a given period provides a measure of rainfall rate.

2.6.5 Capacitance Gauge

The device collects water into a measuring chamber, which surrounds a capacitance probe. The capacitance of the system changes as the water level, in the chamber, rises. Therefore the rainfall accumulation can be determined. The system is automatically emptied and reset at every predetermined accumulation.

2.7 Attenuation Due to Precipitation

In most radio system design, the operating limit is usually predetermined by the variation about the clear sky level. The negative variation below the mean clear sky level is called excess attenuation [Allnutt, 1989]. Attenuation is usually measured in decibels denoted by unit of dB. The access attenuation of a radiowave due to precipitation is formed from two components. The components are described as absorption and scattering.

Signal attenuation on a path is sometimes referred as extinction. Extinction is the algebraic sum of component due to scattering and absorption [Oguchi, 1983]. The relative importance of scattering and absorption is a function of the complex refraction of the absorbing/scattering particle. The complex index of refraction itself is a function of signal wavelength, temperature, and the size of the particle, relative to the

wavelength of the radiowave. It is important to examine the variation of the scattering and/or absorption contributions to extinction, for water spheres of various radii. As illustrated in Figure 2.6 below, it is clear that for longer wavelengths and smaller particles, absorption dominates the extinction process, whereas for shorter wavelengths and larger particles, the scattering dominates [Brussard and Watson, 1995].

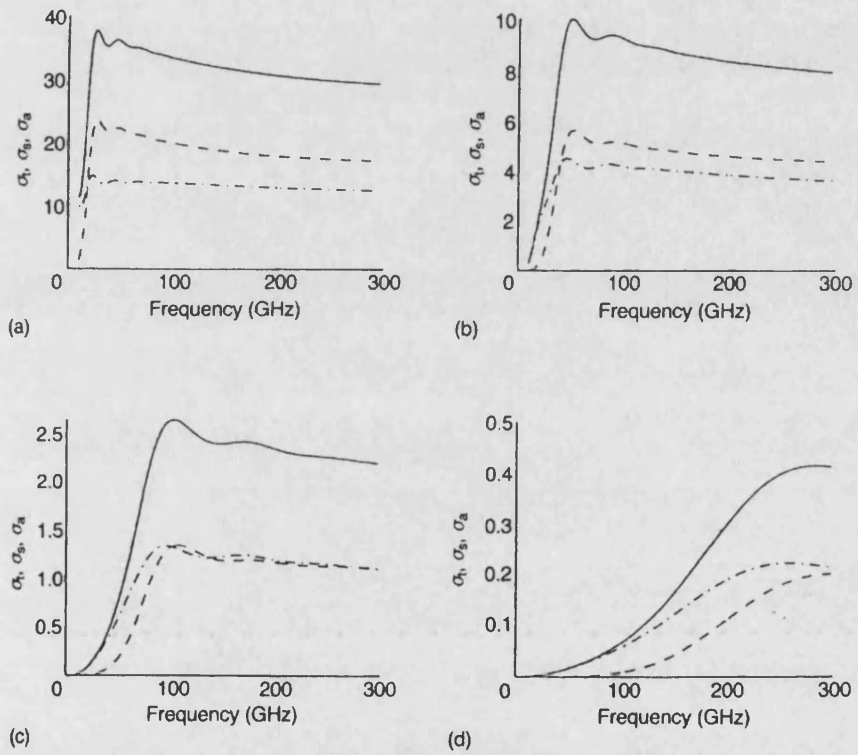

Figure 2.6: Scattering (---), absorption (-·-) and total (–) cross-sections σ_s, σ_a and σ_t in mm^2 for water spheres of various sizes as a function of frequency: (a) a = 2 mm; (b) a = 1 mm; (c) a = 0.5 mm; (d) a = 0.2 mm. [Brussard and Watson, 1995]

In conditions where a particle is very small compared to a wavelength of the radiowave, Rayleigh scattering theory can be applied. In these situations, the signal extinction will be mainly due to absorption. These conditions generally hold for signals well below the frequency of 10 GHz, propagating through an ensemble of hydrometeors. As the frequency goes up, the size of the raindrops becomes a substantial fraction of the wavelength. The raindrops now not only absorb the signal but also scatter it. There is increasing significance of the scattering as the wavelengths

decreases. The imaginary part of the complex permitivity of water becomes significant. In this situation, Mie scattering theory is used.

To calculate the attenuation of a radiowave as it passes through precipitation, it is necessary to aggregate the individual extinction contributions of each raindrop encountered along the path. Since the drops are all of different sizes, it is necessary to invoke a drop size distribution $N(D)$ and integrate the extinction contributions. The attenuation A can be expressed as follows [Allnutt, 1989]:

$$A = 4.343 \times L \int_0^\infty \sigma_t (D)\, N(D)\, dD \qquad \text{(dB)} \qquad (2.1)$$

where $\sigma_t(D)$ is the extinction cross-section or 'total cross-section' of a drop diameter D and, L is the length of path through precipitation in km and the $N(D)$ represents the particle size distribution in $mm^{-1}\ m^{-3}$. If the length of path through precipitation or distance travelled is set equal to 1 km, Equation 2.1 above gives the specific attenuation γ, namely

$$\gamma = 4.343 \int_0^\infty \sigma_t (D)\, N(D)\, dD \qquad \text{(dB km}^{-1}\text{)} \qquad (2.2)$$

In relating such attenuation to the amount of precipitation volume falling in per unit area on the ground, the dependence of terminal velocities of precipitation in still air of radius D must be established. Hence, the rainfall rate R where $V(D)$ as the fall velocity of a particle of radius D in ms^{-1} can be described as follows [Mitra *et al.*, 1987]:

$$R = 4.8\pi \, x\, 10^{-3} \int D^3\, V(D)\, N(D)\, dD \qquad \text{(mm hr}^{-1}\text{)} \qquad (2.3)$$

The calculation of the specific attenuation is quite complicated since characteristics of precipitation vary so much in both space and time. Simplification can be made to

obtain results well within the accuracy achievable in most measurement. The well-known specific attenuation equation given by power-law relationship to the rainfall rate is defined as [Radiocommunication Bureau, 1996]:

$$\gamma_R = kR^{\alpha} \qquad (\text{dB km}^{-1}) \qquad (2.4)$$

where k and α are frequency and polarisation dependent coefficients. Selected values of these two frequency-dependent coefficients as a function of frequency can be found in the Recommendation ITU-R P.838 - '*Specific Attenuation Model For Rain For Use In Prediction Methods*' [ITU-R P.838, 1992].

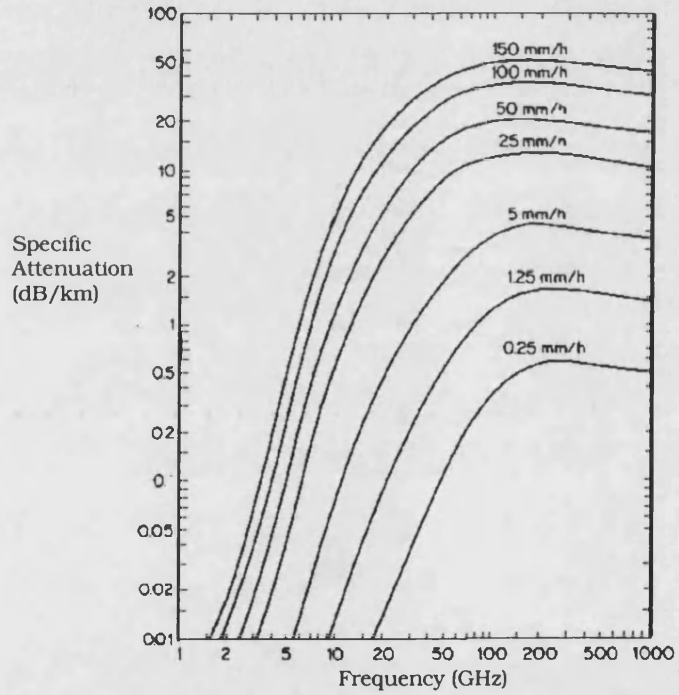

Figure 2.7: Specific attenuation as a function of frequency for coherent wave propagation through uniform rain [Rogers and Olsen, 1976]

Olsen *et al.* [Olsen *et al.*, 1978] have examined the theoretical background of the $A = aR^b$ equation which is the same as Equation 2.4 above. They expanded the Mie coefficients for a sphere in a power series of $ka/2$ where k is the free space propagation constant. Substituting the resulting power series expression of $\sigma_t(D)$ into the attenuation integral shown in Equation 2.1 together with the negative exponential

rain drop size distribution and the modified gamma distribution functions, they found that the $A = aR^b$ (or $\gamma_R = kR^\alpha$) relationship is exact in the limit of low frequencies and low rainfall rates. The relationship is not exact in the higher optical limit because for a very large drop in comparison with the wavelength, the total energy lost from the incident beam is made up of two components. One, energy is removed from the beam by scattering and/or absorption that exactly corresponds to the geometrical cross-section. The other, energy is lost by diffraction in the forward direction that again corresponds to the geometrical cross-section. Figure 2.7 above displays the dependency of specific attenuation with rainfall rate and frequency. The curves are based on the Laws and Parsons drop size distribution, terminal velocities of Gunn and Kinzer and rain temperature of 20° C.

In frequency range between two extremes such as microwave and millimetre wave regions, the relationship could not be exact. There is possible error in assuming Rayleigh scattering instead of Mie scattering or vice versa for various cases as the frequency increases. However, examinations showed that the $\gamma = kR^\alpha$ relationship is a good approximation to the exact relationship. The values of k and α were obtained from logarithmic regression, fit to the exact specific attenuation values in the frequency range of 1-1000 GHz for the drop size distribution functions and for the temperature of 20, 0 and -10^0C. A comparison of the exact Mie calculations and calculations based on $\gamma = kR^\alpha$ relationship showed that the accuracy of the approximate expression is reasonably good for the frequencies, temperature and rainfall rates used in the regressions.

Oguchi reviewed some of the features of the calculated single-scattering properties of non-spherical raindrops in the Mie scattering region. For a distorted raindrop, the cross-section σ_t depends on polarisation. Thus, the attenuation is polarisation dependent. Several measurement results did suggest that the general procedure of calculating cross-section from Mie theory with a known refractive index could also be

valid. This because sometimes the σ_t may be slightly lower than that of calculated for spherical drops and sometimes may be slightly larger.

The Recommendation ITU-R P.838 for calculating the specific attenuation for rain-induced attenuation used in prediction recommendation was based on Law and Parson drop size distribution. Gloaguen and Lavergnat did imply that the use of drop size distribution established for another climate or type of rain can lead to significant errors when applied to attenuation predictions. Therefore, ITU recommendations should be used with caution since drop size distribution of rain for different regions of the world is different.

2.8 Conclusion

A theoretical framework for the development of this thesis is based upon has been presented in this chapter. Radiowave propagation mechanisms have been discussed briefly and propagation impairments affecting space communications have been highlighted. Definition of rainfall rate and description of different equipment that can be utilised to measure rain intensity have been presented. The relevance between rain and signal attenuation has been described on conceptual basic.

A factor that complicates the determination or prediction of rain-induced attenuation along the slant path is its variability in space and time. The rain specific attenuation depends on the microstructures of rain fall i.e. size distribution, temperature, terminal velocity and shape of the rain drops [Radiocommunication Bureau, 1996] and these structures need to be identified at each point of radio path to calculate the attenuation accurately. Microstructure such as rain drop size distribution varies according to type of precipitation. Some of the rain microstructures are climate dependent. One climate differs from another, and brief narrations of world climate types have also been presented in this chapter.

Chapter 3

Analyses of Rainfall Intensity Measurements

3.1 Introduction

Rainfall intensity or rainfall rate is one of the most critical meteorological phenomena that causes severe degradation of satellite-Earth communications above 10 GHz. At frequencies above 10 GHz rain strongly attenuates and depolarises radio waves and constitutes a major impediment to satellite link performance [Pratt and Bostian, 1986]. Therefore, an understanding of the statistical characteristics of rainfall intensity is extremely crucial for the planning of any microwave or millimetre-wave telecommunication systems, especially in the heavy rainfall regime of tropical regions.

The characteristics of the rainfall in tropical regions must be investigated in every design of communication links through this region in order to meet the system's operational reliability. It is common knowledge that rainfall rate cumulative distributions vary greatly from region to region. High rainfall rates and the consequent high rain induced attenuation in the tropical regions is arguably the greatest constraint to the usability of the K_u-bands and above in the tropics

This chapter presents analyses of rainfall intensity measurements taken in Bukit Jalil, Malaysia over a period of twenty months, from August 96 to March 98. The statistical analyses presented include seasonal variations, diurnal variations, and annual cumulative distribution. In addition, the procured measurement results are then compared with available ITU-R rainfall intensity models to test their validity.

3.2 Climate of the Peninsula of Malaysia

The Peninsula of Malaysia is situated between 3° and 7° N of the Equator. Its position in the equatorial zone guarantees a classic wet tropical climate with relative humidity levels usually around 90% [Hulbert, 1973]. There are no distinct seasons and weather is fairly hot and humid all year round. The temperatures vary very little the year round, ranging from 21° to 32° C in the daytime, with the exception of the cooler climates of the central highlands. The Peninsula of Malaysia experiences short intense showers almost daily. The mornings are usually hot and sunny with showers in the afternoon [Kendrew, 1922]. It is rare to have a day without showers and unusual to have a day without sunshine. The average annual rainfall varies from 2,000 to 2,500 mm.

The climate is dominated by the effect of two monsoons or "rainy seasons", which affect different parts of the peninsula of Malaysia to varying degrees. The northeast monsoon blows between October and February; and from March to September; the peninsula of Malaysia is affected by the southwest monsoon [Jackson, 1989]. It is however difficult to generalise about the nation's climate, as rainfall differs on the east and west coasts according to the prevailing monsoon winds, northeast or southwest. The seasonal wind flow patterns coupled with the local topographic features determine the rainfall distribution patterns over the country. During the northeast monsoon season, the exposed areas like the east coast of peninsular Malaysia experiences heavy rain spells. On the other hand, inland areas or areas which are sheltered by mountain ranges are relatively free from its influence.

Over the rest of the peninsula with the exception of the southwest coastal area, the monthly rainfall pattern shows two periods of maximum rainfall separated by two periods of minimum rainfall. The primary maximum generally occurs in October to November while the secondary maximum generally occurs from April to May. Over the northwestern region, the primary minimum occurs in January to February with the

secondary minimum from June to July while elsewhere the primary minimum occurs from June to July with the secondary minimum in February.

3.3 System Location and Geographical Information

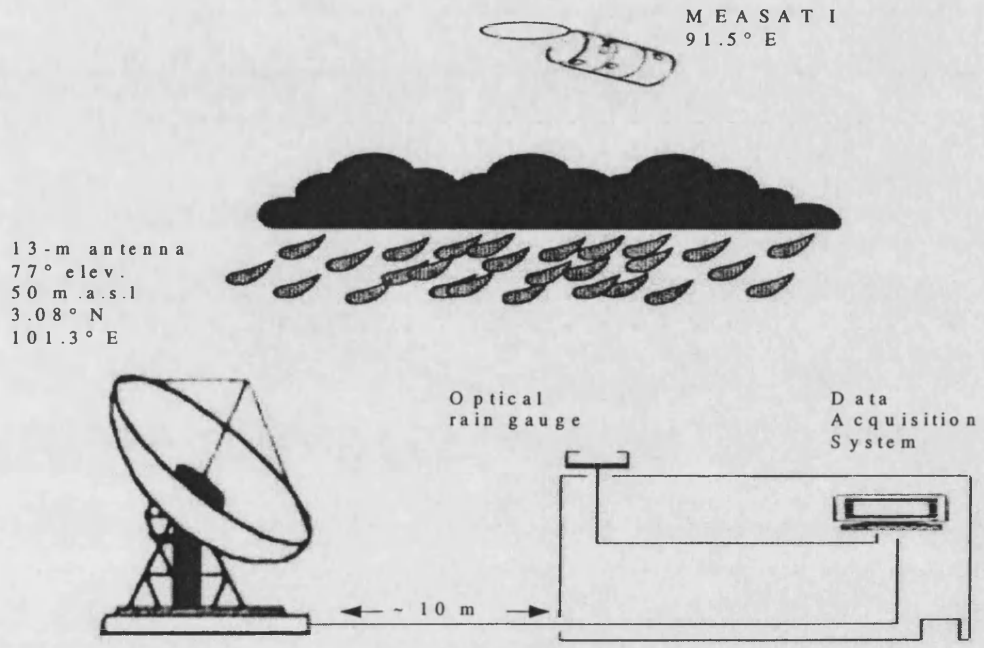

Figure 3.1: The system scenario

MEASAT Broadcast Network Systems (MBSN) Sdn Bhd installed a beacon signal attenuation and rainfall intensity measurement system at The MEASAT All Asia Broadcast Centre earth station, Bukit Jalil Kuala Lumpur Malaysia. The system measures the transmitted K_u-band signals from MEASAT satellites. A 13-m diameter parabolic antenna with vertical polarisation is used as the receiver. The antenna type is an offset reflector with Cassegrain feed optics. Situations where the satellite dish could be flooded by rainfall are very unlikely to happen. Each panel is equally spaced with each other. There is approximately 1.0 cm gap between the panels and this will allow water to trickle down. Also appropriate holes have drilled near the bottom surface of the dish so that water does not accumulate at the surface. In addition, there is a blower installed to prevent rain from going into the feeder. The blower is

automatically activated when the sensor on the outer side of the antenna panel detects moisture.

The beacon signals are transmitted from MEASAT I satellite operating from its orbital slot at 91.5° E. The general scenario of MEASAT signal measurement campaign is shown in Figure 3.1 above. The earth station is located at Bukit Jalil, Kuala Lumpur with longitude of 101.32° E and latitude of 3.08° N. The height above sea level for the earth station is approximately 50 metres. With reference to MEASAT I satellite, the earth station yields an antenna elevation angle of 77.33°. The signal attenuation in dB during precipitation together with the rainfall intensity readings are simultaneously measured. The results from analyses for beacon signal attenuation as well as rainfall intensity statistics are presented in the following sections.

3.4 Measurements Analyses

Rainfall rates are noted to be highly variable in terms of locations and times, and therefore include diurnal, seasonal and yearly variations. In this campaign, the rainfall intensity has been measured by the optical rain gauge described briefly in Chapter 2. The Transmission Department of MBNS has been carrying out the K_u-band beacon signal attenuation and local rainfall intensity measurement works from August 1996 until today. The measurements were recorded into databases. The hope is that, new findings based on collected databases can lead to improvements in technology resulting in more reliable satellite transmission. It is important to explore such technology before initiating new service applications in the Ku frequency bands through MEASAT satellites.

3.4.1 Events Assessment

Rainfall intensity distribution is inhomogeneous in space and time. When considering links of K_u-band and above, radiowave propagation in rainy condition is the major

concern for telecommunication system engineers. This section introduces the first investigative work carried out on K_u-band beacon signals with simultaneously measured rainfall intensity events in Malaysia. The measured event data are stored in monitoring files on a daily basis when applicable. Each monitoring file contains data of detected precipitation intensities and calibrated signal levels. From each monitoring file database acquired from MBSN, time-series plots for every measured event can be produced by use of computer software. Table 1 below presents a summary description of the site related to this study

Location	Latitude	Longitude	Climate	Dry Months	Duration
Kuala Lumpur	3°08' N	101°32' E	Equatorial	Nil	20 Months

Table 3.1: Description of the experimental site

Figure 3.2 and Figure 3.3 are two examples of time-series plots of attenuation and rainfall intensity as observed on the Earth-space link at 11 GHz obtained from MEASAT databases. Shown in the figures below are simultaneous measurements of the rainfall intensity and the K_u-band MEASAT satellite signal attenuation at 10 s sampling time. The measurement system samples the point rainfall rate data from the optical rain sensor at 10-second time interval which is also the integration time. When the system receives measured rain intensity value, it immediately polls the antenna control unit (beacon receiver) for its RF signal level. During precipitation events, (e.g. as shown in the figures below) the rain intensity and attenuation measurements are recorded at every 10-second interval; otherwise the data are stored at every 10-minute sampling [TWI System Inc., 1996].

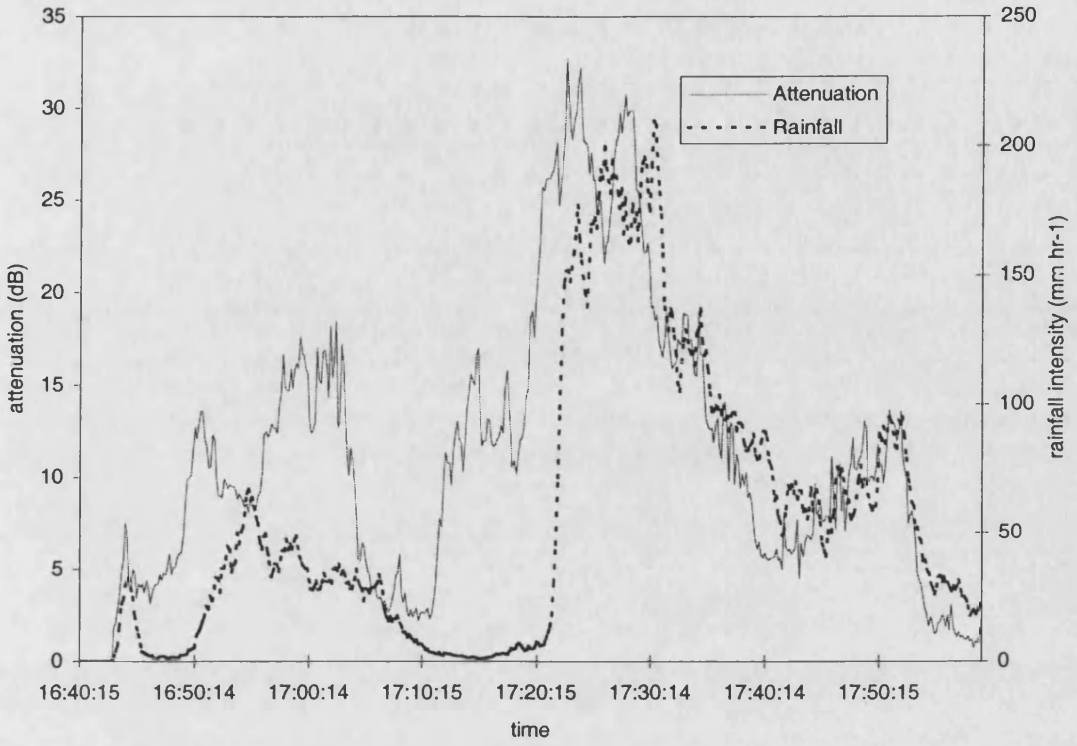

Figure 3.2: Event measurements 20/07/97

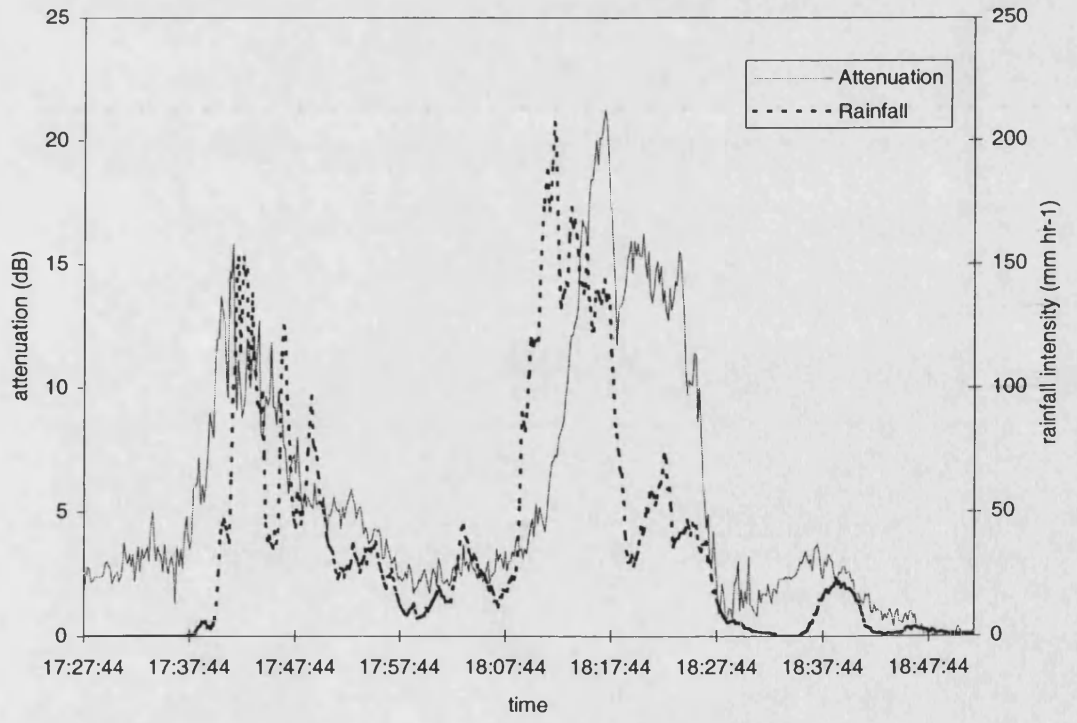

Figure 3.3: Event measurements 04/07/97

In general, a good correlation between the fading and the intensity of the rainfall can be observed in time-series plots. Within the 20 months recording period, more than 200 events with rainfall intensity higher than 100 mm hr^{-1} and attenuation exceeded 7-10 dB level were recorded. Several fades that exceeded the 30 dB level were also recorded. Rainfall intensity as high as 385.9 mm hr^{-1} was detected on 15th March 1998.

3.5 Seasonal Variation Rainfall Intensity

Areas subject to intense thunderstorms experience more severe propagation problems from rainfall compare to areas with a high average rainfall but with less frequent thunderstorms [Bostian *et al.*, 1993]. Monthly cumulative distributions of rainfall intensity have been compiled in the process to investigate the existence of seasonal variations in Malaysia. The monthly cumulative distributions are grouped together in Figure 3.4 and Figure 3.5 for 12 consecutive months, so that each represents 1-year worth of observation. The first group consists of the monthly cumulative distributions from August 1996 until July 1997. The monthly cumulative distributions from April 1997 until March 1998 are grouped together the other figure.

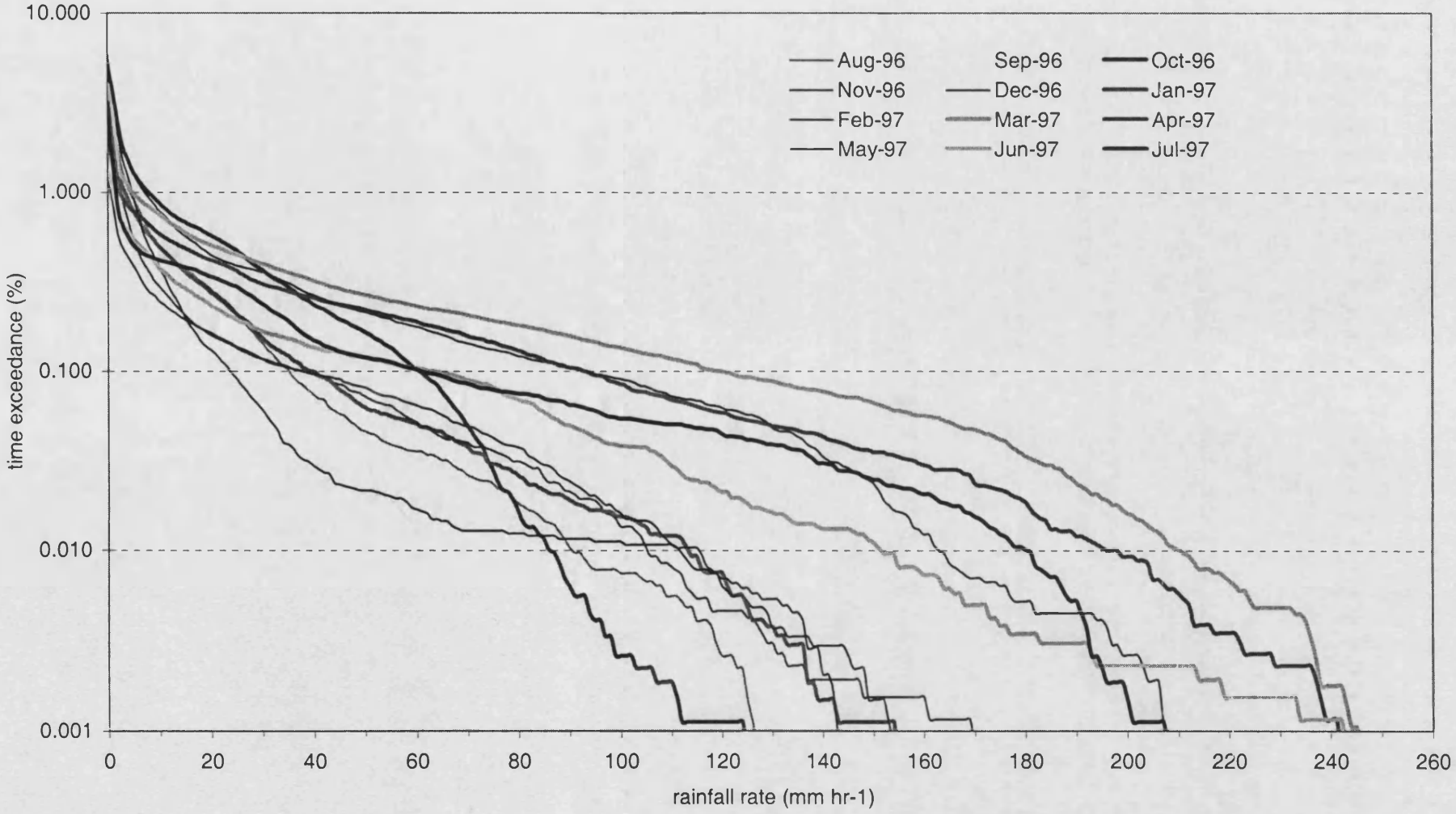

Figure 3.4: Monthly distribution of rainfall intensity (08/96-07/97)

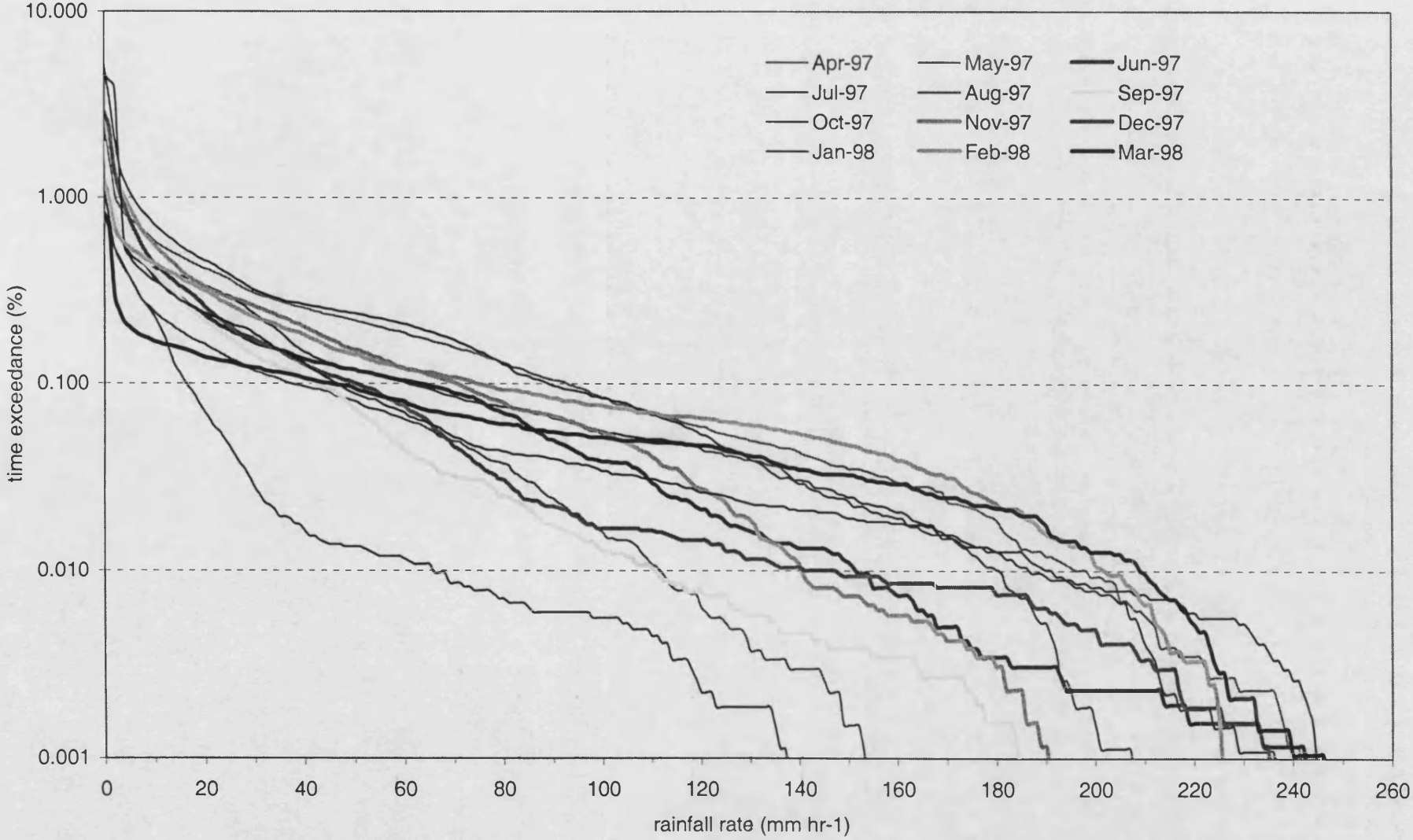

Figure 3.5: Monthly distribution of rainfall intensity (04/97-03/98)

Caution should be exercise in the interpretation of the cumulative distribution curves at the low time exceedance level since data present in this region is of dubious statistical significant.

Plot for each month is marked with different colour to contrast the other months. From Figure 3.4, within the period of first twelve months, rainfall intensity in March 1997 substantially exceeded rainfall intensity observed in other months at all percentages of time. The greatest impact on the annual rainfall intensity cumulative distribution curve is due to measurements of this month. This in other words, March 1997 can considerably influenced the annual rainfall intensity statistic. In Figure 3.5, there is no one specific month that dominates the time percentages. April 1998 is the one with highest measurement at 0.1% exceedance. Where else at time exceedance of 0.01%, it is the month of March 98. From observation upon the figures, it can be concluded that months of March in both 12 months group are subjected to the most severe rainfall intensity for time fractions lower than 0.01%.

In Figure 3.6, we present in a bar chart form the histogram of rain intensity at threshold of 10, 50, 70, 100, 150 and 200 mm hr^{-1} are exceeded monthly within the twenty months period. Histogram of rain intensity exceeded the 0.1%, 0.01% and 0.001% of each month from August 1996 to March 1998 can also be observed in Figure 3.7 below. From twenty months data we cannot yet comment on the long-term seasonal effects. However, it is expected that most locations in the west coast area of peninsula Malaysia will show some seasonally from the effects of the southwest monsoon in the higher rainfall intensities in month of March or April.

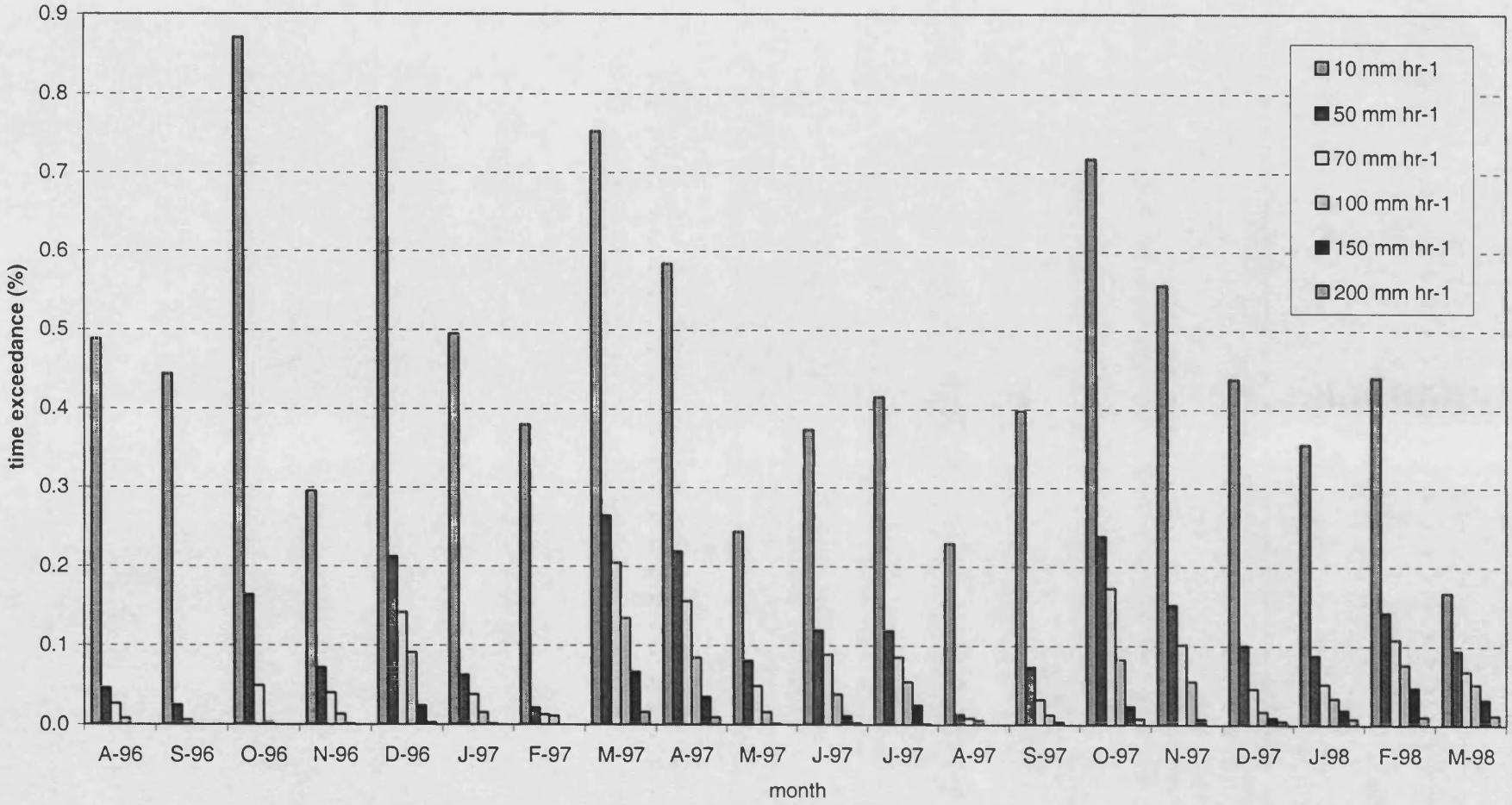

Figure 3.6: Histogram of specific threshold of rain intensity is exceeded monthly within the twenty months period

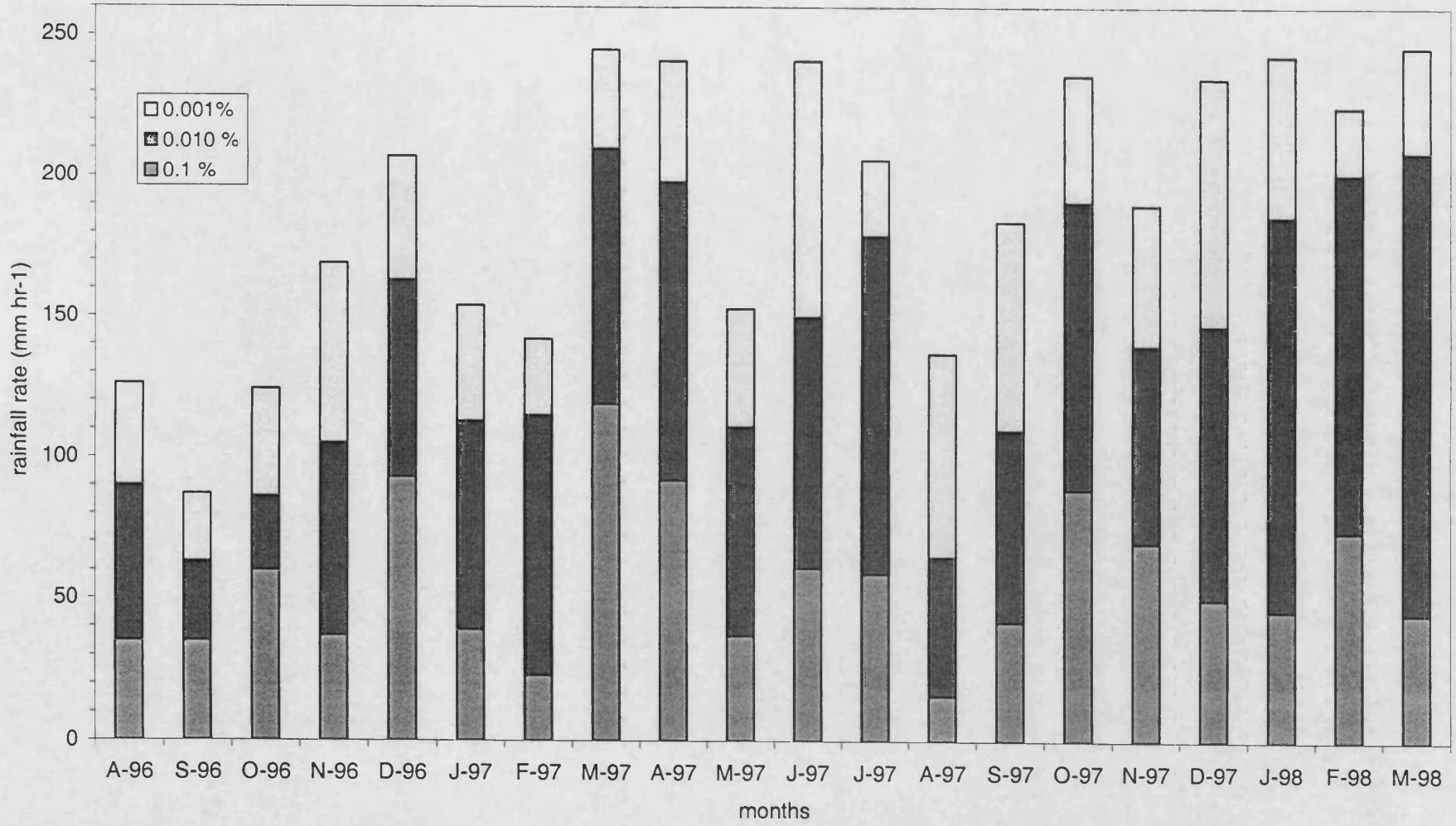

Figure 3.7: Histogram of rain intensity is exceeded for 0.1%, 0.01% and 0.001 % of each month from August 1996 to March 1998

3.5.1 Monthly Accumulated Rain

According the Meteorology Office, based on their observation, for over the rest of the peninsula Malaysia with the exception of the southwest coastal area, the monthly rainfall pattern shows two periods of maximum rainfall separated by two periods of minimum rainfall. The primary maximum generally occurs in October-November while the secondary maximum generally occurs in April-May. MEASAT earth station is located middle part of the peninsula and approximately 40 km from the west seacoast. Using the rain gauge measurement data we are able to calculate the monthly accumulation of rain and the results can be observed in the figure below. Based on our calculation the driest month within the twenty months period is August 1997 where 76.4 mm of rain was estimated. This information qualifies Bukit Jalil, Malaysia to be grouped under the equatorial climate classification where the criterion 'all month have at least 60 cm of rainfall' is met [Donald, 1994].

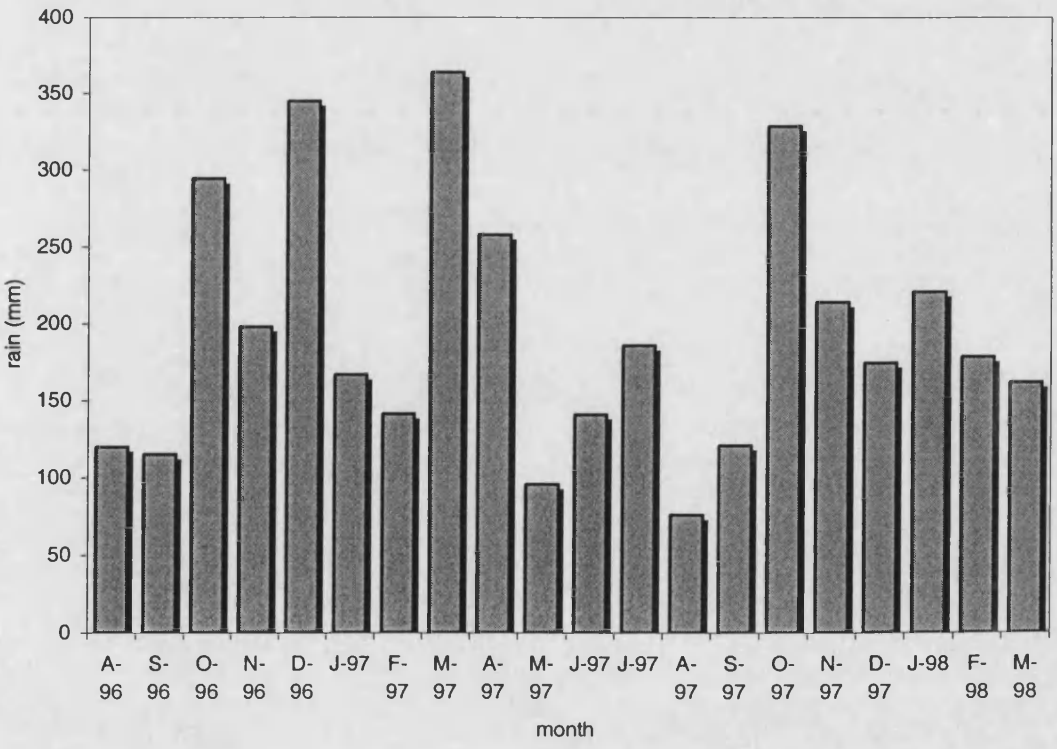

Figure 3.8: Calculated rainfall of Bukit Jalil, Kuala Lumpur Malaysia

3.6 Annual Cumulative Distributions of Rainfall Intensity

The severity of rain-induced attenuation depends on how hard it is raining described by the 'rainfall rate' in millimetres of accumulation per hour. It does not depend at all on the total rain accumulation. Thus, areas subject to intense thunderstorms (which is especially true for the tropical regions) experience more severe propagation problems from rain than do areas with a high average rainfall but fewer thunderstorm occurrences.

Several propagation models employed in the design of microwave systems make use of the long-term point rainfall rate cumulative distribution. Deviations from these predictions may therefore be expected for any single year since rainfall itself is a natural time varying phenomenon. Whenever applicable rainfall rate databases exist for a certain location, these data should be used to determine the appropriate cumulative distribution. Whereas in absence of such knowledge, the value presented in ITU-R recommendation can be employed.

The annual cumulative distribution of rainfall intensity is obtained from compilation of the monthly cumulative distributions. The monthly cumulative distributions for two 12-consecutive months for August 1996 to July 1997 and April 1997 to March 1996 have been presented in the previous section. Using these cumulative distributions, we acquire two annual cumulative distributions of measured rainfall rates for Bukit Jalil. The annual cumulative distributions of measured rainfall rates for Bukit Jalil is shown in Figure 3.9 below.

The figure consists of cumulative distribution plots for the two one-year periods and the other is for the extrapolated two-year period placing double weight on the 4 months April-July 1997. The cumulative distributions that have been acquired show a very good resemblance to each other.

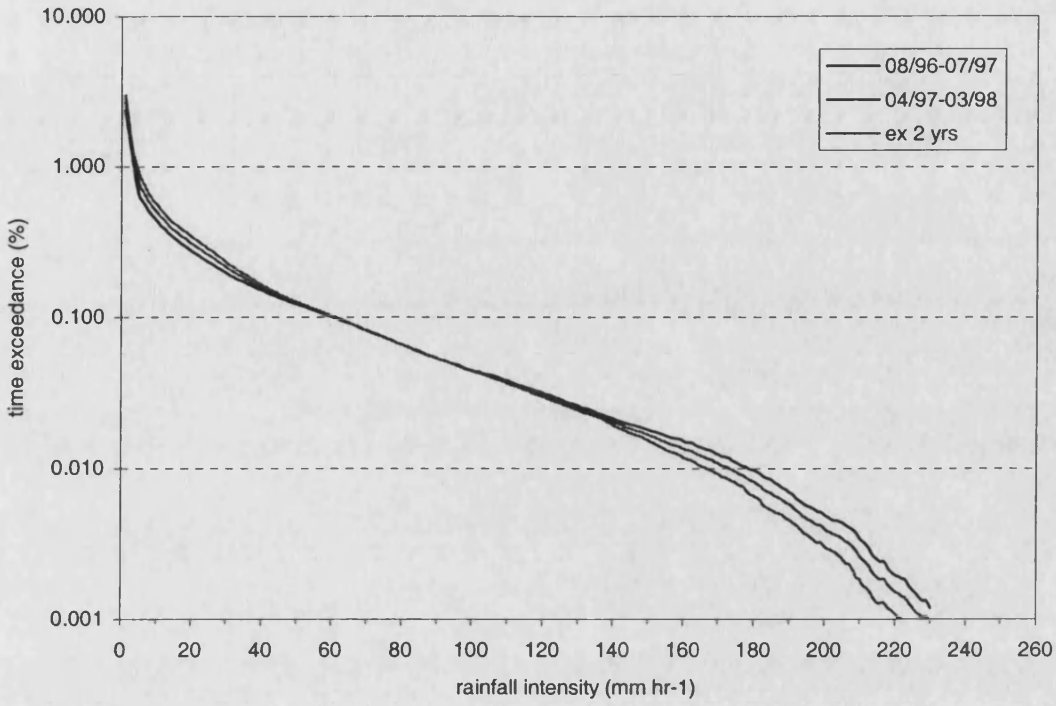

Figure 3.9: Annual cumulative distributions of rainfall rate

What is presented above is the annual statistics of rainfall rates for period of operation collected at 10-second sampling time. Situations where extremely heavy rainfall is detected in one of the countries in the tropics (in this case, Malaysia) can be observed in here. For 0.113% time exceedance, equivalent to 10 hours of the year, Bukit Jalil had experienced rainfall rate of approximately 50 mm hr^{-1}. In Section 3.8, investigation is carried out to determine the variance between rainfall rate statistics measured at 10 second with other integration times.

3.7 Diurnal Variation of Rainfall Intensity

Further investigations were carried out to determine the diurnal variability of the measured rainfall rate using procured databases from MEASAT. We tried to quantify the diurnal effects on the rainfall rate using the twenty months data from Bukit Jalil. Figure 3.10 gives the cumulative distributions for specific hours of the day determined at 6 non-overlapping time intervals. The rainfall rates measurements were inspected for every 4-hour grouping in order to gather additional rainfall characteristic

information. Intervals hour selected are defined by [00:00, 04:00], [00:04, 08:00], [08:00, 12:00], [12:00, 16:00], [16:00, 18:00], [18:00, 24:00]. The cumulative distributions shown in the figure are compiled based on twenty months measurements.

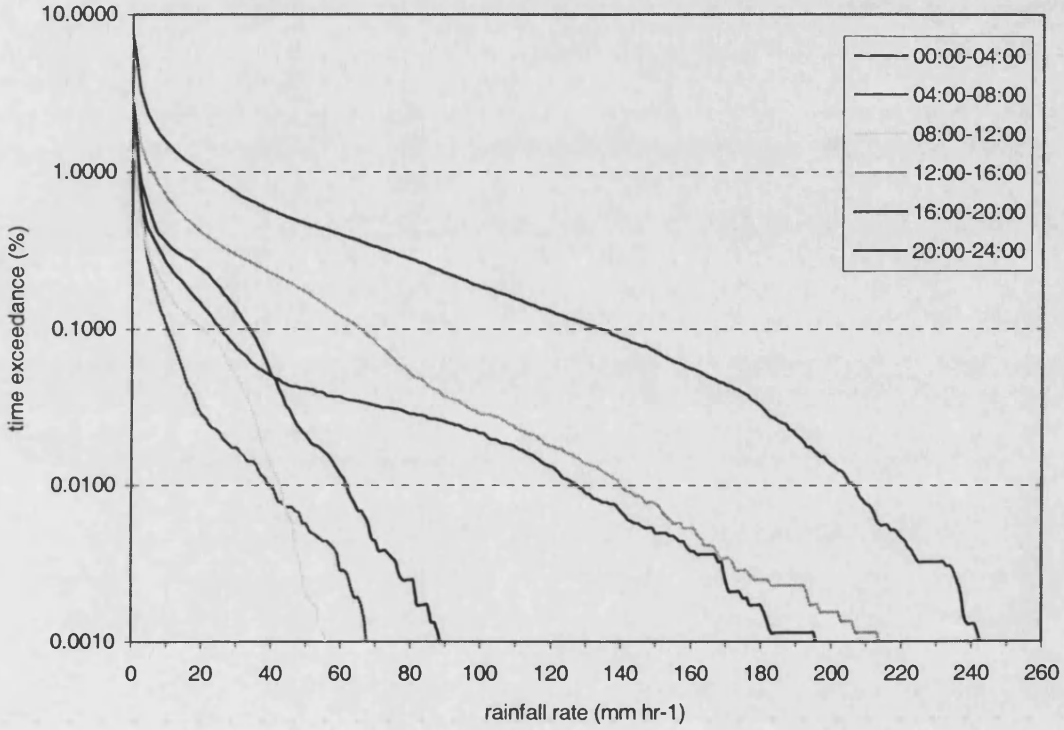

Figure 3.10: Diurnal variation of rainfall rate

From the above figure, it is possible to assume those heavy rain downpours and occasion thunderstorms are most likely to take place during late afternoon and early evening. It is observed that severe rainfall rates are detected between interval hours of 12:00 and 20:00. Hence, the signal degradations are most likely to happen between the same time intervals as well. The finding from this investigation has managed to confirm that rainfall intensity in an equatorial country such as Malaysia is subjected not only to seasonal, but also to diurnal variations.

From literature review, we found that rainfall rate measured in Bandung, Indonesia [Lekla *et al.*, 1998] also exhibited almost similar diurnal variation characteristics as

those observed at Bukit Jalil, Malaysia. It is reported that Bandung's local convective rainfall occurs very frequently during the afternoon between 13:00 and 17:00.

3.8 Integration Time Assessments

An integration time of 1-minute is selected by the ITU as a compromise between experimental accuracy and the amount of rainfall data collected. In many countries all over the world, long-term rain statistics are only available for long integration time of perhaps one hour or more. Since rainfall rate data at higher than 1-minute integration time are more readily available than 1-minute integration time data, methods for the conversion of rainfall rate distribution with variable integration time to the equivalent 1-minute would be very helpful. This is because most rain induced attenuation prediction methods available (to name a few; the ITU-R model [ITU-R P.618-6, 1999], the DAH model [Dissanayake *et al.* 1997], the Crane models [Crane, 1980; Crane and Shieh, 1989]) utilise the 1-minute rainfall rate data for a certain range of time percentage.

The power law relationships can be utilised to approximate the association between the rainfall rate at 1-minute integration time and that obtained at other integration times. One method [Segal, 1986] to convert rainfall data with finite integration time to equivalent 1-minute integration time is expressed as the following:

$$R_1(P) = aP^b R_\tau(P) \tag{3.1}$$

Based on 49 years of rainfall rate data measured in Barcelona, Spain, investigators [Burgueno *et al.*, 1988] suggested that the relationship could be expressed as:

$$R_1(P) = aR_\tau(P)^b \tag{3.2}$$

Where $R_1(P)$ and $R_\tau(P)$ are the rainfall rates exceeded with equal probability P for integration time of 1 minute and τ minutes respectively. The parameter of a and b for the conversions from τ-minute to 1-minute rainfall rate statistics is given in the table below.

τ (minute)	Segal's Method		Burgueno's Method	
	a	b	a	b
5	1.156	0	1.28	0.98
10	1.263	0	1.69	0.94
30	1.569	-0.015	1.32	1.06
60	1.759	-0.054	0.92	1.24

Table 3.2: Values for a and b coefficients for Segal and Burgueno 1-minute conversion formula

Recent developments in weather measuring equipment enable researchers to adopt an instantaneous or pre-selected integration time in computing the rainfall intensity. MEASAT has acquired a 'scintillation' type rain gauge with programmable integration time facilities. Acquired databases from MEASAT contain measurements of rainfall rate that are mostly detected at 10-second interval (there are several occurrences where the time stamp is either 9 seconds or 11 seconds). As mentioned in earlier section, the measurement system is assigned to take measurement at every 10-minute interval for each day. Whenever the system's sensor detects precipitation, the systems automatically changed its measurement time interval to 10 seconds. In other words, all measurements during 'non-rain' conditions were recorded at interval time of 10 minutes.

Recorded measurements from MEASAT rainfall databases at every 10-second interval enable us to compute the cumulative distributions of rainfall rates with 1, 5, 10, 30 and 60-minute integration time. Curves for rainfall rate cumulative distributions obtained with 10-second integration time and five others selected integration time are shown in Figure 3.11. From this figure, comparison can be made between the distributions of rainfall rates procured using various integration times. There are

reasonably good agreements for the percentage of the time exceedance greater than 0.01% among plotted statistics for 10 second, 1 minute and 5 minute. Plot drawn for computed 1-minute integration time exhibits very good agreement with the curve of measured rainfall rate at 10-second integration time at all time percentages.

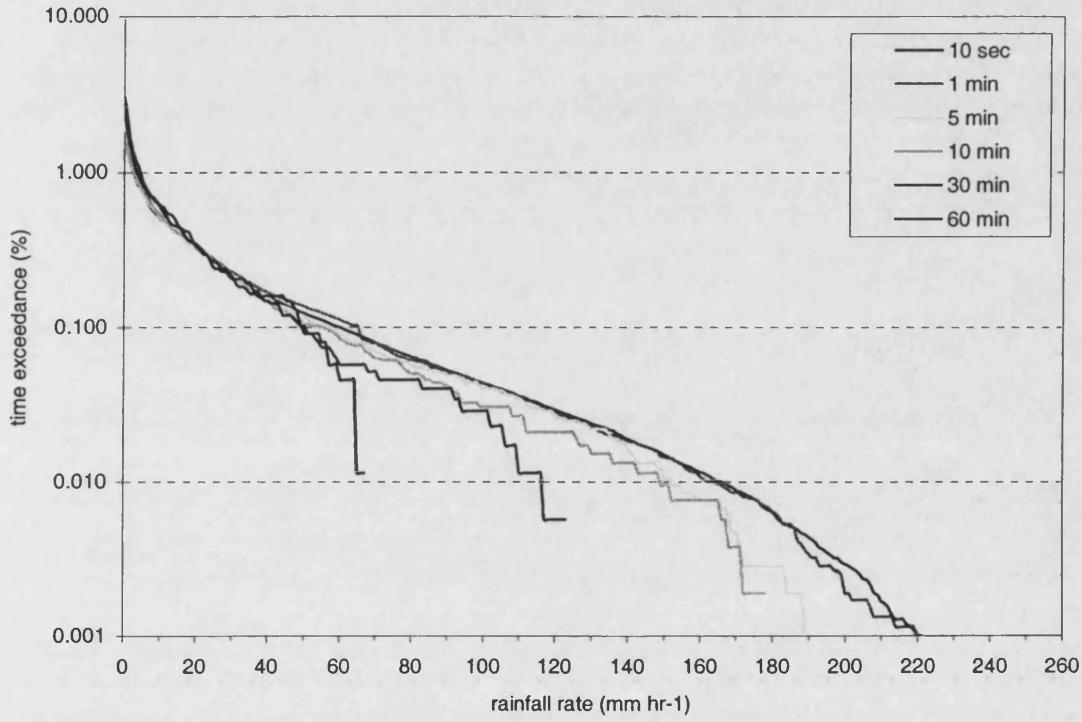

Figure 3.11: Rainfall cumulative distributions with different integration time

Using the acquired information from above we were able to examine the suitability of the proposed conversion formulas. We can observe from Figure 3.12 below that the 1-minute integration time statistics of rainfall rate estimated using Segal and Burgueno conversion formulas (for 10 minute and 30 minute) are higher than that of measured rainfall rate statistics at 1-minute integration time.

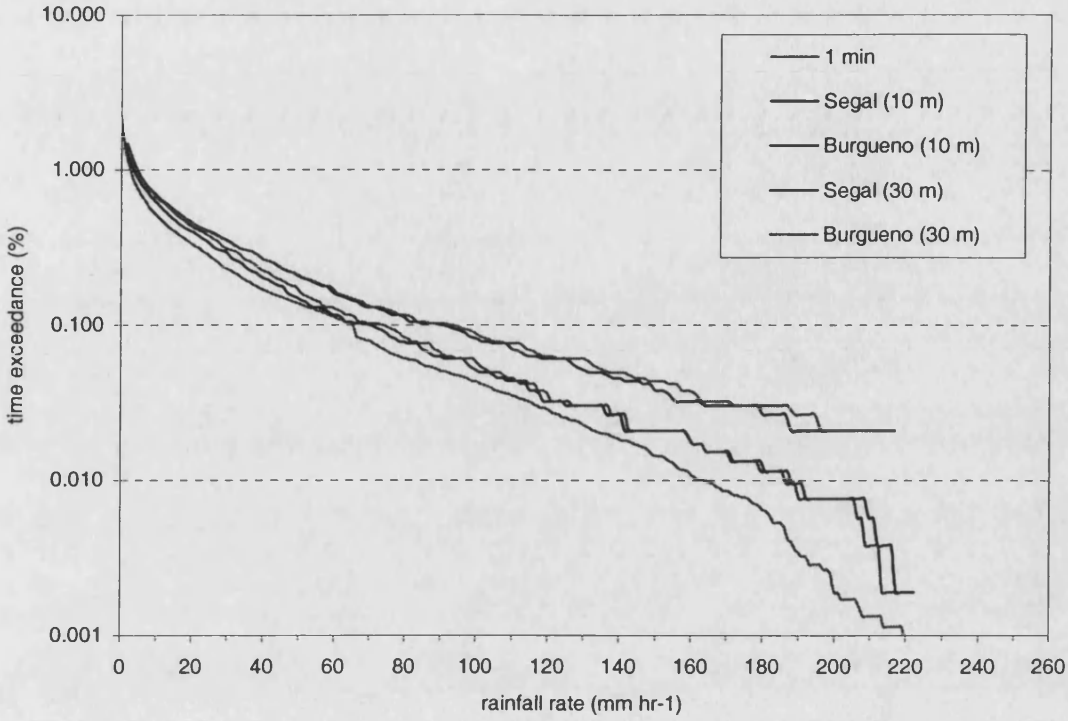

Figure 3.12: Comparison between 1-minute integration statistics with Segal and Bergueno estimations

From our analysis of the rainfall rate data measured at Bukit Jalil over the period of twenty months, we identified that the statistics of rainfall rate at 1-minute integration time could be obtained from other integration time statistics using the power law relationship expressed as:

$$P_{01}(R) = \alpha P_{\tau}(R)^{\beta} \tag{3.3}$$

In the above expression, the $P_{01}(R)$ and $P_{\tau}(R)$ are the probability exceeded with equal rainfall rates for integration time of 1 minute and τ minutes respectively. The parameter of α and β for the conversions from τ-minute to 1-minute rainfall rate statistics is provided in the Table 3.3.

Owing to the high rainfall rates encountered in Malaysia and tropical regions, the statistics of rainfall rates acquired is very dependent on the integration time employed. The integration time selected could determine the accuracy of some rain attenuation

prediction models. From the figure above, we can observe that the value of rain intensity measured at 0.01% of the time decreases as the integration time increases.

τ (min)	α	β
5	0.8153	0.8671
10	0.8643	0.8557
30	0.7387	0.7235
60	0.7205	0.6794

Table 3.3: Values for α and β coefficients for the time conversion formula

3.9 Comparison of Rainfall Rate Models

With the annual measured rainfall rate cumulative distribution, association with appropriate climatic zone as suggested by the ITU-R can be warranted. Table 3.4 was constructed using values obtained from locally measured rainfall rate distribution, Recommendation ITU-P 837-1 [ITU-R P.837-1, 1994] climatic zone P and climatic zone N, and the newly revised world rain map Recommendation ITU-P 837-2 [ITU-R P.837-2, 1999]. The annual statistics of rainfall rate for the first 12 consecutive months collected at Bukit Jalil are re-plotted in Figure 3.13. The rainfall rate statistics for climatic zone P, climatic zone N, and ITU-R new rain map for Bukit Jalil are also shown in the same figure. According to the ITU-R recommendation 837-1, Malaysia comes under climatic zone P. Our results also suggest that the rainfall rates bellow 200 mm hr-1 are close to that for Climatic Zone P.

The ITU-R climatic zones of rainfall intensity as presented by recommendation ITU-R P.837-1 have developed as a result of combining databases in various rain climates. It has decided in themselves by broad climatic considerations and thus can be improved by local knowledge. Since the recommendation is subjected to continual revision and improvement, perhaps result obtained from the investigation that was measured by a 'state of the art' optical rain gauge should be taken into consideration by ITU.

Percentage of time (%)	Zone N	Zone P	New ITU-R Rain Map	Measured
1.0	5	12	4	4
0.3	15	33	22	21
0.1	35	65	50	57
0.03	65	105	83	113
0.01	95	145	114	163
0.003	130	200	148	196
0.001	180	250	179	220

Table 3.4: Rainfall intensity exceeded (mm hr^{-1})

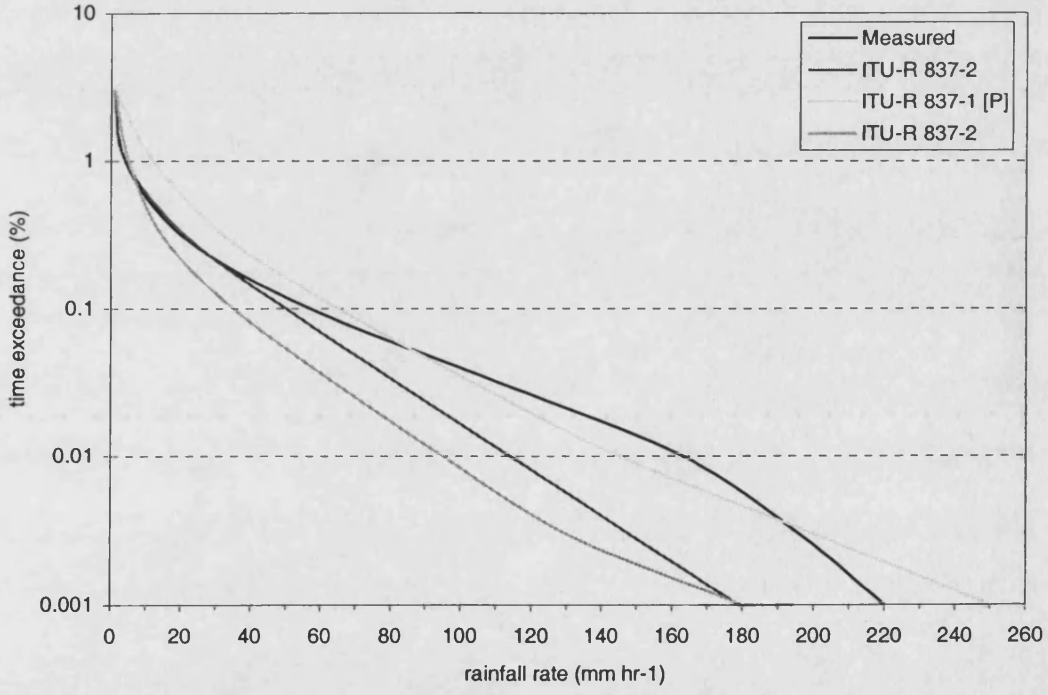

Figure 3.13: Comparison between rain climatic zones

3.10 Conclusion

Rainfall rate statistics and characteristics acquired from the analyses are important findings that need to be addressed in studying the effect of signal fading during rainfall events. We presented here in this chapter, results obtained from the study of twenty-month rainfall rate data collected in Malaysia. From our findings we conclude

that rainfall rate statistics are subjected to seasonal and diurnal variations. From our observation, the annual statistics seem to be influenced primarily by the rainfall experienced during the month of March and to the lesser extend by the month of August. As far as the diurnal variations are concerned, the day is divided into six equal periods and the most severe rainfall rate was detected during the period from 16:00 to 20:00. Nevertheless, to draw significant conclusions, this type of analysis requires data set over a longer period of time say perhaps at least 7 years to have confidence in the results [Burgeuno *et al.*, 1987].

In this chapter, the rainfall rates statistics with 10-second integration time to that with different integration time has been presented. The results show that the 10-second rainfall rate statistics very much agrees with that of 1-minute rainfall rate statistics for all measurements higher than 0.01% of the time. There is also a reasonably good agreement between 1-minute rainfall rate statistics with that of 5-minute rainfall rate statistic within 0.05% to 1% of the time, but differ obviously at the percentage of time smaller than 0.01%.

The precipitation characteristics in the tropics differ appreciably from those of the temperate region in that empirical relationships obtained in the latter may not be very suitable for system design in the former. This problem is further intensified by lack of dependable rain measurements and the present ITU-R rain intensity recommendations may be able to perform satisfactorily for the calculations of predicted rain induced attenuation in the tropics. In this chapter, we conclude that based on comparison between the available rainfall rate models, the locally measured annual cumulative distribution of rainfall rate shows that Malaysia is located within ITU-R climatic zone P as suggested by the previous ITU-R recommendation 837-1. From our assessment, the new rain map value seems to underestimate the measured rain intensity especially at higher time percentages.

Chapter 4

Analyses of Path Attenuation Measurements

4.1 Introduction

There has been a confined usage of K_u-band satellite links for commercial operations in tropical countries mainly due to high attenuation. The high attenuation experienced in the tropics is caused by significantly higher rainfall rates compared to other parts of the world. In this region, rain is the main consideration, as the occurrence of other hydrometeors is very rare [Mitra *et al.*, 1987; Ajayi, 1996].

Due to the growth in the use of frequency spectrum in the C-band operation, new and existing satellite operators in tropical regions may soon have no other alternative but to progress up to the K_u-band and above. This is expressly true with the increasing demand for television broadcasting uplinks and other additional services [Johannsen and Cuevas, 1993]. Nevertheless, the effects of rainfall on satellite signals at K_u-band frequencies in the tropics have not yet been fully detailed. Additional measured data, research, experiments and investigations are considered necessary in order to obtain more knowledge in this area. The databases made available to this study from measurement campaigns in Malaysia provide excellent opportunities to examine the propagation characteristics in the tropical region.

We present in this chapter the analyses of measured attenuation or fading due rainfall over the twenty-month period (previously mentioned in Chapter 3). The statistical analyses that comprise seasonal variations, diurnal variations, and annual cumulative distribution are presented here. This chapter also includes the finer details available in propagation measurements beyond the common cumulative statistics in dimensioning the links for new K_u-band services

4.2 Seasonal Variation of Path Attenuation

The annual cumulative distribution of rain induced attenuation enables link margin for a service to be developed but it does not provide any insight into potential variations of service due to propagation effects that exist over smaller intervals of time. To develop a better system, more information is required about the likely impairments to be encountered on the satellite-Earth link. Hence, in such attempt, finer temporal detail is required of the propagation conditions to be encountered on the path, particularly at the seasonal and monthly level.

The concept of four seasons such as Spring, Summer, Autumn, and Winter has no meaning in a country with a wet tropical or equatorial climate such as Malaysia. In most locations in Malaysia, is more common to have what is considered as 'wet' and 'dry' season. The seasons experienced could however fluctuate in length, time of occurrence, and severity. The detailed analyses for the monthly rainfall intensity measurements and rain accumulation have been presented earlier in Chapter 3. It was observed from the result of calculated rain accumulation that the Bukit Jalil site experienced dry months sometimes around August or September.

We broke down the attenuation data from Malaysia into each individual month. Figures 4.1 and 4.2 show the cumulative distributions for measured beacon attenuation on a monthly basis. In each figure, we grouped together the monthly cumulative distributions for 12 consecutive months to represent one-year observation. From Figure 4.1, within the period of the first twelve months, the measured attenuation in March 1997 substantially exceeded all measurements observed in other months at all percentages of time.

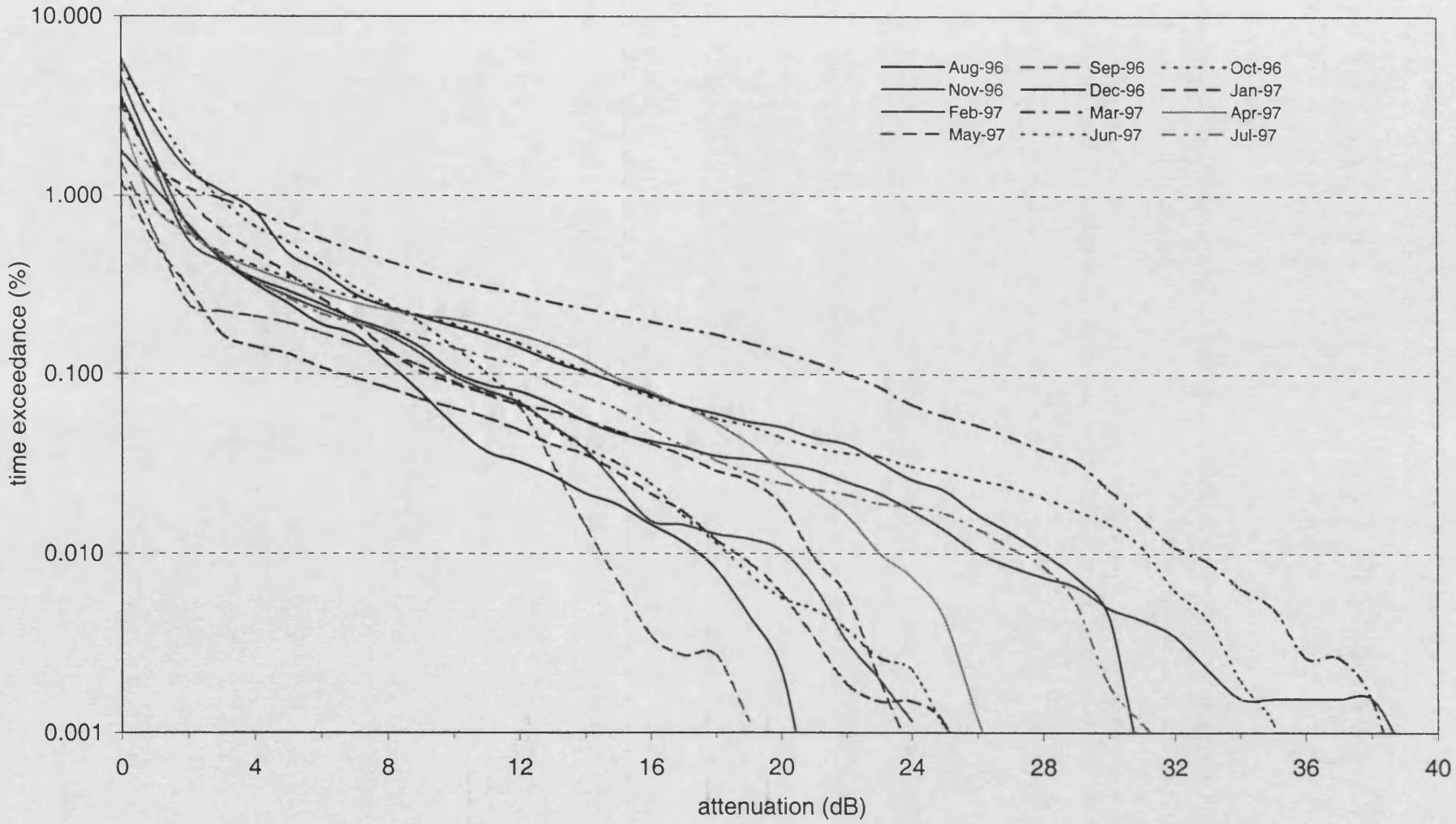

Figure 4.1: Monthly distribution of attenuation (08/96-07/97)

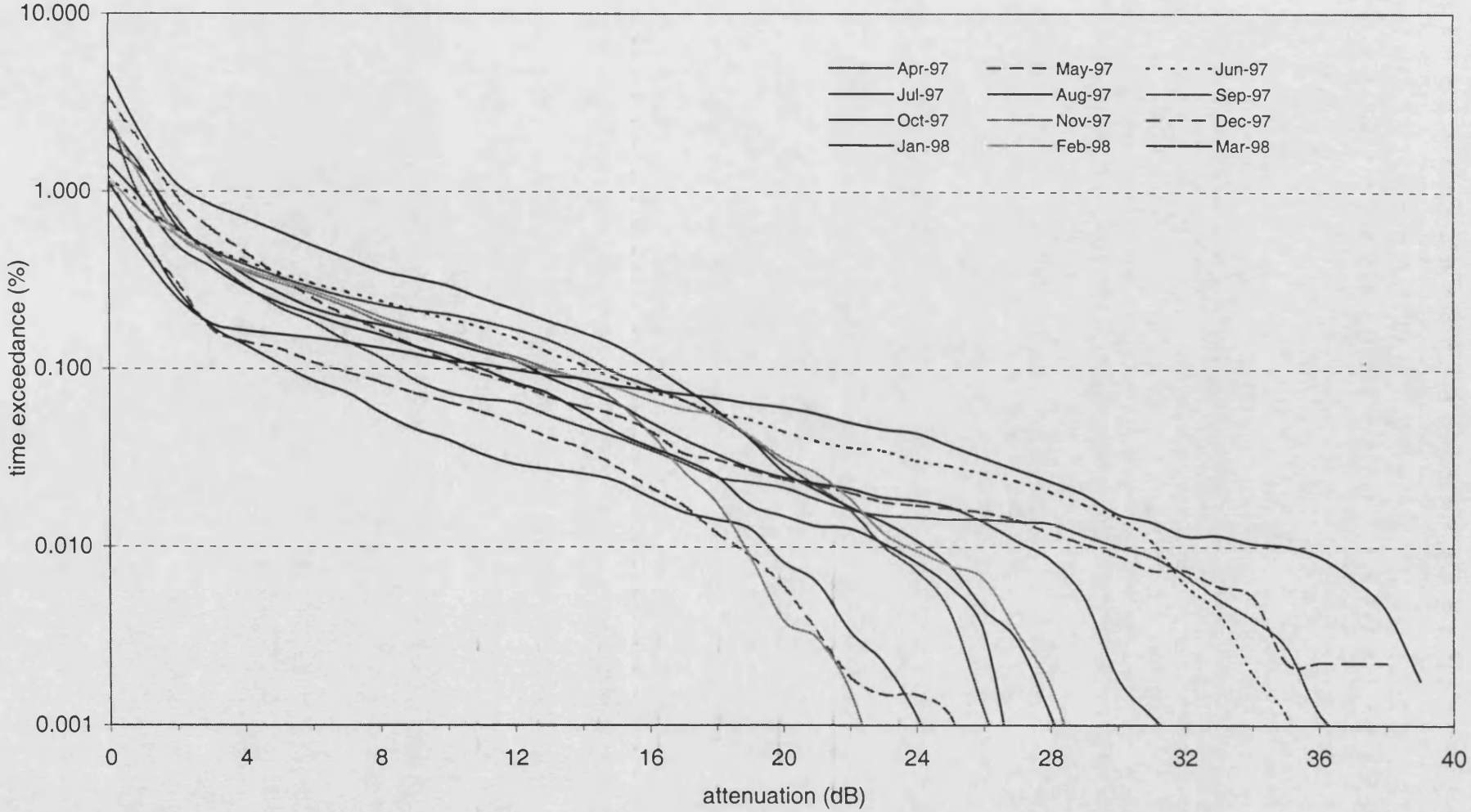

Figure 4.2: Monthly distribution of attenuation (04/97-03/98)

Similar rainfall intensity characteristics have been observed earlier for this particular year in Figure 3.4 and 3.5, and therefore demonstrate the principle that attenuation is subjected to the intensity of the rainfall. In Figure 4.2, there is no one specific month that dominates the time percentages.

A bar chart of rain fades at selected threshold of 5, 10, 20, 25 and 30 dB are exceeded monthly for each month from August 1996 to March 1998 is provided and labelled as Figure 4.3. We note from Figure 4.3 that attenuation level of 5 dB is rather constant and not really subjected to any strong monthly or seasonal variation (i.e. detected in every month). The 5 dB level is slightly higher only in March 97. From the figure, we can be observed that the most severe fading was detected in the month of March 1997.

Histogram of fading on a monthly basis for the twenty-month period from August 1996 to March 1998 is given in Figure 4.4. The number of fades equals or exceeding 10 dB level, detected at each month with duration equal or greater than 10 seconds are noted on top of each column. According to the measured data, the satellite-Earth link experiences a total of 356 fades from August 1996 until March 1998 at 10 dB threshold. It is recognised that the monsoon winds reverse in March/April and September/October each year during which periods there is increased convectivity activity causing the most extreme rainfalls. Nevertheless, it is noted that at Bukit Jalil site, significant rainfall and fading occur each month, with 10 dB fades between 5 and 39 times for every month of the year.

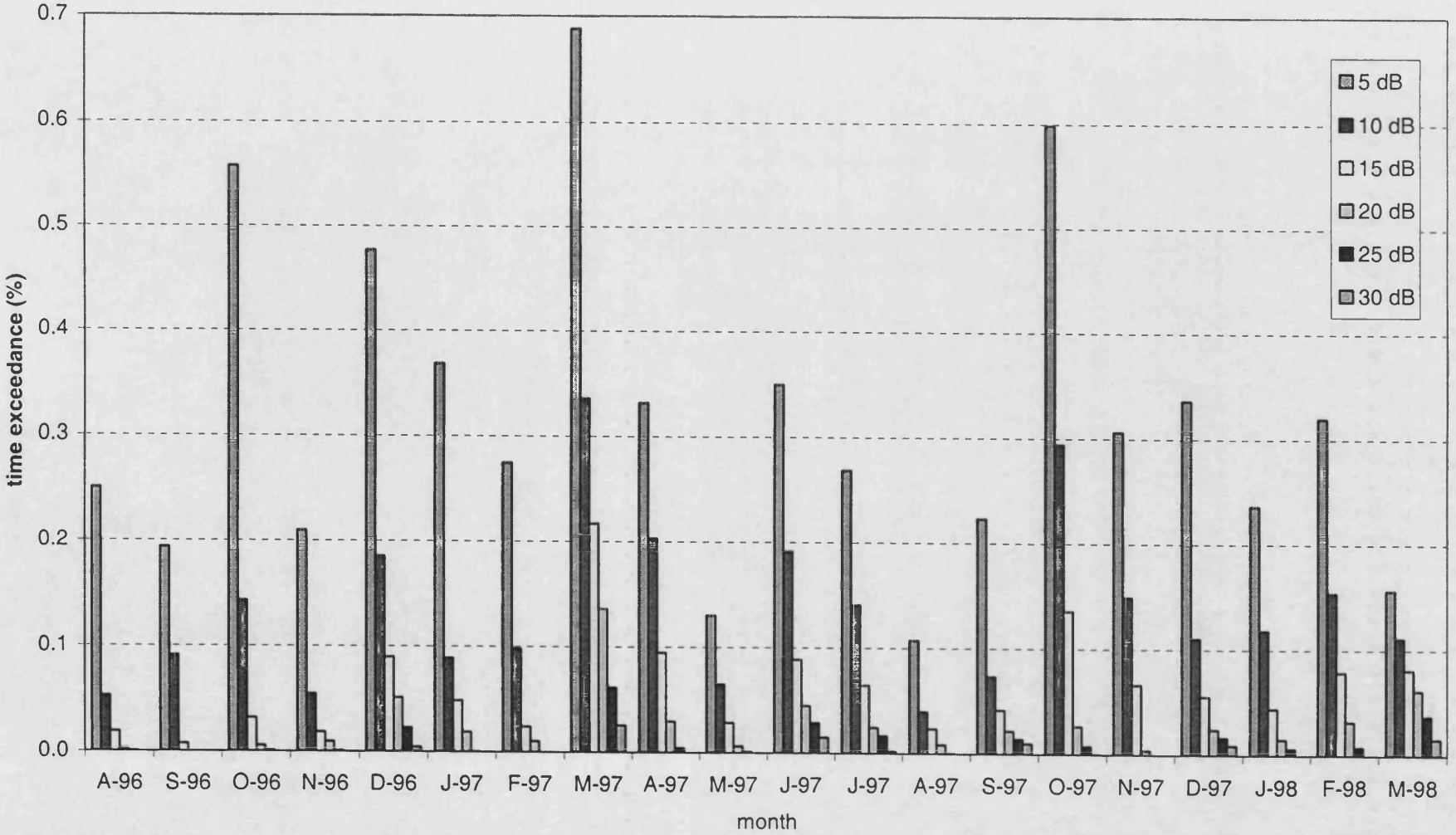

Figure 4.3: Histogram of specific threshold of attenuation is exceeded monthly

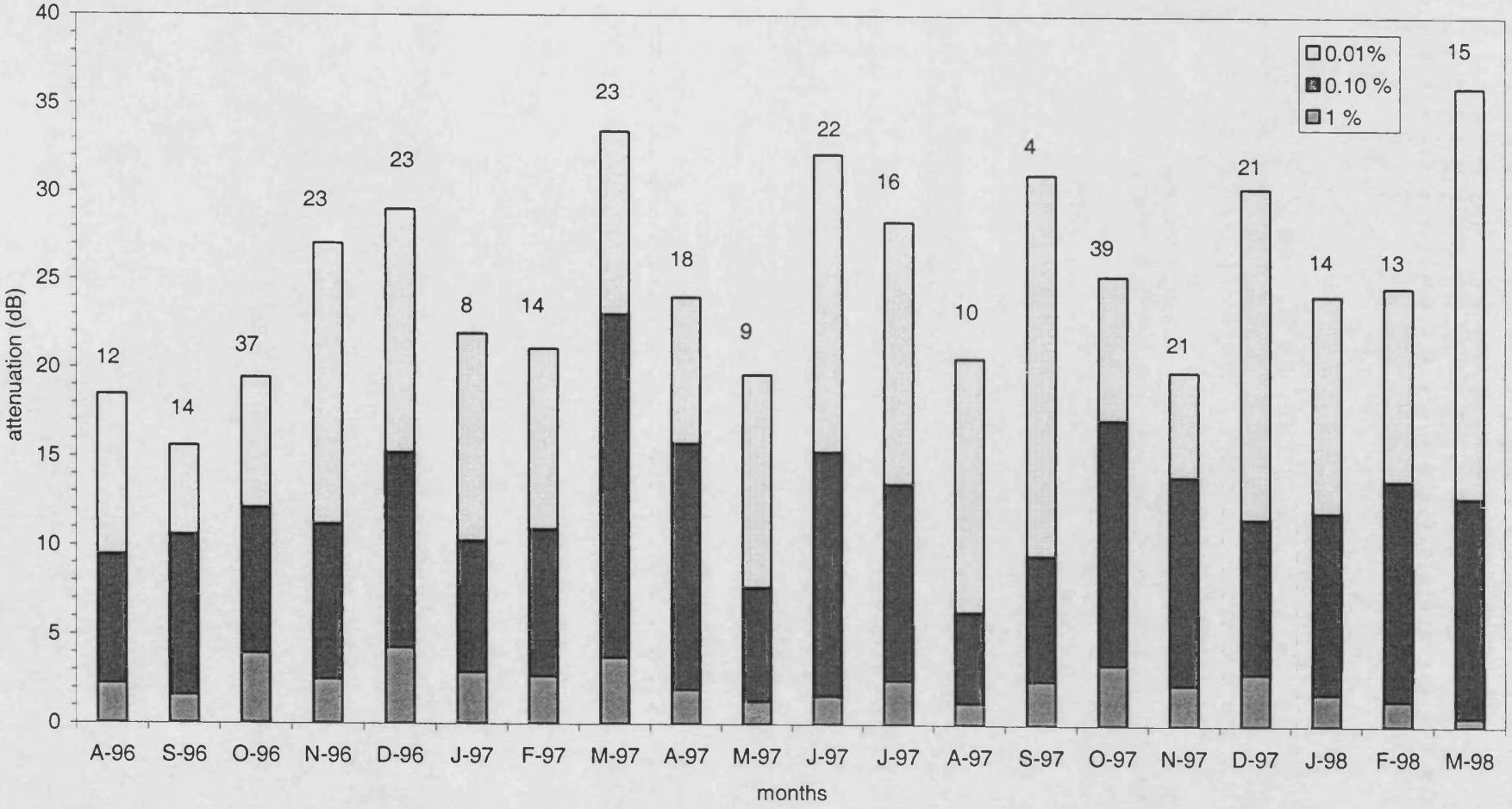

Figure 4.4: Histogram of attenuation is exceeded for 1%, 0.1% and 0.01 % of each month. The number of fades in excess of 10 dB and lasting 10 seconds or more is on the top.

4.3 Annual Cumulative Distributions of Path Attenuation

In designing communications links, cumulative distributions are the most effective presentation format for long-term data. For instance, link availability or exceedance at a point can be determined from its annual cumulative distribution. Thus, appropriate rain induced attenuation margins can be put into the system to acquire the desired link performance.

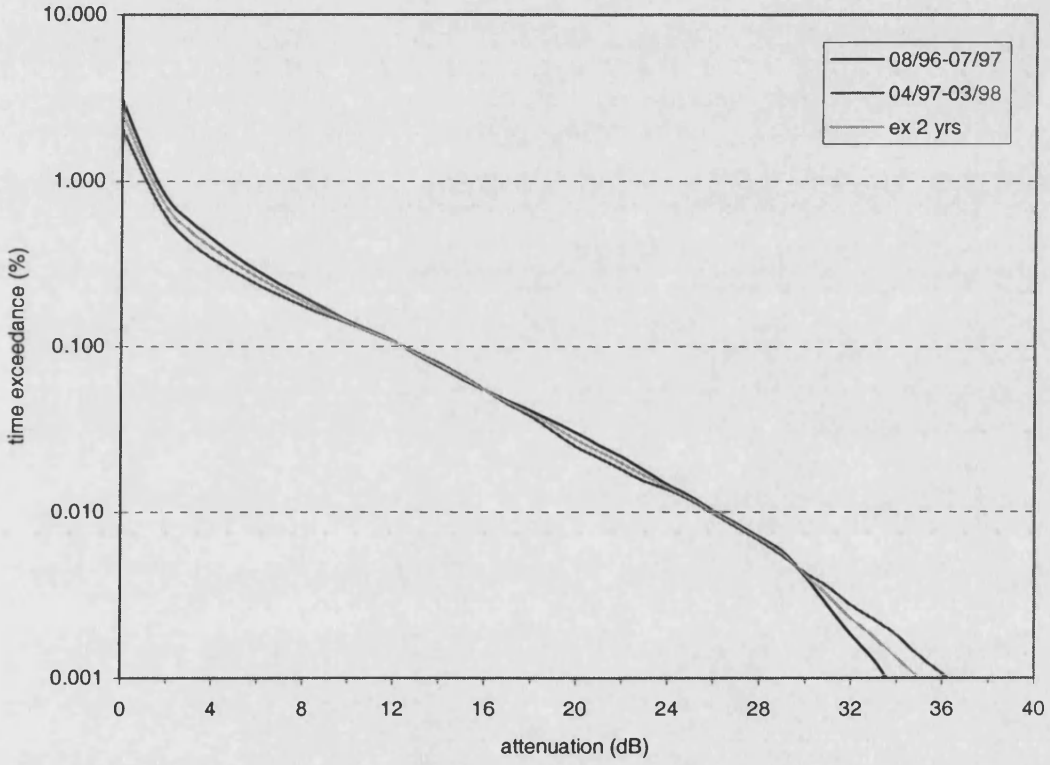

Figure 4.5: Annual cumulative distribution of beacon attenuation

The cumulative distribution of measured beacon attenuation during precipitation at MEASAT earth station for the first year and the extrapolated two years based the measurement data are obtained through research work. The annual cumulative distributions of attenuation due to rain measured at 11 GHz of the MEASAT I satellite beacon signal are presented in Figure 4.5 above. These cumulative distributions are very important since they provide information concerning the estimation of rain induced attenuation margins required for a given link reliability.

The distribution is expressed in percent and it is equivalent for a given link reliability expressed in hours or minutes From Figure 4.5 above, for 1 hour per year (08/96-07/97), 0.011% link outage, equivalent to 99.99% link availability, approximately 25 dB margin would have been required. A link with a 1-hour per year outage is considered a high quality link, similar to what specified for the national telephone system [Ippolito, 1986]. Similarly, margins of 16 dB and 11.5 dB would have been required for outages of 10 hours (0.114%) and 5 hours (0.057%) respectively.

Comparisons are also made between the annual cumulative distributions of attenuation due to rainfall obtained in Malaysia with other measured distributions in the tropics. Findings from several measurements that were carried out in equatorial countries such as Singapore, Indonesia, Brazil, and Papua New Guinea have been gathered through literature reviews. The frequency of interest in all experiments conducted is within the K_u-band frequencies.

The attenuations exceeded for 99.7%, 99.9% and 99.99% of the average year are reported in Table 4.1 and compared with data from the nearest stations in terms of climate and location. We note the remarkably low year-to-year variability of the annual cumulative distributions for the two years over the 0.1% to 0.01% exceedance range detected in Malaysia. We also note the similarity of the data reported from Singapore [Ong and Zhu, 1997; Lekla *et al.*, 1995] and Indonesia [de Maagt *et al.*, 1993] measured at distinct elevation angles and taken over a different measurement periods. The data measured in Papua New Guinea [Pan and Bryant, 1992; Pan and Allnutt, 2001] and in Belem, Brazil [de Miranda *et al.*, 1998], both in equatorial region, show considerably less fading than those for South-East Asia as listed in Table 4.1. With the variety of rain climates to be characterised, considerably more data are thus required for the development of satisfactory physically based models for prediction.

Site and reference	Elev (degree)	Period of Measurement	Instrument type	Attenuation exceeded for specific % times (dB)		
				0.3%	0.1%	0.01%
Malaysia Bukit Jalil	77.4	Aug 96- Mar 98 Weighted to 2 years	Beacon receiver	6.5	12.5	26.2
Singapore [Ong and Zhu, 1997]	42.9	Nov 92-Apr 94	Beacon receiver	6.2	13.4	32.0
Singapore [Lekla *et al.*, 1995]	39.4	Mar 92-Feb /93 Mar /92-Feb 93 Mar 92-Feb 93	Radiometer	5.7 6.5 6.5	Not avail.	Not avail.
Indonesia Surabaya [de Maagt *et al.*, 1993]	20	Apr 92 Jan 92	Radiometer	8.4 7.7	16.1 14.5	Not avail.
Papua New Guinea [Pan and Bryant, 1992]	72.8	Feb 91-Jan 92	Beacon	7.0	10.4	13.5
U site PNG [Pan and Allnutt, 2001]	72.8	Jun 94-May 95	Beacon	4.5	8.2	17.8
P site PNG [Pan and Bryant, 2001]	72.8	Jun 94-May 95	Beacon	Not avail.	6.0	16.4
Brazil, Belem [de Miranda *et al.*, 1998]	89	I year during 96/7	Beacon and radiometer	4.5	9.0	22.0

Table 4.1: Comparison of measured annual cumulative statistics of slant path attenuation measured in equatorial climate

4.4 Diurnal Variation of Path Attenuation

Investigations are also carried out to determine the diurnal variability of signal loss due to precipitation experienced at the Bukit Jalil Earth station. The following

presented results can be the basis for both the determination of satellite link availability and the development of fade countermeasures to reduce communication link outages.

The cumulative distributions of attenuation for specific hours of day at interval hours [00:00, 04:00], [00:04, 08:00], [08:00, 12:00], [12:00, 16:00], [16:00, 18:00], [18:00, 24:00] are presented in Figure 4.6 below. From inspections carried out for every 4-hour time interval, it can be observed that severe signal degradations are most likely to occur between 16:00 and 20:00. We can infer that this is due to the weather condition during the same period based on our previous analysis results in Chapter 3. From Figure 4.6, considerable less attenuation is measured during [04:00, 08:00] and [08:00, 12:00] where severe rain events are rare (indicated by low rainfall rates measured)

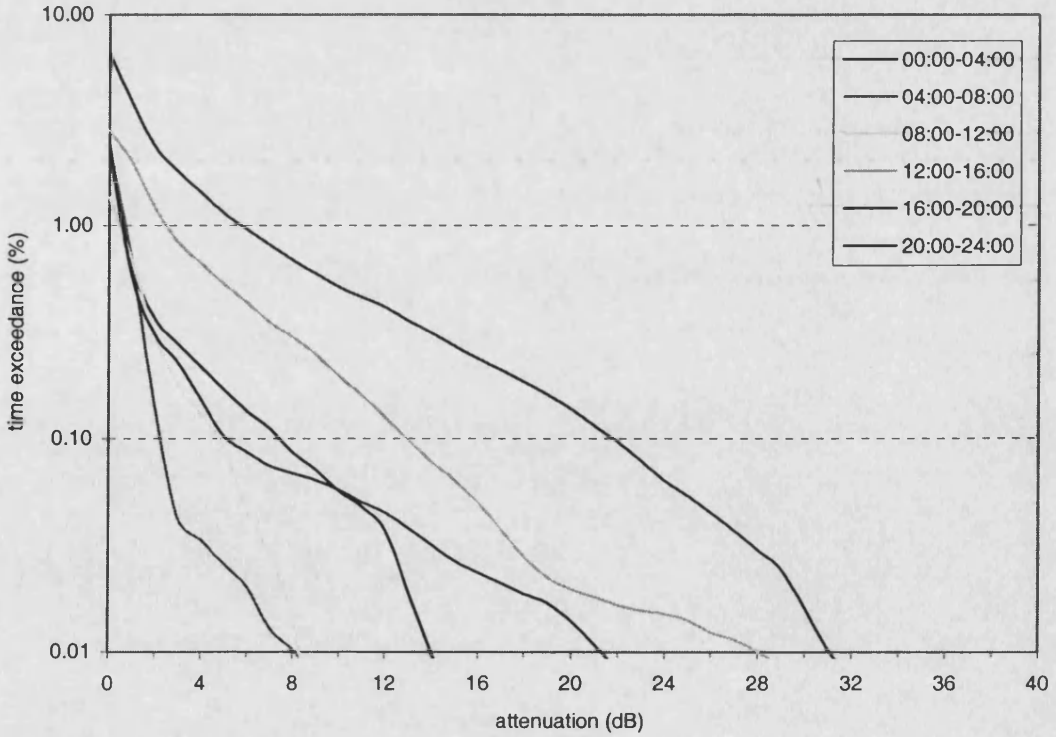

Figure 4.6: Diurnal variation of beacon attenuation

Outcomes from extended analyses demonstrate that attenuation in an equatorial country such as Malaysia is subjected not only to seasonal, but also to diurnal variations. The findings correspond to the investigation results carried out on rainfall rate distributions obtained from MEASAT databases that gave identical results. Significant diurnal variations for both components (attenuation and rainfall rate) have been observed. The diurnal variations of attenuation may have important influence on certain particular applications. For example, at point rainfall in climates where possibilities of severe signal degradations due to rainfall are higher at certain time of the day, the uplink power can be pre-programmed with additional margins to combat the uplink rain induced attenuation.

Comparisons were made between findings from Bukit Jalil site with previously reported experimental results in equatorial region to investigate any possible similarity or distinct pattern of rain fade diurnal characteristics. Investigators [De Maagt *et al.*, 1993b.] reported that based on measurement campaign data, a greater probability for excess attenuation is expected during the hours from 08:00 to 16:00 detected at Surabaya, Indonesia.

4.5 Probability of Exceeding Specific Attenuation

The depths of selected fades over the twenty months are presented in detail to highlight the severity of rain-induced attenuation encountered in tropical region. Investigation results are presented below by the probability of exceeding a specific threshold of attenuation level statistics. The outcomes that are presented through this type of statistics were derived from the cumulative distribution of attenuation. The results are more suitable for the presentation of diurnal effects than the cumulative distribution of attenuation because comparisons between specific attenuation levels at a specific time interval are easier to observe.

We presented in Figure 4.7 and 4.8 the probabilities that a specific attenuation level such as 5 dB, 10 dB, 15dB, 20 dB and 25 dB are exceeded. The respective probability was denoted in the process of revealing and determining the monthly or seasonal and detailed diurnal variations. The statistics for selected rain induced attenuation fades for twenty consecutive months are shown in Figure 4.7. This figure is the presentation of monthly variations.

From Figure 4.7, it can be observed that probabilities of getting denoted attenuation levels are higher in the month of March 1997 therefore confirming the existence of 'worst month' of attenuation. On the other hand, denoted attenuation levels can be observed with extremely low values in the month of September 1996, justifying the month as 'best' month'. This is the month with very limited rain induced attenuation where probability of getting attenuation level exceeding 20 and 25 dB are zero.

Figure 4.8 on the other hand is the histograms for the percentage time exceedance of specific attenuation of 5 dB, 19 dB, 15 dB, 20 dB and 25 dB for diurnal characteristics. Figure 4.9 below shows the corresponding probability of exceeding specific attenuation level with respect to diurnal variations for whole period of measurements.

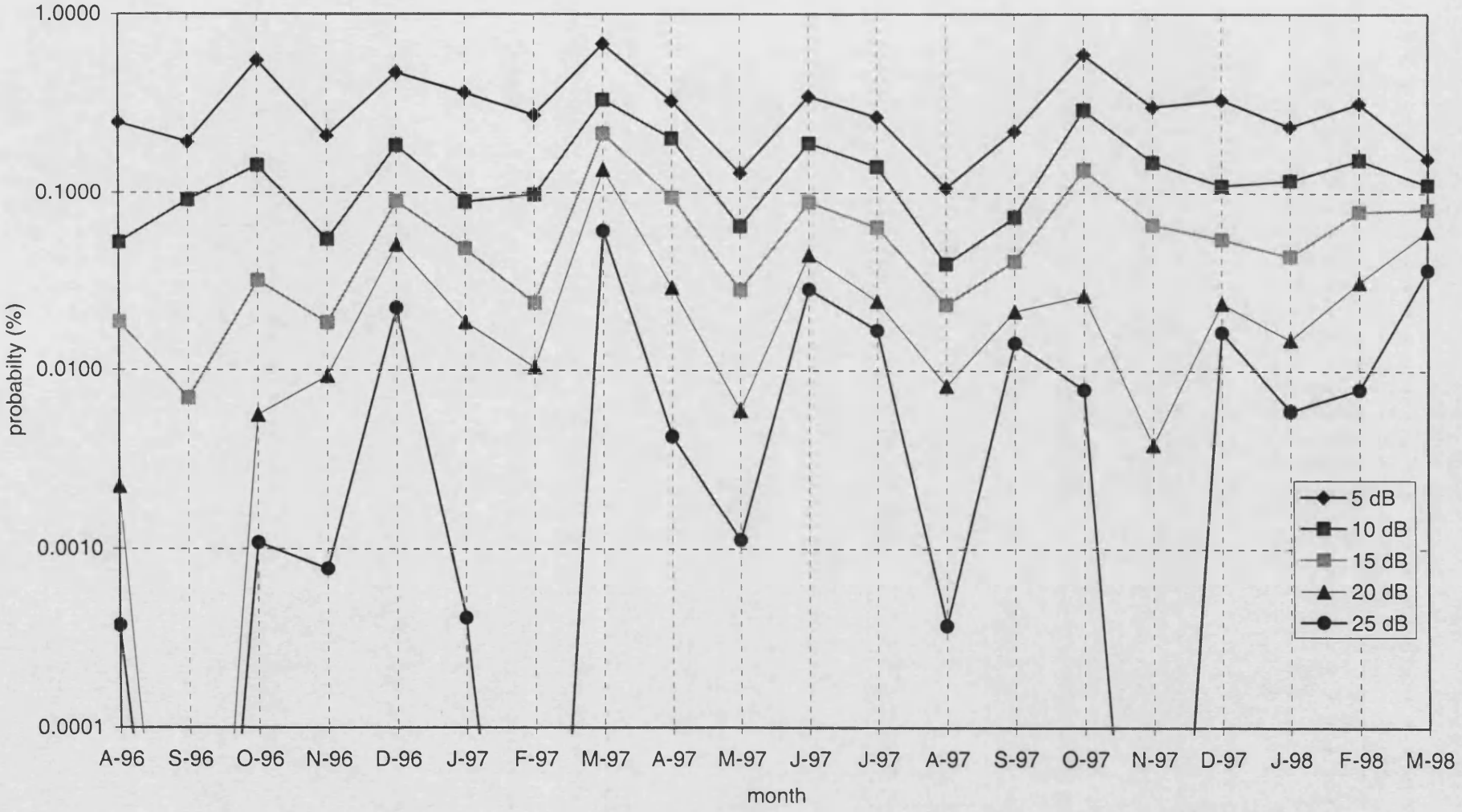

Figure 4.7: Probability of specific threshold of attenuation is exceeded

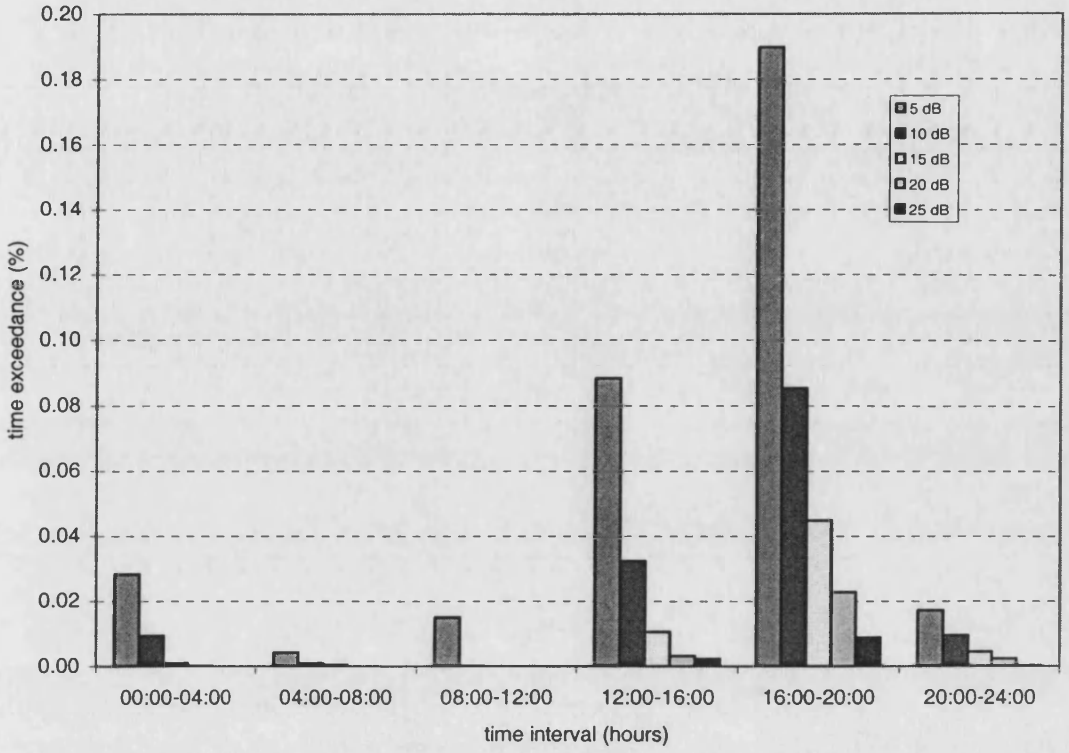

Figure 4.8: Histogram of specific threshold of attenuation is exceeded diurnally

As indicated in previous section, the resolution concerned is a 4-hour time interval such as there is 6 measured values for a day. From our data assessment, only probabilities of denoted attenuation levels of 5 and 10 dB are detected for time period [08:00-12:00]. Probability of getting specific threshold of attenuation 10 dB level detected is at value of extremely low. Probability of exceeding specific threshold of attenuation levels denoted perceived in general, depended on actual time of the day. It can be concluded that the probabilities are smallest during the first half of the day and largest in the second half. Probability of exceeding higher attenuation level reveals even stronger diurnal variations with large peaks in the late afternoon and early evening hours.

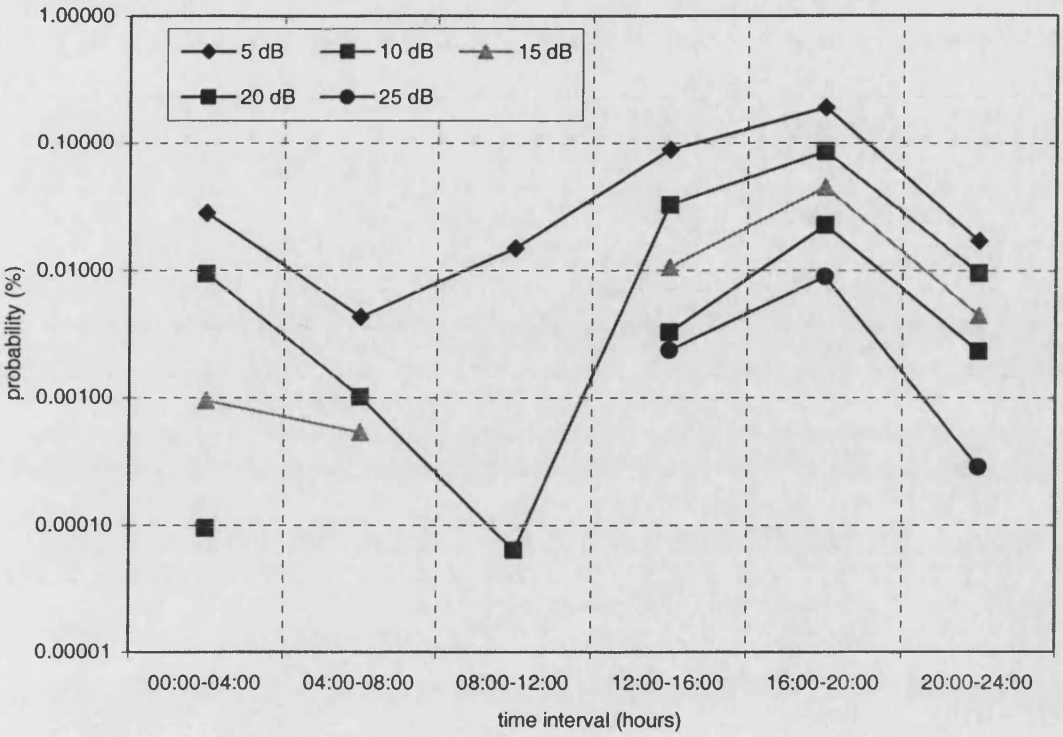

Figure 4.9: Probability of specific threshold of attenuation is exceeded

The specific attenuation level at 5 dB is not strongly subjected to diurnal variation as compared to other selected levels. In other words, it can be commonly accepted that rain induced attenuations lower than that of 5 dB are due to normal rainfalls (stratiform) as opposed to heavy rainfalls (convective). Heavy rainfalls are rainfalls that take place during thunderstorms. Note was also made where normal (stratiform) rainfall may be seen as being independent of the time of the day, where heavy rainfalls (thunderstorms) are most likely to occur in the evening hours. Furthermore, normal rainfall usually lasts considerably longer than heavy rainfall. Thus normal rainfall contributes much more to the probability of exceeding 5 dB than thunderstorm rainfall

4.6 Duration of Individual Fades

Strong rainfalls that typically occur during thunderstorms cause attenuation of more than 20 dB. In Malaysia, these incidents are quite rare in the morning but occur very

often in the afternoon and evening. This can be confirmed with Figure 4.8 and Figure 4.9 where such probability of exceeding 20 dB and 25 dB are low in the morning but high in the evening hours

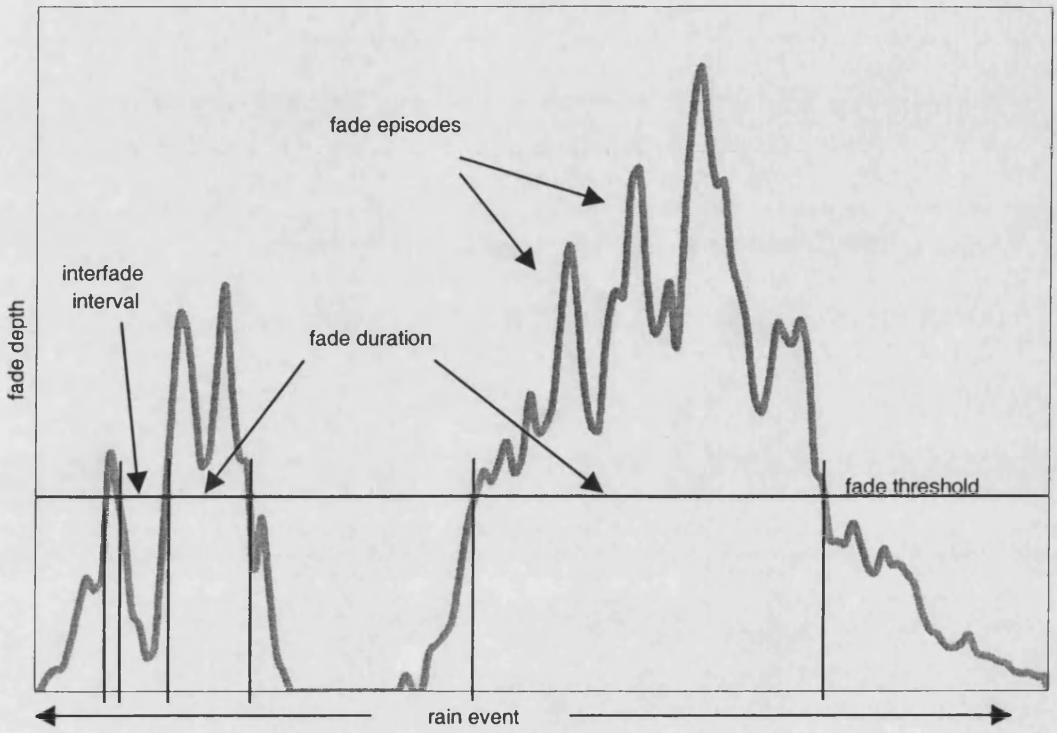

Figure 4.10: Features commonly used in characterising precipitation events

Figure 4.10 above Illustrates the features commonly used in characterising precipitation events. The statistics of fade duration for the period of campaign are shown in Figure 4.11 below for selected fade thresholds of 3, 5, 8, 10, 13, 15, 18, 20, 23, and 25 dB. The fade duration is measured for 10 seconds and above. From these statistics there could be 43 occasions within the twenty consecutive months when a 10 dB fade depth lasts for longer than 600 seconds (equivalent to 10 minutes). Such analyses of the fade duration for different fade thresholds observed at MEASAT Earth station is used to evaluate the effects of rain induced attenuation on the operational aspect of their various satellite services like the television broadcasting and telecommunication services.

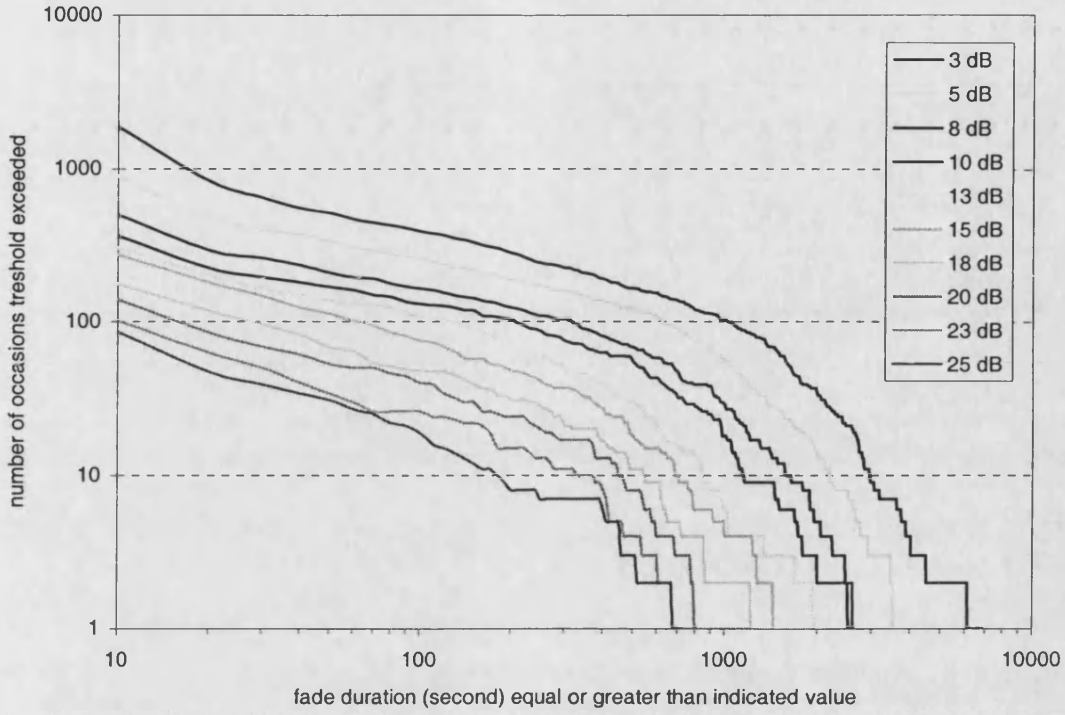

Figure 4.11: Statistics of fade duration of rain induced attenuation measured for 06/98-03/98

Attenuation and rainfall rate statistics or characteristics compiled are important findings that to be addressed in determining the effect of signal fading during rainfall events. This is especially true for the K_u-band satellite-earth link services in tropical region. The further analysis of the fade duration for various fade depths observed at MEASAT earth station can be used to study the effects of rain induced attenuation on operational aspect of various Earth-space satellite services like TV broadcasting, VSAT and other telecommunication services.

4.7 Daily Concentration of Events

Combining the knowledge of the fading duration, number of occasions when the threshold is exceeded and the time of occurrence, the daily diurnal distribution for any specific fade level can be produced. As an example, Figure 4.12 shows the daily distribution of attenuation events exceeding 10 dB in Bukit Jalil near Kuala Lumpur Malaysia.

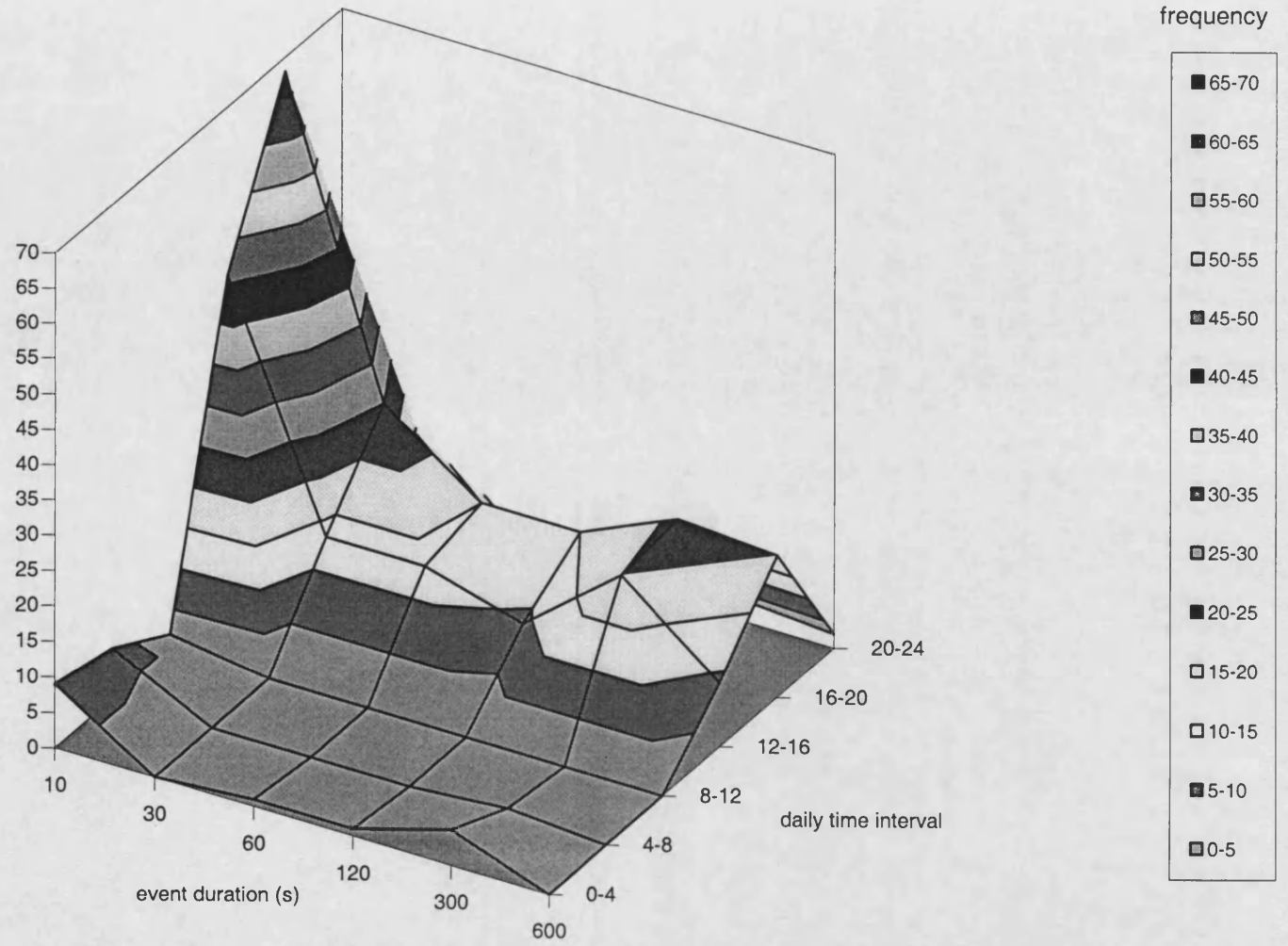

Figure 4.12: Illustration of diurnal concentration at 10-dB threshold based on 20 months data (number of events)

The events appear to be concentrated between late afternoon and early hour of the day at the earth station site with duration tending to be less than 1 minute. The late afternoon diurnal distribution between 16:00-20:00 hours in Bukit Jalil has two fade duration modes as evidence of long lasting heavy rainfall events occurring evenly during the year. We reproduce Figure 4.12 for easier observation and labelled it as Figure 4.13 below. This is a typical characteristic of equatorial climate as observed from similar results procured at another location in Brazil [de Miranda *et al.*, 2000]. It is of particular interest to acquire detailed information concerning the conditions during which the satellite-Earth links are most impaired for the development of the fade countermeasures.

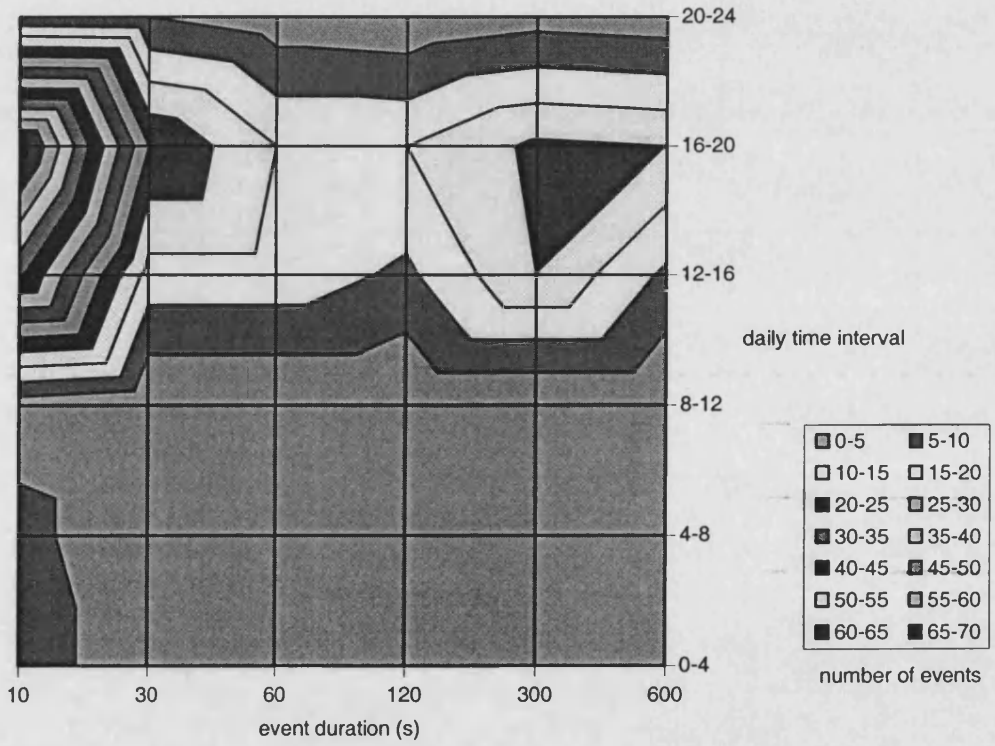

Figure 4.13 Illustration of diurnal concentration at 10-dB threshold based on 20 months data in 2-D (number of events)

4.8 Average fade Duration and Inter-fade interval

The corresponding average fade duration and the inter-fade interval as the function of fade depth on a tropical satellite-earth link are given in Figure 4.14. From the analyses

of the twenty months data, the average fade duration is found to be almost independent of the fade depth. We obtain the average values by dividing total measured time with number of fades equal or exceeding each fade level (with duration equal to or exceeding 10 seconds).

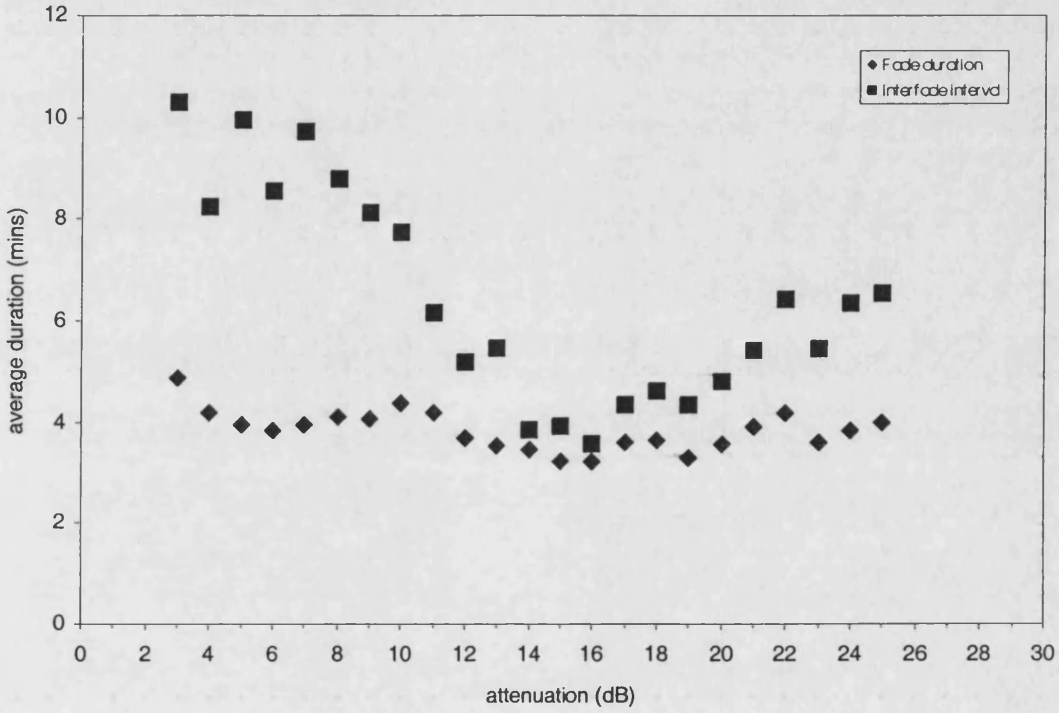

Figure 4.14: Average fade duration and inter-fade interval for K_u-band link

Similar findings have also been reported in several Australian locations [Flavin, 1992]. The frequency of fading increases with the decrease of fade threshold as can be observed in Figure 4.14 above without any noticeable relationship between these two parameters. It is suggested that the average fade duration is independent from the fade value because the larger time percentage for which lower fade threshold is exceeded is distributed among a larger numbers of fades, whereas the lower time percentage at higher fade threshold is distributed among fewer numbers of fades.

Average fade duration of approximately 4 minutes for most fade threshold can be observed in the figure above. Usually, the spread of fade duration around the average

value is expected to increases with the decrease of fade threshold because of the region is subjected to extreme and severe widespread events. But actually the results at the lower fade threshold is very much dependent to the integration time applied, since the events are influenced by scintillation spikes. A shorter integration time will definitely detect a higher number of occurrences of specific fade threshold compared to a longer one. The variation of inter-fade interval with fade depth (using blue markers) is also included in Figure 4.14. It can be observed that the inter-fade interval lies between 8 and 3 minutes above the 10 dB fade threshold.

4.9 Conclusions

It is worthwhile noting that rain induced attenuation is strongly dependent on the operating frequency. Attenuation due to rain at 4 GHz is minimal even for very heavy rainfall but at 11 GHz it can be significant. Experimental findings obtained by the use of ESA's OLYMPUS satellite signals at 12.5, 20 and 30 GHz [Ruckus, 1993] confirm that fade levels are dependent on frequencies. In the tropics, high rainfall intensity and the consequent high rain induced attenuation is the greatest constraint to the usability of the K_u-band and above. The characteristics of the path attenuation in a particular region must be investigated in the design of communication links through the region in order to meet the system's operational reliability. It is has been shown in this chapter that the cumulative distributions of path attenuation due to rain vary greatly from region to region.

This chapter presented detail findings for seasonal and diurnal variations analyses based on measurements in Kuala Lumpur, Malaysia. By comparing cumulative distribution curves and histograms, it can be concluded that attenuation is most likely to be experienced in the interval [16:00-20:00] of a day and least likely to be endured in the interval [08:00,12:00]. Inspection upon attenuation measurements did show diurnal variation and the variations are very much dependent on the attenuation level considered. The probabilities of attenuation exceeding 10, 15, 20, and 25 dB levels

depend on the time of the day. Probabilities are at highest value in the interval [16:00-20:00] (late afternoon and early evening), which perhaps due to heavy thunderstorm and severe downpours that usually occur.

Most of the attenuation studies on earth-satellite paths have been conducted in the temperate region of the world. The increasing use of satellites for telecommunications and broadcasting services have necessitated more than before the need for earth-space attenuation research in the tropics. Some new data, which inspect the finer detail of rain induced attenuation seasonal and diurnal distributions, have been presented in this chapter. It is important that data such as these should be used in determining the likely user acceptance of the new Digital to Home (DTH) and the Very Small Aperture Terminals (VSAT) services. Developing an appreciation for the variations in service quality over monthly and seasonal periods may also allow the service provider to modify the dimensioning of the link with the month and/or season. This might be particularly worthwhile if the service provider is offering service to more than one country, or over a very large continent. Varying the distribution of transmitted power in the spacecraft antenna to take account of seasonal variability would confer substantial competitive lead to the service providers.

Chapter 5

Prediction of Rain Fading and Possible Countermeasure on Tropical Satellite-Earth Link

5.1 Introduction

The K_u-band satellite links have been widely used for communications in countries with temperate climates since margins can be built into link budget to cope with fading in those climates. Initially, contributions on rain induced attenuation measurements in the tropics are very limited and prediction models of rain induced attenuation in satellite links have to depend almost entirely on measurements in temperate climates. Even until recently, still very few experimental results are made available on earth-space communication links in tropical-equatorial region. Sufficient measurements are required to understand the complete propagation mechanisms in this region.

Rain induced attenuation is given as probabilistic value because of the statistical variation in rainfall rates. This is often expressed as attenuation or signal loss exceeded for certain percentage of time such as perhaps 0.1% of the year. Rainfall is a serious cause of attenuation for radiowave propagation at frequency bands above 10 GHz. It is important to accurately predict the fading outage due to rain. A reliable prediction of attenuation by rain is necessary for a system designer to realistically determine link availability, establish the link margin and provide means to combat rain effects [Tri, 1990].

5.2 Predictions of Rain Induced Attenuation

Methods have been proposed for predicting rain induced attenuation statistics. Among currently available prediction models are the models recommended by the radiocommunications sector of the ITU [ITU-R P.618-4/5/6, 1995/1996/1999], the Dissanayake, Allnut and Haidara (DAH) rain induced attenuation model [Dissanayake *et al.* 1997], the Crane-Global model [Crane, 1980], the Crane-Two Component model [Crane and Shieh, 1989], the Garcia-Lopez model [Lopez *et al.*, 1988] and Moupfouma model [Moupfouma, 1987]

The ITU and the DAH attenuation models are similar in design. They differ in the complexity of the model used in the regression analysis. They both represent different ways to summarise the data in the ITU-R data bank and use those data to predict cumulative distribution for different location and path parameters. Both models basically generate attenuation prediction at a 0.01% probability level then extrapolate that prediction to other probability levels. The Cranes models are quite different from the first two models mentioned earlier. Both models appear to be dependent on the model of an entire rainfall rate distribution and not just expected rainfall rate at 0.01% of a year. They also appear to be dependent on different models for spatial structure of rain.

In this thesis, comparisons are made between the measured cumulative distributions with the predicted cumulative distributions of the three ITU-R models. The latest published ITU-R method to predict attenuation due to precipitation along a slant propagation path identified as Recommendation ITU-R P.618-6 - '*Propagation Data And Prediction Methods Required For The Design Of Earth-Space Telecommunication Systems*' is described in detail in this chapter. In our analyses, we also evaluated the prediction values calculated using two previously published recommendations, the ITU-R P618-5 and the ITU-R P618-4.

5.3 The Basis of ITU-R Prediction Methods

The procedure currently adopted in all ITU-R prediction models is based on the estimation of the attenuation exceeded at 0.01% of the time, which is derived from the rainfall rate exceeded at the same time exceedance percentage. From a theoretical point of view, the concept of equiprobable analysis is not consistent with meteorological information and not entirely satisfying. Nevertheless, the accuracy obtained in most cases with the prediction method is consistent with the quality and variability of available rain intensity data.

For a given value of rainfall rate at 0.01 time exceedance percentage $R_{0.01}$, the specific attenuation γ_R is calculated. When multiplied with the effective path length L_E, the corresponding attenuation value at 0.01% time exceedance $A_{0.01}$ is produced. Hence, calculation of attenuation can be expressed as:

$$A_{0.01} = \gamma_R \cdot L_E \tag{5.1}$$

where the effective path length L_E is the product of slant path lengths, horizontal path reduction factor $r_{0.01}$ and vertical path reduction factor $\upsilon_{0.01}$. The empirical expression as can be observed in Equation 5.1 can be used for scaling the other time percentage, in order to provide a complete rain induced attenuation distribution. The schematic presentation of an Earth-space path giving the parameters to be input in to the attenuation prediction process is given in Figure 5.1 [Radiocommunication Bureau, 1996] below.

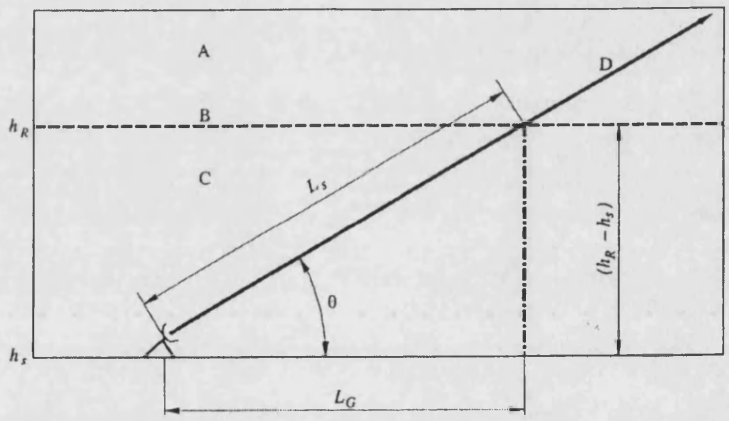

Figure 5.1: Schematic presentation. A: frozen precipitation, B: rain height, C: liquid precipitation, D: Earth-space path, L_G: horizontal projection, L_S: slant-path length, h_r: rain height, h_s: station height, θ: elevation angle

The set expression for the estimation of $A_{0.01}$ is based on two assumptions. With reference to the above figure, the first assumption is that the spatial structure of rain can be modelled by equivalent rain cell; with a rectangular cross-section of equivalent length L_G and effective height h_R-h_S in the plane of the path. The second assumption is that the equivalent rain cell can assume any position with respect to the path with equal probability.

5.3.1 Effective Rain Height

Techniques have been proposed by investigators in order to consider the vertical structure of rain into account. The technique is an extension of those developed for

terrestrial paths [Brussaard, 1981]. Whereas some have been derived based on extensive studies on the rain structure [Leitao and Watson, 1986; Li *et al.*, 1986]. In the current version of the prediction method in Recommendation ITU-R P.618-6, the vertical structure of rain is taken into account by the use of an effective rain height h_R, derived from experimental data, in the expression of L_S. For vertical paths, the effective path length coincides with the effective rain height, which at any latitude may differ from the 0° C isotherm height h_{FR}, as specified in their recommendation, '*Rain Height Model For Prediction Methods*' [ITU-R P.839-2, 1997]. The RAL, U.K. has carried out studies at specific locations such as PNG and Singapore with radar equipment to determine accurately the effective rain height in the tropics [Ladd *et al.*, 1997; Ong *et al.*, 2000].

5.3.2 Specific Attenuation

Researchers [Olsen *et al.*, 1978] have reported that the relationship between specific attenuation '*A*' or 'γ_R' and rainfall rate *R* as given in Equation 5.1 can be approximated by using power-law. As mentioned earlier in Chapter 2, based on assumption of spherical drops, values of *k* and α have been calculated at various frequencies between 1 and 1000 GHz for several drop temperatures and drop size distributions. Values of *k* and α coefficients based on the Laws and Parson drop size distribution and a drop temperature of 20°C have also been calculated. The curves of specific attenuation can be observed in Figure 2.7. The calculations were computed by assuming oblate spheroidal drops, aligned with a vertical symmetry axis and with dimensions related to equal volume spherical drops. Values for horizontal and vertical polarisation of *k* and α at various frequencies can be obtain from Table 1 of Recommendation ITU-R P.838.

Values of *k* and α at frequencies other than those in the table can be estimated by interpolation using logarithmic scale for frequency *f*, a logarithmic scale for *k*, and a linear scale for α. For linear and circular polarisation, and for all path geometries, the *k* and α coefficients for the specific attenuation equation can be calculated from using the following equations:

$$k = \left[k_H + k_V + (k_H k_V)\cos^2\theta\cos 2\tau\right] / 2 \tag{5.2}$$

$$\alpha = \left[k_H\alpha_H + k_V\alpha_V + (k_H\alpha_H k_V\alpha_V)\cos^2\theta\cos 2\tau\right] / 2k \tag{5.3}$$

where θ is the path elevation angle and τ is the polarisation tilt angle relative to the horizontal (τ = 45° for circular polarisation).

However, there are measurements [Manabe *et al.*, 1987], that suggest at about and above 40 GHz, the values of k in Table 1 of the ITU-R P.838 may be underestimated, and the values of α are overestimated. This result may indicate or perhaps confirm that the Laws and Parson drop size distribution is not appropriate at frequencies above 40 GHz. A new theoretical formulation [Moupfouma, 1997] was proposed for calculating the specific attenuation due to precipitation particles. In his proposal, the values of frequency-dependent coefficients k and α are no longer necessary to be utilised. This is because, in the formulation, the frequency is already one of the parameters to be used.

5.4 Calculation and Comparison for Predicted Rain Induced Attenuation Statistics

For the satellite-Earth link at Bukit Jalil, Kuala Lumpur, Malaysia predicted values of rain-induced attenuation using ITU-R P.618-6 was obtained through the following procedure.

Earth station and satellite information:

Earth station (All Asia Broadcast Centre):

longitude (degree), l_{es} : 101.42° E

latitude (degrees), φ : 3.08° N

height above mean sea level of the earth station (km), h_S : 0.05

Satellite: (MEASAT I):

longitude (degree), l_{st} : 91.5° E

frequency (GHz), f: 10.98

polarisation: vertical

Rain data: $R_{0.01}$ = 164 mm hr^{-1} (point rainfall rate for Bukit Jalil for 0.01% of the year)

This value is the rainfall rate exceeded during 0.01% of one-year at integration time 1 minute obtained from measurements at Bukit Jalil as shown in previous chapter, Figure 3.11. For comparison purposes, the rainfall rates time exceedance of 0.01%

from the new climatic zone map recommendation ITU-R P.837-2 that equals to 114 mm hr^{-1} was also used in determining ITU-R predicted attenuation values.

Step 1: Calculation of the elevation angle θ, for the earth-space link.

$$\theta = \tan^{-1}\left[\frac{\cos\phi - \frac{R_E}{R_E + R_O}}{\sqrt{1-\cos^2\phi}}\right] = 77.4°$$

where:

$$\phi = \cos^{-1}\left(\cos\varphi\cos|l_{st} - l_{es}|\right) = 0.9836$$

R_E = radius of earth (km) = 6378

R_O = altitude of the satellite (km) = 35, 786

Step 2: Calculation of the polarisation angle τ:

$$\tau = \tan^{-1}\left[\frac{\sin|l_{st} - l_{es}|}{\tan\varphi}\right] = 72.7°$$

Step 3: The effective rain height, h_R, for the latitude of the station φ was determined to be according to ITU-R P.839-2:

h_R = 5 km

since 0° ≤ φ ≤ 23° Northern hemisphere

Step 4: For θ ≥ 5° computation of the slant-path length, L_S, below the rain height is as follows:

$$L_s = \frac{(h_R - h_S)}{\sin\theta} = 5.072 \text{ km}$$

Step 5: Calculation of the horizontal projection, L_G, of the slant-path length from:

$$L_G = L_S\cos\theta = 1.106 \text{ km}$$

Step 6: The rain intensity, $R_{0.01}$, exceeded for 0.01% of an average year is 164 mm hr^{-1} at integration time 1 minute

Step 7: Determination of the k and α values using the frequency-dependent coefficients, k_H, k_V, α_H, and α_V from Table 1 of the ITU-R P.838. Since values of k_H, k_V,

α_H, and α_V are at frequency f other than those in the table. New values of k_H and k_V were calculated through interpolation of logarithmic scale f and logarithmic scale *k*.

$$k_H = 10\text{^}\left[\left(\frac{\log_{10} k_{H1} - \log_{10} k_{H2}}{\log_{10} f_1 - \log_{10} f_2} * \log_{10} f_1 - \log_{10} f_2\right) + \log_{10} k_{H2}\right] = 0.0138982$$

$$k_H = 10\text{^}\left[\left(\frac{\log_{10} k_{V1} - \log_{10} k_{V2}}{\log_{10} f_1 - \log_{10} f_2} * \log_{10} f_1 - \log_{10} f_2\right) + \log_{10} k_{V2}\right] = 0.0123151$$

Meanwhile new values of α_H, and α_V were obtained through interpolation of logarithmic scale f and linear scale α

$$\alpha_H = \left(\frac{\alpha_{H1} - \alpha_{H2}}{\log_{10} f_1 - \log_{10} f_2} * \log_{10} f_1 - \log_{10} f_2\right) + \alpha_{H2}$$
$$= 1.24569$$

$$\alpha_V = \left(\frac{\alpha_{V1} - \alpha_{V2}}{\log_{10} f_1 - \log_{10} f_2} * \log_{10} f_1 - \log_{10} f_2\right) + \alpha_{V2}$$
$$= 1.23112$$

where:

f_1 = 10 GHz; f_2 = 11 GHz

k_{H1} = 0.0101; k_{H2} = 0.0188

k_{V1} = 0.00887; k_{V2} = 0.0168

α_{H1} = 1.276; α_{H2} = 1.217

α_{V1} = 1.264; α_{V2} = 1.200

Therefore the calculation of the frequency-dependent coefficients *k* and α;

$$k = \left[k_H + k_V + (k_H k_V)\cos^2\theta\cos 2\tau\right] / 2 \quad = 0.0130758$$

$$\alpha = \left[k_H\alpha_H + k_V\alpha_V + (k_H\alpha_H k_V\alpha_V)\cos^2\theta\cos 2\tau\right] / 2k \quad = 1.2385593$$

Step 8: The specific attenuation, γ_R, using the frequency-dependent coefficients calculated above and the rainfall rate, $R_{0.01}$ was obtained by using:

$\gamma_R = k\,(R_{0.01})^{\alpha} = 7.2$ dB km^{-1}

Step 9: Calculate the horizontal reduction factor, $r_{0.01}$, for 0.01% of the time:

$$r_{0.01} = \frac{1}{1 + 0.78\sqrt{\frac{L_G \gamma_R}{f}} - 0.38\left(1 - e^{-2L_G}\right)} = 0.7532 \qquad (5.$$

Step 10: Calculate the vertical adjustment factor, $v_{0.01}$, for 0.01% of the time:

$$\zeta = \tan^{-1}\left(\frac{h'_R - h_s}{L_G\, r_{0.01}}\right) = 80.45°$$

For $\zeta > \theta$,

$$L_R = \frac{L_G\, r_{0.01}}{\cos\theta} = 3.821 \text{ km}$$

Since $|\varphi| < 36°$,

$$\chi = 36 - |\varphi| = 32.92°$$

$$v_{0.01} = \frac{1}{1 + \sqrt{\sin\theta}\left(31\left(1 - e^{-(\theta/(1+\chi))}\right)\frac{\sqrt{L_R \gamma_R}}{f^2} - 0.45\right)} = 0.5716$$

Step 11: The effective path length is:

$$L_E = L_R\, v_{0.01} = 2.19896 \text{ km}$$

Step 12: The predicted attenuation exceeded for 0.01% of an average year is obtained from:

$$A_{0.01} = \gamma_R L_E = 15.92 \text{ dB}$$

Step 13: The estimated attenuation to be exceeded for other percentages of an average year, in the range 0.001% to 5%, is determined from the attenuation to be exceeded for 0.01% for an average year:

since $p < 1\%$ and $|\varphi| < 36°$ and $\theta \geq 25°$:

$$\beta = -0.005(|\varphi| - 36) = 0.1646$$

Step 14: The estimated attenuation to be exceeded for other percentages of an average year, in the range 0.001% to 1%, is determined from the attenuation to be exceeded for 0.01% for an average year by using:

$$A_p = A_{0.01}\left(\frac{p}{0.01}\right)^{-(0.655 + 0.033\ln(p) - 0.045\ln(A_{0.01}) - \beta(1-p)\sin\theta)}$$

For calculation according to Recommendation ITU-R P.618-5 and ITU-R P.618-4, several changes are involved in the procedures where:

1) The effective rain height h_R, according to ITU-R P.618-4 for the latitude of the station φ was determined to be: h_R (ITU-R P.618-4) $= 3.0 + 0.028\varphi = 3.086$ since $0° \leq \varphi \leq 36°$

2) Determination of the equivalent length L_0: for measured $R_{0.01} > 100$ mm hr^{-1}, the value 100 mm hr^{-1} was used in place of $R_{0.01}$ $L_0 = 35 \exp(-0.015\, R_{0.01}) = 7.809$ km

3) Calculation of the reduction factor, $r_{0.01}$, for 0.01% of the time using $R_{0.01} = 100$ mm hr^{-1}: $r_{0.01} = \dfrac{1}{1 + L_G / L_0}$

4) The predicted attenuation exceeded for 0.01% of an average year is obtained from: $A_{0.01} = \gamma_R L_S r_{0.01}$ dB

Table 5.1 lists parameters calculated according to the each recommendation. A few selected predicted values obtained in terms of percentage time availability are presented in Table 5.2. Cumulative distributions of predicted values and measured value are plotted together in Figure 5.2 for comparison purposes. We reproduce the figure using the recommended rainfall rate value of 114 suggested by the Recommendation ITU-R P.837-2 to investigate the variations between the ITU-R prediction values without the use of local rain information. The plots can be observed in Figure 5.3 below

	ITU-R P.618-6	ITU-R P.618-5	ITU-R P.618-4
$R_{0.01}$ (mm hr^{-1})	164.0	164.0	164.0
h_S (km)	0.05	0.05	0.05
θ (°)	77.42	77.42	77.42
φ (°)	3.08	3.08	3.08
τ (°)	72.65	72.65	72.65
f (GHZ)	10.98	10.98	10.98
R_e (km)	8500	Not Applicable	Not Applicable
H_R (km)	5.000	5.000	3.086
L_S (km)	5.072	5.072	3.110
L_G (km)	1.106	1.106	0.677
α	1.239	1.239	1.239
k	0.013	0.013	0.013
γ_R (dB/km)	7.267	7.267	7.267
L_O (km)	Not Applicable	7.809	7.809
$r_{0.01}$ (mm hr^{-1})	0.7532	0.876	0.920
ξ (°)	80.45	Not Applicable	Not Applicable
L_R (km)	3.847	Not Applicable	Not Applicable
χ (°)	32.98	Not Applicable	Not Applicable
$v_{0.01}$ (mm hr^{-1})	0.5716	Not Applicable	Not Applicable
L_E (km)	2.1990	Not Applicable	Not Applicable
$A_{0.01}$ (dB)	15.92	32.29	20.49
β	0.1646	Not Applicable	Not Applicable

Table 5.1: Calculated parameters using ITU-R recommendations

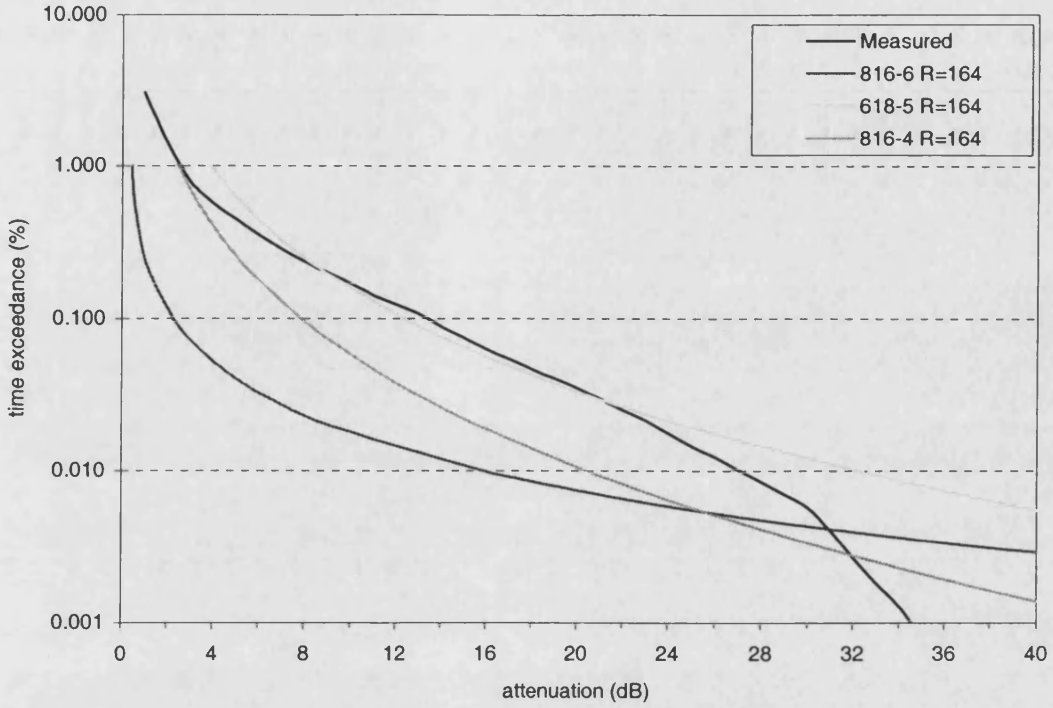

Figure 5.2: Plots of annual predicted statistics (using local rain) and measured attenuation statistic.

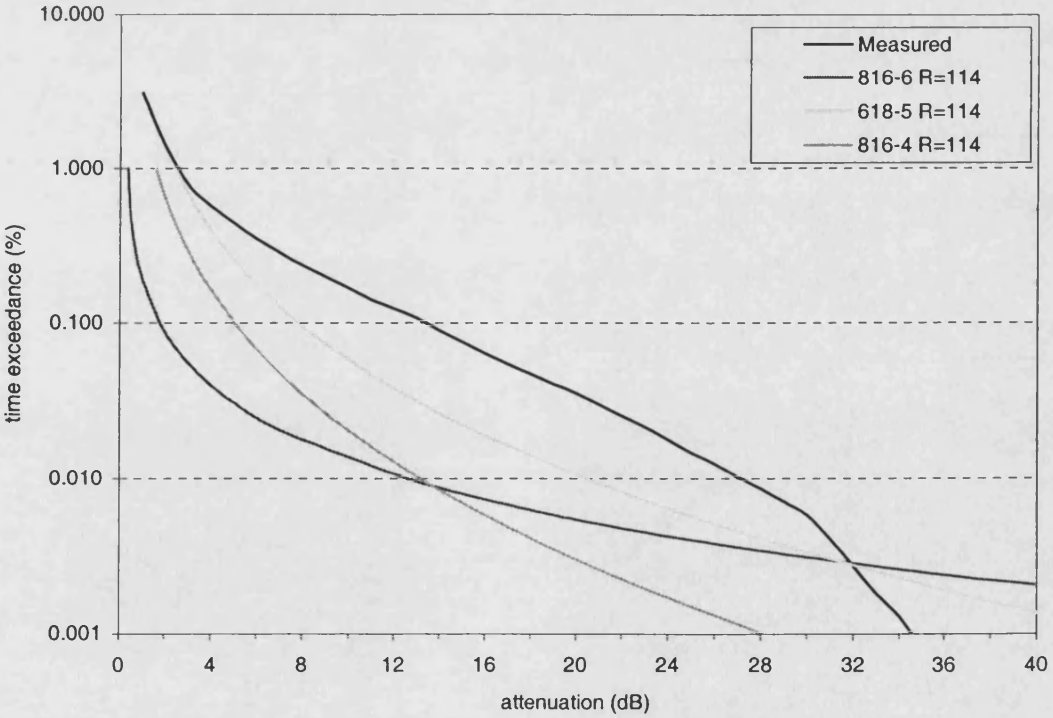

Figure 5.3: Plots of annual predicted statistics (with ITU-R rain) and measured attenuation statistic.

Availability (%)	Predicted Attenuation (dB)			
	ITU-R 618-6	ITU-R 618-5	ITU-R 618-4	Measured
99.90	2.26	12.4	8.0	12.5
99.91	2.48	13.1	8.3	13.0
99.92	2.75	13.8	8.8	13.6
99.93	3.10	14.6	9.3	14.2
99.94	3.55	15.7	10.0	15.5
99.95	4.16	16.9	10.8	16.7
99.96	5.05	18.7	11.9	18.1
99.97	6.47	21.1	13.5	20.2
99.98	9.09	24.8	15.9	22.5
99.99	15.92	32.3	20.5	26.3

Table 5.2: Comparison of annual predicted and measured values

Table 5.2 above lists measured and predicted attenuation values for MEASAT satellite-Earth link in Malaysia for comparison. For space-earth links in tropical country like Malaysia, the results of these analyses suggest that recommendation ITU-R 618-6 and ITU-R 618-4 do not give accurate prediction for rain-induced attenuation. The predicted values are even lower when using recommended rainfall rate at 0.01% time exceedance from the new world rain map [ITU-R P.837-2, 1999]. The recommendation ITU-R 618-5 seems to give good approximation values similar to those of measured with the use of local rainfall rate information for time exceedance greater than 0.01%. The Recommendation ITU-R 618-6 that was published in 1999 severely underestimates the measured signal attenuation for the time exceedance between 1% and 0.005%. At certain time exceedance percentage, the measured rain induced attenuation readings are almost double than predicted values by recommendation ITU-R 618-6. In this recommendation, new vertical correction factor was introduced. We suspect that the reduction factor proposed has been inappropriately applied to correct the overestimation at the low time exceedance percentages in the previous ITU-R 618-5 and 618-4 prediction models. Further analyses of vertical attenuation variability with height will be discussed later in chapter 7 of this thesis.

By comparing calculation procedures of each recommendation, we were able to identify the variation in the parameters for each recommendation. Recommendation ITU-R P 618-4 varies from ITU-R P 618-5 in term of the suggested effective rain height. It has been observed that the recommendations have proposed different formulations to estimate the rain height h_R. The investigation of rain height based on radar measurements will be discussed further in Chapter 7

5.5 Worst-month rain statistics for Tropical K_u-band fading

The study of the worst month statistics is very important to the designers of tele-communication systems. The ITU definition of 'worst' month now copes with that situation since accumulation of an outage in one month could have a worse effect on transmission links than if the accumulation were distributed throughout the year. In situations when system planning requires the attenuation value exceeded for a time percentage p_W of the worst month, there is a procedure in Recommendations ITU-R P.618-6 that can be used to estimate the attenuation exceeded for a specified percentage based on the average year probability p.

By comparing individual monthly distributions, the 'worst month' can be identified. According to ITU [ITU-R P.581-2, 1981], they recommend that the fraction of time during which a pre-selected threshold is exceeded in the worst month of a year is referred to as 'the annual worst-month time fraction of excess'. In other words, the probability distribution:

P_{wm} = Probability that s > s in the worst month period of the average year

is the ITU-R definition of 'average annual worst month', where s is the random variable in question such as rain intensity or attenuation and s is a chosen threshold for exceedance measure [Watson, 1997]. The introduction to the concept of 'worst month' statistics was led by condition where it has always recognised by ITU that the average

yearly exceedance of cumulative distribution may be inapt in illustrating the variability of attenuation from month to month, season to season or year to year. Hence, it is obviously worthwhile to take into account the occurrence of pronounced monthly or seasonality of a specific region.

We include here in this section the study of the worst-month rain induced attenuation statistics for tropical environment, a continuation from our monthly variability analyses discussed earlier in Chapter 4. In our study, the beacon attenuation measurements processed at 10 seconds integration time that were collected at MEAS'AT earth station are utilised to derive the annual worst-month statistics and its relationship with the average annual distribution. The relationship between the measured worst month and the yearly probabilities was investigated and we made comparison with the ITU-R model. From our analyses, new values for the parameters Q_1 and β are proposed based on measurements in Bukit Jalil, Malaysia.

The study is based on the recommendation of the ITU-R P581-2 where the definition for worst-month statistics applied to rain induced attenuation is established. The annual worst month for a pre-selected threshold is defined as the month with the highest probability of exceeding that threshold within the period of 12 consecutive months. A worst month can therefore be established for each threshold level. In our case, observed in Figure 4.1 in previous chapter, at probability exceeding 0.1 and 0.01 time percentage, the month of March 1997 is the worst month for the period from August 1996 to July 1997. The envelope of the highest monthly probability value of all the monthly cumulative distributions from that year can be obtained using the highest detected attenuation at each time exceedance percentages.

Worst month statistics are related to annual statistics by the parameter Q, which is the ratio between the worst-month and annual probability and is given by:

$$Q = \frac{p_w}{p} \tag{5.4}$$

where as defined earlier p_w is the average worst-month probability and p is the average annual probability. Studies of the relationship between worst-month and annual statistics have been conducted at various locations for different propagation effects and the Q_1 and β values are available in Table 1 of the ITU database [ITU-R P.841, 1992]. However no values for Q_1 and β have been quantified for rain effect slant path in the tropical region. It is suggested by ITU-R that the Q_1 and β could be approximated for $(Q_1/12)^{1/\beta} < p_w(\%) < Q_1 3^{(1-\beta)}$ by a power law relationship of the form of:

$$Q = Q_1 p^{-\beta} \tag{5.5}$$

Substituting the above equation into Equation 5.1, giving new expression:

$$p_w = Q_1 p^{(1-\beta)} \tag{5.6}$$

The ITU-R states that values of Q_1= 2.85 and β = 0. 13 can be used for global planning purposes. For tropical region, the only values Q_1 and β available are from Indonesia that is determined from terrestrial microwave rain effect experiment. From the measured data, the rain induced attenuation cumulative distributions for the average year and the worst month envelope were obtained and plotted in Figure 5.4. In the same figure we include the ITU-R predicted average worst month for comparison. The ratio of exceedances between the average year and the average worst month, Q can be procured using the values taken from measurement data. The Q values vary from 2 to 5.5 over the 6 to 20 dB attenuation range as can be observed in Figure 5.5.

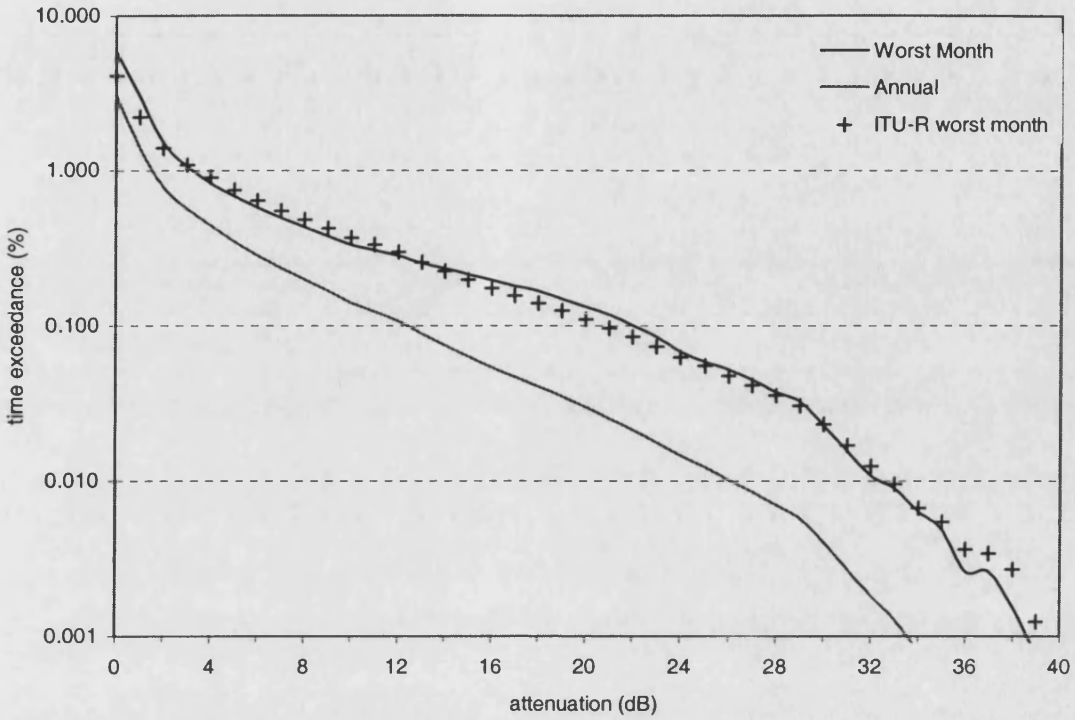

Figure 5.4: Plots of annual and worst month attenuation cumulative distributions

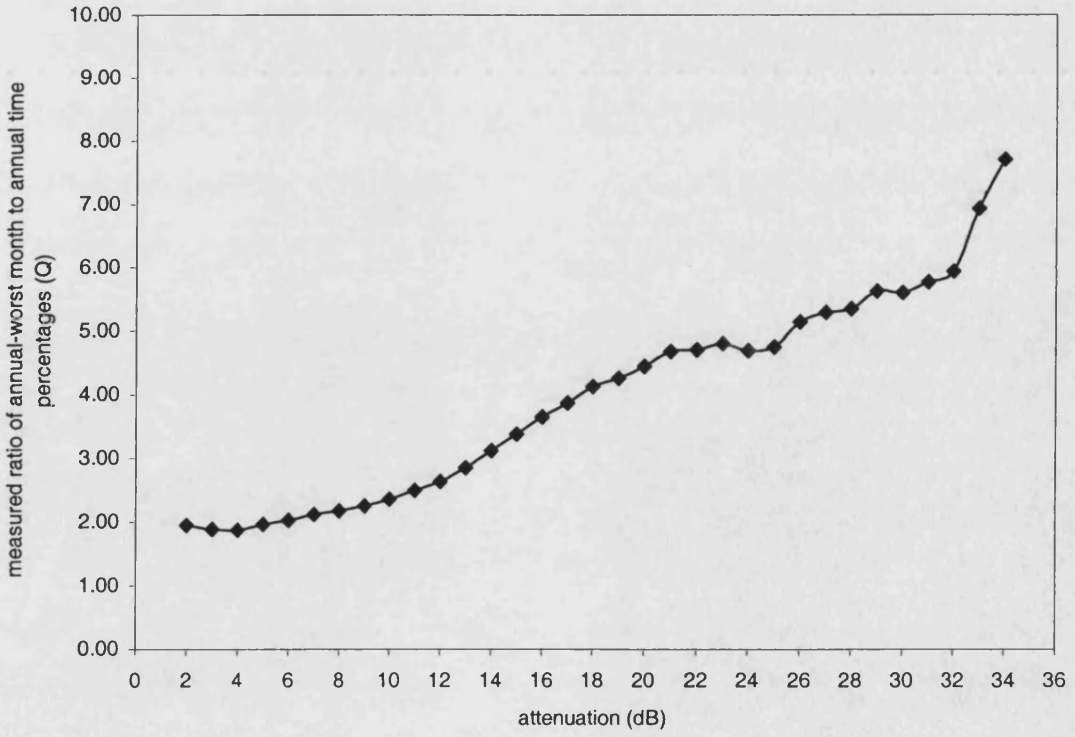

Figure 5.5: Ratio of exceedances between average year and average worst month (Q) as a function of attenuation

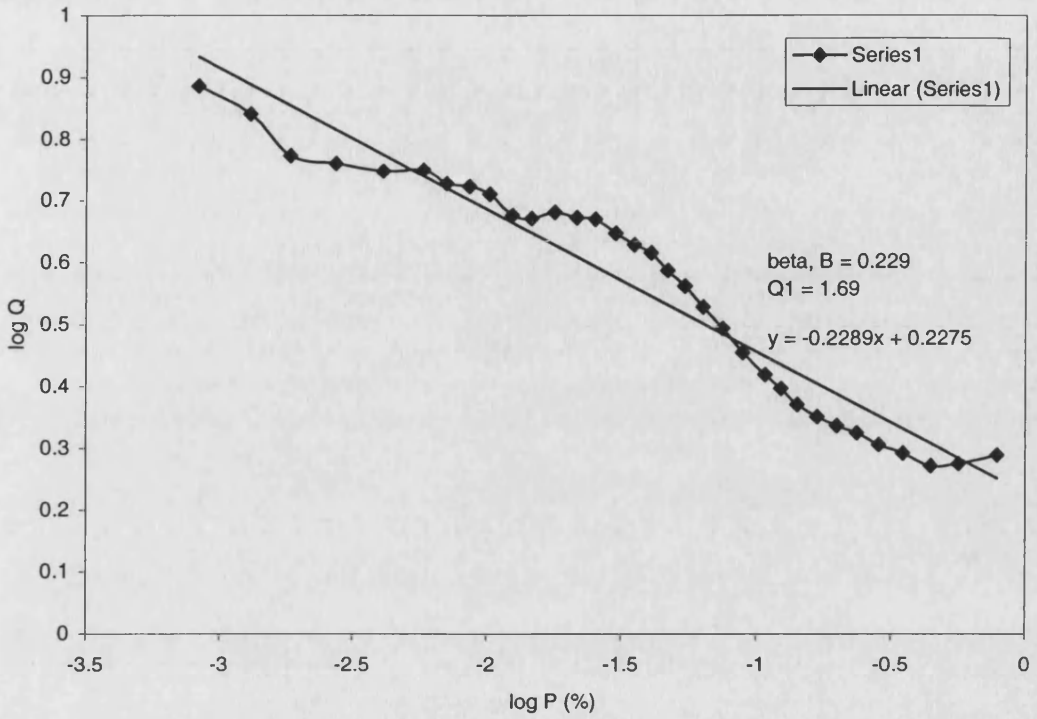

Figure 5.6: Linear regression method applied to estimate Q_1 and β values

As for comparison, in European region, researchers [Brussard and Watson, 1978] have concluded that the factor for conversion from annual worst month to annual cumulative statistics of attenuation on Earth-space 11 GHz radio paths is typically in the range 6.0 to 7.0 varying inversely with the percentage exceedance of interest.

Table 5.6 shows the values for the regression parameters Q_1 and β which are determined from the measured data using the least square method. These are only known values derived for the Q_1 and β for slant path rain effect in the tropic. The values of these parameters obtained at Bukit Jalil are in almost exact agreement with those of the ITU-R values.

However, we would suggest that the worst month relation in Equation. 5.6 with the recommended values β = 0.229 and Q_1 = 1.69 to be used for slant path links in tropical environment. From Figure 5.4 above, it can be observed that the power law relation in Equation 5.6 with ITU-R recommended values for β and Q_1 can give good

estimation for the worst-month envelope based on the average year statistic. New values based on our analyses for the parameters β and Q_1 are proposed in order to obtain a better estimate for the slant path rain effect worst-month statistics in the tropics.

	Q_1	β
Bukit Jalil, Malaysia (Slant path)	1.69	0.229
Indonesia (Terrestrial) [Juy *et al.*, 1989]	1.7	0.22

Table 5.3: Available measured values for Q_1 and β in tropical propagation

The worst-month statistics of rainfall rate are very useful in designing high quality communication networks since the maximum occurrence of events that lead to the degradation of the network is expected to be higher in the worst month. For satellite broadcast application, fading at 99% of the worst month is usually of greatest concern as proposed by ITU [ITU-R P.679-2, 1999]. Observed in the Figure 5.4, the attenuation for time exceedance of 1% of the worst month is 4 dB. Should the margin be adopted for satellite link operating in the tropical region such as Malaysia, yearly average availability of just 99.5% can be achieved which is less then the operating standard 99.7%. Therefore conventional worst month criterion is not appropriate for equatorial climate based on our analyses.

5.6 Development of a Countermeasure Techniques

In specifying the performance of a satellite link that incorporates digital networks; the implementation of fade mitigation techniques such as power control, diversity, coding and resource sharing should be taken into consideration. To overcome the effect of severe localised rain fades at important reception or transmission sites, it is possible to interconnect two earth stations separated by a distance greater than the likely size of the rain cell. Such arrangement is called space diversity 'reception' or 'transmission'. If the rain cell is likely to affect reception or transmission from one

earth station to satellite, the signal can be switched to the second earth station which statistically speaking, very unlikely to be suffering the same rainfall fade conditions. This sort of arrangement is of great value for transmission uplinking because fading at the uplinking site will affect all receiving sites. Rainfall fades on downlink on the other hand only effect the local area around the rain cell.

5.7 Satellite Countermeasures and Diversity Techniques

There are basically four types of diversity techniques that can be used in satellite system operations to overcome impairments at a given earth station. Such diversity techniques or schemes can be identified as space diversity, orbital diversity, frequency diversity, and time diversity. A brief outline of each technique is provided in the following subsections.

5.7.1 Space Diversity

Space diversity technique in telecommunication systems involves the provision of alternate propagation paths for signal transmission. The systems then have the option of selecting the least impaired propagation path when condition warrants. The implementation of path diversity for satellite communication systems requires the deployment of two or more interconnected earth terminal at spatially separated sites. As mentioned earlier, implementation of additional diversity terminals to operate with a main station would be complex and very expensive.

Measurements obtained by researchers [Witternigg *et al.*,1993; Bosisio and Riva, 1996] indicate that significant increases in availability can be obtained by simultaneously operating with more than two terminals

5.7.2 Orbital Diversity

The difference between orbital diversity [Matricciani, 1997; Capsoni *et al.*, 1990] and site diversity is that only one earth station is used. The earth station uses two antennas that can access different satellites simultaneously to achieve the measure of diversity. Orbital diversity does not require the diversity interconnect link between sites as required for site diversity. The angle between two paths at the earth station must be large in order to obtain significant de correlation of concurrent attenuation along the two paths. The achievable diversity is reported to be fairly small, generally being at most about 2-3 dB in the K_u-band frequencies

5.7.3 Frequency Diversity

This technique requires that multiple frequency bands to be simultaneously available at the earth station in question. Some applications of technique have been studied by and reported [Carassa and Matricciani, 1988; Capsoni *et al.*, 1988]. It is acknowledged that, path losses caused by particles on the path increase as the frequency increases. If the earth terminal is capable to switch communications from an impaired high-frequency band to a lower-frequency band, significant increases in availability might be achieved.

In addition, the technique also requires that there must be spare capacity available in the lower frequency band whenever needed. This implies that significant spare capacity must be provided if the link is a high-capacity channel. Frequency diversity technique definitely requires significant investment. However, should such dynamic network control features be in place and the additional capacity in the lower frequency be available on call, this technique can undoubtedly provides large increases in availability.

5.7.4 Time Diversity

Current technology enables satellite-broadcasting systems to employ digital transmission to yield a high-quality and realistic sound and visual environment. The information can be divided into basic and additional (or redundant) information. Home viewers can enjoy television broadcast at conventional quality by receiving only the basic information. Viewers can enjoy a more realistic sound and picture by receiving additional information couple together with the basic information.

In Figure.5.7 [Fukuchi, 1992] below, the proposed broadcasting satellite that incorporates the time diversity countermeasure will be transmitting the basic and two sets of the additional information 'α'. The additional set of information is sent with a certain delay 'T' relative to one another. Therefore even during severe rain conditions, the basic information '1-α' should be received with a certain quality by using sophisticated source and channel coding technologies and the damaged or deteriorated information should be recovered from additional information transmitted

with the delay and in less severe condition. The re-broadcasting method, which uses a delay 'T', is the principle of this time-diversity model

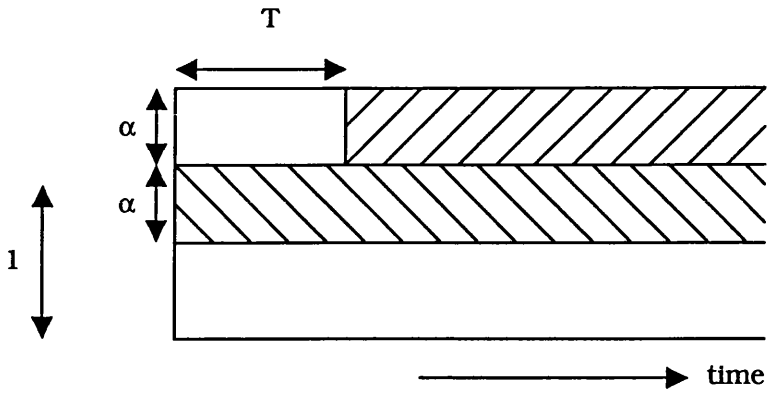

α = 0 : normal program
α = 'α (0<α<1) : partial time diversity
α = 1 : full time diversity (rebroadcast)

Figure 5.7: Concept of time diversity transmission of broadcast

For such sophisticated satellite broadcasting technique, it is favoured that the household receiving equipment to have an intelligent large-capacity random-access memory, which has the capability to store information in order to get error-free information. Although rainy conditions will reduce real-time full quality broadcasting performance, in due time a high quality program library will be created before the receiver owner is aware of it.

The time-diversity technology appears to be beneficial not only for millimetre satellite broadcasting systems but also for point-to-multipoint communication systems in which a real-time capability is not strongly required

5.8 Reducing the Incidence of Outage

Not all satellite operators have the luxury to build additional earth stations. Perhaps, a second earth station is considered necessary for system calibration and maintenance service but a proposal to building the third and so forth really has to be taken into

serious consideration coupled with the fact that the severity of rainfall at undetermined location in tropical regions. In view of these situations, several diversity techniques are currently in ongoing research all over the world. At the All Asia Broadcast Centre, the MEASAT earth station has the capability to boost the transmission power of its 13-metre uplink antennas up to 2.2 kW, its full capacity, during a thunderstorm in order to overcome the potential rain fading on the uplink side. Combine with information of diurnal statistics of the slant path link based on our analyses; appropriate margin can be implemented to ensure required signal strength is able to reach the satellite. The power required on a clear day is only 12 watts or just 0.5% of the available capacity. Therefore, the rain fading that pose real threat to quality of service promised to MEASAT's customer is on the downlink side.

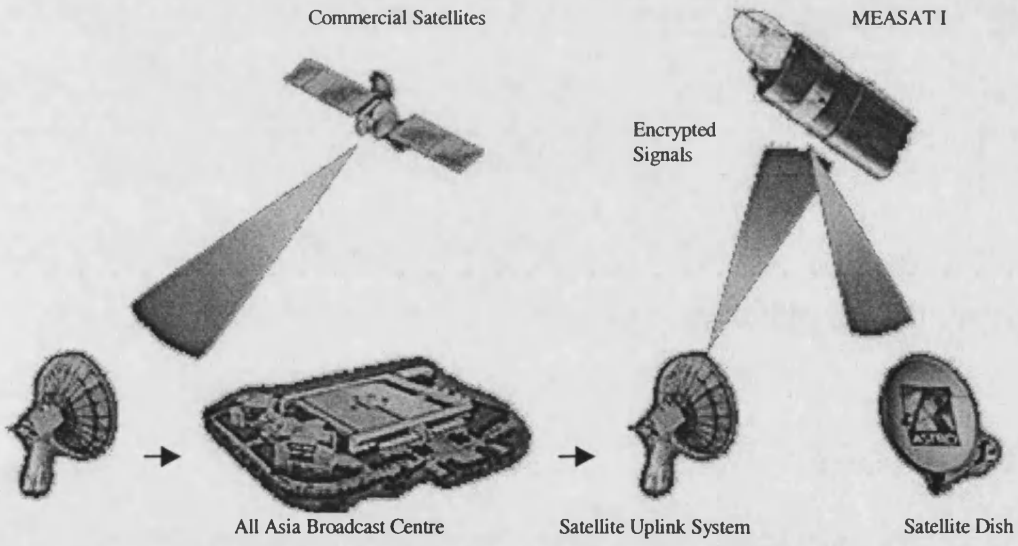

Figure 5.8: Operation of MEASAT

5.9 Use of Time Diversity

Severe rain events do not usually last long at given location. Such characteristic enables the use of communication means that do not require instantaneous interaction between the caller and the receiver. For example, electronic mail, e-mail and facsimile transmissions fit this category, provided messages are successfully sent

without errors within customers agreed period, the service can be said as accepted. The scheme realised by retransmission of information several times with a certain time delay is considered time diversity [Fukuchi, 1992; Fukuchi *et al.*, 2000] technique. This feature could be also used with advantage to determine the capacity requirements of a given link for optimal economic performance. If a link is sized for maximum anticipated capacity, it will have excess capacity for most of the time. If some transmission can be delayed and sent, for example at off-peak times for most of the time, the capacity requirement can be reduced. The time delay could therefore be used at times of peak capacity. The same technique can be applied when earth station is undergoing a severe rain event. Transmissions can be delayed and sent after such rain event has diminished. This particular technique can be applied in commercial application such as video-on -demand with time delay programme repeats. The technique can be implemented where customer receiver with the use of sophisticated memory function is able to accumulate information obtained in better receiving condition.

5.9.1 Diversity Gain and Diversity Improvement Factor

In our analyses, the possible use of time diversity as a fade countermeasure technique is investigated using the MEASAT beacon data. Assessments are carried out upon the concept of applying time delay on the transmission link. Figure 5.9 gives an example of a fading event where the approach was implemented. The original signal was delayed at selected time of study and the plot was redrawn in the same figure. Comparisons were made between the original and the delayed signal values. The lower values among the two measurements then are selected and recorded.

The figure shows how the retransmission technique can improve the performance of the satellite earth link. In the above figure, the original transmitted signal exceeded the 10-dB fade level eight times. The users experienced eight occurrences of receiver outage if the system utilise margin of 10 dB for the path link. Delaying the signal by

10 minutes later, a stronger signal level can be received by the users. The outages now are reduced to just two occurrences.

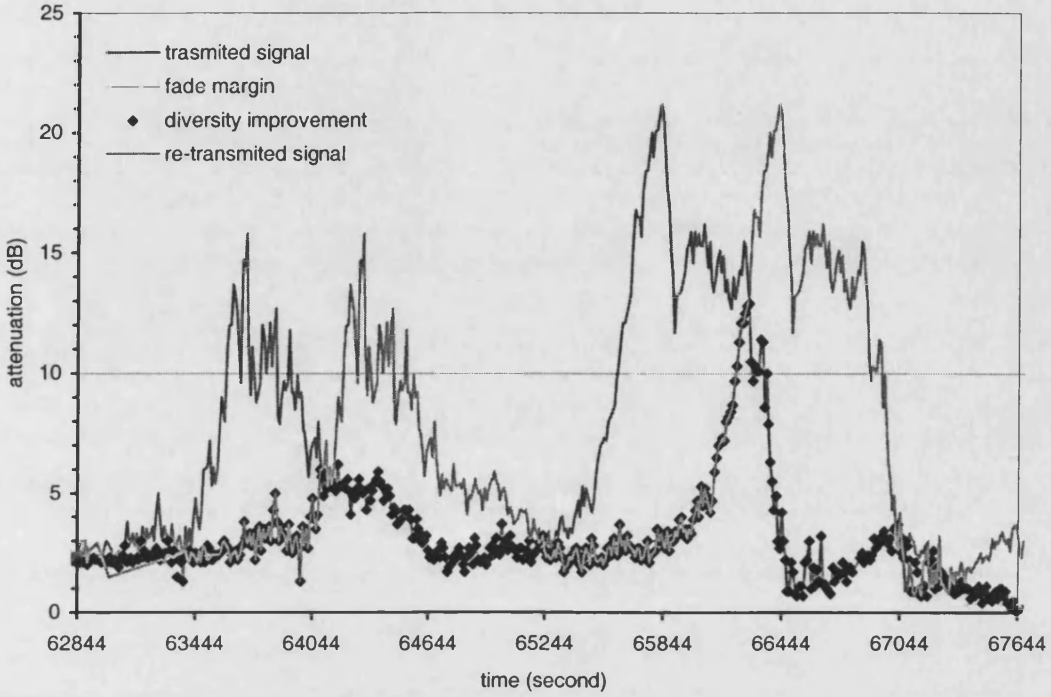

Figure 5.9: Time diversity of 10 minutes delay implementation

The diversity gain of any countermeasure techniques is defined as the difference between the path attenuation associated with single terminal and diversity mode of operation for a given percentage of time [Hodge, 1973]. In the use of time diversity, the diversity gain can be graphically presented on the attenuation cumulative distribution plots. The difference between the original signal A_m and diversity signal A_{div} cumulative distribution attenuation values at the same percentage time can be expressed by:

$$G(p) = A_m(p) - A_{div}(p) \tag{5.7}$$

where *G(p)* is the diversity gain for the system at that percentage of time. The values can be clearly observed from plots in the next page. Diversity performance can also be

described in terms of outage times by a factor know as diversity improvement [Hodge, 1974] or diversity advantage. The diversity improvement factor, *I*, is given by:

$$I(A) = \frac{p_m(A)}{p_{div}(A)} \tag{5.8}$$

where $p_m(A)$ is the percentage time associated with original distribution and $p_{div}(A)$ is the percent time associated with diversity distribution, both at the same value of attenuation. In the application of site diversity technique, the above equation can also be expressed according to ITU-R P618-6 as:

$$\frac{p_m}{p_{div}} = \frac{1}{(1+\beta^2)}\left(1+\frac{100\beta^2}{p_m}\right) \approx 1+\frac{100\beta^2}{p_m} \tag{5.9}$$

where β is a parameter depending on link characteristics. The approximation on the right-hand side of Equation 5.9 is acceptable since β^2 is generally small.

The time-diversity effects are discussed quantitatively in the following sections, by making use of attenuation time series data measured along the satellite-Earth link in Malaysia. For the statistical analysis of time-diversity effect, delay times from several minutes to one hour were assumed considering the time series characteristics of the rain-induced attenuation.

5.9.2 Performance of Time Diversity

Investigation was carried out for various time delay values of interest. Curves of original measured attenuation distribution and improved distribution with time diversity for the range 1 to 60 minutes are presented in Figure 5.10. The improved cumulative distributions are obtained using the lower values obtained through

previously described procedure for all events within the twenty-month period. From figure below, increase of diversity gain values can be observed as the time delay increases.

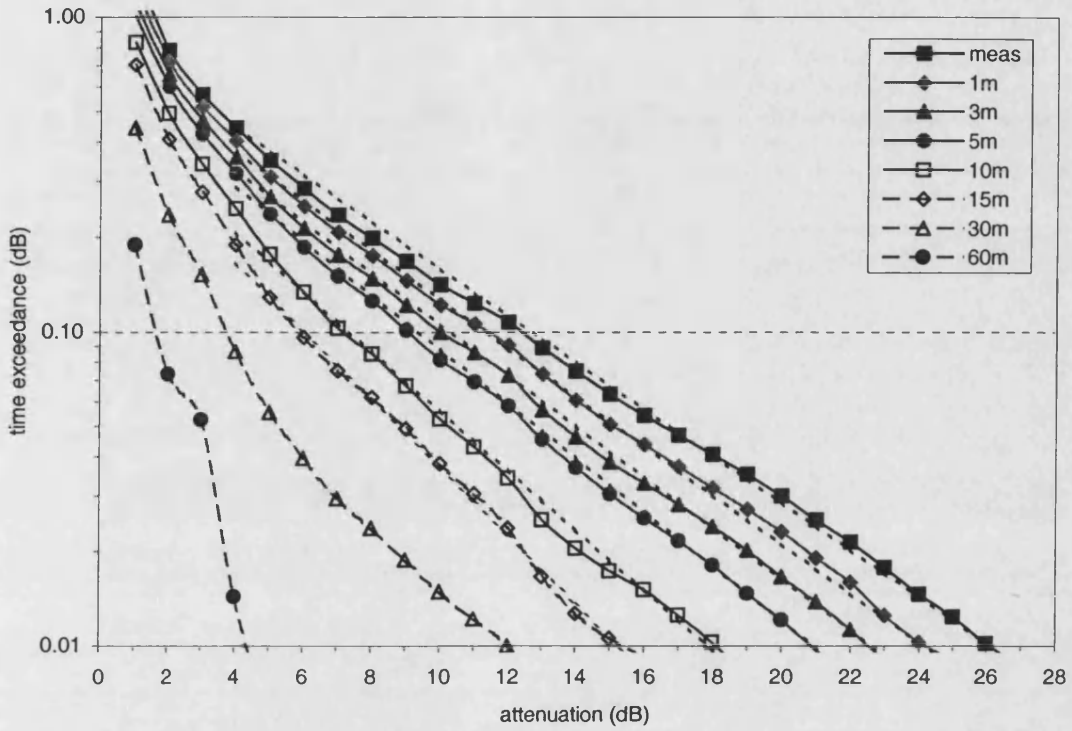

Figure 5.10: Time diversity gain as a function of delay.

Ideal time diversity is assumed with full recovery in the inter-fade interval. In Figure 5.10, it can be observed that diversity gain at time exceedance 0.1% with the implementation of 5 minutes delay is approximately 4 dB. The performance is in keeping with the observed average fade duration of about 4 minutes as shown in Figure 5.8.The value was obtained by subtracting the diversity signal distribution value from the original attenuation distribution value at the same time percentage. Diversity gain at the 99.9% exceedance threshold varies depending on the minute delay applied.

5.9.3 Proposed Recovery Strategy

Apparently there is significant and increasing diversity gain for delays between 1 and 30 minutes but for delays above 30 minutes, proportionately less gain is seen per 1-minute unit of delay. The time diversity technique might have potential for the use on the downlink, building in memory and switches into domestic receivers. Considering practical intervals for time-repeated material between 15 to 30 minutes leads to the conclusion that a recovery strategy must operate with a frame length considerably shorter than the repeat period. The dashed curves without marker in Figure 5.10 above are the fitted exponential distribution for each time diversity improvement. The attenuation and time-delay improved cumulative distributions may be represented, for A > 4 dB, by exponential distributions of the form:

$$P(A) = \beta \exp(-\alpha A) \tag{5.10}$$

where the coefficients α and β are given in Table 5.4. The distribution for other selected time diversity delay can also be determined within an error of ± 0.34 dB as a function of delay Δt using expressions:

$$\alpha = 0.005\Delta t + 0.1726 \tag{5.11}$$

$$\beta = -0.0224\Delta t + 0.7575 \tag{5.12}$$

The linear regression to estimate the relationship between selected time delay and coefficient α and β can be observed in Figure 5.11 below.

Delay (minutes)	α	β
0	0.1715	0.8807
1	0.1793	0.7611
3	0.1866	0.6828
5	0.1982	0.6372
10	0.2181	0.4950
15	0.2499	0.4494
30	0.2801	0.2654

Table 5.4: Coefficients for exponential approximations to time diversity gain relationship

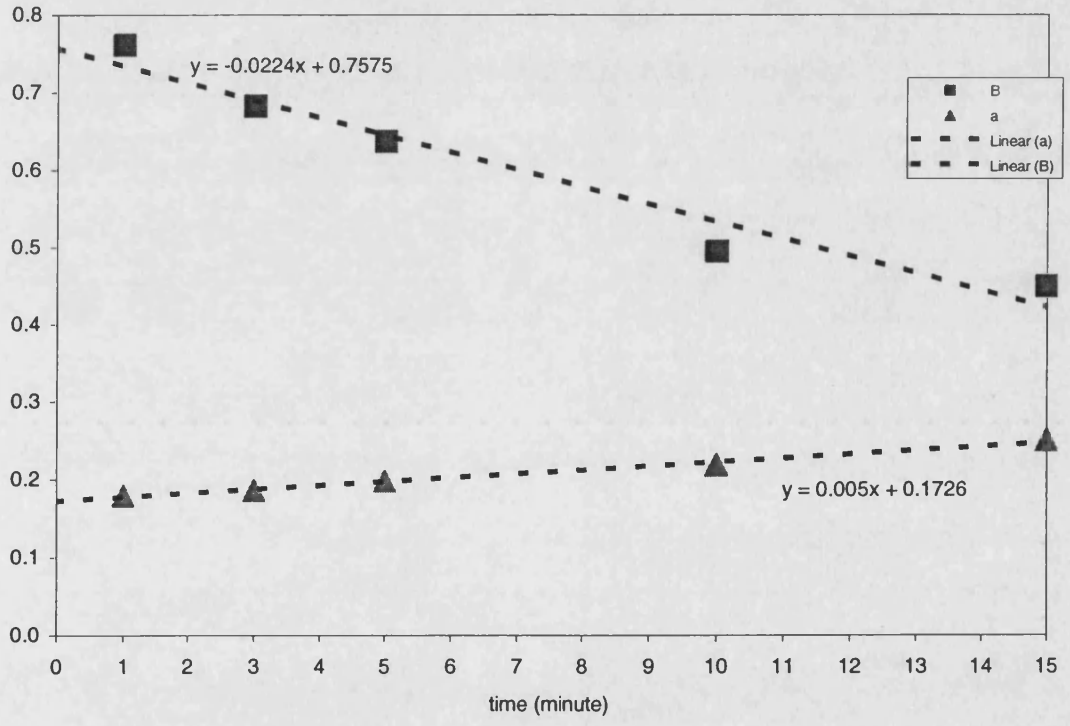

Figure 5.11: Estimation of α and β vales for various selected time diversity delays

5.10 Conclusion

Analyses of rain induce-attenuation measurement at K_u-band recorded at Bukit Jalil, Kuala Lumpur indicate that latest ITU-R recommendation 618-6 for predicting annual attenuation statistic severely underestimate the annual measured attenuation

statistics at time exceedance 0.006% and above. The previously published recommendation ITU-R p.618-5 gave good estimation for beacon attenuation measured in Malaysia. The results also suggested that the prediction method ITU-R 618-5 with local measured rainfall rate gave the best estimation of rain induced attenuation values than other predictions methods. There is a serious deficiency in the latest ITU-R prediction model and satellite designers are advice to use with extreme caution.

Due to the severity of the rain induced attenuation encountered, findings suggest that commercial satellite K_u-band operation and other tropical region may not be feasible to operate at 99.7% availability without the use of one or more techniques to alleviate the effect of rain induced attenuation. The techniques may include site diversity [Hodge, 1992; Pan and Allnutt, 2001], uplink power control [Lin *et al.*, 1993] and uplink receiver such as facilities at the satellite. Based on findings in Malaysia, we conclude that, applying margin taken from the value at 0.1% time exceedance of the worst month is not sufficient enough to ensure adequate annual availability.

The chapter presents the research findings of possible countermeasure time diversity that could be employed to reduce the effect of rain-induced attenuation. The performance of the diversity technique cannot yet be compared since there is no other diversity measurement available for tropical climate at similar location, elevation and frequency in order to make a comparison. Considerable amounts of diversity gain have been observed and confirmed from plots of time diversity distribution as the selected time delay increases. More than 3 dB diversity gain can be observed at 0.1% of time exceedance with time diversity of 300 seconds. Satellite designers and engineers should extend their research in this area since significant improvements from proposed techniques have been observed based on the statistics obtained. This is an encouraging finding for the new concept of future satellite broadcasting systems that could provide higher quality visual and audio broadcast; but at the expense of real-time viewing.

Chapter 6

Tropical Rain Drop Size Distribution Analyses

6.1 Introduction

Drop size distribution is one of the important rain characteristics that are required in calculation of rain-induced attenuation. The knowledge of rainfall drop size distribution is a fundamental subject in such calculation at frequencies above 10 GHz. The negative exponential model of rain drop size distribution based on data collected in temperate region is currently adopted by the ITU-R for scattering due to raindrops in the calculation of specific attenuation γ (dB km^{-1}). The distribution is normally characterised by the Law and Parson model, and its analytic form in negative exponential function has been proposed Marshall and Palmer.

Nevertheless, numbers of investigators suggested that such relations are not adequate to describe the rain drop size distribution characteristics in measured the tropical region [Maciel and Assis, 1990; Jassal *et al.*, 1994, Timothy *et al.*, 1995; Tharek and Din, 1992; Vilar *et al.*, 1997, Maitra, 2000]. Several researchers have suggested that the lognormal or the gamma distributions are more applicable models than the negative exponential distribution model for countries with tropical climate [Ajayi and Olsen, 1985; Ong and Shan, 1997]. In this chapter, we attempt to present comprehensive results of the tropical rain drop size distribution analyses based on measurement data collected in Papua New Guinea observing closely the previous approaches by researchers [Ong and Shan, 1997, Shan 1996] as guidelines.

6.2 Experimental Data

A 3-GHz vertical pointing Doppler radar and a co-located distrometer belonging to RAL were installed out in the open space on the rooftop of PNG University of Technology's electronics laboratory. RAL started their observation campaign for monitoring precipitation in the tropical region starting December 1996. Measurements were recorded for 6 continuous months

Unitech, PNG is located at Lae with latitude and longitude 7° S and 147° E respectively. PNG is classified to be between the M and the P zone according to the earlier ITU-R rain climatic regional map [ITU-R P.837, 1994]. PNG has the climate that is typical of tropical region with daytime temperature of around 32° C with relative humidity higher than 85% all year around. PNG experiences annual rainfall of approximately 4500 mm. In accordance with the new ITU-R rain map recommendation [ITU-R P.837-2, 1999] PNG is computed to experience rain intensity of 100 mm hr^{-1} for the annual percentage time of 0.01.

The distrometer used in the PNG campaign is capable to provide records of the number of rain drops in individual diameter ranges over a period of 60 seconds. This enabled the characteristics of the rain drop size distribution in PNG to be investigated through what is classified as the surface based measurement method. The distrometer used was an impact type and identified as the Joss-Waldvogel distrometer, model number RD-69. It has a sampling area of 50 cm^2 and sorts the rain drops into 20 intervals ranging from approximately 0.3 to 6.5 mm in diameter.

Meanwhile, the RAL's polarmetric S-band pulse Doppler radar measured and recorded the co-polar reflectivity (*Z*), linear depolarisation ratio (*LDR*) and the full Doppler spectrum. The radar ran continuously providing vertical profiles for every 3.2 seconds up to the height of 10 km and the range bin (gate) resolution for each profile is 75 m.

6.3 Parameters for Distrometer

The distrometer data furnish us with measurements of the number of rain drops $n(D_i)$ that fell onto the distrometer's sensor within 60-second integration time. The measurements are recorded according to sizes in 20 individual categories corresponding to the range of drop diameters D_i between 0.3 to 6.5 mm. The program utilised to acquire the $n(D_i)$ measurements from the binary data is written in IDL language. The program is a modified version from one provided by Dr. Merhala Thurai from RAL. The original supplied program uses integration time of 30 seconds and hence is modified to suit our data requirement. The original program is capable to compute the estimates of rainfall rate, R and radar co-polar reflectivity (Z) factor at 3 GHz based on the collected drop size data. The readings can be displayed on the screen and saved into datafile. The datafile format listed is not adequate for further data processing in the interest of drop size distribution analyses. We included an additional file saving function feature for the D_i and its associated $n(D_i)$ in our revised program. We formatted the measurement datafiles in text format. In our analyses, Microsoft Excel 97 is utilised as our data processing tool. Microsoft Excel 97 is able to retrieve directly all text format datafiles.

The parameter D_i is the representative diameter for that channel i with the assumption that the rain drop shape is spherical. Where else the $n(D_i)$ is the measurement of number of drops in channel i. The upper and lower diameter values D_{iu} and D_{il} of particular channel i can be determined from parameters D_i and the mean value of the range, ΔD_i supplied in the program. The parameters D_{iu} and D_{il} can be calculated from D_i and ΔD_i the values using the following expressions:

$$D_{il} = D_i - \frac{\Delta D_i}{2} \tag{6.1}$$

$$D_{iu} = D_i + \frac{\Delta D_i}{2} \tag{6.2}$$

Table 6.1 below shows the detail parameters configured for each channel of the distrometer employed in the measurement campaign.

Channel i	Mean value D_i (mm)	Dia. interval ΔD_i (mm)	Lower bound D_{il} (mm)	Upper bound D_{iu} (mm)
1	0.3590	0.092	0.313	0.405
2	0.4550	0.100	0.405	0.505
3	0.5495	0.089	0.505	0.594
4	0.6565	0.125	0.594	0.719
5	0.7740	0.110	0.719	0.829
6	0.9135	0.169	0.829	0.998
7	1.1135	0.231	0.998	1.229
8	1.3315	0.205	1.229	1.434
9	1.5130	0.158	1.434	1.592
10	1.6625	0.141	1.592	1.733
11	1.9115	0.357	1.733	2.090
12	2.2690	0.358	2.090	2.448
13	2.5995	0.303	2.448	2.751
14	2.8915	0.281	2.751	3.032
15	3.1885	0.313	3.032	3.345
16	3.5410	0.392	3.345	3.737
17	3.9440	0.414	3.737	4.151
18	4.3850	0.468	4.151	4.619
19	4.8820	0.526	4.619	6.145
20	6.4470	0.605	6.145	6.750

Table 6.1: Parameters for each drop size channel

The correlation between the terminal velocities of water drops with the drop sizes is mentioned in various literatures. The results of Gunn and Kinzer measurement have been widely quoted in most of the papers. The distrometer program adopted their results where their values are used in this study to calculate the terminal fall velocity of drops, $v(D_i)$. The estimated velocity values for each channel i are given in Table 6.2 and Figure 6.1 illustrates the curves of the fitting result to that of data by Gunn and Kinzer.

Channel i	Mean value D_i(mm)	Terminal fall velocity $v(D_i)$ (m s^{-1})
1	0.36	1.35
2	0.46	1.81
3	0.55	2.24
4	0.66	2.70
5	0.77	3.18
6	0.91	3.70
7	1.11	4.37
8	1.33	6.02
9	1.51	6.49
10	1.66	6.85
11	1.91	6.38
12	2.27	7.01
13	2.60	7.48
14	2.89	7.83
15	3.19	8.13
16	3.54	8.42
17	3.94	8.68
18	4.39	8.91
19	4.88	9.10
20	6.45	9.26

Table 6.2: Terminal velocity for each channel

The Gunn and Kinzer results are said not be very ideal because in their experiment, the drops were allowed to fall in an environment of air of only 50% relative humidity. The shortcoming has been noticed and discussed investigator who then examined the drops falling in water-saturated air and at different pressure levels [Pruppacher and Beard, 1970]. Their results which were just for the terminal velocity of water drops of diameter between 0.02 and 0.95 mm however agreed quite closely with those of Gunn and Kinzer. Based on such consideration, the Gunn and Kinzer results can be accepted to assign the velocity of drops in PNG where the relative humidity is higher than 85%.

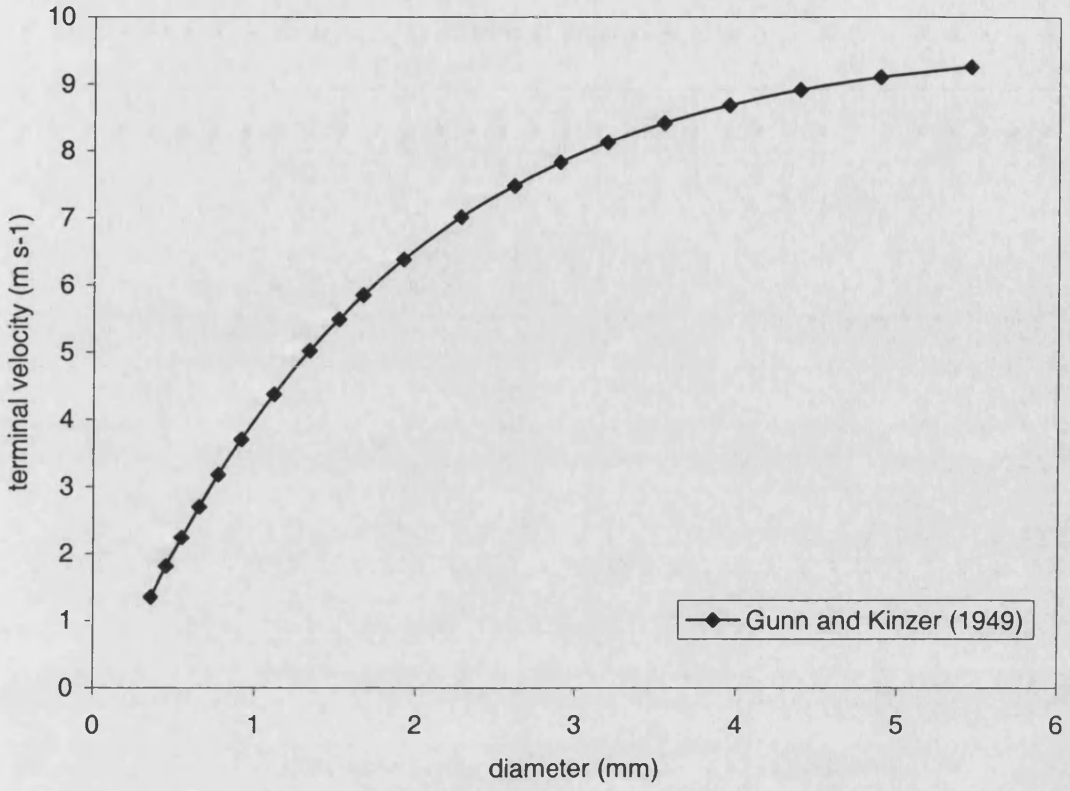

Figure 6.1: Terminal velocity versus the drop diameter of each channel

The common expression of rain drop size distribution $N(D_i)$ is given in terms of the number of drops per cubic metre of air per millimetre interval of drop diameter (m^{-3} mm^{-1}). In our analyses, the integration time T for the distrometer is 60 seconds. The sample area of the distrometer S is 5000 mm^2. With the terminal velocity of rain drop in ms^{-1}, $v(D_i)$ values specified in the table above and the extracted $n(D_i)$ value from the data, the number of rain drops per unit volume per unit diameter $N(D_i)$ for each category i can then be calculated by the following formula [Goddard and Cherry, 1984]:

$$N(D_i) = \frac{n(D_i)\times 10^6}{v(D_i)\times T \times S \times \Delta D_i}$$

$$= \frac{n(D_i)\times 10^6}{v(D_i)\times 60 \times 5000 \times \Delta D_i}$$

$$= \frac{n(D_i)}{v(D_i) \times 0.3 \times \Delta D_i} \tag{6.3}$$

In addition to the number of rain drops per unit volume per unit diameter $N(D_i)$, the rain rate R (mm hr^{-1}) can also be calculated using the $n(D_i)$ values and the parameters as defined in Equation (6.3). With $\frac{\pi}{6} D_i^3$ as the volume of a drop for the average diameter D_i within ΔD_i in channel i, the rainfall rate R (mm hr^{-1}) from Equation 2.3 can be calculated as follows:

$$R = \int_0^{D\max} \frac{\pi}{6} D_i^3 n(D_i) \frac{3600}{ST}$$

$$= \sum_{i=1}^{20} \frac{\pi}{6} D_i^3 n(D_i) \frac{3600}{ST}$$

$$= \frac{6\pi \times 10^2}{ST} \sum_{i=1}^{20} D_i^3 n(D_i)$$

$$= \frac{6\pi \times 10^2}{5000 \times 60} \sum_{i=1}^{20} D_i^3 n(D_i)$$

$$= 6.283 \times 10^{-3} \sum_{i=1}^{20} D_i^3 n(D_i) \tag{6.4}$$

6.4 Classification of Rain Events

By visual inspection, the radar data are categorised into two events i.e. stratiform and convective. The criteria used to characterise the two events are; based on the presence of a clear bright-band enhancement in the co-polar reflectivity in identifying stratiform events, as well as the occurrence of significant updrafts in the case of convective events. From the data logged over the six-month period, 62% of the events are classified as stratiform, 19% convective and 19% 'mixed' events [Ladd *et al.*, 1997]. Based on the six-month data, various rain events are inspected. For purpose of rain

drop size distribution modelling, the simultaneously recorded distrometer data are catalogued in accordance with the radar classification. We then conducted the analyses on distrometer data for stratiform and convective classifications.

Figure 6.2 illustrates a colour plot example of stratiform event that occurred on February 20th 1996 for duration of 90 minutes. Clear identification of the melting layer can be observed in the measured co-polar reflectivity parameter. Figure 6.3 shows the rainfall rate curve estimated from the distrometer data using integration time of 60 seconds. The curve is a time series of the rainfall rate computed by the Microsoft Excel 97 software using Equation 6.4 above. The event illustrated here starts at 13:02:35 (hr:min:sec). During stratiform events, the rainfall intensities detected are usually at low values. The curve displayed reached its maximum intensity of approximately 6.3 mm hr^{-1}. The rain intensity during stratiform events usually remained constant for the whole period.

Most of the recorded convective events lasted for at least one hour. Figure 6.4 is one convective event example recorded during the RAL's campaign in PNG. The co-polar reflectivity (Z) radar scan indicates there is no clearly defined melting layer in this profile. It can be observed that there is a considerable updraft and there are areas of strong turbulence. The corresponded rainfall rates computed from raw data provided by the distrometer is shown in Figure 6.6. In this plot, the rain intensity fluctuates several times reaching peaks of higher than 80 mm hr^{-1} for at least 5 times within the 90 minutes duration. In general, during most convective events, rain reaches the maximum intensity very rapidly. The rain then remains heavy for a few minutes then it decreases a much slower rate than it increases. From our observation, lower rainfall rates occurred during the decreasing period.

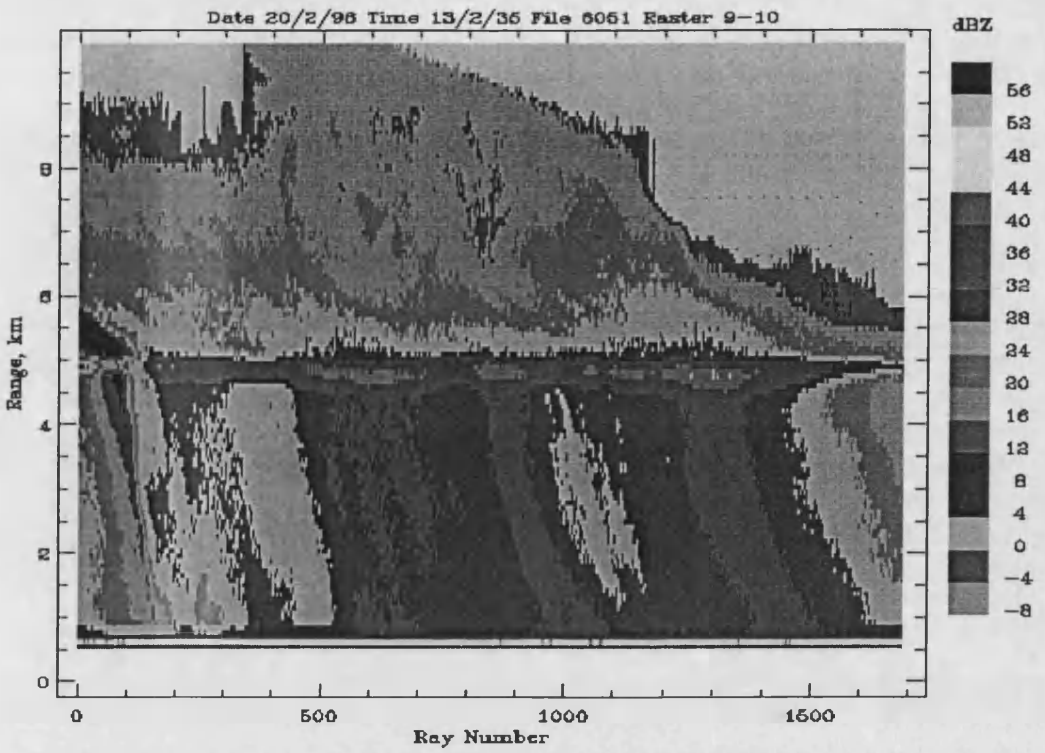

Figure. 6.2: An example of PNG stratiform precipitation event

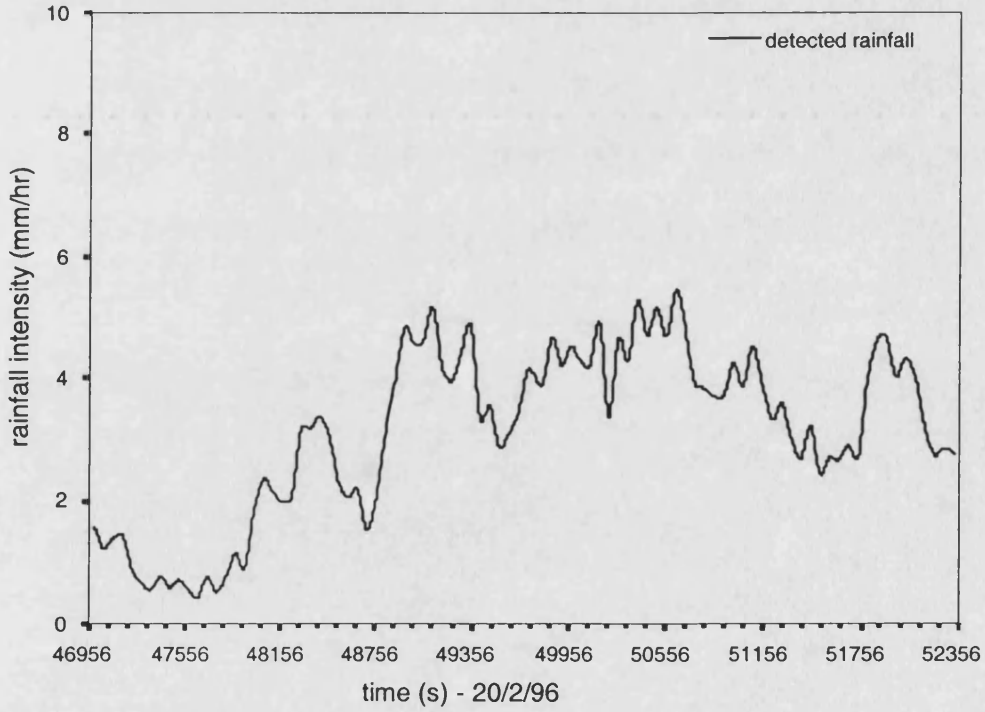

Figure. 6.3: Simultaneous ground-truth rainfall intensity computed using the distrometer data for the above stratiform event.

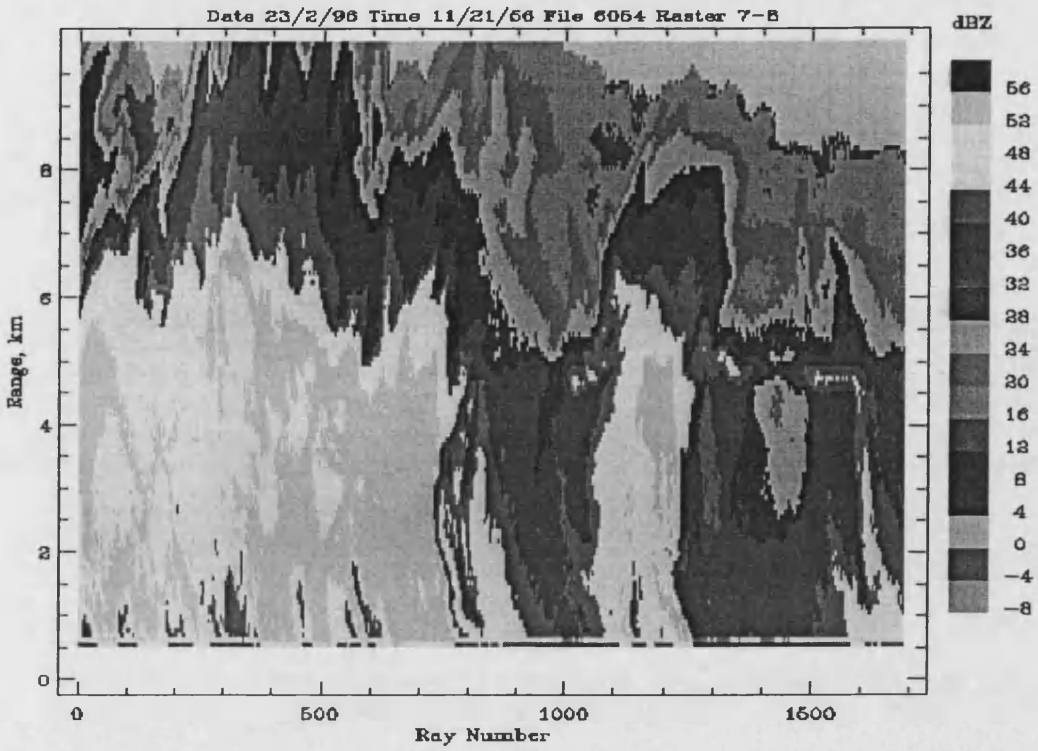

Figure. 6.4: An example of PNG convective precipitation event

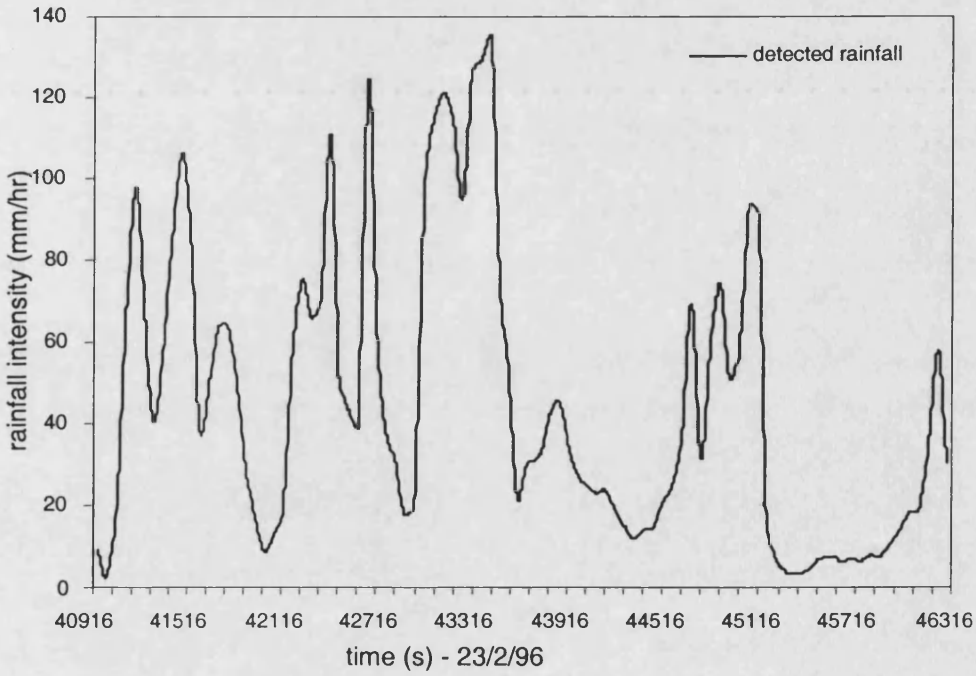

Figure. 6.5: Simultaneous ground-truth rainfall intensity computed using the distrometer data for the above convective event

The recorded convective events in most cases show that they are very often followed by stratiform events of less intense rainfall rate. We notice that in the case of stratiform rain events there are no case where the rainfall intensity exceeds 20 mm hr^{-1}. In fact, in most cases, the rainfall rate for stratiform events is less than 10 mm hr^{-1}. While for convective events the rainfall intensity is usually greater than this value

6.5 Measured Data Analyses

The investigation of the drop size distribution in tropical rain has been the subject of continued concern in view of varied climatological conditions and the lack of experimental observations in this part of the world. In temperate climate, the drop size distribution can be well represented by the Law and Parson model. The experiment was conducted using the 'floor method' in Washington DC for various types of rain. Floor method is where a pan containing fine flour was exposed to rain and size of pellets produced by the rain was measured.

Marshall and Palmer based on theirs and Law and Parson's measurements proposed a negative exponential relation for raindrop size distribution such as follows:

$$N(D) = N_0 e^{-\Lambda D} \tag{6.5}$$

where $N(D)$ is the number of drops in a unit volume with diameter in the interval from D to $D + \Delta D$. Coefficient N_0 is a constant determined empirically and the rainfall rate R is in unit of mm hr^{-1}. We initiated our analyses by making comparison between the Marshall and Palmer's negative exponential function with measured raindrop size distribution calculated by the distrometer. The parameters of exponential size distribution of Marshall and Palmer can be observed in Table 6.3 below. Figure 6.6 gives two comparison examples carried out for stratiform and convective rain. It is evident that the negative exponential model does not fit each observation particularly

for small drops. Hence, it is essential to consider a new relation that is more appropriate to represent the measured distribution.

	Type of rain	N_0 (m^{-3} mm^{-1})	Λ (mm^{-1})
Marshall and Palmer	All	8000	$4.1R^{-0.21}$
Joss et al.	Drizzle	30000	$5.7R^{-0.21}$
	Widespread	7000	$4.1R^{-0.21}$
	Thunderstorm	1400	$3.0R^{-0.21}$

Table 6.3: Parameters of exponential size distributions of Marshall and Palmer, and Joss *et al.*

Modern measurements campaigns have been conducted by the use of more advanced instrumentation such as a distrometer. Joss *et al.* with their distrometer measured the size distribution of rain at Locarno, Switzerland and found that the distributions vary considerably for different type of rainfalls [Joss *et al.*, 1968]. The parameters of average exponential distribution have been acquired for three different types of rain. The values are tabulated in Table 6.3 above. The drizzle distribution is associated with very light widespread or stratiform rain composed mostly of small drops, while thunderstorm distribution is characterised for the drop size distribution of convective rain with relatively high concentration of large rain drops. The rain drop distributions as proposed by Joss *et al.* were plotted against measured distributions obtained in PNG.

It can be observed in Figure 6.7 that the proposed Joss *et al.* distributions overestimate the number of drop will small sizes for both stratiform and convective rains. It has been suggested that in the measurements, the number of very small drops, e.g., in radius range less than 0.1 mm is only sufficiently know because of the difficulty of measurements. Nonetheless, contributions of such small size drops are crucial in calculation of rain-induced attenuation for the any wavelengths shorter than several millimetres.

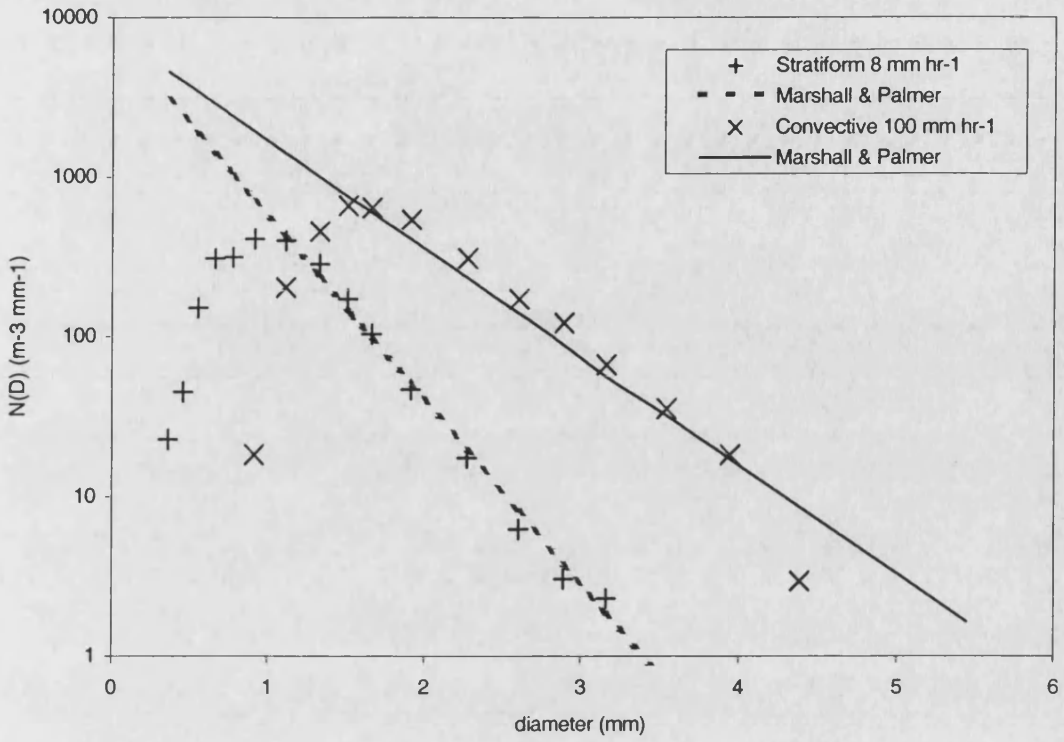

Figure. 6.6: Comparison between measured drop size with Marshall Palmer distributions at R = 8.0 mm hr^{-1} for stratiform rain distribution and at R = 100.0 mm hr^{-1} for convective rain

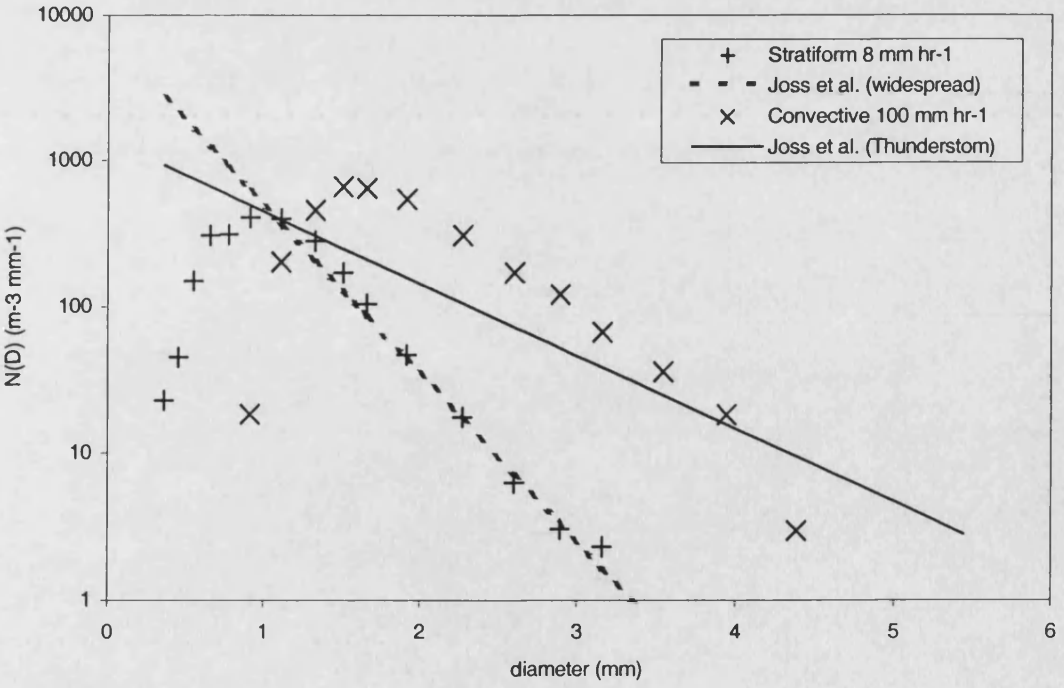

Figure. 6.7: Comparison between measured drop size with Joss *et al.* distributions at R = 8.0 mm hr^{-1} for stratiform rain distribution and at R = 100.0 mm hr^{-1} for convective rain

6.5.1 Stratiform Event

In this section, we first introduce the measured raindrop size distributions obtained from the stratiform rain events. Stratiform events generally cover the rainfall intensity range of below 20 $mmhr^{-1}$. Subsequently we then present the raindrop size distribution obtained from convective events. For each rain classification, we studied samples from more than 20 different rain events to ensure that the statistics are reliable. The aim of this section is to study the characteristic of rainfall rate and inspect various structure of the raindrop size distribution in building a preliminary plot for the modelling attempts.

Ten selected rainfall rates ranging from 0.5 mm hr^{-1} to about 16.5 mm hr^{-1} from various stratiform events are chosen to analyse the raindrop size distribution. The first three selected rainfall rates in ascending orders can be observed in Figures 6.8.1 (a) through (c). The remaining drawings are included in Appendix A. We followed the practice adopted by previous researchers in displaying our results where the horizontal axis diameter of raindrop D is represented in linear scale and the vertical axis for $N(D_i)$, the number of raindrops per unit volume per unit diameter is represented in a logarithmic scale. There are four curves in every figure representing the number of raindrops per unit volume per unit diameter $N(D_i)$ acquired from distinct events having the same rainfall rate.. Plotted in each figure are the $N(D_i)$ values computed from the distrometer data $n(D_i)$ using Equation (6.3), versus the raindrop diameter D (mm). We then determined the average $N(D_i)$ and plotted the values labelled as 'average' in the same figure.

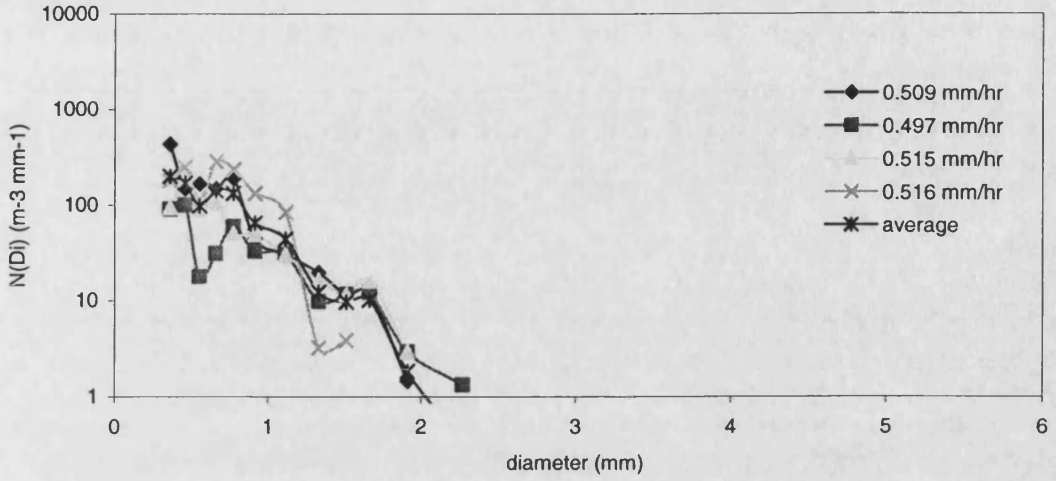

Figure 6.8.a: Measured distributions for stratiform rainfall rates at ~ 0.5 mm hr^{-1}

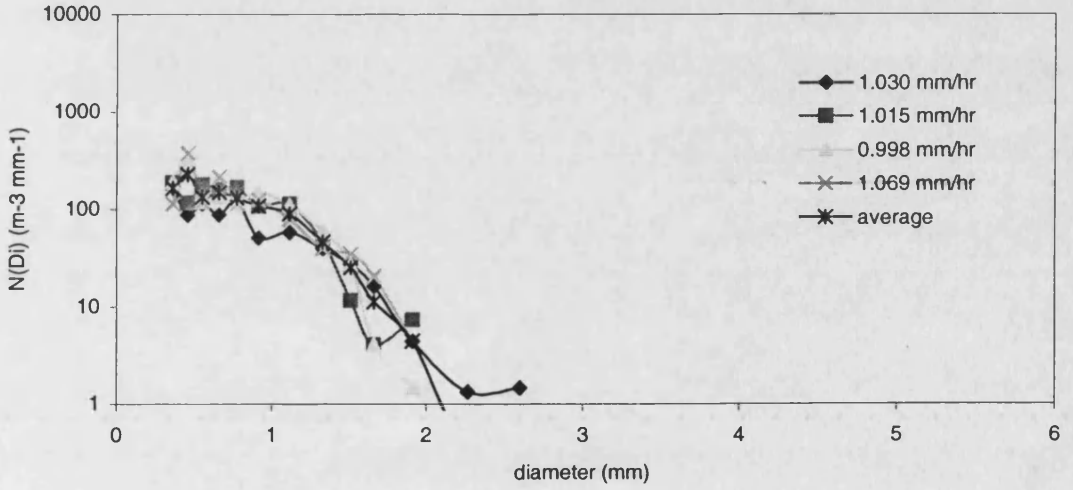

Figure 6.8.b: Measured distributions for stratiform rainfall rates at ~ 1.0 mm hr^{-1}

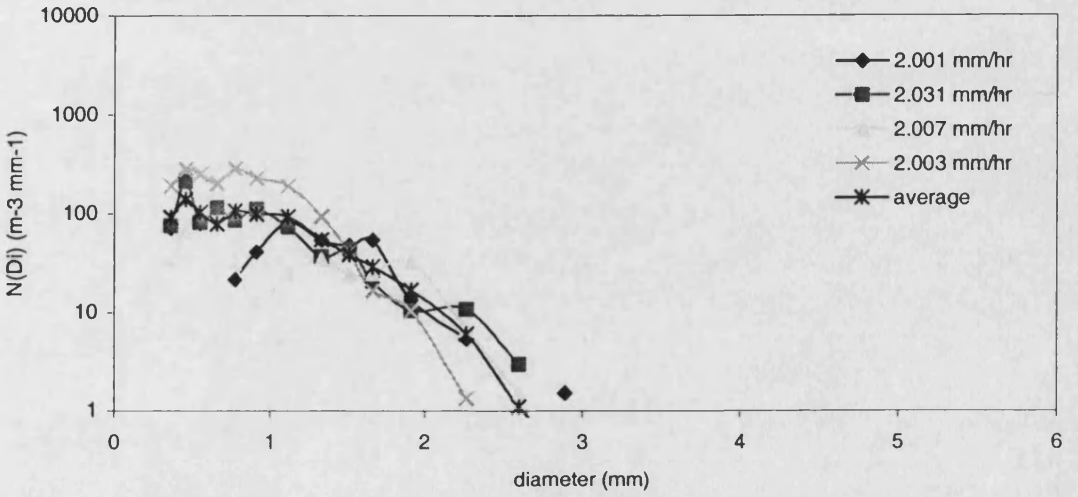

Figure 6.8.c: Measured distributions for stratiform rainfall rates at ~ 2.0 mm hr^{-1}

It appears that $N(D_i)$ shape for rainfall rate below 5 mm hr^{-1} is not that uniform. The shapes of the drop size distribution curves for such rates seem not very alike to one another. We encountered several measurements where there were only several big drops within one minute integration time and disregard such cases. Such deviation denotes that it is difficult to predict the behaviour of drop size distribution at lower rainfall rates. In general, we observed that from these figures, the shape of the raindrop size distribution under the same curve for rain intensity higher than 5 mm hr^{-1} exhibit almost similar tendency. The trend is such as that the $N(D_i)$ increases with the drop diameter until it reaches the peak and then $N(D_i)$ decrease gradually.

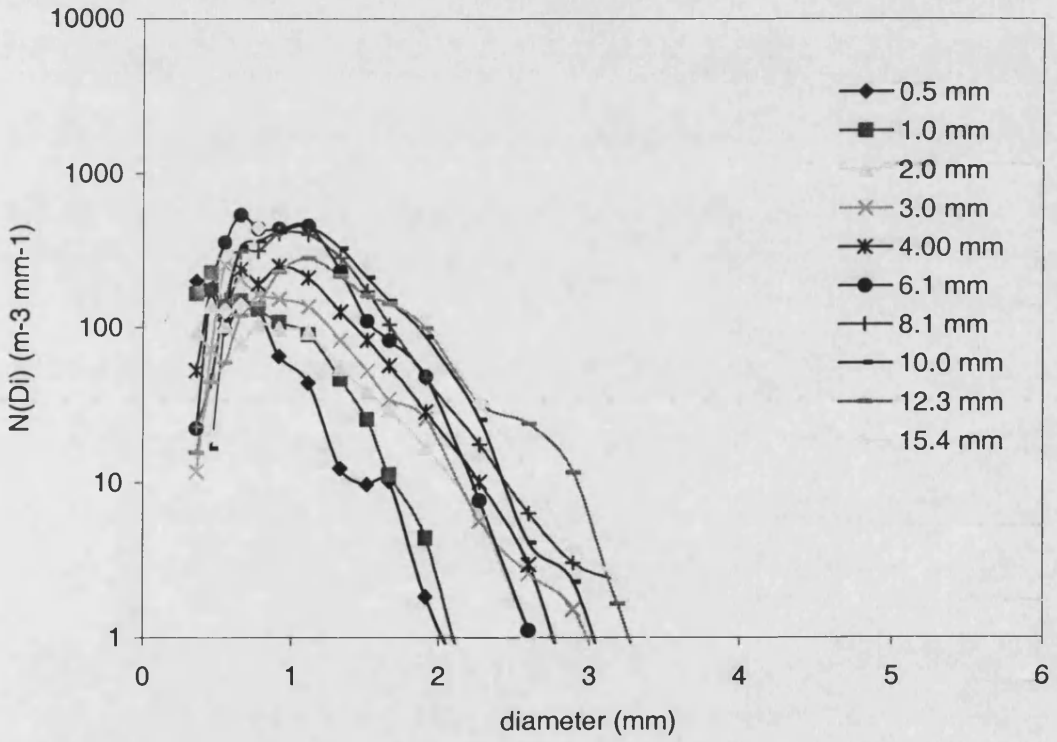

Figure 6.9: Drop size distribution for various rainfall rates during stratiform events

Figure 6.9 above illustrates the average $N(D_i)$ for each selected rainfall rate obtained from the figures. We can make further assessments on the rainfall characteristics by comparing the plot of ten different rainfall rates in one graph. The data enable us to investigate the dynamic range of $N(D_i)$ for the selected rainfall rates. We noticed the increase of the maximum diameter of the raindrop values as the rainfall rate

increases. In Figure 6.9, the maximum diameter detected for 3 mm hr^{-1} is at about 3.19 mm and for 15.4 mm hr^{-1}, it is at 4.39 mm. We include our findings in Table 6.4 below. Slight increase in the dynamic range as the rainfall rate increases can be observed. This may suggests that the higher rainfall intensity is dependent on the large raindrops than small ones.

We expressed Figure 6.9 in several different ways to assess the variation of the diameter corresponding to the peak of $N(D_i)$ as the rain rate increases. The diameter corresponding to the peak of $N(D_i)$ is identified as mode diameter D_m. Using linear scale representation of $N(D_i)$ and logarithmic scale of D, the divergence of D_m can be clearly observed more easily. It can be seen in Figure 6.10 that for rainfall smaller than 8.1 mm hr^{-1}, the mode diameter is less than 1 mm. While for rainfall rates of 10 mm hr^{-1} and higher, the mode diameter is around 1.11 mm. We listed the average mode diameters in Table 6.4. It seems that the mode diameter variation for stratiform rain events is not large.

Rainfall rate (mm hr^{-1})	Mode diameter D_m (mm)	Dynamic range (mm)	
		D_{imin}	D_{imax}
0.5	Not detected	0.3590	2.2690
1.0	0.4550	0.3590	2.5995
2.0	0.4550	0.3590	2.2815
3.0	0.4550	0.3590	3.1885
4.0	0.9135	0.3590	3.5410
6.1	1.1135	0.3590	3.5410
8.1	0.9135	0.3590	3.5410
10.0	1.1135	0.4450	3.5410
12.3	1.1135	0.3590	3.9440
15.4	1.1135	0.4450	4.3850

Table 6.4: Mode diameter and dynamic range for stratiform rainfall rates

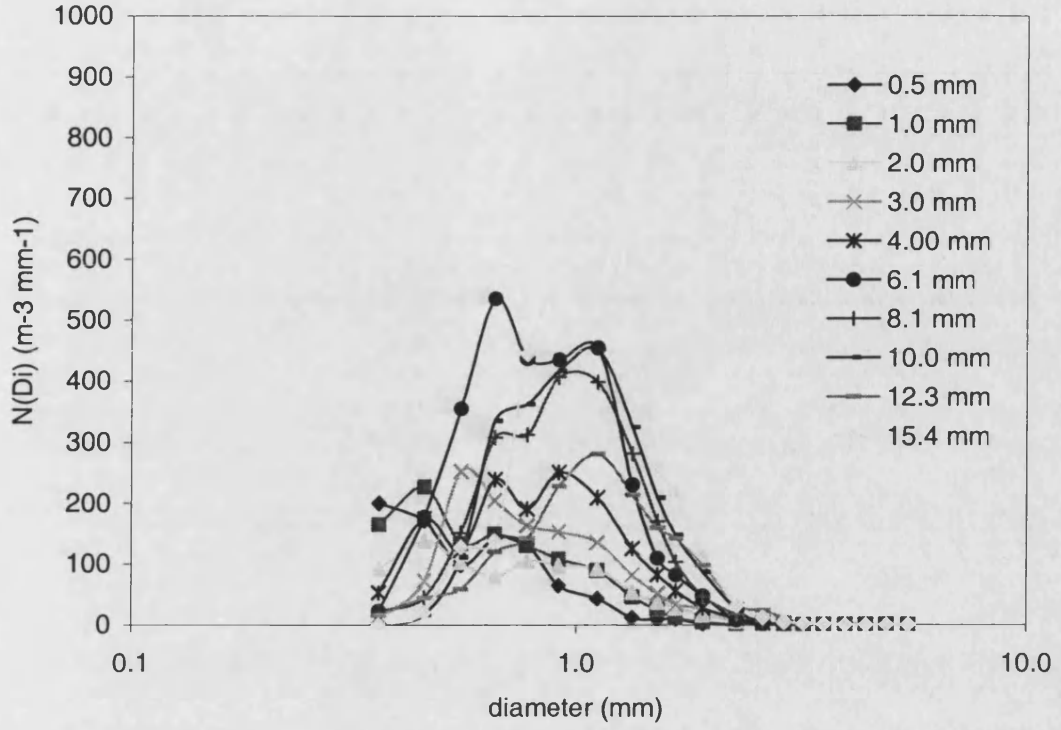

Figure 6.10: Drop size distribution for various rainfall rates during stratiform events with logarithmic scale x-axis and linear scale y-axis

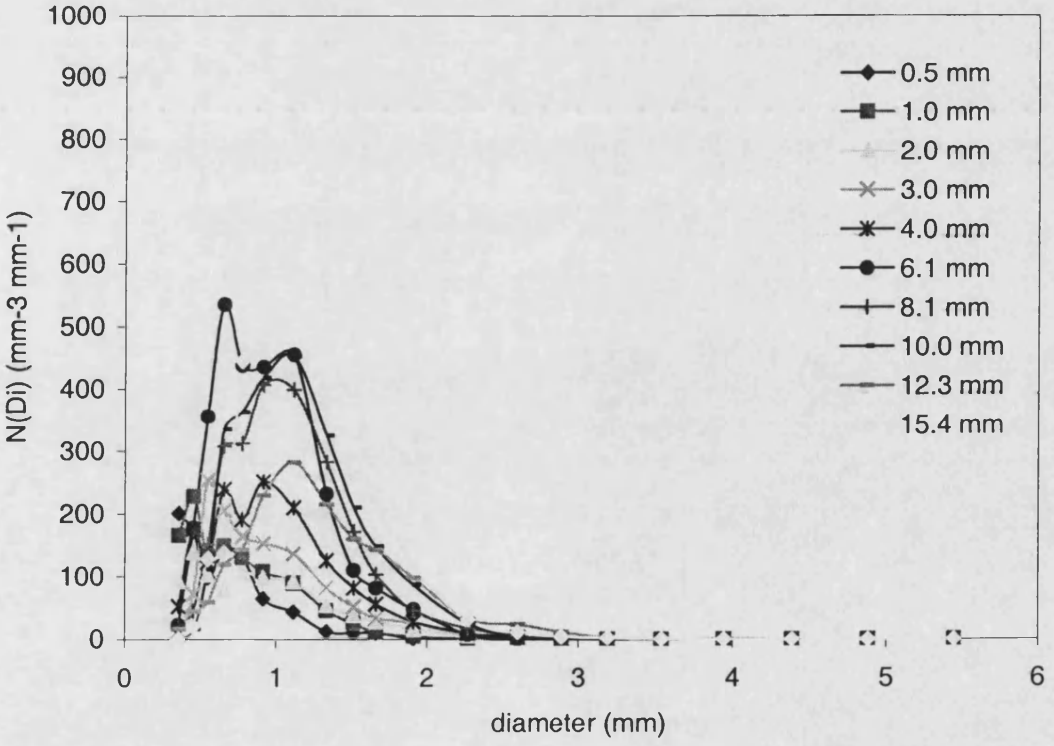

Figure 6.11: Drop size distribution for selected rainfall rates during stratiform events plotted with linear scale on both axes

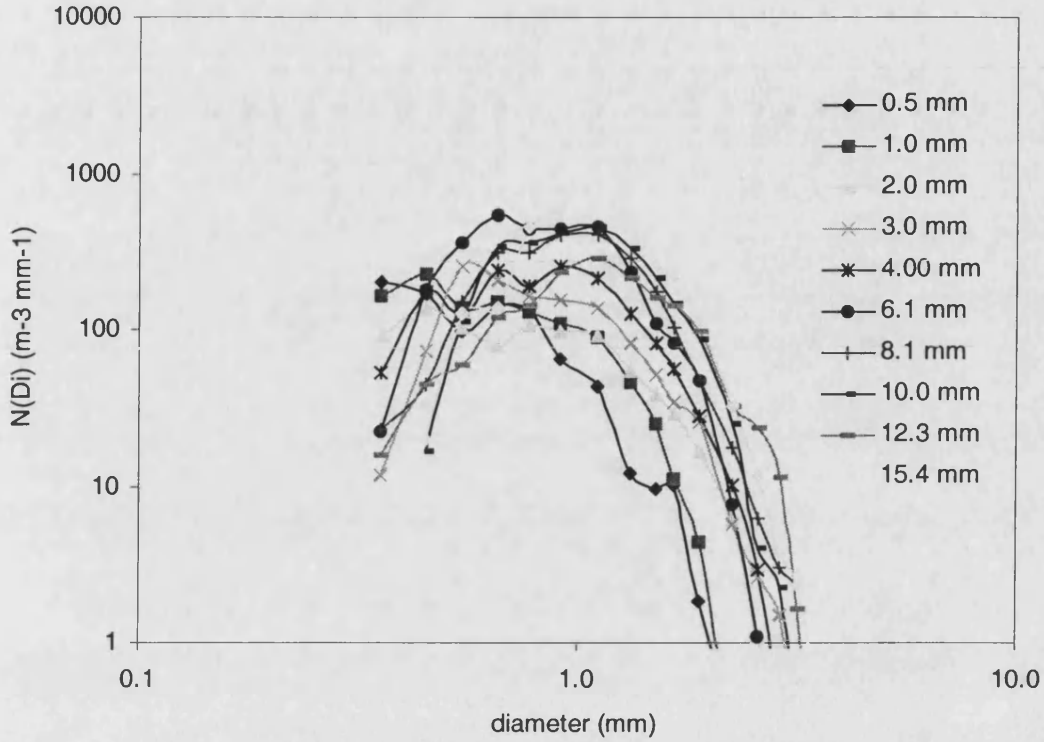

Figure 6.12: Drop size distribution for selected rainfall rates during stratiform events plotted with logarithmic scale on both axes.

We redrawn Figure 6.9 in order to observe the result from different perspectives. In Figure 6.11, we drew the distribution using linear scale for its horizontal and vertical axes. Where as for Figure 6.12 the axes shown are represented using the logarithmic axis scale. These figures then can be compared with available general statistical distribution models.

6.5.2 Convective Events

This is the section where we present the findings from the analyses of the measured convective events' rain drop size distribution. We repeated the same assessments as previously conducted for stratiform events. In our investigation, we tried our best to accumulate drop size distribution data at approximately the same rainfall rate for each event classification in order to make the statistics to be reliable. It was a difficult task to obtain the exact rainfall rate from different events when processing the

convective samples from our datafiles. We tried to obtain at least 3 sets of data with approximately the same rainfall rate for every selected rainfall rate of interest.

Figures 6.13 (a) through (c) are the first three drawings of measured drop size distributions for 10 selected rainfall rates during convective events. We included the remaining seven in Appendix B. Three distributions are plotted for each selected rainfall rate and the mean was determined. The figures show almost similar observations to those gathered from the analyses of stratiform events. It is more perceptible from these figures that the $N(D_i)$ increases with drop diameter D until reaches the peak, then the $N(D_i)$ decreases gradually with D.

We combined the 'average' distributions in one graph labelled as Figure 6.14. The curves showed almost similar tendencies as to Figure 6.9. Because of the wider selection of rainfall rates range involved, it is more visible from the from Figure 6.14 graph that the $N(D_i)$ increases as the rainfall becomes heavier. This clearly supports the suggestion that heavy rainfall is much more dependent on large raindrops than small ones. We also investigated the mode diameter D_m of drops during convection events. The variation of the mode diameters of raindrop detected for rain intensities during convective rain events is not large. We list the mode diameters and the dynamic range for the convective events' rainfall rates in Table 6.5 for comparison. Figure 6.14 is also redrawn using various combination scales of axis.

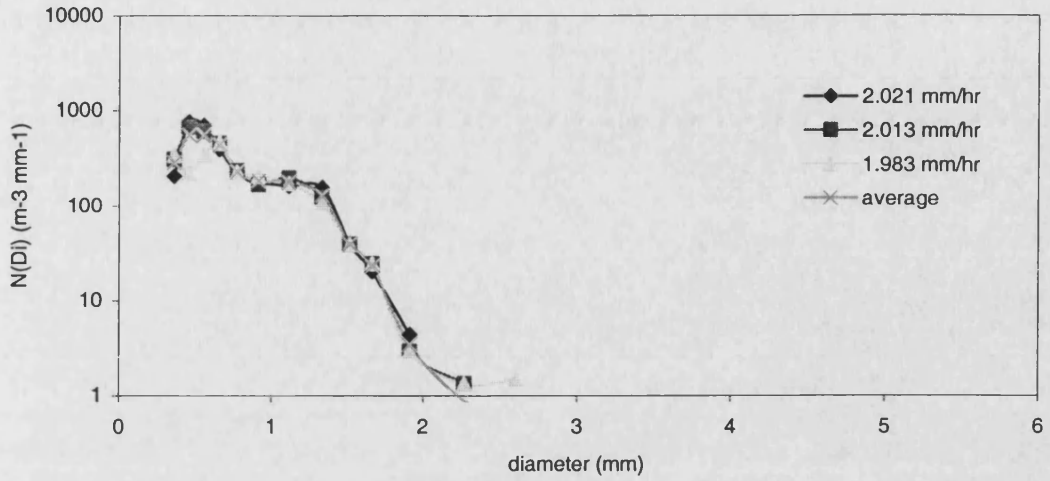

Figure 6.13.a: Measured distributions for convective rainfall rates at ~ 2.0 mm hr^{-1}

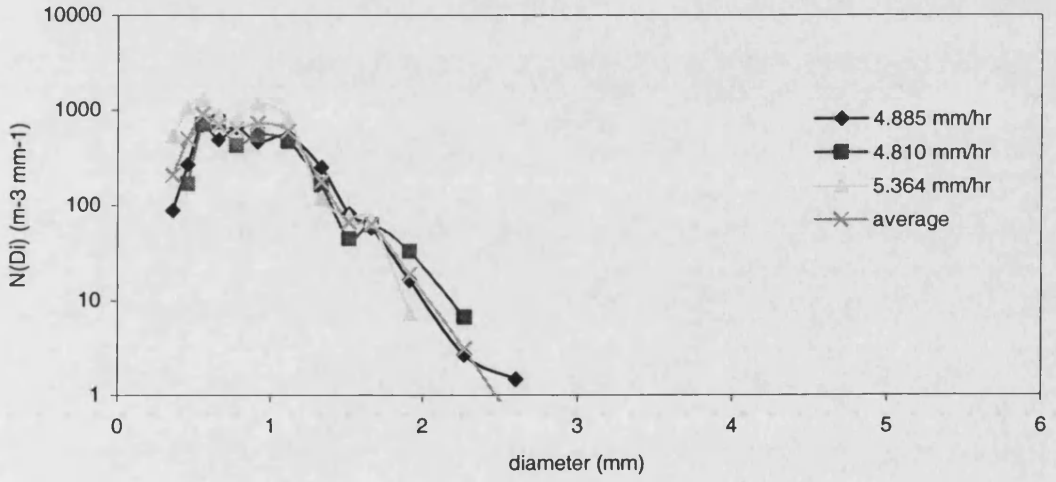

Figure 6.13.b: Measured distributions for convective rainfall rates at ~ 5.0 mm hr^{-1}

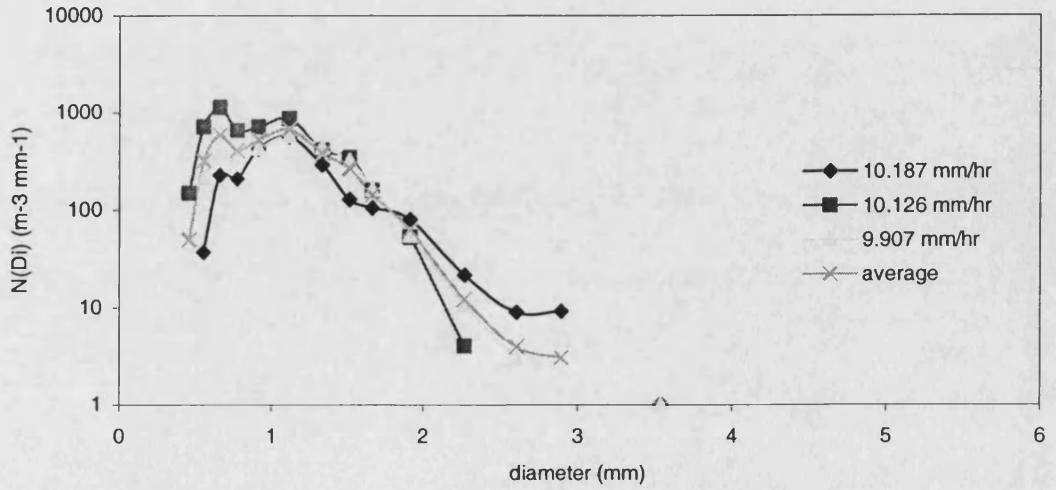

Figure 6.13.c: Measured distributions for convective rainfall rates at ~ 10.0 mm hr^{-1}

Rainfall rate (mm hr^{-1})	Mode diameter D_m (mm)	Dynamic range (mm)	
		D_{imin}	D_{imax}
0.5	0.5495	0.3590	2.5995
1.0	0.5495	0.3590	3.5410
2.0	1.1135	0.3590	2.5995
3.0	1.1135	0.7740	3.9440
4.0	1.1135	0.6565	3.5410
6.1	1.3315	0.7740	4.3850
8.1	1.3315	0.7740	5.4470
10.0	1.5130	0.9135	4.8820
12.3	1.6625	1.1135	5.4470
15.4	1.6625	0.9135	4.8820

Table 6.5: Mode diameter and dynamic range for convective rainfall rates

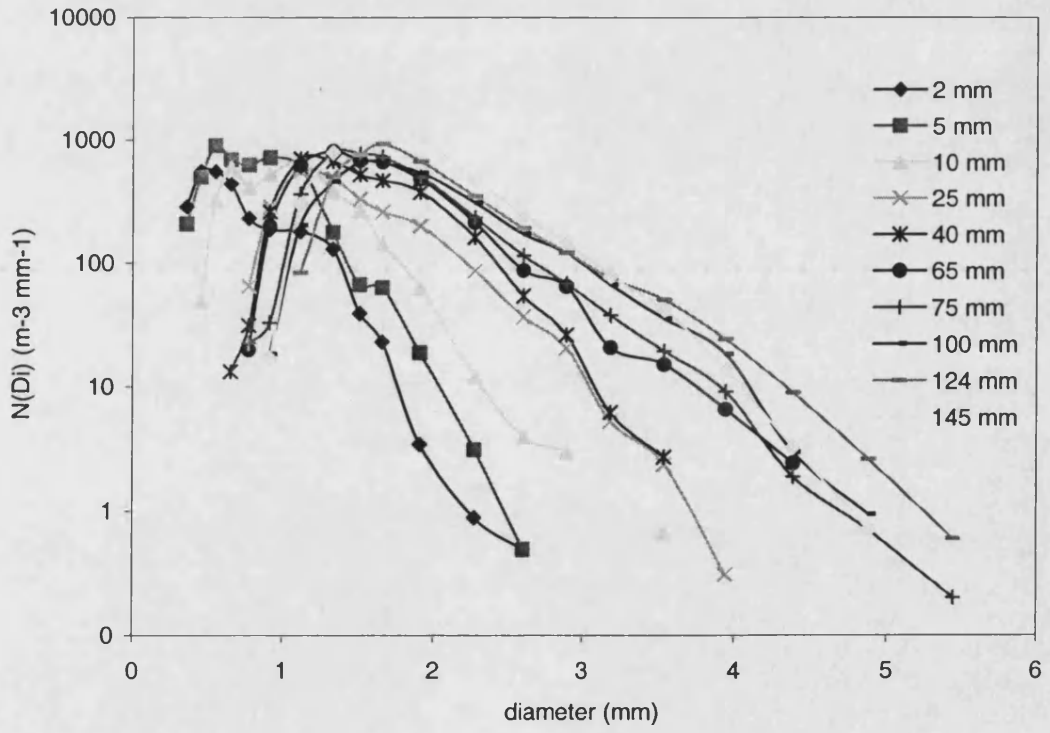

Figure 6.14: Distribution for various rainfall rates during convective events

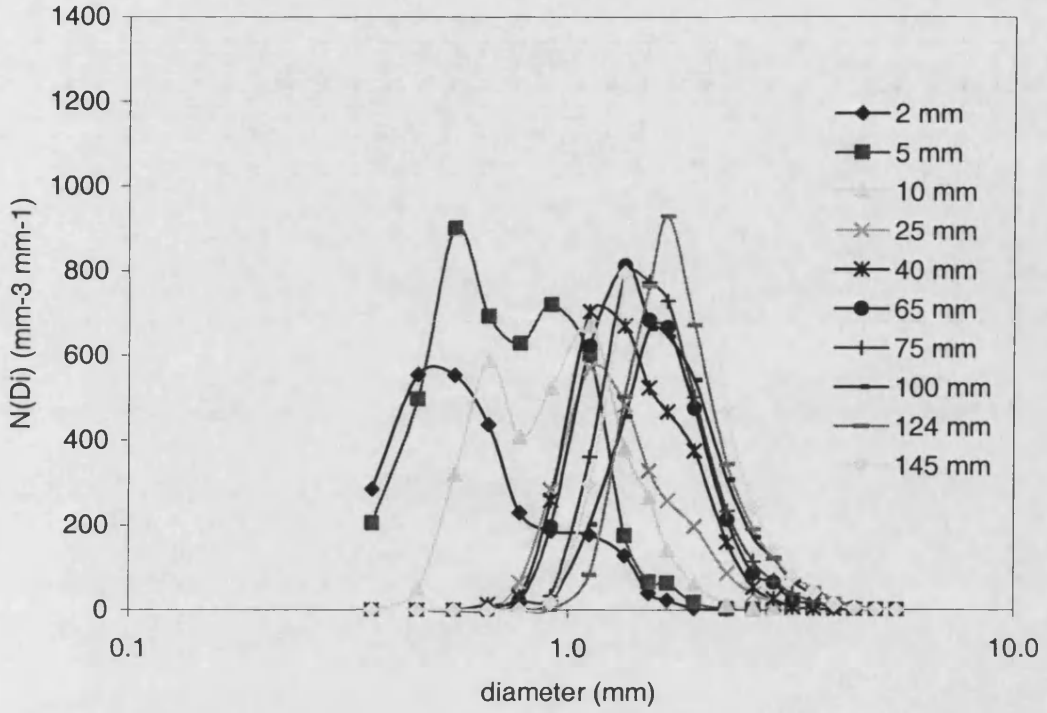

Figure 6.15: Drop size distribution for various rainfall rates during convective events plotted with logarithmic scale x-axis and linear scale y-axis

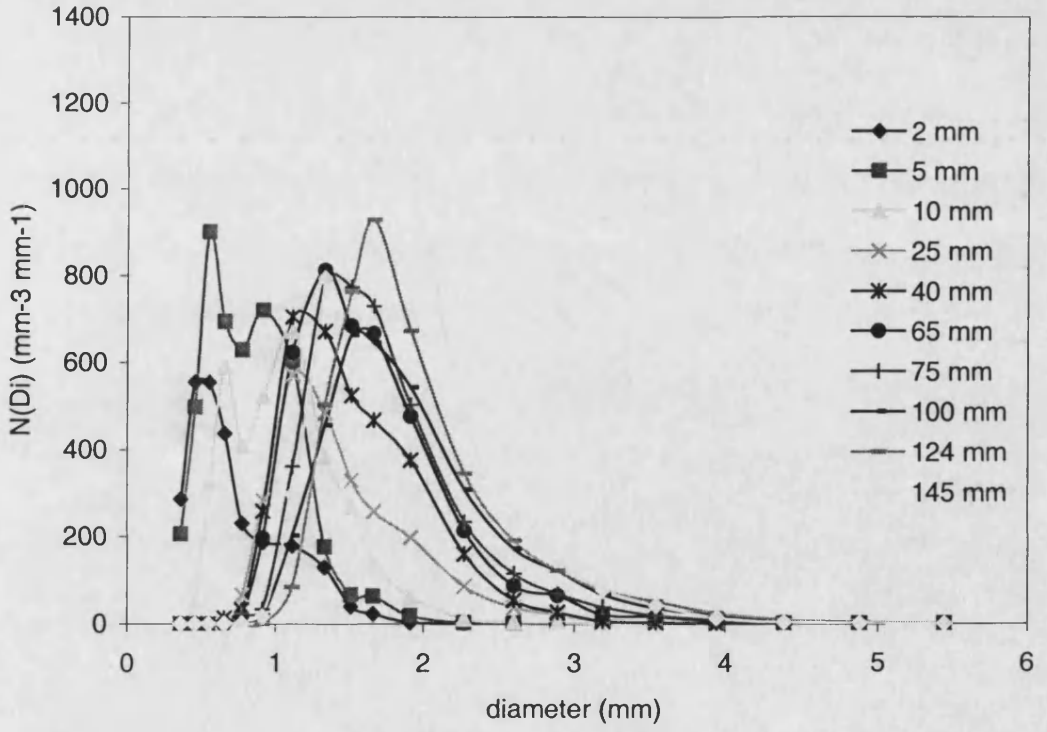

Figure 6.16: Drop size distribution for various rainfall rates during convective events plotted with linear scale on both axes

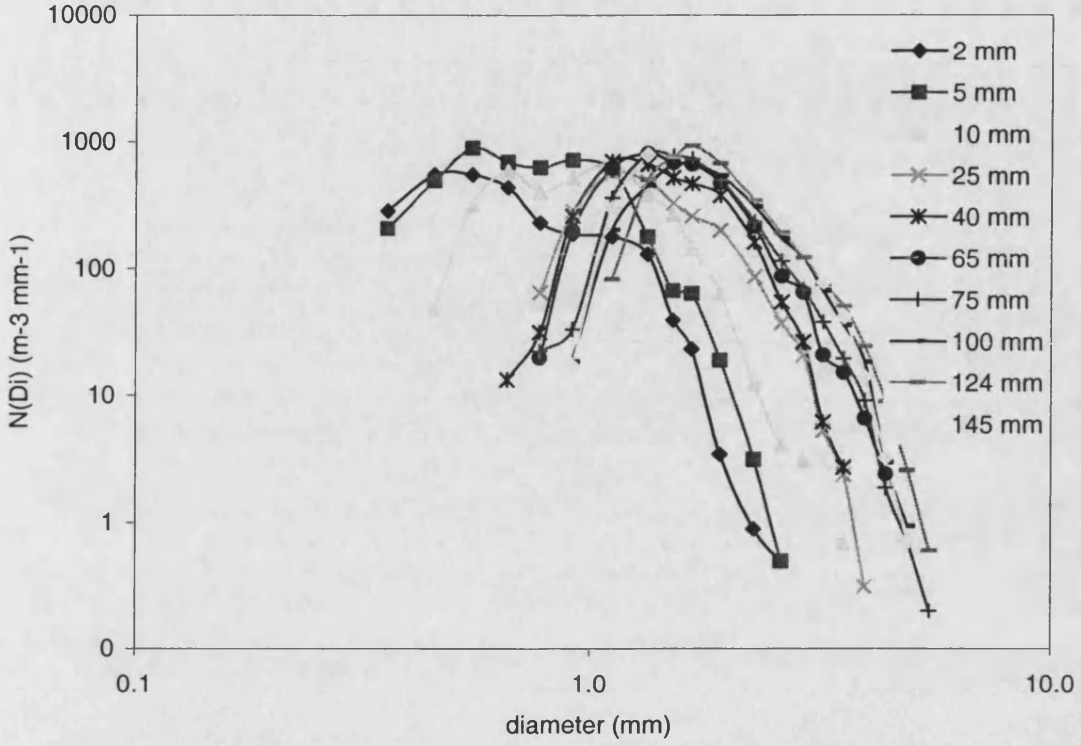

Figure 6.17: Drop size distribution for various rainfall rates during convective events plotted with logarithmic scale on both axes

6.6 Assessment Summary

From the 6 months data, various rain intensities were measured and recorded by the RAL's distrometer. PNG experiences equatorial climate where rain is copious throughout out the year with no apparent dry month. Very high rainfall rates were encountered where rainfall rate of approximately 180 mm hr^{-1} that lasted for more than 1 minute was recorded.

Analyses of stratiform rain cover 10 selected rainfall rates of interest ranging from 0.5 to 15.4 mm hr^{-1}. Samples were taken from more than 20 separate events for the study. 10 rainfall rates ranging from around 2.0 to 150 mm hr^{-1} were selected for the analyses of convective events. We obtained measurement data from 15 individual events. The recorded raw data number of drops $n(D_i)$ were processed using Microsoft Excel 97 to obtain the measured drop size distribution by considering the drop

There are very limited literatures that offer detail and systematic procedures on how to model the drop size distribution. In our analyses, we adapted the procedures employed by investigators [Ong and Shan, 1997, Shan 1996, Ajayi and Olsen, 1983] in their modelling attempt. The derivations of the general calculation and equations those are suitable to be applied for our measured data were obtained from their publications.

Our modelling attempt initiated with the selection of suitable statistical models for the measured drop size distribution analyses then followed by the estimations of the parameters for every models. We calculated the parameters for the proposed distribution models using the method of maximum likelihood and/or method of moments where applicable.

6.8 Selection of Models

The plots of the rain drop size distribution in previous section for both stratiform and convective events dismiss the possibility that they can be represented by either the exponential or Gaussian distributions. Observed from the Figure 6.9 and 6.14, the exponential distribution is clearly inappropriate because of the projection of the distribution curve for each rainfall rates. Is also not possible to model the drop size with Gaussian distribution considering the distribution curve is not symmetry.

Apart from the exponential and Gaussion distributions, other types of distribution have also been used by investigators in their studies to model the rain drop size distribution. Other known models are identified as the lognormal, shifted-lognormal, Weibull and gamma. It is not possible to distinguishing between them simply by observing the plots of the measured rain drop size distribution in the previous section. In most literature, two types of models that are popularly nominated for describing the rain drop size distribution are the three-parameter lognormal and the gamma models.

The three-parameter distribution models are considered more flexible than two-parameter models in accounting for a wide variability in drop sizes detected in the tropics [Maitra, 2000]. In our analyses, we selected both functions are as possible models to represent the tropical rain drop size distribution in PNG.

6.9 Modelling Approach

In our analyses, we tried to determine the most appropriate functions that can represent the raindrop size distribution for stratiform and convective rain in the Papua New Guinea. We concentrated the modelling of the PNG rain drop size distribution using measured data presented in section 6.5. Brief introduction to the selected distribution models in presented the next sections. The special equations suitable for processing the measured 20-channel data recorded by the distrometer in PNG data are reproduced in the next section for convenience. These equations enable us to estimate the parameters of the lognormal function using the method of maximum likelihood and the method of moments. The maximum likelihood estimators for the gamma function do not exist and therefore we can only estimated the parameter for the gamma function using the method of moments. For both types of rain, the distribution models for PNG are first established for each rainfall rate. Afterwards, the general models suitable for all rainfall rates are determined by least-square fitting method.

6.9.1 Lognormal Model

The lognormal distribution occurs in practice whenever we encounter a random variable that is such that its logarithm has a normal distribution. Its probability density is commonly expressed as [Miller and Freund, 1985]:

$$f(x) = \frac{1}{\sqrt{2\pi}\beta} x^{-1} e^{-(\ln x - a)^2 / 2\beta^2} \qquad (6.6)$$

where ln x is the natural logarithm of x. The three-parameter lognormal function proposed for our rain drop distribution is structured as [Vilar *et al.*, 1997; Montanari *et al.*, 1996]

$$N(D) = \frac{N_t}{\sigma D\sqrt{2\pi}} \exp\left[\frac{-(\ln(D)-\mu)^2}{2\sigma^2}\right] \tag{6.7}$$

where $N(D)$ is the drop size distribution, D is the drop diameter, N_t is the total number of drops per cubic metre, σ is the standard deviation of ln D and μ is the mean of ln D. The mean of D and variance of D can be expressed as:

$$E[D] = e^{\mu+\frac{\sigma^2}{2}} \tag{6.8}$$

$$Var[D] = e^{2\mu+\sigma^2}(e^{\sigma^2}-1)$$

$$= e^{E^2[D]}(e^{\sigma^2}-1) \tag{6.9}$$

The relationships between N_t, μ, σ and rainfall rate R can be any form i.e. polynomial or exponential. Proposed in previously published papers, the parameters N_t, σ and μ are related to the rainfall rate R with such expression such as:

$$N_t = \alpha R^{\beta}$$

$$\mu = A_\mu + B_\mu \ln R \tag{6.10}$$

$$\sigma^2 = A_\sigma + B_\sigma \ln R$$

6.9.2 Gamma Model

The three-parameter gamma distribution model of interest is given as

$$N(D) = \Lambda_1 D^p e^{-\Lambda_2 D} \tag{6.11}$$

Researchers assumed that parameters had power law relationships with rainfall rates [Ajayi and olsen, 1983; Gloaguen and Lavergnat, 1995] The parameters Λ_2, Λ_1 and p are associated to the rainfall rate R with equations below.

$$\Lambda_1 = \alpha_1 R^{-\beta_1}$$

$$\Lambda_2 = \alpha_2 R^{-\beta_2} \tag{6.12}$$

$$p = \alpha_p R^{-\beta_p}$$

6.10 Models for Each Rainfall Rate

The parameters for both lognormal and gamma models are determined using the special equations described in Appendix C. The parameters of the lognormal and gamma model for 10 selected rainfall rates ranging from 0.5 to 15.4 mm hr^{-1} in stratiform rain are listed in Table 6.6 and Table 6.7, respectively. We listed the parameters for the models calculated for 10 individual rainfall rates from 2 to 145 mm hr^{-1} in convective rain in Table 6.8 and 6.9.

The LN-li column in the table is for parameters N_t, μ. and σ^2 for lognormal model that are estimated by employing the method of maximum likelihood. LN-m12, LN-m23, LN-m56, LN-m36 columns are the four solutions for parameters of the lognormal model calculated by method of moments. The notation LN-m12 is for solution calculated using combination of the 1st and 2nd moment, same labelling applies for other notations as well. Combinations of the moments are selected because of their physical significance. Moment 2 is proportional to the optical extinction coefficient, moment 3 is proportional to the liquid water content and moment 6 is the reflectivity factor.

		LN-li		LN-m_{12}		LN-m_{23}		LN-m_{56}		LN-m_{36}	
RR (mm hr^{-1})	Nt/M_0	μ	σ^2	μ	σ^2	μ	σ^2	μ	σ^2	μ	σ^2
0.5	103.9	-0.44380	0.17435	-0.44552	0.18308	-0.43969	0.17725	-0.35157	0.13420	-0.39865	0.14989
1.0	138.4	-0.32557	0.19442	-0.31985	0.18199	-0.30075	0.16289	-0.21099	0.11621	-0.25047	0.12937
2.0	120.5	-0.14588	0.23596	-0.13403	0.20478	-0.10610	0.17685	0.01848	0.11261	-0.03794	0.13142
3.0	173.9	-0.08664	0.16794	-0.08716	0.17245	-0.08050	0.16579	-0.00249	0.12732	-0.04310	0.14086
4.0	236.4	-0.06165	0.17134	-0.05594	0.15511	-0.04362	0.14279	0.02818	0.10676	-0.00732	0.11859
6.1	441.4	-0.06921	0.13243	-0.06727	0.12751	-0.06171	0.12196	-0.03050	0.10595	-0.04489	0.11075
8.1	379.4	0.05170	0.12512	0.05216	0.12336	0.05214	0.12338	0.06440	0.11822	0.05536	0.12123
10.0	430.6	0.09893	0.11543	0.10009	0.11281	0.10454	0.10836	0.14376	0.08899	0.12344	0.09576
12.3	292.4	0.21235	0.15393	0.21640	0.14143	0.22390	0.13392	0.26480	0.11324	0.24504	0.11983
15.4	613.3	0.14577	0.09194	0.14452	0.09528	0.14146	0.09834	0.13706	0.10137	0.13677	0.10146

Table 6.6: Parameters for the lognormal function derived for each stratiform rainfall rate

	ga_{1210}			ga_{2310}			Ga_{2320}			ga_{5610}			ga_{5650}		
RR (mm hr^{-1})	p	Λ^2	Λ^1	P	Λ^2	Λ^1	P	Λ^2	Λ^1	p	Λ^2	Λ^1	p	Λ^2	Λ^1
0.5	3.97719	7.09114	76821.3	3.25077	6.22933	28011.6	3.25077	6.22933	28689.5	4.29394	6.99390	100146.2	4.29394	6.99390	-52761.1
1.0	4.01000	6.29837	57363.4	4.03423	6.32376	59190.4	4.03423	6.32376	59155.3	5.33339	7.38597	293552.7	5.33339	7.38597	143045.3
2.0	3.40030	4.54173	9267.7	3.65265	4.75396	17255.1	3.65265	4.75396	10965.3	7.41257	7.08768	-24501.9	7.41257	7.08768	92601.6
3.0	4.31324	5.31820	32122.0	3.66881	4.77534	729.0	3.66881	4.77534	20193.6	4.49590	5.22370	-528.6	4.49590	5.22370	24987.8
4.0	4.95990	5.83247	77365.8	4.83036	5.72392	80659.3	4.83036	5.72392	69891.0	6.51089	6.76163	41839.4	6.51089	6.76163	170216.5
6.1	6.35305	7.37891	756187.8	5.90057	6.97919	152587.2	5.90057	6.97919	526770.1	4.80300	6.21900	10842.6	4.80300	6.21900	248293.1
8.1	6.61695	6.79739	352824.5	5.61466	6.00675	180541.4	5.61466	6.00675	160939.8	3.55616	4.67674	-159100.4	3.55616	4.67674	45240.0
10.0	7.37392	7.16082	575114.3	6.93074	6.82227	420692.4	6.93074	6.82227	410498.4	7.78239	7.31697	559571.1	7.78239	7.31697	613416.7
12.3	5.58245	4.93967	32251.0	5.19325	4.68611	25775.6	5.19325	4.68611	25334.1	4.46271	4.30671	21398.3	4.46271	4.30671	18888.0
15.4	9.00333	8.25451	2480874.9	7.52204	7.14327	866853.9	7.52204	7.14327	823353.5	4.51983	5.25240	447065.6	4.51983	5.25240	144633.5

Table 6.7: Parameters for the gamma function derived for each stratiform rainfall rate.

		LN-li		LN-m_{12}		LN-m_{23}		LN-m_{56}		LN-m_{36}	
RR (mm hr^{-1})	Nt/M_0	μ	σ^2	μ	σ^2	μ	σ^2	μ	σ^2	μ	σ^2
2.0	321.2	-0.35823	0.17265	-0.35719	0.17448	-0.34339	0.16067	-0.25278	0.11388	-0.29362	0.12749
5.0	628.4	-0.21042	0.13504	-0.20657	0.12425	-0.19868	0.11636	-0.16781	0.10039	-0.18164	0.10500
10.1	564.3	0.02755	0.11490	0.02904	0.11071	0.03154	0.10822	0.02701	0.10981	0.03127	0.10839
24.8	495.6	0.33821	0.08715	0.33554	0.09588	0.33297	0.09845	0.35125	0.09037	0.33892	0.09448
40.0	715.9	0.39132	0.08111	0.39084	0.08318	0.39174	0.08228	0.41113	0.07292	0.40042	0.07649
64.9	854.7	0.45558	0.08634	0.45275	0.09498	0.44787	0.09987	0.44326	0.10338	0.44194	0.10382
74.8	820.5	0.51897	0.07769	0.51547	0.08809	0.50877	0.09478	0.49359	0.10365	0.49736	0.10240
99.8	772.5	0.61773	0.08328	0.61567	0.08978	0.61310	0.09235	0.62607	0.08696	0.61631	0.09021
124.1	887.1	0.64258	0.07477	0.63818	0.08797	0.63039	0.09575	0.62572	0.09997	0.62240	0.10108
144.8	1349.7	0.59038	0.06651	0.58799	0.07362	0.58341	0.07820	0.57424	0.08373	0.57600	0.08314

Table 6.8: Parameters for lognormal function derived for each convective rainfall rate.

	ga_{1210}			ga_{2310}			ga_{2320}			ga_{5610}			ga_{5650}		
RR (mm hr^{-1})	p	Λ^2	Λ^1	p	Λ^2	Λ^1	P	Λ^2	Λ^1	p	Λ^2	Λ^1	p	Λ^2	Λ^1
2.0	4.24599	6.87176	225999.5	4.01609	6.61882	167146.7	4.01609	6.61882	168296.5	5.68658	8.04368	1265648.9	5.68658	8.04368	419225.2
5.0	6.55863	8.73325	3894143.3	6.40522	8.57672	3241112.7	6.40522	8.57672	3247657.6	5.42337	7.77830	1020068.6	5.42337	7.77830	1766446.2
10.1	7.54159	7.85028	1623339.0	6.85764	7.28756	1005492.1	6.85764	7.28756	927571.3	3.33672	4.96774	-43935.0	3.33672	4.96774	113419.4
24.8	8.93815	6.77274	283129.3	7.53498	5.90392	131402.8	7.53498	5.90392	128588.0	6.85089	5.50209	94556.3	6.85089	5.50209	88793.1
40.0	10.52966	7.48194	669125.5	9.72669	7.00246	443435.3	9.72669	7.00246	440202.1	9.77335	7.00145	429379.3	9.77335	7.00145	423957.9
64.9	9.03599	6.08565	161473.5	7.28304	5.11900	74953.8	7.28304	5.11900	73447.1	4.43946	3.79521	38147.6	4.43946	3.79521	32522.5
74.8	9.85958	6.20610	127939.8	7.69853	5.07523	55489.9	7.69853	5.07523	54426.1	4.09833	3.48577	27774.9	4.09833	3.48577	23579.6
99.8	9.64549	5.49903	37008.4	8.18741	4.81052	24383.2	8.18741	4.81052	24134.3	7.14852	4.35775	19752.6	7.14852	4.35775	19118.0
124.1	9.87517	5.49765	36724.2	7.54360	4.41824	19692.6	7.54360	4.41824	19365.9	5.00797	3.39751	14419.4	5.00797	3.39751	13476.5
144.8	12.08938	7.00764	262851.1	9.93032	5.93379	128060.8	9.93032	5.93379	126636.4	6.48257	4.43533	65308.0	6.48257	4.43533	61839.9

Table 6.9: Parameters for gamma function derived for each convective rainfall rate.

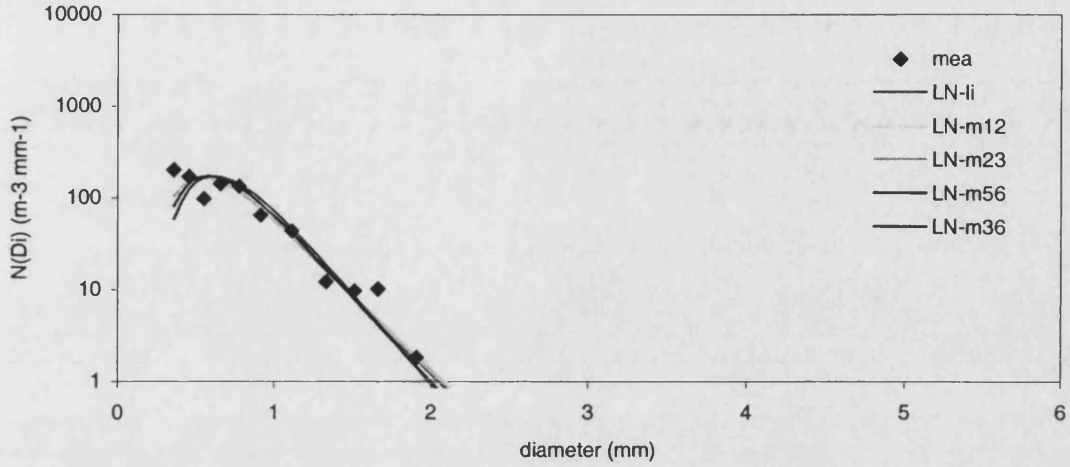

Figure 6.18.a: Comparison between various lognormal distributions with measured data distribution for stratiform rainfall rate of 0.5 mm hr^{-1}.

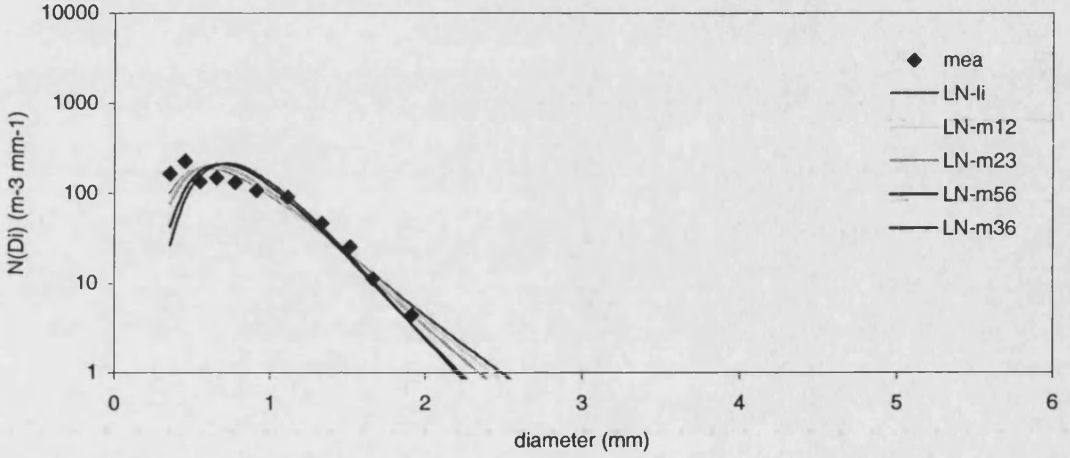

Figure 6.18.b: Comparison between various lognormal distributions with measured data distribution for stratiform rainfall rate of 1.0 mm hr^{-1}.

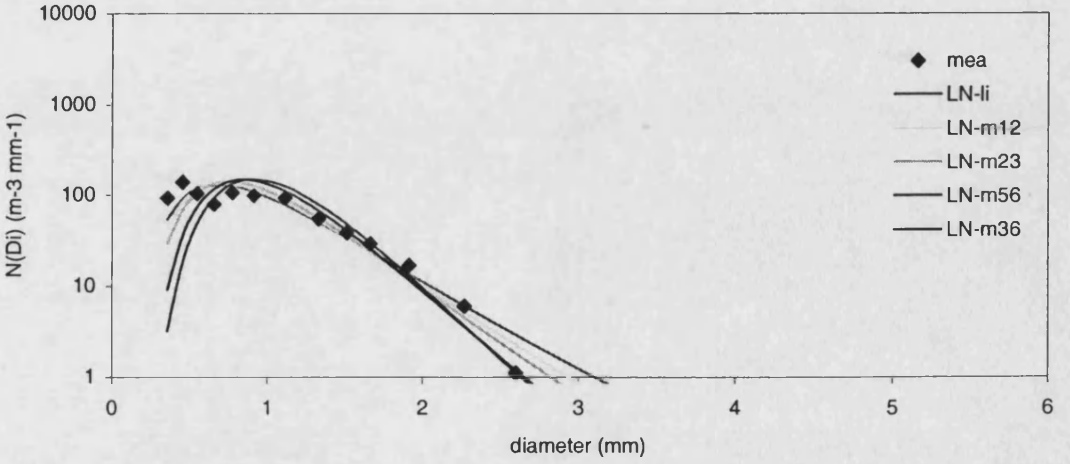

Figure 6.18.c: Comparison between various lognormal distributions with measured data distribution for stratiform rainfall rate of 2.0 mm hr^{-1}

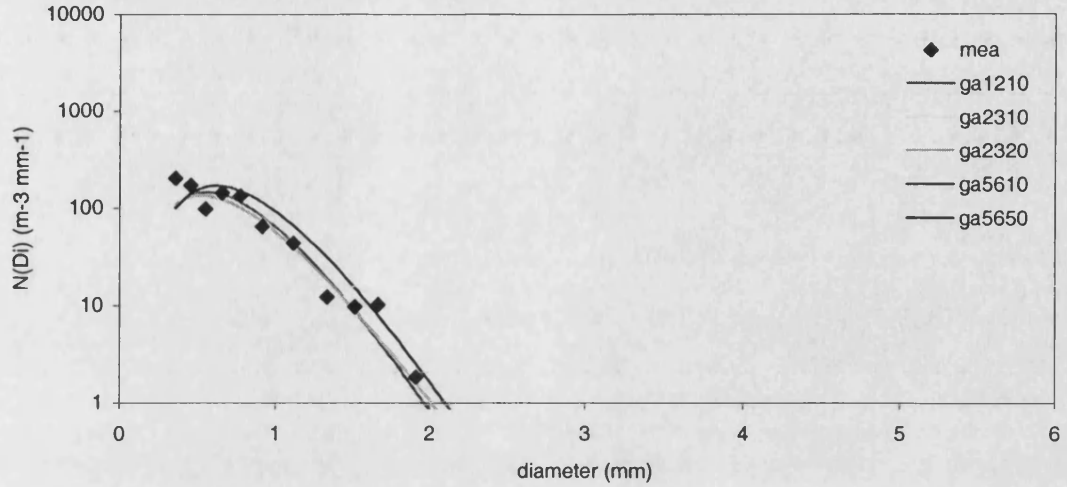

Figure 6.19.a: Comparison between various gamma distributions with measured data distribution for stratiform rainfall rate of 0.5 mm hr^{-1}.

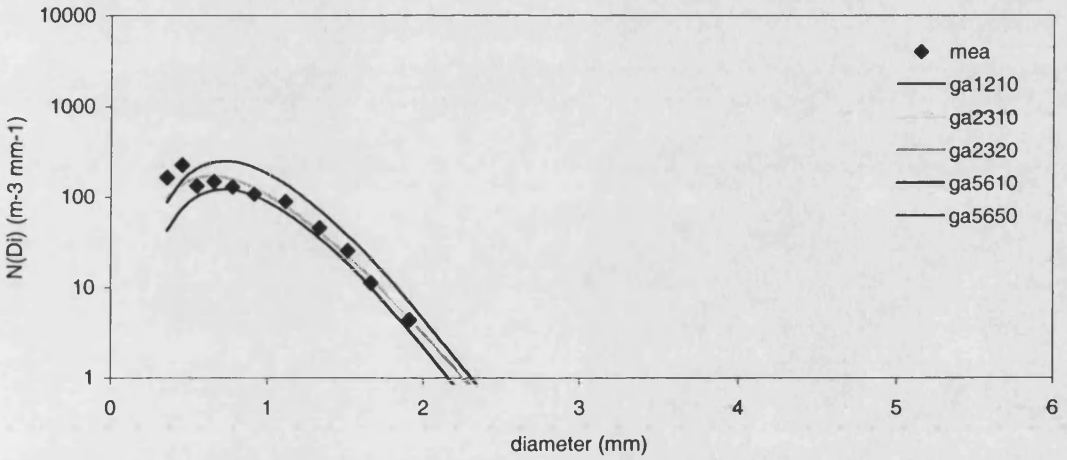

Figure 6.19.b: Comparison between various gamma distributions with measured data distribution for stratiform rainfall rate of 1.0 mm hr^{-1}.

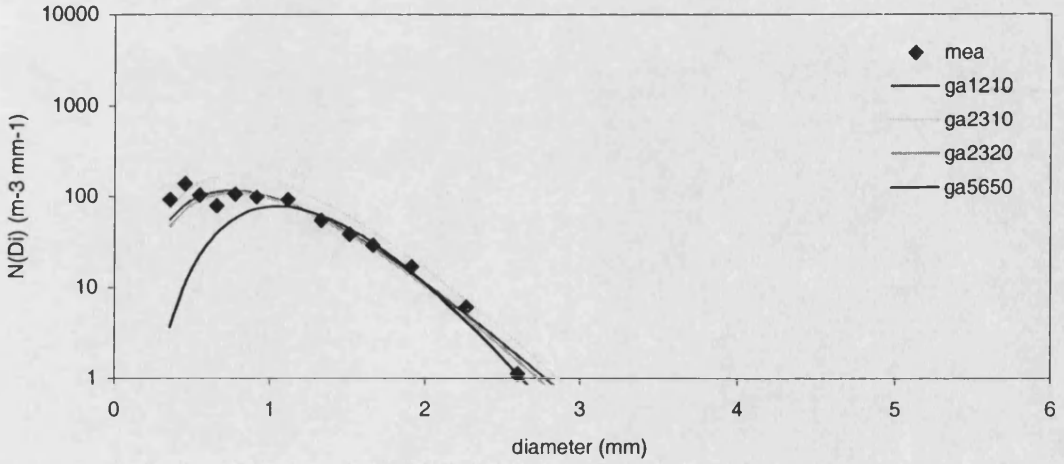

Figure 6.19.c: Comparison between various gamma distributions with measured data distribution for stratiform rainfall rate of 2.0 mm hr^{-1}.

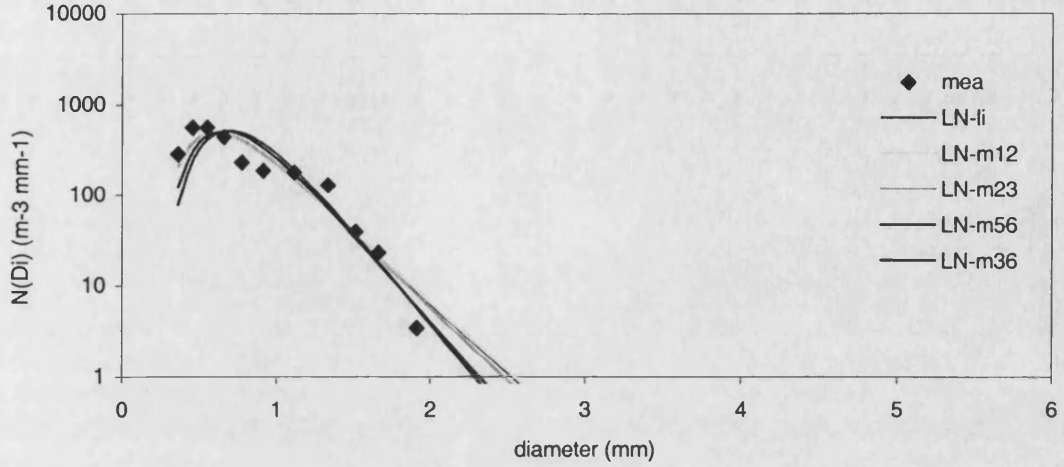

Figure 6.20.a: Comparison between various lognormal distributions with measured data distribution for convective rainfall rate of 2.0 mm hr^{-1}

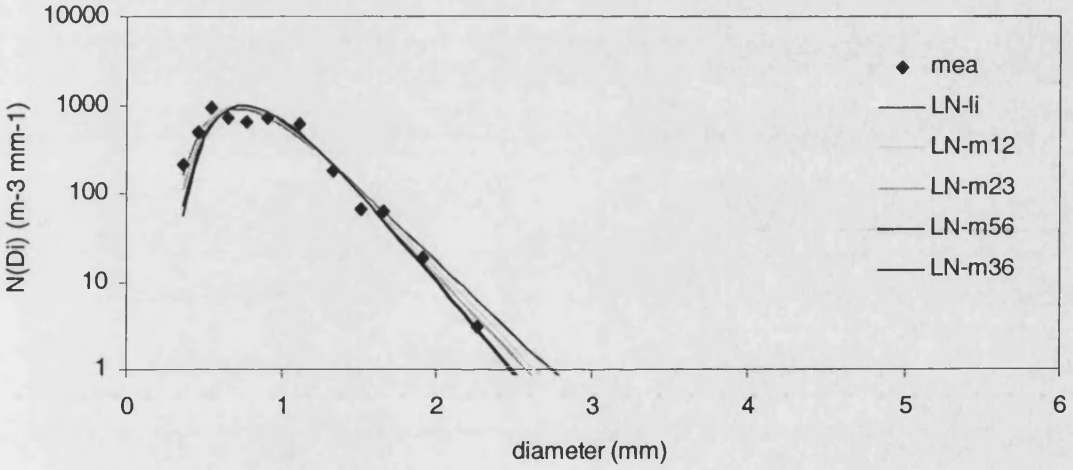

Figure 6.20.b: Comparison between various lognormal distributions with measured data distribution for convective rain fall rate of 5.0 mm hr^{-1}

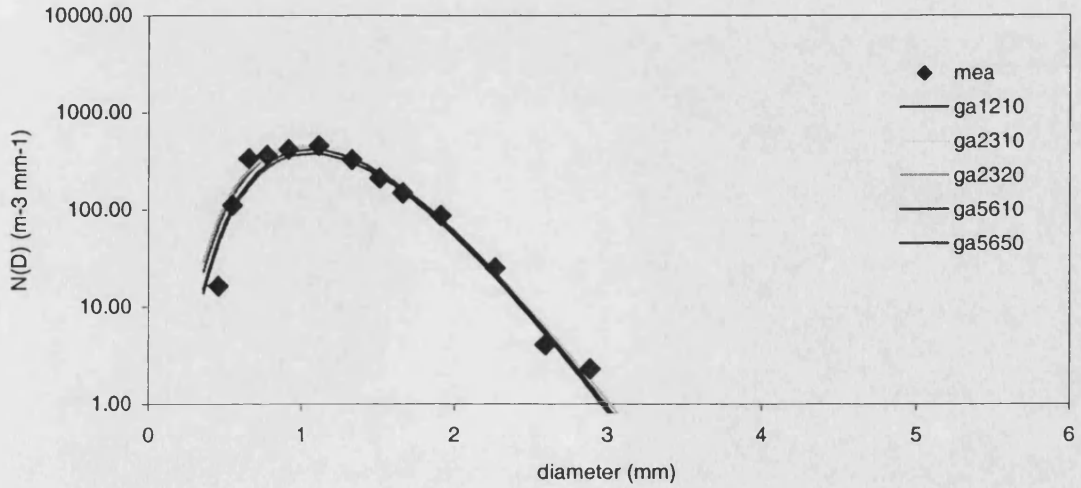

Figure 6.20.c: Comparison between various lognormal distributions with measured data distribution for convective rain fall rate of 10.1 mm hr^{-1}

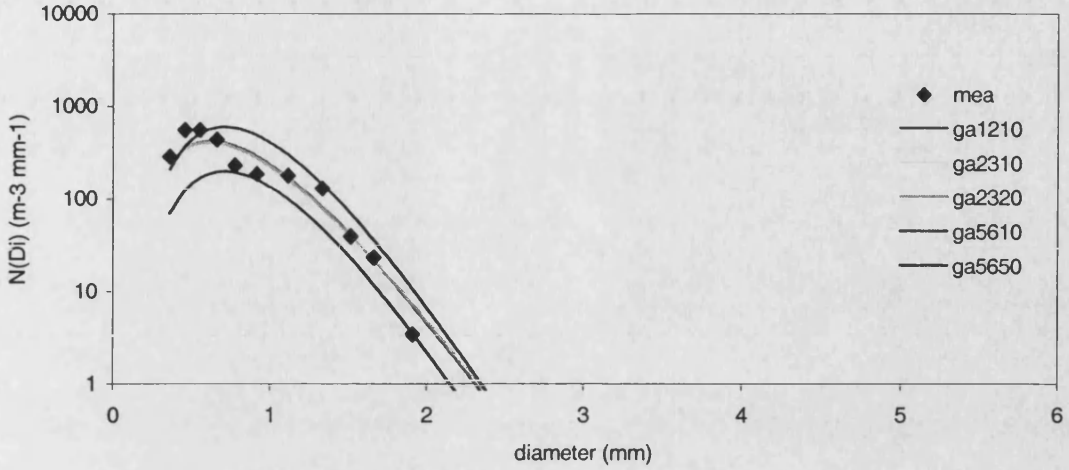

Figure 6.21.a: Comparison between various gamma distributions with measured data distribution for convective rainfall rate of 2.0 mm hr^{-1}.

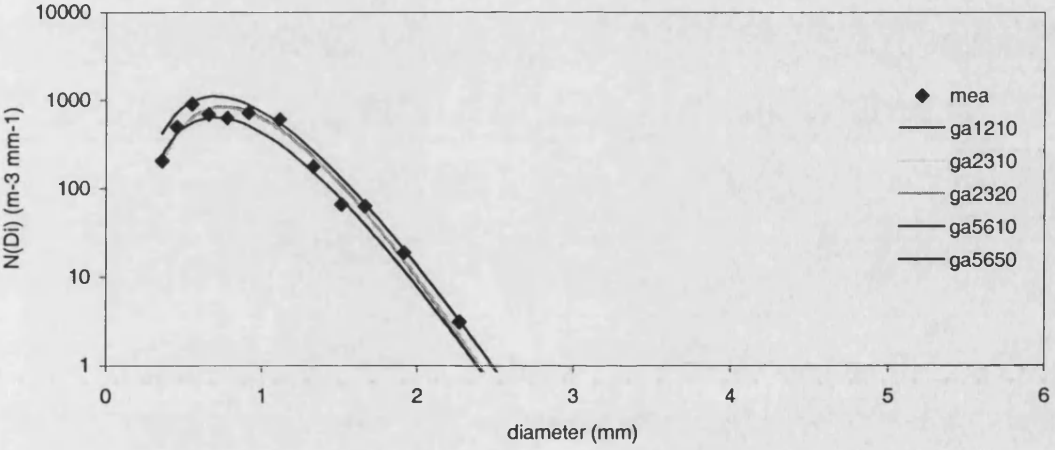

Figure 6.21.b: Comparison between various gamma distributions with measured data distribution for convective rainfall rate of 5.0 mm hr^{-1}.

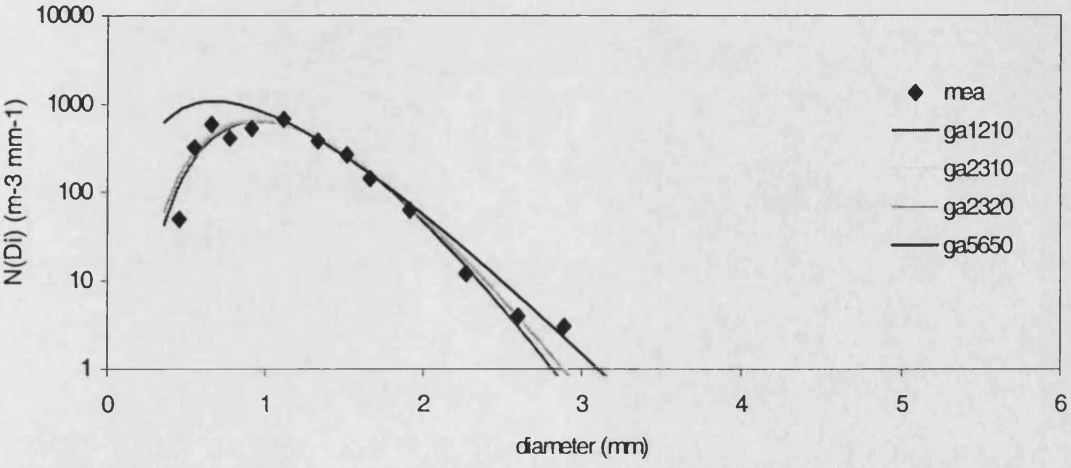

Figure 6.21.c: Comparison between various gamma distributions with measured data distribution for convective rainfall rate of 10.1 mm hr^{-1}.

There are five solutions for parameters of the gamma function determined using the method of moments i.e. ga1210, ga2310, ga2320, ga5610 and ga5620. In the gamma tables, column ga1210 is for the solutions calculated using the 1st and 2nd moments for p and Λ2, and the 1st and 0th moments for Λ1. The same applies for other notations as well. The first three associated plots in each category can be observed in figures above labelled as Figure 6.18 (a) to (c), Figure 6.19 (a) to (c), Figure 6.20 (a) to (c) and Figure 6.21 (a) to (c). The subsequent plots for each criterion are included in Appendix D, E, F and G.

6.11 General Models

In the previous section, listed in the four tables are the parameters determined for each rainfall rate. We then attempt to derive general models that suitable for all rainfall rates involved. The lognormal general models are achieved by employing the least square fitting method for the 10 rainfall rates selected. Coefficients α, β, A_μ, B_μ, A_σ and B_σ for the theoretical lognormal models obtained from the such method for stratiform and convective rain are given below in Table 6.10 and Table 6.12. We employed the same approach to obtain the coefficients α_1, β_1, α_2, β_2, α_p and β_p for the general gamma models. Out of five modified gamma solutions, only the general gamma model identified as ga1210, ga2310 and 2320 are calculated since results obtained from high moments ga5610 and ga5650 observed in previous section are not that satisfactory. The coefficients of the gamma model for the stratiform and convective rain are listed in Table 6.11 and 6.13.

The three parameters for the lognormal and gamma models for both type of rain are recalculated using appropriate coefficients from the tables below. The new values of parameters N_t, μ,σ^2, Λ_1, Λ_2 and p are given in Table 6.14, Table 6.15, Table 6.16 and Table 6.17. The first three plots of general model distribution compared to the measured data for each case study are given in Figures 6.22 (a) to (c), Figure 6.23 (a)

to (c), Figure 6.24 (a) to (c) and Figure 6.25 (a) to (c]. We included the succeeding plots in Appendix H, I, J and K

	N_t		μ		σ^2	
	α	β	A_μ	B_μ	A_σ	B_σ
LN-li	123.623	0.501	-0.314	0.180	0.194	-0.027
LN-m12	123.623	0.501	-0.310	0.179	0.187	-0.027
LN-m23	123.623	0.501	-0.295	0.175	0.173	-0.022
LN-m56	123.623	0.501	-0.198	0.146	0.124	-0.008
LN-m36	123.623	0.501	-0.245	0.160	0.139	-0.012

Table 6.10: Coefficients of general lognormal models for stratiform rain

	Λ_1		p		Λ_2	
	α_1	β_1	α_p	β_p	α_2	β_2
Ga1210	38839.33	-0.85682	3.828217	-0.23502	5.9841	-0.03203
Ga2310	18182.68	-0.83043	3.560085	-0.22513	5.716475	-0.01959
Ga2320	27943.87	-0.79335	3.560085	-0.22513	5.716475	-0.01959

Table 6.11: Coefficients of general gamma models for stratiform rain

	N_t		μ		σ^2	
	α	β	A_μ	B_μ	A_σ	B_σ
LN-li	315.647	0.229	-0.534	0.243	0.173	-0.022
LN-m12	315.647	0.229	-0.530	0.241	0.165	-0.018
LN-m23	315.647	0.229	-0.515	0.237	0.150	-0.014
LN-m56	315.647	0.229	-0.444	0.220	0.112	-0.005
LN-m36	315.647	0.229	-0.474	0.226	0.122	-0.007

Table 6.12 Coefficients of general lognormal models for convective rain

	Λ_1		P		Λ_2	
	α_1	β_1	α_p	β_p	α_2	β_2
ga1210	2462064	0.643275	4.449124	-0.189	8.467759	0.066694
ga2310	2018677	0.745579	4.504965	-0.14127	8.615356	0.107357
ga2320	1987259	0.746211	4.504965	-0.14127	8.615356	0.107357

Table 6.13 Coefficients of general gamma models for convective rain

		LN-li		LN-m_{12}		LN-m_{23}		LN-m_{56}		LN-m_{36}	
RR (mm hr^{-1})	Nt/M_0	μ	σ^2	μ	σ^2	μ	σ^2	μ	σ^2	μ	σ^2
0.5	88.1	-0.43526	0.21270	-0.43114	0.20537	-0.41341	0.18764	-0.29715	0.12884	-0.35326	0.14754
1.0	125.4	-0.30883	0.19357	-0.30518	0.18652	-0.29054	0.17188	-0.19432	0.12329	-0.24100	0.13885
2.0	175.4	-0.18823	0.17533	-0.18503	0.16854	-0.17333	0.15684	-0.09623	0.11800	-0.13391	0.13056
3.0	214.0	-0.11695	0.16454	-0.11401	0.15791	-0.10405	0.14795	-0.03826	0.11488	-0.07062	0.12566
4.0	247.6	-0.06457	0.15661	-0.06182	0.15010	-0.05314	0.14142	0.00435	0.11258	-0.02411	0.12207
6.1	306.2	0.01158	0.14509	0.01404	0.13875	0.02087	0.13193	0.06628	0.10924	0.04351	0.11683
8.1	352.1	0.06169	0.13751	0.06397	0.13128	0.06957	0.12568	0.10704	0.10704	0.08801	0.11339
10.0	392.9	0.10106	0.13155	0.10319	0.12541	0.10783	0.12077	0.13906	0.10532	0.12296	0.11068
12.3	435.3	0.13775	0.12600	0.13975	0.11994	0.14349	0.11620	0.16891	0.10371	0.15555	0.10816
15.4	486.6	0.17778	0.11994	0.17963	0.11397	0.18239	0.11121	0.20146	0.10195	0.19109	0.10541

Table 6.14: Parameters for lognormal function recalculated using general model coefficients for each stratiform rainfall rate.

	ga_{1210}			ga_{2310}			ga_{2320}		
RR (mm hr^{-1})	p	Λ^2	Λ^1	p	Λ^2	Λ^1	p	Λ^2	Λ^1
0.5	3.26640	5.85606	21776.4	3.05799	5.64134	10378.0	3.05799	5.64134	16353.7
1.0	3.85326	5.98942	39773.8	3.58239	5.71958	18606.5	3.58239	5.71958	28565.8
2.0	4.51111	6.11946	70657.8	4.16625	5.79523	32474.4	4.16625	5.79523	48632.1
3.0	4.95157	6.19765	99234.8	4.55514	5.84042	45133.7	4.55514	5.84042	66603.9
4.0	5.30243	6.25574	127366.7	4.86387	5.87384	57484.9	4.86387	5.87384	83919.3
6.1	5.85732	6.34116	183078.2	5.35039	5.92278	81711.0	5.35039	5.92278	117427.3
8.1	6.25378	6.39801	232452.6	5.69681	5.95521	102987.5	5.69681	5.95521	146482.3
10.0	6.58399	6.44304	280416.2	5.98463	5.98081	123521.7	5.98463	5.98081	174268.4
12.3	6.90743	6.48528	333989.8	6.26597	6.00477	146330.4	6.26597	6.00477	204891.5
15.4	7.27840	6.53168	404166.5	6.58796	6.03101	176039.6	6.58796	6.03101	244464.3

Table 6.15: Parameters for gamma function recalculated using general model coefficients for each stratiform rainfall rate.

		LN-li		LN-m_{12}		LN-m_{23}		LN-m_{56}		LN-m_{36}	
RR (mm hr^{-1})	Nt/M_0	μ	σ^2	μ	σ^2	μ	σ^2	μ	σ^2	μ	σ^2
2.0	370.2559	-0.36480	0.15765	-0.36193	0.15197	-0.35024	0.14028	-0.29083	0.10923	-0.31651	0.11779
5.0	456.9442	-0.14214	0.13770	-0.14064	0.13537	-0.13298	0.12772	-0.08895	0.10498	-0.10880	0.11159
10.1	536.0795	0.02691	0.12254	0.02739	0.12276	0.03197	0.11818	0.06432	0.10175	0.04890	0.10689
24.8	659.2293	0.24578	0.10293	0.24492	0.10644	0.24553	0.10583	0.26277	0.09757	0.25308	0.10080
40.0	735.4482	0.36158	0.09255	0.36002	0.09780	0.35852	0.09930	0.36776	0.09536	0.36110	0.09758
64.9	821.6942	0.47894	0.08203	0.47667	0.08905	0.47304	0.09267	0.47417	0.09311	0.47059	0.09431
74.8	849.0278	0.51358	0.07892	0.51109	0.08647	0.50684	0.09072	0.50558	0.09245	0.50290	0.09335
99.8	907.0545	0.58355	0.07265	0.58064	0.08125	0.57511	0.08677	0.56902	0.09112	0.56818	0.09140
124.1	953.4851	0.63639	0.06791	0.63315	0.07731	0.62667	0.08379	0.61693	0.09011	0.61747	0.08993
144.8	987.8606	0.67388	0.06455	0.67041	0.07451	0.66325	0.08168	0.65092	0.08939	0.65244	0.08888

Table 6.16: Parameters for lognormal function recalculated using general model coefficients for each convective rainfall rate.

	ga_{1210}			ga_{2310}			ga_{2320}		
RR (mm hr^{-1})	p	Λ^2	Λ^1	p	Λ^2	Λ^1	p	Λ^2	Λ^1
2.0	5.07453	8.08373	1573570.6	4.97036	7.99516	1201531.0	4.97036	7.99516	1182310.4
5.0	6.03533	7.60394	872131.3	5.65817	7.24523	606273.8	5.65817	7.24523	596229.7
10.1	6.88457	7.25876	557164.0	6.24328	6.72319	360679.6	6.24328	6.72319	354548.2
24.8	8.16397	6.83504	311916.2	7.09159	6.10279	184123.0	7.09159	6.10279	180889.9
40.0	8.93443	6.62096	229476.5	7.58610	5.79805	129005.6	7.58610	5.79805	126702.1
64.9	9.78953	6.41082	168126.3	8.12249	5.50471	89953.9	8.12249	5.50471	88320.7
74.8	10.05717	6.35009	153379.1	8.28791	5.42101	80874.2	8.28791	5.42101	79398.7
99.8	10.62042	6.22915	127414.6	8.63246	5.25579	65230.8	8.63246	5.25579	64029.1
124.1	11.06654	6.13936	110763.5	8.90209	5.13437	55457.1	8.90209	5.13437	54428.0
144.8	11.39438	6.07644	100287.1	9.09848	5.04993	49424.6	9.09848	5.04993	48502.6

Table 6.17: Parameters for gamma function recalculated using general model coefficients for each convective rainfall rate.

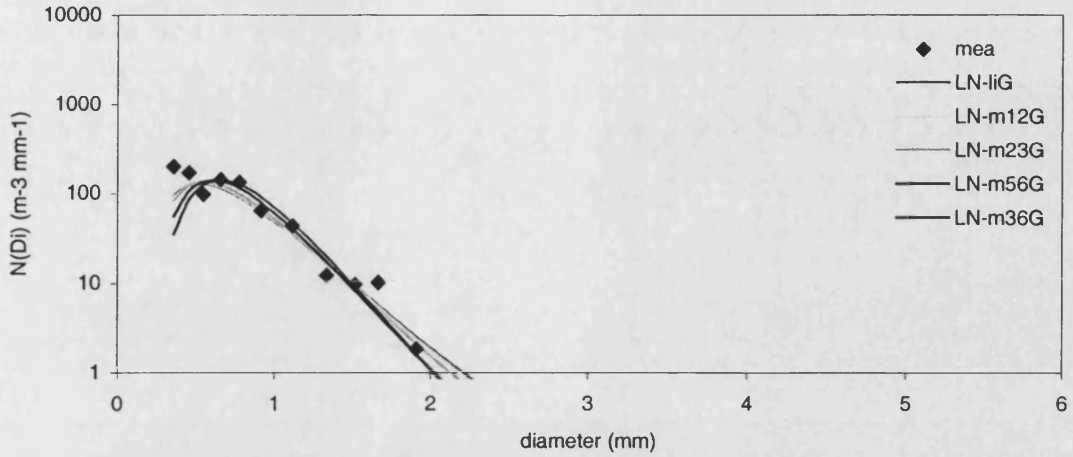

Figure 6.22.a: Comparison between various generalised lognormal distributions with measured data distribution for stratiform rainfall rate of 0.5 mm hr^{-1}.

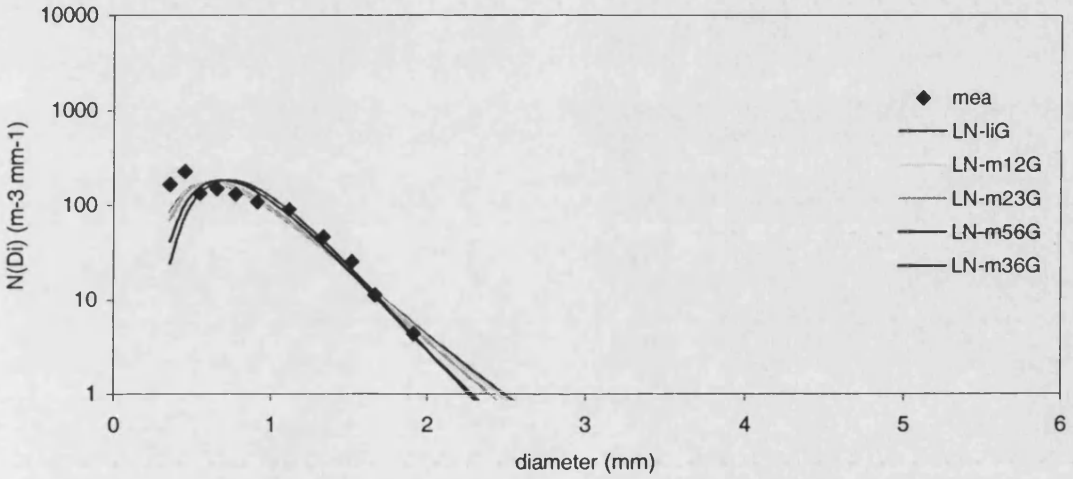

Figure 6.22.b: Comparison between various generalised lognormal distributions with measured data distribution for stratiform rainfall rate of 1.0 mm hr^{-1}.

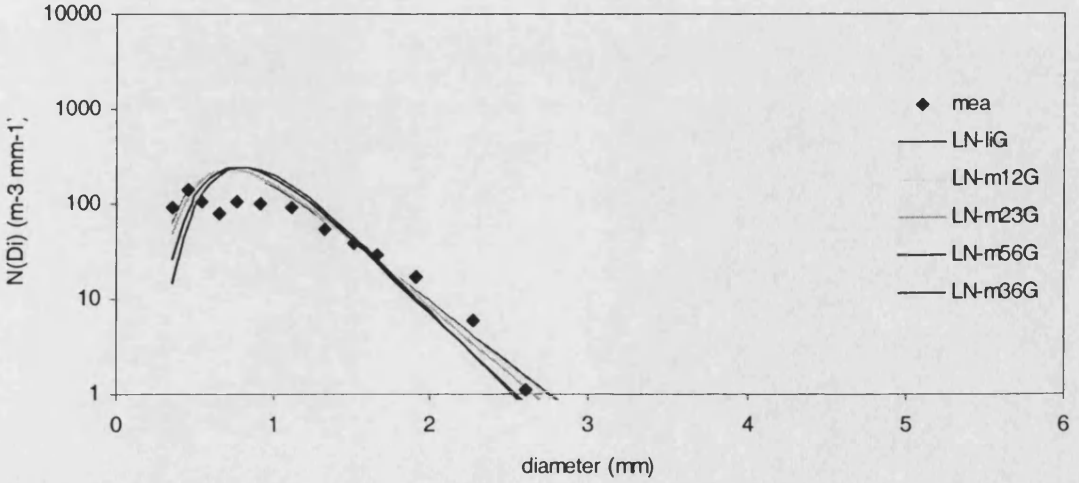

Figure 6.22.c: Comparison between various generalised lognormal distributions with measured data distribution for stratiform rainfall rate of 2.0 mm hr^{-1}.

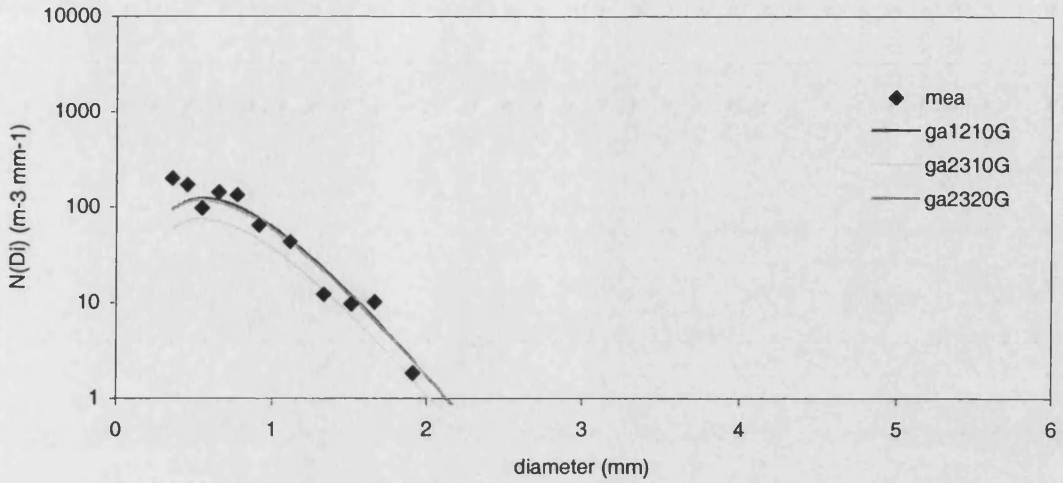

Figure 6.23.a: Comparison between various generalised gamma distributions with measured data distribution for stratiform rainfall rate of 0.5 mm hr^{-1}.

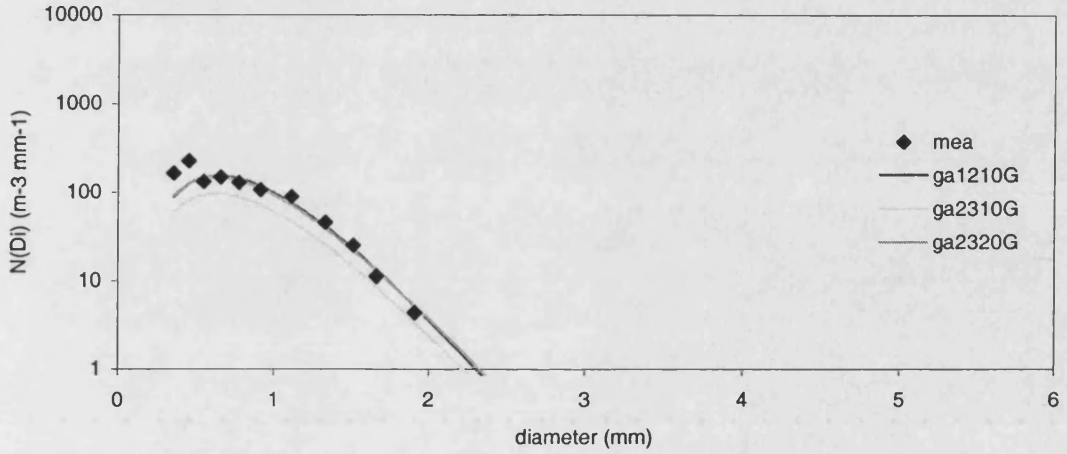

Figure 6.23.b: Comparison between various generalised gamma distributions with measured data distributions for stratiform rainfall rate of 1.0 mm hr^{-1}

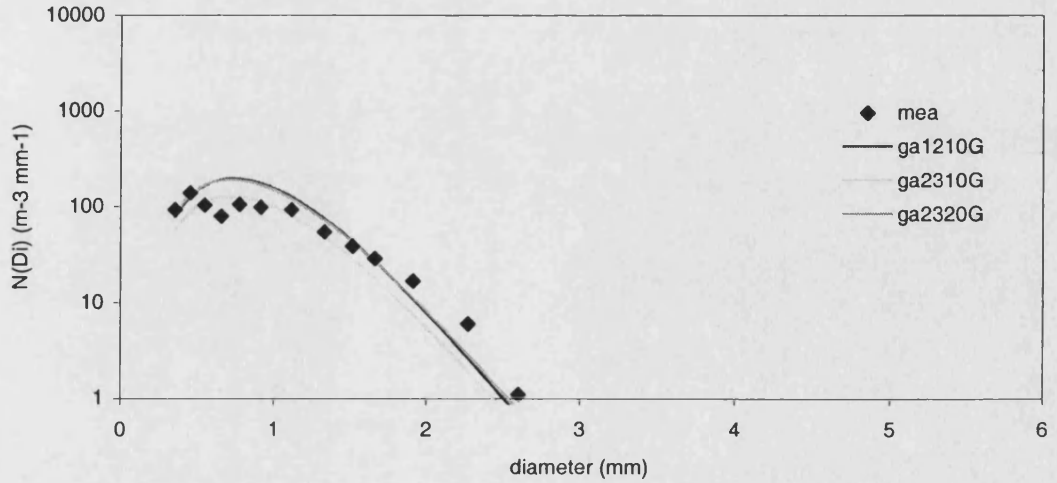

Figure 6.23.c: Comparison between various generalised gamma distributions with measured data distribution for stratiform rainfall rate of 2.0 mm hr^{-1}.

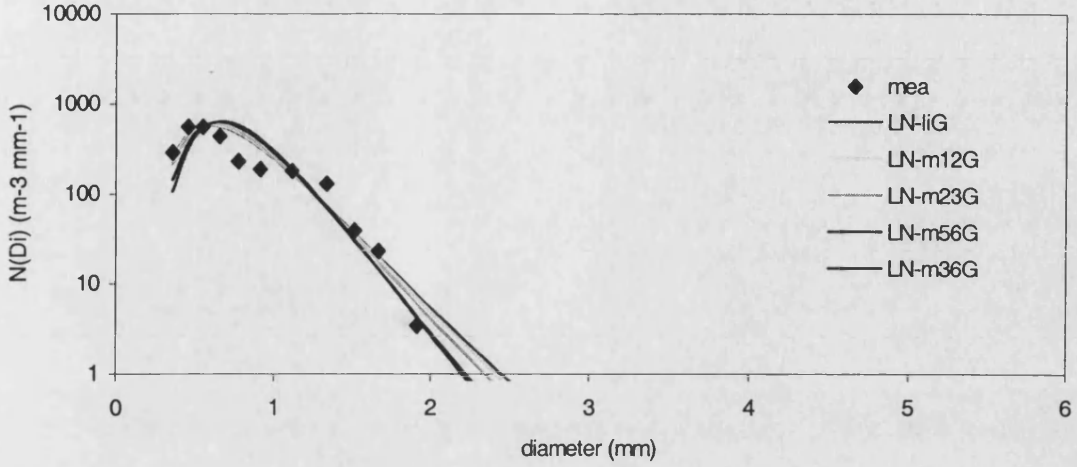

Figure 6.24.a: Comparison between various generalised lognormal distributions with measured data distribution for convective rainfall rate of 2.0 mm hr^{-1}

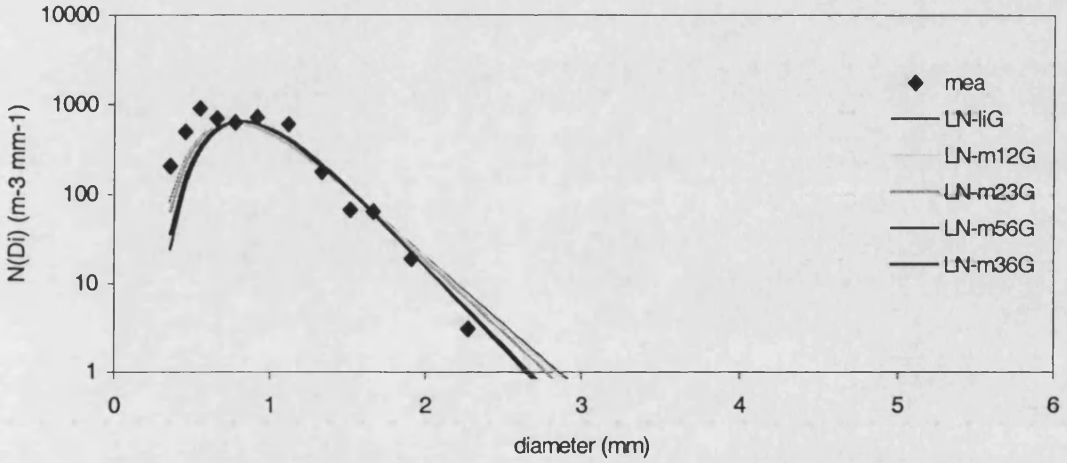

Figure 6.24.b Comparison between various generalised lognormal distributions with measured data distribution for convective rainfall rate of 5.0 mm hr^{-1}

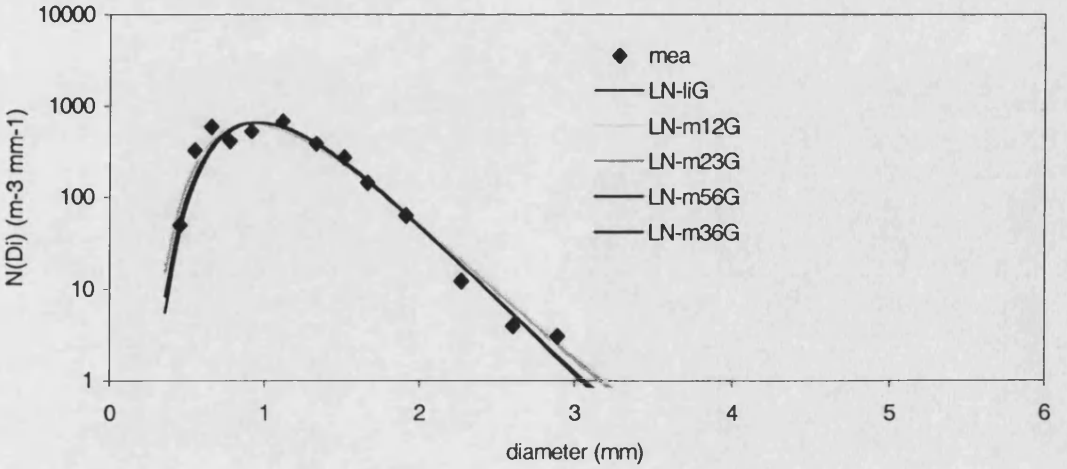

Figure 6.24.c: Comparison between various generalised lognormal distributions with measured data distribution for convective rainfall rate of 10.0 mm hr^{-1}

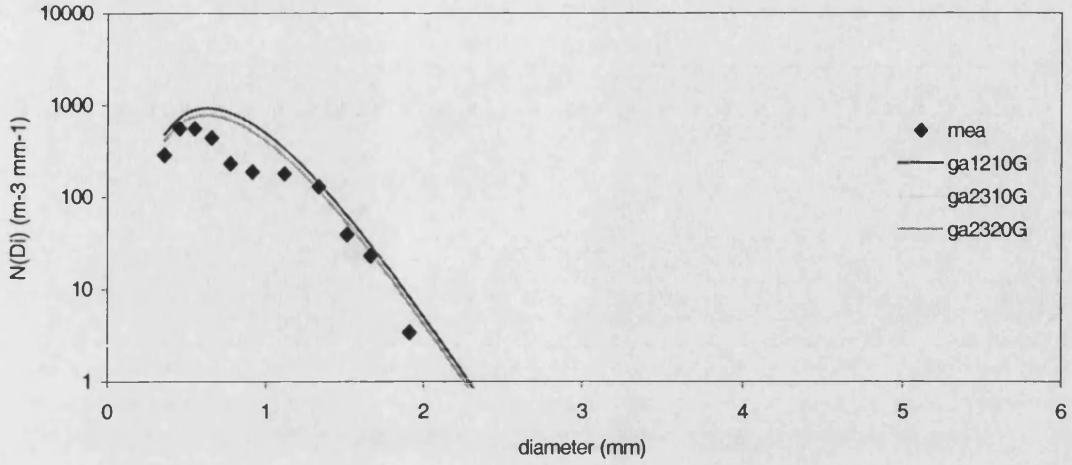

Figure 6.25.a: Comparison between various generalised gamma distributions with measured data distribution for convective rainfall rate of 2.0 mm hr^{-1}.

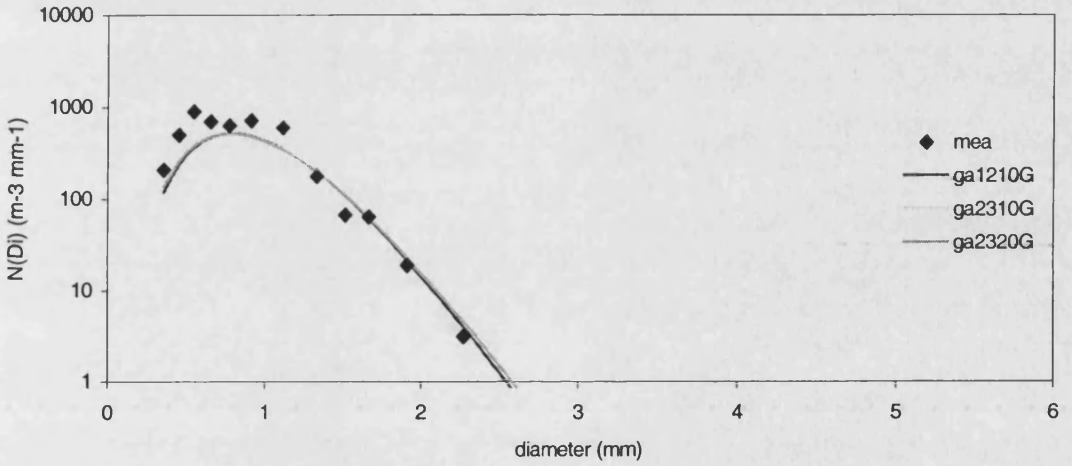

Figure 6.25.b: Comparison between various generalised gamma distributions with measured data distribution for convective rainfall rate of 5.0 mm hr^{-1}.

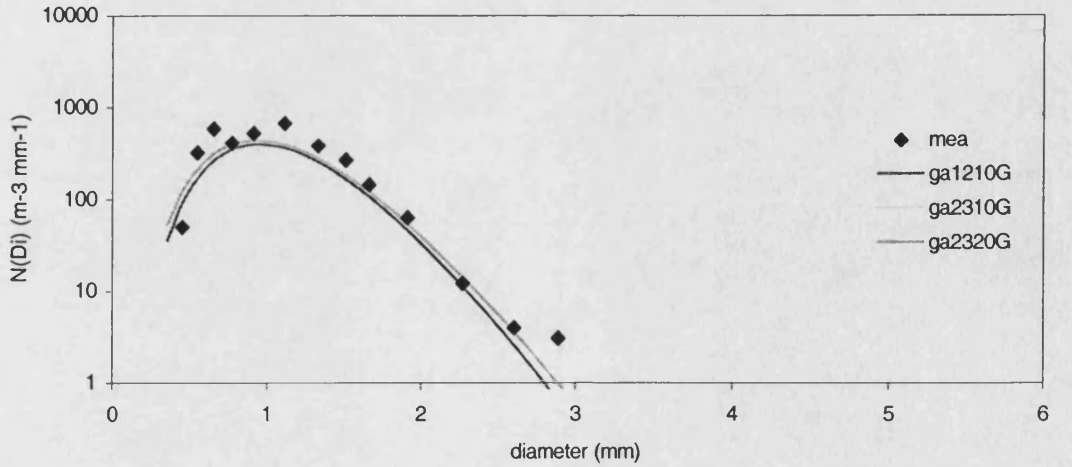

Figure 6.25.c: Comparison between various generalised gamma distributions with measured data distribution for convective rainfall rate of 10.0 mm hr^{-1}.

6.12 Comparison between the Two Models

From figures labelled as Figure 6.18 (a)-(c), Figure.19 (a)-(c), Figure 20 (a)-(c), Figure 21 (a)-(c) and figures from Appendix H, I J and K. It can be commonly observed that the lower moment solutions fit better the small drop diameters. The higher moment solutions meanwhile give better match to the large drop diameters. We noticed as well that the lower moment solutions give a good fit to measured data especially for low rainfall rates in both stratiform and convective rain. It can be perceived from the figures of convective rain that the higher moment solutions give a good match to the measure data for rainfall rates greater than 80 mm/hr. The results of higher moment solutions for the gamma models are not satisfactory where the models overestimate the distributions of small drops. We rejected solutions ga5610 and ga5620 from our choice of possible model.

Comparing the general models with measured data, it can be observed that the plots of LN-li, LN-m12 and LN-m23 are very similar to that of measured data for most rainfall rates. The lognormal model with high moments, LN-m56 and LN-m36 this time seem no longer able to match the measured distribution in most cases. The general gamma models seem not to be able to give good match to PNG measured data especially in the case of convective rain. It is very difficult simply decide one model that is most appropriate for PNG measured distribution out of eight available choices based merely on our visual observation. In the next section, tests that are impartial are applied on every model to objectively determine the best model for describing the distribution.

6.13 Models Verification

It is hard to determine the appropriate models from plotted curves in the previous section. To simply accept a model based on visual judgement is clearly subjective and non-quantitative. Hence we employed the goodness of fit test procedure to evaluate the

various proposed models in order to be more impartial and quantitative. Combining this procedure together with our visual inspections, the best model or models that represent the PNG rain drop size distribution then could be decided. There are two model verification tests that were performed to assess the proposed generalised models.

6.13.1 The Chi-Square (χ^2) Test

In this section we briefly introduce the notion of the χ^2 test adapted from the related literatures [Miller and Freund, 1985; Mendenhall and Sincich, 1988; Soong, 1981]. Let us assume $X_1, X_2, \ldots, X_n$ to be a sample of size n. The range space of X is distributed into k mutually exclusive intervals $A_1, A_2, \ldots$, and A_k. Let N_i be the number of X_j's falling into A_i, $i = 1, 2, \ldots, k$. The Observed Probabilities from measured data $P(A_i)$ are given by

$$Observed\ P(A_i) = \frac{N_i}{n} \quad i = 1, 2, \ldots, k \tag{6.13}$$

Whilst, the Theoretical Probabilities $P(A_i)$ can be obtained from the hypothesised distribution denoted by

$$Theorethical\ P(A_i) = p_i \quad i = 1, 2, \ldots, k \tag{6.14}$$

A logical selection of a statistic giving a measure of deviation can be defined as

$$D = \sum_{i=1}^{k} c_i \left[\frac{N_i}{n} - p_i \right]^2 \tag{6.15}$$

which is a natural least-square type deviation measure. If taking $c_i = n/p_i$, then the equation above can be rewritten such as

$$D = \sum_{i=1}^{k} \frac{n}{p_i}\left[\frac{N_i}{n} - p_i\right]^2$$

$$= \sum_{i=1}^{k}\left[\frac{N_i - np_i}{np_i}\right]^2$$

$$= \sum_{i=1}^{k} \frac{N_i^{\,2}}{np_i} - n \qquad (6.16)$$

where D is a statistic since it is a function of N_i. The distribution of statistic D approaches a χ^2 distribution with k-1 degrees of freedom as $n \to \infty$. If the significance level α is defined as

$$P(D > \chi^2_{k-1,\alpha}) = \alpha \qquad (6.17)$$

then the χ^2 test suggests that proposed distribution is rejected whenever

$$d = \sum_{i=1}^{k} \frac{N_i^{\,2}}{np_i} - n > \chi^2_{k-1,\alpha} \qquad (6.18)$$

and is accepted otherwise. d is the sample value of D based on the sample values x_i, $i = 1, \ldots, n$.

We then performed the χ^2 test based on the recommended procedure. Listed below are the recommended step-by-step procedure for carrying out the χ^2 test when the distribution of X is completely specified.

1. Divide range space of X into k mutually exclusive and numerically convenient intervals A_i, i =1, 2, ..., k. Let n_i be the number of sample values falling into A_i. As a rule, if the number of sample values in any A_i is less than five, combine the interval A_i with either A_{i-1} or A_{i+1}.
2. Compute the Theoretical Probabilities $P(A_i) = p_i$, $i = 1, 2, \ldots, k$, by means of the hypothesised distribution.

3. Construct d as given by equation (6.29).
4. Choose a value of α and determine from table for the χ^2 distribution of (k-1) degrees of freedom the value of $\chi^2_{k-1,\alpha}$.
5. Reject hypothesis distribution if $d > \chi^2_{k-1,\alpha}$. Otherwise, accept hypothesis distribution.

6.13.2 Results of the Chi-Square Test

N_t is removed from the drop size distribution $N(D)$ equation for the Theoretical Probability. This gives us the probability density function $n(D)$ such that the $\int n(D)dD = 1$. From here we can recognise that the goodness of fit test actually tests the profile of the distribution. In our case that also considers the N_t, the observation is still partially needed. In our analyses, the Theoretical Probability can now be expressed by

$$p_i = \int_1^{i+1} n(D_i)dD_i \tag{6.19}$$

and the Observed Probabilities can be calculated from the distrometer measured data by

$$n_i = N(D_i)\times\Delta D_i \tag{6.20}$$

where

$$\sum_{i=1}^{k} n_i = \sum_{i=1}^{k} N(D_i)\times\Delta D_i = N_t = n \tag{6.21}$$

We illustrate here one χ^2 test sample calculation carried out on rainfall rate R = 40.0 mm hr^{-1} observed during convective events. In this example, we performed the χ^2 test

to evaluate the LN-li model. The essential steps in implementing the χ^2 test are summarised in Table 6.18. The N_i values in the table were computed using equation (6.31) above. The Theoretical Probabilities $P(A_i) = p_i$ were calculated using the lognormal distribution equation (6.30) according to appropriate A_i interval. For example p_1 is expressed as

$$p_1 = P(A_1) = \int_{0.313}^{0.405} \frac{N_t}{\sigma D_1 \sqrt{2\pi}} \exp\left[\frac{-(\ln(D_1) - \mu)^2}{2\sigma^2}\right] dD$$

Channel i	Lower bound D_{il} (mm)	Upper bound D_{iu} (mm)	Mean value D_i (mm)	Observed number n_i	Theoretical $P(A_i)$	Ni^2/np_I
1	0.313	0.405	0.3590	0.000	1.57E-05	0
2	0.405	0.505	0.4550	0.000	0.000281	0
3	0.505	0.594	0.5495	0.000	0.001564	0
4	0.594	0.719	0.6565	1.660	0.009652	0.398606
5	0.719	0.829	0.7740	3.428	0.024022	0.683496
6	0.829	0.998	0.9135	43.717	0.080479	33.17139
7	0.998	1.229	1.1135	162.591	0.188748	195.6403
8	1.229	1.434	1.3315	137.409	0.193781	136.1019
9	1.434	1.592	1.5130	82.773	0.134504	71.15298
10	1.592	1.733	1.6625	65.943	0.09896	61.38058
11	1.733	2.090	1.9115	134.206	0.159507	157.7298
12	2.090	2.448	2.2690	57.412	0.068802	66.91929
13	2.448	2.751	2.5995	16.409	0.023425	16.05501
14	2.751	3.032	2.8915	7.365	0.009269	8.174699
15	3.032	3.345	3.1885	1.929	0.00428	1.214948
16	3.345	3.737	3.5410	1.058	0.001882	0.830515
17	3.737	4.151	3.9440	0.000	0.00059	0
18	4.151	4.619	4.3850	0.000	0.00018	0
19	4.619	5.145	4.8820	0.000	4.76E-05	0
20	5.145	5.750	5.4470	0.000	1.11E-05	0

Table 6.18 Table for χ^2 test of LN-li model at convective rainfall rate 40 mm hr^{-1}

We obtained the values of the Theoretical $P(A_i)$ by the use of the IDL programming language. The parameters involve are such as $\mu = 0.3616$ and $\sigma^2 = 0.0925$ determined by $\mu = A_\mu + B_\mu \ln R$ and $\sigma^2 = A_\sigma + B_\sigma \ln R$. Then from equation (6.18) we computed the value of d such as

$$d = \sum_{i=1}^{k} \frac{N_i^2}{np_i} - n$$

$$= 749.45 - 715.90$$

$$= 33.55$$

From Table A.5 in reference [Soong, 1981] for the χ^2 distribution with 19 degrees of freedom and $k = 20$, it is stated that $\chi^2_{19,0.05} = 30.144$ and $\chi^2_{19,0.01} = 36.191$. Since $d < \chi^2_{k-1,\alpha}$, only when $\alpha = 0.01$, this indicates that the hypothesis can be accepted only at 1% significance level and did not satisfy the 5% significant level test. In this example, our hypothesis is that a lognormal distribution can represent the measured data distribution for convective rainfall rate. Table 6.19 below lists the test results d for the lognormal and gamma models determined for stratiform rainfall rates. The results in bold are values accepted at 5% significance level.

RR (mm hr^{-1})	LN-liG	LN-m12G	LN-m23G	LN-m56G	LN-m36G	Ga1210G	ga2310G	ga2320G
0.5	**10.52**	**10.08**	**13.76**	66.19	32.01	**13.63**	**12.09**	**12.09**
1.0	**13.78**	**14.03**	**19.46**	93.36	46.50	**12.27**	**10.24**	**10.24**
2.0	**20.17**	**21.69**	**28.32**	95.05	55.76	**16.93**	**14.25**	**14.25**
3.0	**12.82**	**12.57**	**15.28**	38.53	**24.98**	**19.12**	**17.51**	**17.51**
4.0	**11.68**	**13.52**	**17.69**	76.44	41.21	**7.73**	**6.48**	**6.48**
6.1	36.98	39.32	46.11	131.59	81.59	42.68	39.09	39.09
8.0	**7.13**	**6.32**	**6.74**	**27.80**	**14.12**	**12.67**	**14.64**	**14.64**
10.0	**11.55**	**10.42**	**10.37**	**21.73**	**14.01**	**16.38**	**19.29**	**19.29**
12.3	49.13	47.15	44.85	31.94	38.49	57.73	60.64	60.64
15.4	44.56	39.45	38.20	43.50	38.44	64.22	73.30	73.30

Table 6.19: χ^2 test of models for stratiform rainfall rates

Table 6.20 lists the test results for the lognormal and gamma models for convective rainfall rates, where the bold is accepted at 1% significance level. We lowered the acceptance value since all models failed to satisfy the 5% significance level. It was observed from Table 6.19 that several models passed the 5% confidence level test. This indicates that for the stratiform rainfall rates, several model can be accepted to represent the rain drop size distribution for R = 0.5 to 14.5 mm hr^{-1}. On the other hand, all the proposed models for convective rainfall rates for R = 2 to 144.8 mm hr^{-1} failed the 5% confidence level test. Only when we decrease the confidence level to 1% then a few models can be accepted. This suggests that the proposed lognormal and gamma distribution profiles were not really that suitable and could not accurately represent the measured distribution for convective cases.

RR (mm hr^{-1})	LN-liG	LN-m12G	LN-m23G	LN-m56G	LN-m36G	Ga1210G	ga2310G	ga2320G
2.0	37.28	40.12	48.20	110.55	80.32	40.07	38.62	38.62
5.0	64.64	66.86	79.25	217.12	143.77	57.16	52.60	52.60
10.1	**34.97**	**35.04**	**35.23**	55.36	42.83	40.57	42.26	42.26
24.8	58.73	58.67	58.30	48.39	53.99	79.80	85.18	85.18
40.0	**33.55**	**35.78**	39.46	**34.00**	37.29	51.43	70.82	70.82
64.9	39.02	**34.57**	**33.51**	**34.14**	**33.18**	77.95	74.70	74.70
74.8	42.61	42.86	45.85	47.47	48.49	95.25	101.05	101.05
99.8	54.94	37.92	36.97	39.80	40.37	71.76	73.74	73.74
124.1	104.12	81.60	80.19	85.03	84.77	151.25	145.28	145.28
144.8	212.13	186.74	174.15	164.85	166.38	266.84	255.02	255.02

Table 6.20: χ^2 test of models for convective rainfall rates

However after reviewing the figures labelled Figure 6.24 (a) – (j) it seems the fittings were not too bad to be accepted visually. It seems that, for establishing the theoretical model for rain drop size distribution, there is no absolute good theoretical model because the range of rainfall rates involved during convective is too large, and the data are too dispersed. It only exists the relatively better model. Previous investigators indicated [Hall and Barclay, 1989] that there is no single model for drop size distributions can be claimed as the only representative of the physical reality, even as

a statistical mean over many rain events. We noticed that in discussing the modelling of the rain drop size distribution; many literatures just conclude their results visually.

Based on the χ^2 test, coupled with our visual observation, we then grade our results. For the models for stratiform rainfall rate, LN-m12 > LN-li> LN-m23 > ga1210> ga-2310 > ga2320 > LN-m56 > LN-m36 where > indicates "better than". For the general models for convective rainfall rates LN-m12 > LN-m23 > LN-li > LN-m56 > LN-m36 >ga1210 > ga2310 >ga2320. It seems that the lognormal with combination moment 1 and moment 2 is the most appropriate model for stratiform and convective rain.

6.13.3 The Kolmogorov-Smirnov (K-S) Test

The K-S test is based on statistics that measures the deviation of observed cumulative histogram from the hypothesised cumulative distribution function. The step-by-step procedure for executing the K-S test was outlined in literature [Soong, 1981]:

1. Rearrange sample values x_1, x_2,..., x_n in increasing order of magnitude and label them $x_{(1)}$, $x_{(2)}$,..., $x_{(n)}$.
2. Determine the observed distribution function $F^0(x)$ at each $x_{(i)}$ using $F^0(x_{(i)}) = i/n$.
3. Determine the theoretical distribution function $F_x(x)$ at each $x_{(i)}$ using the hypothesised distribution.
4. Form the differences $F^0(x_{(i)}) - F_x(x_{(i)})$ for $i = 1, 2, ..., n$.
5. Calculate $d_2 = max^i_{n=1} [F^0(x_{(i)}) - F_x(x_{(i)})]$. The determination of this maximum value required enumeration of n quantities. It can plot $F^0(x)$ and $F_x(x)$ as functions of x; the location of maximum is obtained by inspection.
6. Choose a value of a and determine from Table A.6 of reference [Soong, 1981] the value of $c_{n,\alpha}$.
7. Reject hypothesis distribution if $d_2 > c_{n,\alpha}$. Otherwise, accept.

6.13.4 Results of the Kolmogorov-Smirnov Test

Table 6.21 and Table 6.22 list the test results for various parameters for the general lognormal model and the general gamma model for stratiform and convective rain, where the bold value is the accepted at 5% significance level. The last column is the c value calculated from $c_{n,0.05} = 1.36/\sqrt{n}$ since for different rainfall rate.

RR (mm hr^{-1})	LN-liG	LN-m12G	LN-m23G	LN-m56G	LN-m36G	Ga1210G	ga2310G	ga2320G	5% SL
0.5	**0.090**	**0.093**	**0.107**	0.208	0.161	**0.117**	**0.109**	**0.109**	0.133
1.0	**0.098**	**0.103**	0.117	0.194	0.162	**0.106**	**0.096**	**0.096**	0.116
2.0	**0.092**	**0.093**	**0.092**	0.154	**0.123**	**0.070**	**0.071**	**0.071**	0.124
3.0	**0.033**	**0.034**	**0.048**	0.130	**0.093**	**0.040**	**0.049**	**0.049**	0.103
4.0	**0.038**	**0.042**	**0.049**	0.108	**0.077**	**0.026**	**0.019**	**0.019**	0.088
6.1	0.087	0.091	0.101	0.156	0.131	0.103	0.098	0.098	0.065
8.0	**0.031**	**0.027**	**0.027**	**0.063**	**0.047**	**0.039**	**0.039**	**0.039**	0.070
10.0	**0.016**	**0.013**	**0.020**	**0.059**	**0.041**	**0.030**	**0.041**	**0.041**	0.066
12.3	0.151	0.145	0.139	0.102	0.120	0.139	0.156	0.156	0.073
15.4	0.087	0.084	0.084	0.103	0.091	0.104	0.101	0.101	0.055

Table 6.21 K-S test of stratiform models for all rainfall rates

RR (mm hr^{-1})	LN-liG	LN-m12G	LN-m23G	LN-m56G	LN-m36G	ga1210G	ga2310G	ga2320G	5% SL
2.0	**0.076**	**0.080**	0.094	0.168	0.137	0.099	0.093	0.093	0.091
5.0	0.086	0.089	0.100	0.147	0.129	0.081	0.082	0.082	0.065
10.1	**0.041**	**0.041**	**0.043**	0.081	**0.066**	**0.027**	**0.041**	**0.041**	0.069
24.8	0.109	0.114	0.112	0.087	0.100	0.119	0.146	0.146	0.073
40.0	**0.048**	**0.055**	**0.058**	**0.047**	**0.054**	0.069	0.098	0.098	0.061
64.9	0.065	**0.056**	**0.049**	**0.050**	**0.045**	0.063	0.056	0.056	0.056
74.8	**0.033**	**0.038**	**0.048**	**0.051**	**0.054**	0.051	0.087	0.087	0.057
99.8	**0.045**	**0.036**	**0.048**	**0.059**	0.061	**0.045**	0.082	0.082	0.059
124.1	**0.051**	**0.046**	**0.052**	0.064	0.064	0.069	0.092	0.092	0.055
144.8	0.161	0.157	0.151	0.140	0.142	0.182	0.156	0.156	0.044

Table 6.22 K-S test of convective models for all rainfall rates

Comparing Table 6.19 and Table 6.20 for χ^2 test with Table 6.21 and Table 6.22 for K-S test, both for the general models for all rainfall rates, it is found that the results are quite similar, that is to say, when the parameters for a model pass the χ^2 test, they pass the K-S test too. So the similar conclusion can be obtained as in the χ^2 test.

6.14 Comparison with Other Tropical Models

In this section we present the comparisons between the rain drop size distribution model proposed for PNG with those derived in other places of the tropics. All studies agree that the negative exponential distribution model as proposed by Marshall Palmer is unsuitable to model the distribution for this part of the world since it overestimate the number of small size raindrops. Some of recommended drop size distribution models derived from previous investigations in the tropical areas include:

1. The lognormal model in Kuala Lumpur, Malaysia [Tharek and Din, 1992]
2. The lognormal and modified gamma models in Singapore [Ong and Shan, 1997; Ong and Shan, 1997b]
3. The lognormal model at Ile-Ife, Nigeria [Ajayi and Olsen, 1983]
4. The lognormal model at Sao Paulo Brazil [Marciel and Assis, 1990]

6.14.1 Recommendations from Malaysia

Malaysian investigator [Tharek and Din, 1992] conducted the rain drop size distribution analysis using distrometer measurement data at Universiti Teknologi Malaysia (UTM), Kuala Lumpur. They suggested that the rain drop size distribution in Kuala Lumpur can be represented by the lognormal distribution model. The parameters proposed were fitted for rainfall rates ranging from 80 to 260 mm hr^{-1}. From our database, there is no such record of rainfall rates higher than 200 mm hr^{-1} detected in PNG. The parameters of the drop size distribution model for convective rain in our analysis were fitted for rainfall rates between 2 mm hr^{-1} to 145 mm hr^{-1}. We listed parameters from Malaysia together with parameters for PNG convective rain

model in the Table 6.23 below. For their lognormal model, they used combination of the 2nd and 3rd moment to fit their data where else we applied the 1st and 2nd moment.

	α	β	A_μ	B_μ	A_σ	B_σ
Malaysia	47.058	0.618	-0.6808	0.2596	0.5966	-0.0972
PNG	315.647	0.229	-0.5300	0.2410	0.1650	-0.0180

Table 6.23 Parameters for lognormal model in Malaysia and PNG

Figure.6.26 shows the distribution plots for rainfall rates of 80 and 140 mm hr^{-1}. For large drop diameter ranges i.e. greater than 3.5 mm, the number of drops is higher in the Malaysian model than in the PNG model. The rationale may be because the Malaysian model is fitted for rainfall rates range from 80 to 261 mm hr^{-1} that only involves the high rainfall rates data. Where on the other hand, the PNG model covered for mixed rainfall rates range from 2 mm hr^{-1} to 145 mm hr^{-1}.

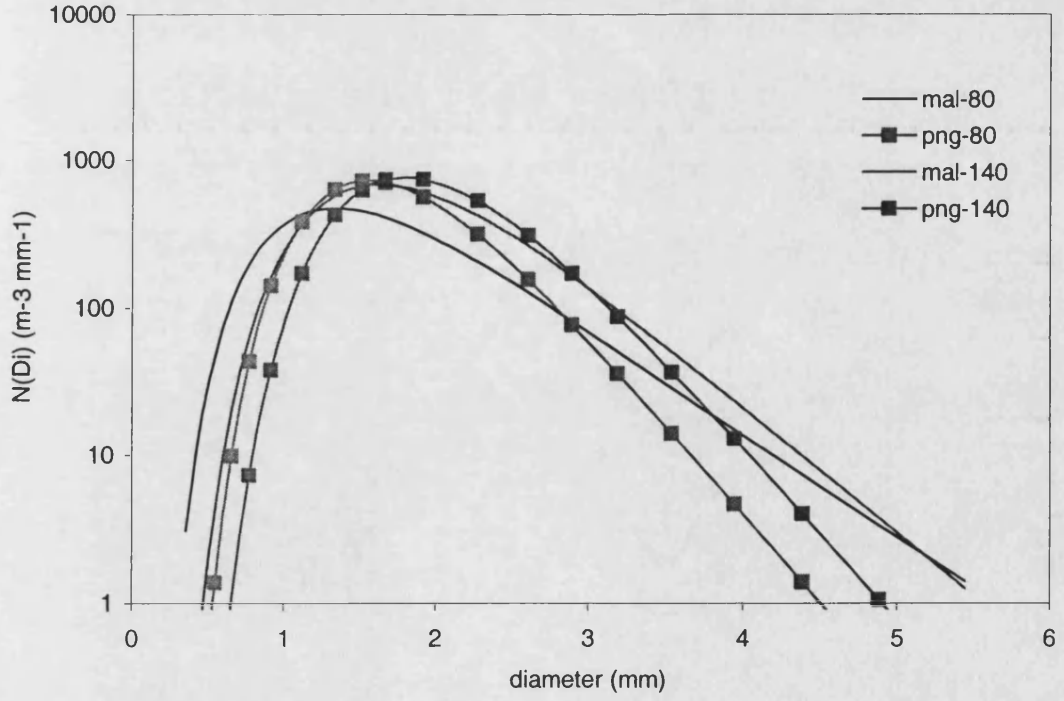

Figure 6.26: Comparison of lognormal model for Malaysia and PNG at rainfall rates of 80 and 140 mm hr^{-1}

6.14.2 Recommendations from Singapore

Researchers in Singapore [Ong and Shan, 1997] initially proposed that the lognormal model could be used to describe the rain drop size distribution of measured data obtained at Nanyang Technology University (NTU), Singapore. Their parameters for the model were fitted for rainfall rates ranging from 1.3 mm hr^{-1} to 147 mm hr^{-1}. The range selected is very similar to our PNG model for convective rain that covers ranges from 2 mm hr^{-1} to 145 mm hr^{-1}. The parameters for the lognormal model in Singapore and PNG are listed in Table 6.24.

	α	β	A_μ	B_μ	A_σ	B_σ
Singapore	276.18	0.381	-0.4286	0.1458	0.1565	-0.0091
PNG	315.65	0.229	-0.5300	0.2410	0.1650	-0.0180

Table 6.24 Parameters for lognormal model in Singapore and PNG

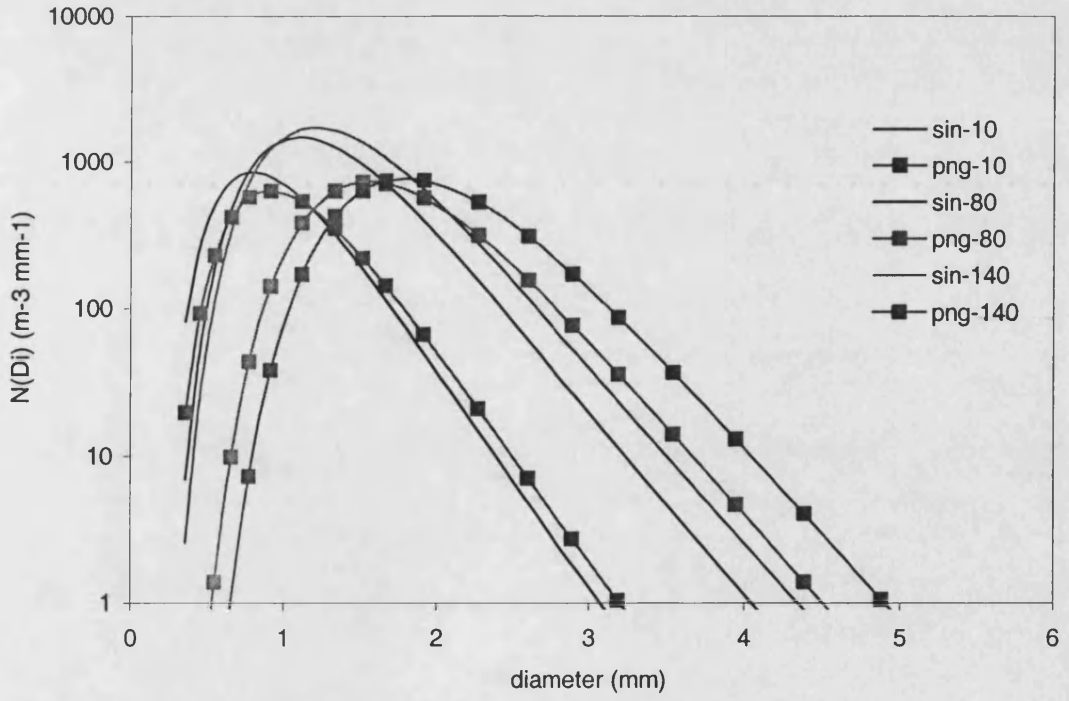

Figure 6.27: Comparison of lognormal model for Singapore and PNG at rainfall rates of 10, 80 and 140 mm hr^{-1}

The drop size distributions at rainfall rates of 10, 80 and 140 mm hr^{-1} can be compared in Figure 6.27 above. It is observed that for rainfall rates of 80 and 140 mm

hr^{-1}, the Singaporean model indicates higher number of small size raindrops compare to the PNG model. In addition, the mode diameters for the selected rain intensity in Singapore are smaller than that of PNG. Higher number of small raindrops may induce severe rain attenuation at high frequencies in Singapore. The distribution plots for the 10 mm hr^{-1} rainfall rates are almost identical. It may be that the two places share similar climatic characteristics where both are islands.

In a later publication [Ong and Shan, 1997b], they proposed that the distribution of the measured data could also be represented by modified gamma functions with the parameters as listed in the table 6.25 below. The comparison between their proposed modified gamma Ga1210 and PNG lognormal distribution plots is given in figure 6.28. We noticed that both models have approximately the same number of drops for drop sizes greater than 1.8 for rain rainfall rate of 80 mm hr^{-1}.

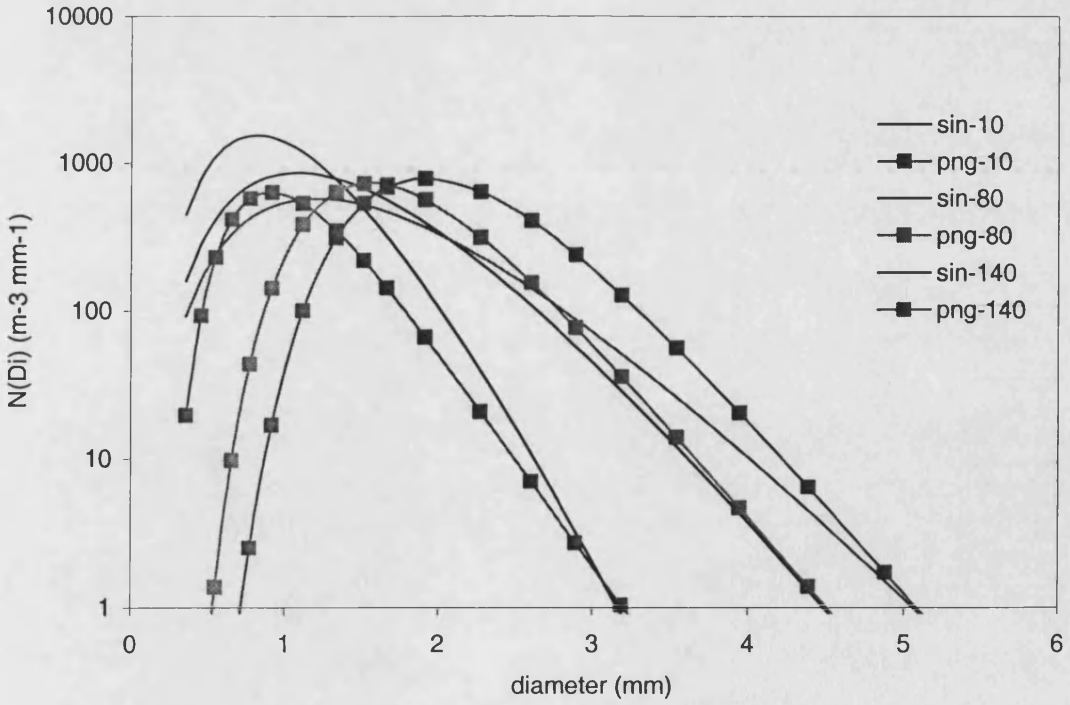

Figure 6.28: Comparison between Singaporean modified gamma GA1210 with PNG distribution for rainfall rates of 10, 80 and 140 mm hr^{-1}.

	Λ_1		P		Λ_2	
	α_1	β_1	α_p	β_p	α	β
Ga1210	10287238	1.32397	5.98084	0.09806	10.0797	0.23443
Ga2310	6482957	1.23981	6.07632	0.1158	10.1169	0.24489

Table 6.25 Parameters for two modified gamma models for Singapore

6.14.3 Recommendation from Nigeria

Lognormal model was proposed to describe the rain drop size distribution of measured data at Ile-Ife (7.5°N, 4.5°E), Nigeria [Ajayi and Olsen, 1983]. They claimed that the parameters for their model are suitable for rainfall rates ranging from 0.23 mm hr^{-1} to 146 mm hr^{-1}. This is very similar to our PNG data range for convective rain and those of Singapore. We list the parameters of the lognormal models proposed for Nigeria and PNG in the table below.

	α	β	A_μ	B_μ	A_σ	B_σ
Nigeria	108	0.363	-0.195	0.199	0.137	-0.013
PNG	315.6	0.229	-0.530	0.241	0.165	-0.018

Table 6.26 Parameters for lognormal model in Nigeria and PNG

Figs.6.29 compares the drop size distributions at rainfall rates of 10, 80 and 140 mm hr^{-1} by the two models. It is observed that for the same rainfall intensity, the Nigerian model indicates lesser number of small size raindrops than the PNG model. The mode diameter in Nigeria is slightly lower than that of PNG.

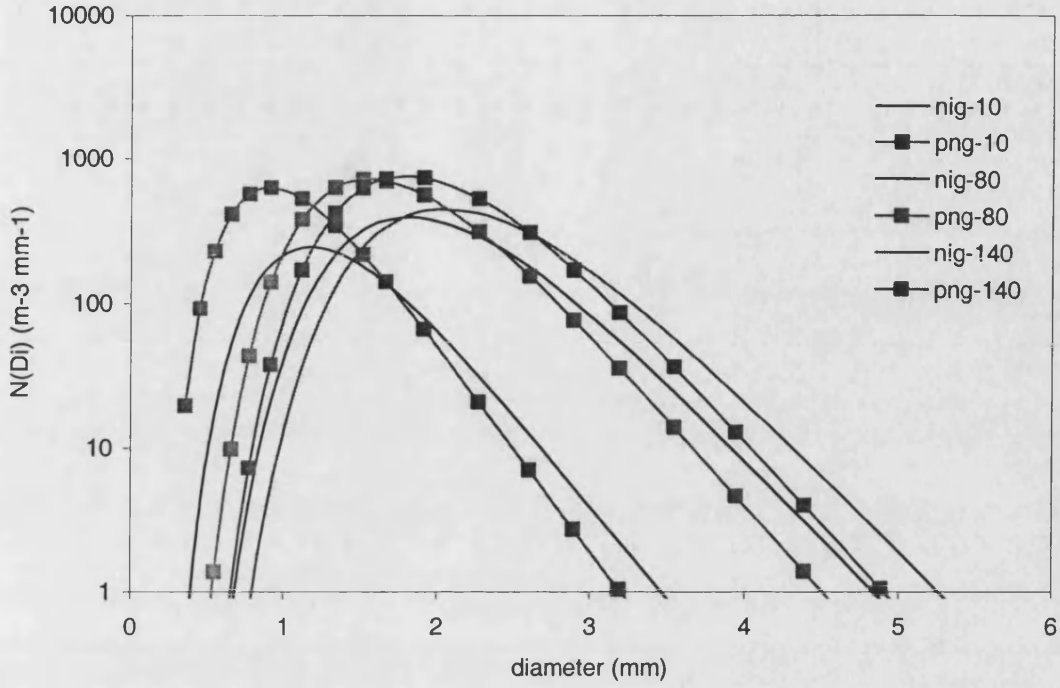

Figure 6.29: Comparison of lognormal model for Nigeria and PNG at rainfall rates of 10, 80 and 140 mm hr^{-1}

6.14.4 Recommendation from Brazil

Investigators suggested the lognormal model could represent the rain drop size distribution measured in Sao Paulo, Brazil [Marciel and Assis, 1990]. They claimed that their model is applicable for range between 70 to 120 mm hr^{-1}. The comparable parameters are given in the Table 6.27

	α	β	A_μ	B_μ	A_σ	B_σ
Brazil	0.859	1.535	-0.023	0.116	0.805	-0.150
PNG	315.6	0.229	-0.530	0.241	0.165	-0.018

Table 6.27 Parameters for lognormal model in Sao Paulo, Brazil and PNG

Fig.6.30 illustrates the comparison between the PNG and Sao Paulo distributions at rainfall rate of 80 and 100 mm hr^{-1}. For rainfall rates of 80 mm hr^{-1}, their model give distribution of result which is very similar to that of the Malaysian lognormal model.

The PNG model is closer to the Brazilian than that to the Nigerian model for rainfall rates of 120 mm hr^{-1}.

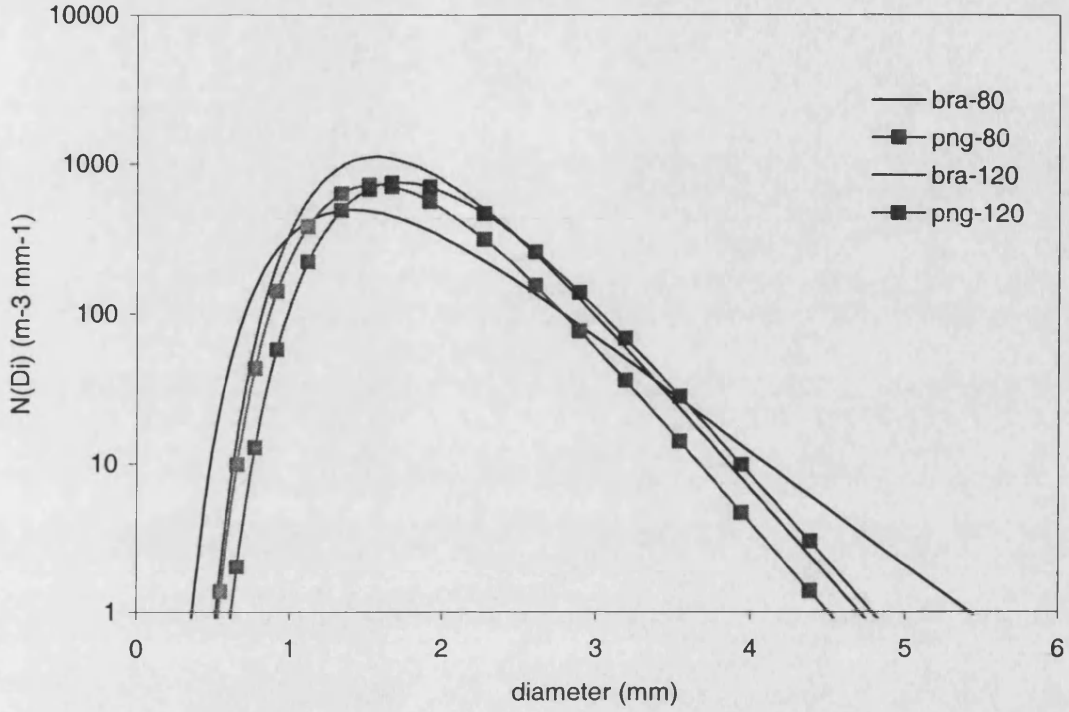

Figure 6.30: Comparison of lognormal model for Sao Paulo, Brazil and PNG at rainfall rates of 80 and 120 mm hr^{-1}

6.14.5 Other Recommendations

Researchers at Universiti Sains Malaysia (USM), Ipoh, also investigated another drop size distribution study in Malaysia [Zainal *et al.*, 1993]. Their finding also suggested that the rain drop size distribution in Malaysia could be modelled by the lognormal distribution. They plotted several curves for their suggested lognormal distribution model in their publication, however they did not furnish the values of the parameters used.

Three raindrop size distribution analyses were carried out in India. Researchers conducted their study at Dehra Dun and proposed that the distribution can be modelled by the lognormal distribution [Jassal *et al.*, 1994]. In their publication, they provided the parameters of their model applicable for rainfall rate of 49.6 mm hr^{-1}. We

list their parameters in the table below. However, this Dehra Dun model did not satisfy the rainfall rate equation and therefore this model cannot be used to represent the Indian model.

	N_t	α	β
Dehra Dun	733.0	0.409	0.606

Table 6.28 Parameters for lognormal model in Dehra Dun

Another study was conducted at Guwahati, India and the investigator also recommended that a lognormal model could model the distribution [Timothy *et al.*, 1995]. Their lognormal model is expressed by equation

$$N(D) = \frac{N_t}{\ln\sigma D\sqrt{2\pi}} \exp\left[-\frac{1}{2}\frac{\left(\frac{\ln(D)}{D_M}\right)^2}{\ln\sigma}\right]$$

where definition of the parameters are such as

$$N_t = \alpha R^{\beta}$$

$$D_M = A_\mu + B_\mu \ln R$$

$$\sigma^2 = A_\sigma + B_\sigma \ln R \qquad [6.22]$$

The third investigator proposed that the rain drop size distribution of measured data obtained at Calcutta (22.34° N, 88.29° E) could also be represented by the lognormal model [Maitra, 2000]. The parameters for their model are suitable for rainfall rates ranging from 5 to 80 mm hr^{-1}. The parameters of the lognormal models proposed for India at Calcutta and Guwahati and are listed in the table below.

	α	β	A_μ	B_μ	A_σ	B_σ
Calcutta	54	0.469	-0.538	0.0174	0.0685	0.075
Guwahati	180	0.39	1.12	0.18	0.48	-0.03

Table 6.29 Parameters for lognormal model in Calcutta and Guwahati

However, when these parameters from both places are used to compute the drop size distribution, the plots did not agree with the distributions shown in their publications. We suspect that this may due to the printing errors for their recommended parameters.

It can be observed from these cases, that several results in published papers can not used by others for redrawing and comparison purposes. The tropical rain drop size distribution measurements are still very rare and sparse for tropical regions. Perhaps with new additional measurements of drop size distribution, one standard distribution model can be established for the tropics.

6.15 Conclusion

In this chapter, a comprehensive analysis is carried on the drop size distribution for tropical rain measured in PNG. Investigation was made to find the possible distribution/s that best fit the measured data. Findings from the studies of the measured distribution narrowed the choice to several distribution options. Among the available choices are the lognormal and the gamma functions. The methods for processing the rain drop size distribution data for the lognormal and gamma models were introduced. The models were derived from distrometer data using special equations. The PNG drop size distribution models for stratiform and convective rain were determined respectively for the lognormal and gamma models. The parameters were configured and listed in the appropriate tables and curves were plotted for comparison between the modelled distributions and the measured data. Several models have been proposed to represent the measured size distribution of raindrops. Tests were carried out on each model by employing two 'goodness of fit' tests in determining the most appropriate representative for size distribution.

We conclude that the lognormal model with the 1st and 2nd moments is the best selection to describe the PNG rain drop size distribution, both for stratiform and convective rain. This is based on the goodness of fit test results together our visual opinion. Our analyses indicate that several lognormal and gamma models can be used to characterise the stratiform rain drop size distribution in PNG. The low moment regression combinations such as the ga1210, ga2310 and ga2320 of the gamma model are able to give good representation of the stratiform rain distribution. Nevertheless, even they passed the goodness of fit tests, the overall results concluded that the proposed lognormal model with combination moment 1 and moment 2 is the best option to represent the PNG stratiform rain drop size distributions.

From the results of the goodness of fit tests, it can be observed that the lognormal model with parameter derived from method of maximum likelihood and several other combinations of the low moments can also describe the drop size distribution in convective rain. The findings suggest that parameters of the models should be selected accordingly and carefully when it is used in the calculation of the attenuation of microwave signal caused by rain.

The PNG rain drop size distribution models were then compared with the other results in the tropical and equatorial regions. There are very limited studies conducted previously due to shortage of measured data. From the observation, it can be said that the rain drop size distributions in these parts of the world can be described by lognormal model and gamma with appropriate parameters. Most models give good agreement with one another regardless the fact that the parameters vary from one place to another place. We suspect that the use of drop size distribution established for another climatic region might result in the prediction error when applied to that of tropics. It appears that it is essential for researchers to gather as many data as possible in all locations.

Chapter 7

Propagation Studies in the Tropics Using Radar System

7.1 Introduction

The nations in the tropical regions today are undergoing a rapid expansion in satellite communications with the increase in demand for long distance telecommunications, broadcastings and data channel requests. Due to rapidly increasing demand for more bandwidth, the radio frequencies used by the current satellite communication systems in these regions have been gradually shifted toward higher bands. Despite such phenomenal growth, available data to describe how the radiowaves behave in tropical conditions is still lacking.

In other words, there are insufficient measured data in the tropical region to accurately model the Earth-space propagation at microwave and millimetre wavelengths. Reliable propagation models are required to support the optimal design of the future satellite communication systems in the high rainfall rate climatic zones [Eastment, 1999]. The introduction of DTH satellite services in tropical regions at K_u-band frequency and above could be hampered by signal attenuation due to heavy rainfall if the correct margin or fade mitigation technique could not be engaged.

This heavy rain in the tropical region can affect radiowave signals profoundly, causing signal fading and interference. A multiparameter radar system is an ideal tool for studying the climate conditions in the tropics. This is the only feasible technique of collecting data that will furnish both the horizontal and vertical structure of precipitation in a way that is practical for studying rain scatter and interference [Currie and Brown, 1987; Kingsley and Shaun, 1992]. The cross-polar and Doppler information from such radar could be used to determine the height of melting layer for

all types of rain condition [Ladd *et. al.*, 1997; Eastment *et al.*, 1995; Watson *et al.*, 1998]. It is of important to ascertain the correct height of the melting layer in a statistically valid way, rather than by studying specific events during short-term campaigns. The characterisation of the melting layer has always been of particular interest in the modelling of radiowave propagation for Earth-space communication path due to its different electromagnetic properties in comparison to those of underlying rain [Salonen *et al.*, 1990].

7.2 Description of the Radar System

The Radio Communication Research Unit (RCRU) engineers from RAL designed, built and installed a fixed 3m vertical (zenith) pointing polarimetric Doppler radar at the Papua New Guinea University of Technology at Lae in 1996. This radar furnished six months' worth of vital climate data before it was disassembled in 1997. The 3-GHz S-band dual polarisation system measured and recorded reflectivity (*Z*), linear depolarisation ratio (*LDR*), radial velocity and velocity spectral width at 3.2 s sampling rate with 75 metre range gates. The primary objective of such system was to obtain information of the vertical structure of precipitation in tropical climate [Eastment *et al.*, 1995]. This was in a way very useful for example to predict attenuation due to rain along the Earth-space paths at high frequencies

In the previous Chapter 6, we have presented how the distrometer and radar data were applied to investigate one of the characteristics of tropical rain, which is the rain drop size distribution. Combine with other detail analyses on additional characteristics of rain such as the appropriate rain height and how different rain cell systems evolve together with the size distribution can ultimately improve the accuracy in predicting radiowave attenuation for satellite communications systems in the tropical regions.

7.3 Measurements and Classification of Rain Events

The radar data from Papua New Guinea are classified into two groups namely stratiform and convective. Previous studies [Tokay and Short, 1996; Ladd *et al.*, 1997] also utilise these two rain classifications. Figures 7.1 – 7.4 below depict time series displays of Z vertical scan recorded on selected days during stratiform events within the period of campaign. It is apparent in the presented figures, that each exhibits clear melting height of approximately 5 km with approximate layer thickness between 200-500 m. The melting layers are the transition regions between snow and rain. They usually start at the 0° C and finish a few degrees above 0° C where the entire snow particles melted and become raindrops.

Examples of convective events can be observed in figures labelled as Figure 7.5 - 7.8. Even though the co-polar reflectivity measurements do not exhibit existence of a melting layer, such enhancement can be seen in the cross-polar reflectivity that indicative of the melting process. Based on the 6 months data, the radar scans were inspected and rain events are identified and recorded. The processed and classified radar results can be observed in Appendix L.

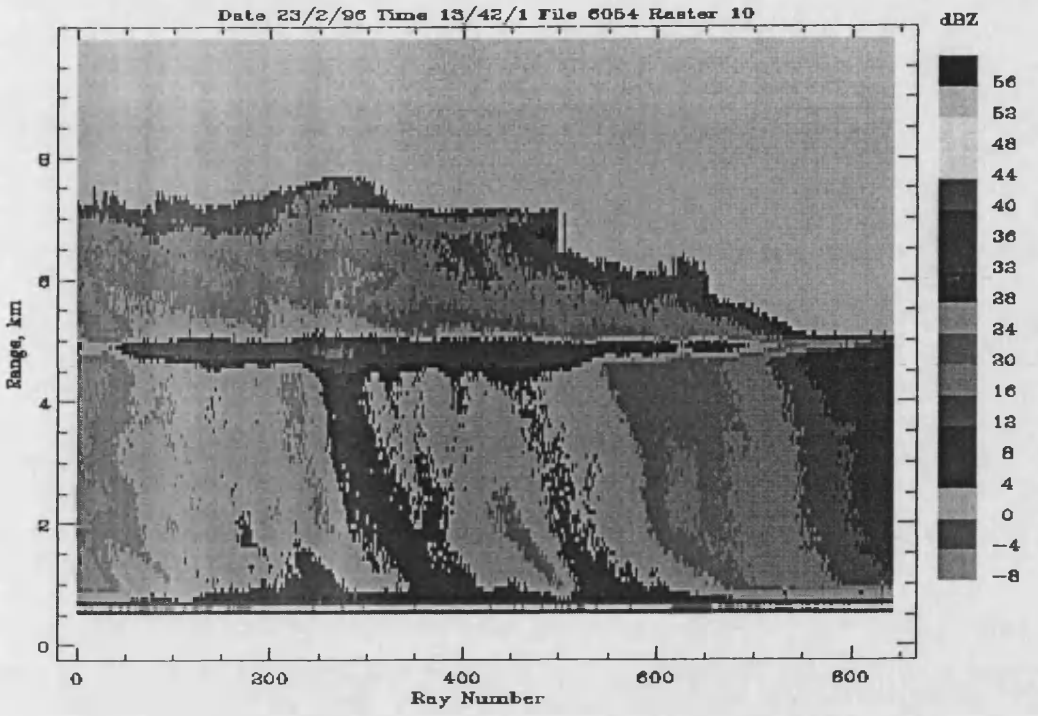

Figure 7.1: Stratiform event on 23/2/96

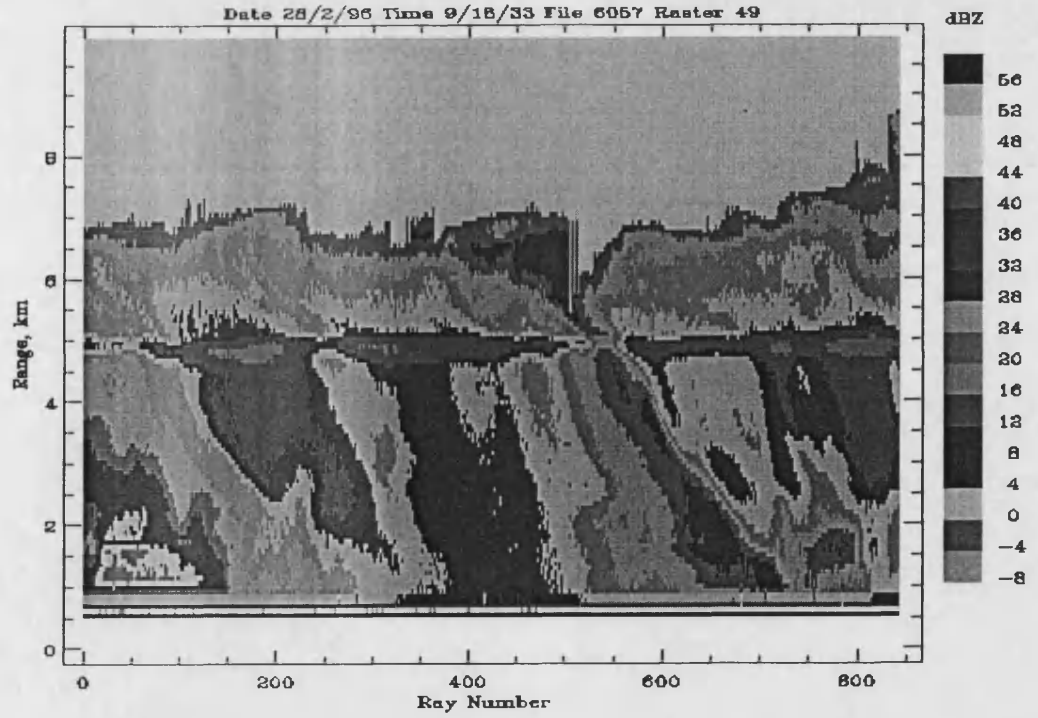

Figure 7.2: Stratiform event on 28/2/96

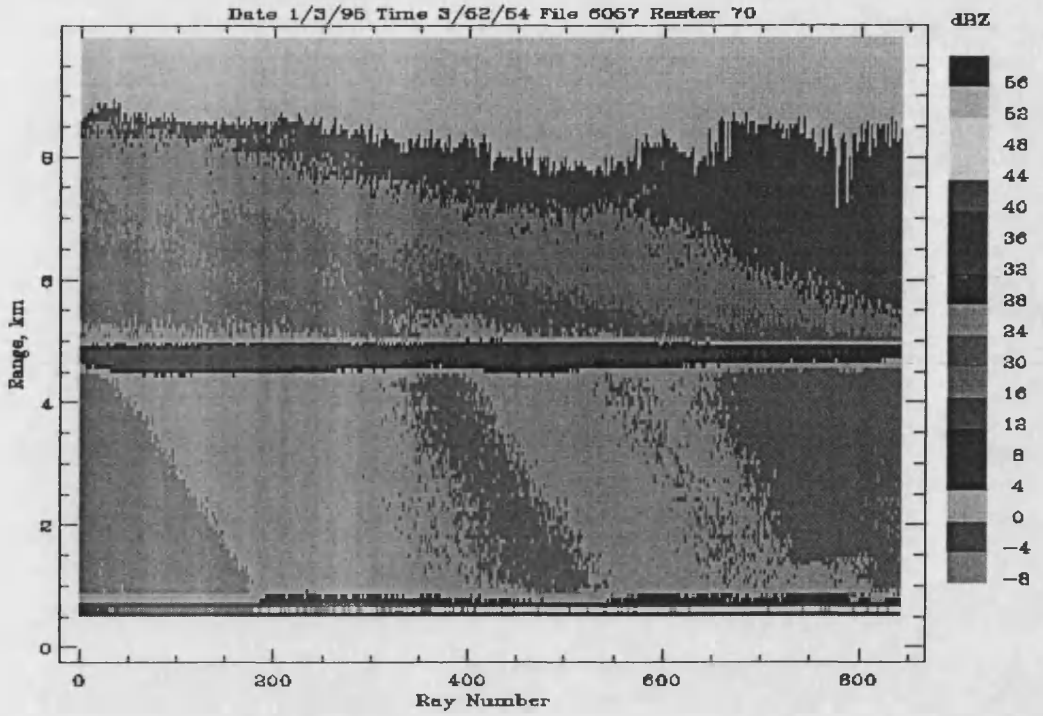

Figure 7.3: Stratiform event on 1/3/96

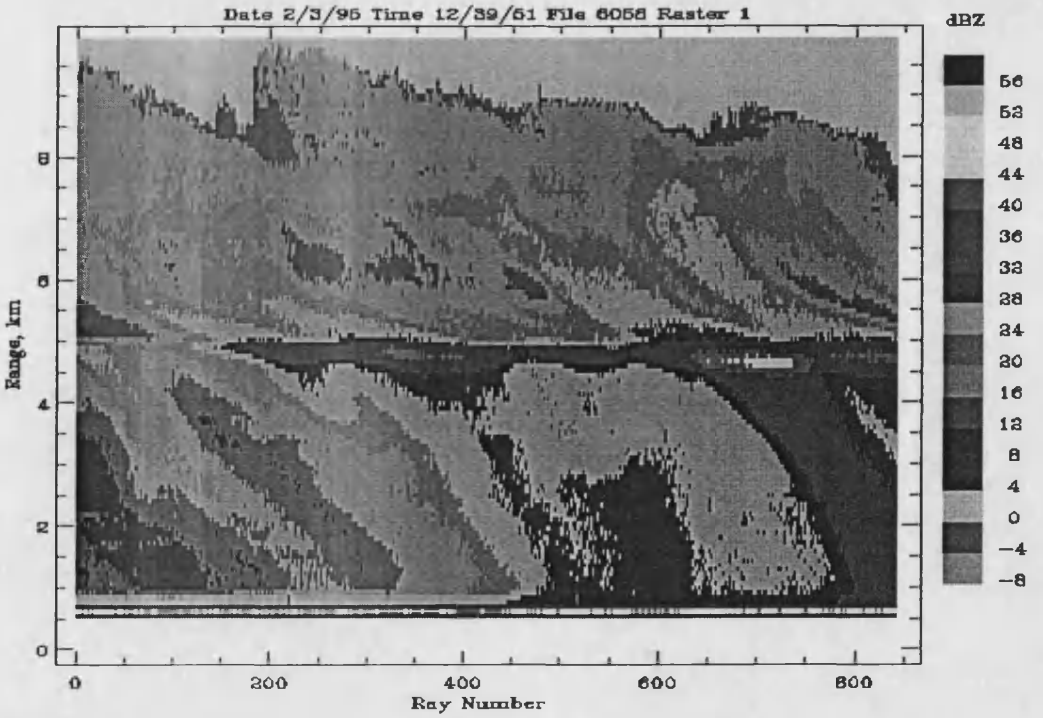

Figure 7.4: Stratiform event on 2/3/96

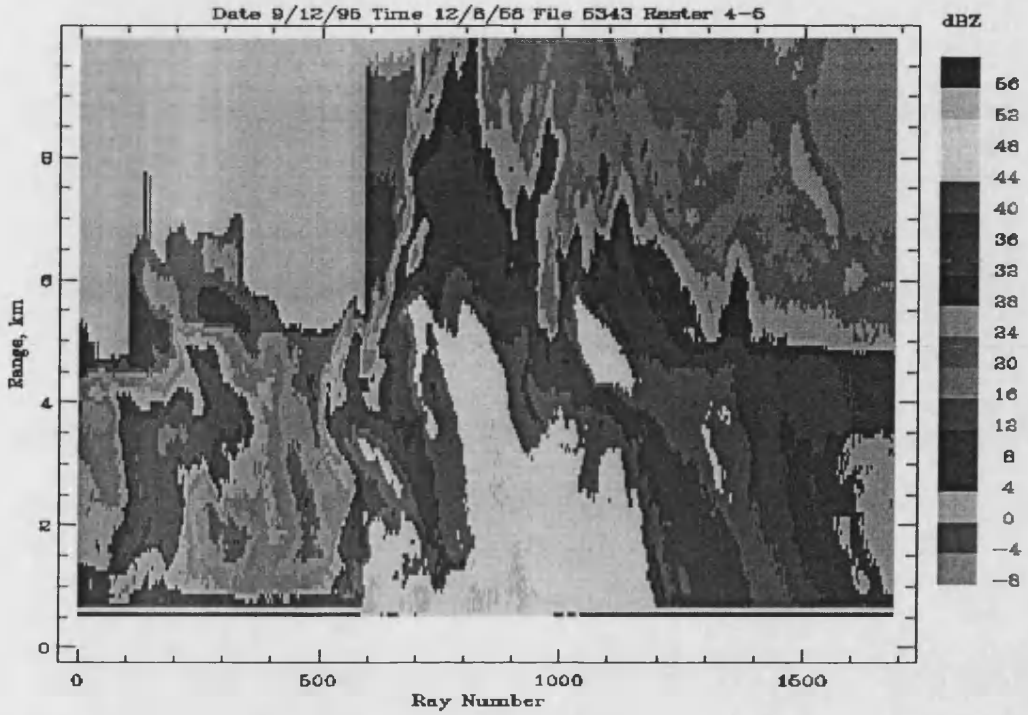

Figure 7.5: Convective event on 9/12/95

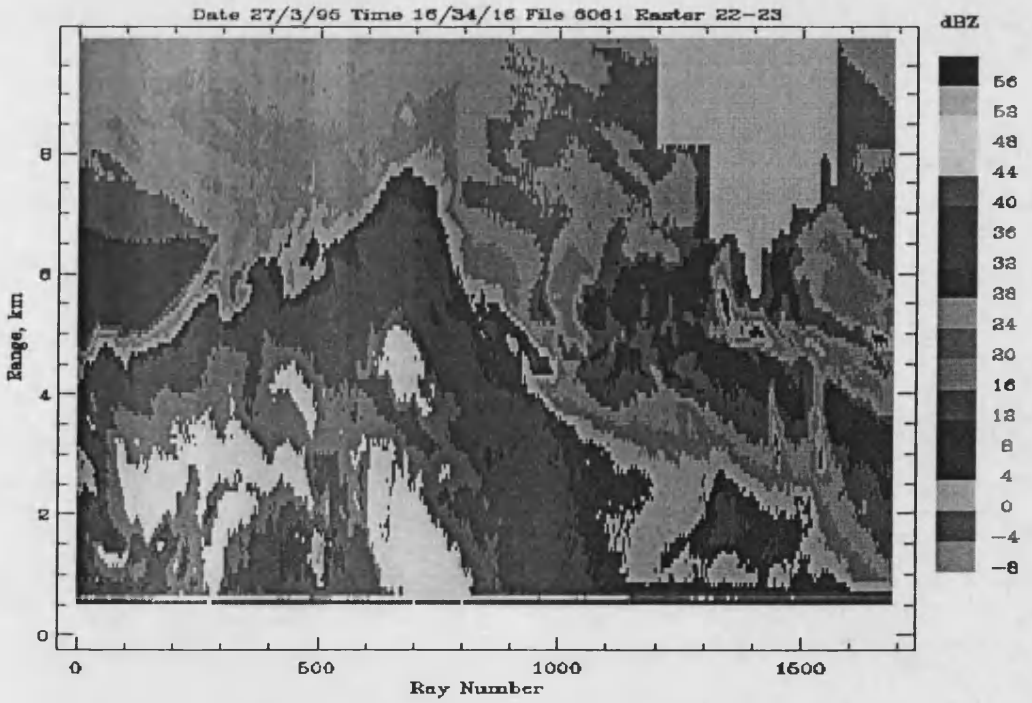

Figure 7.6: Convective event on 27/3/96

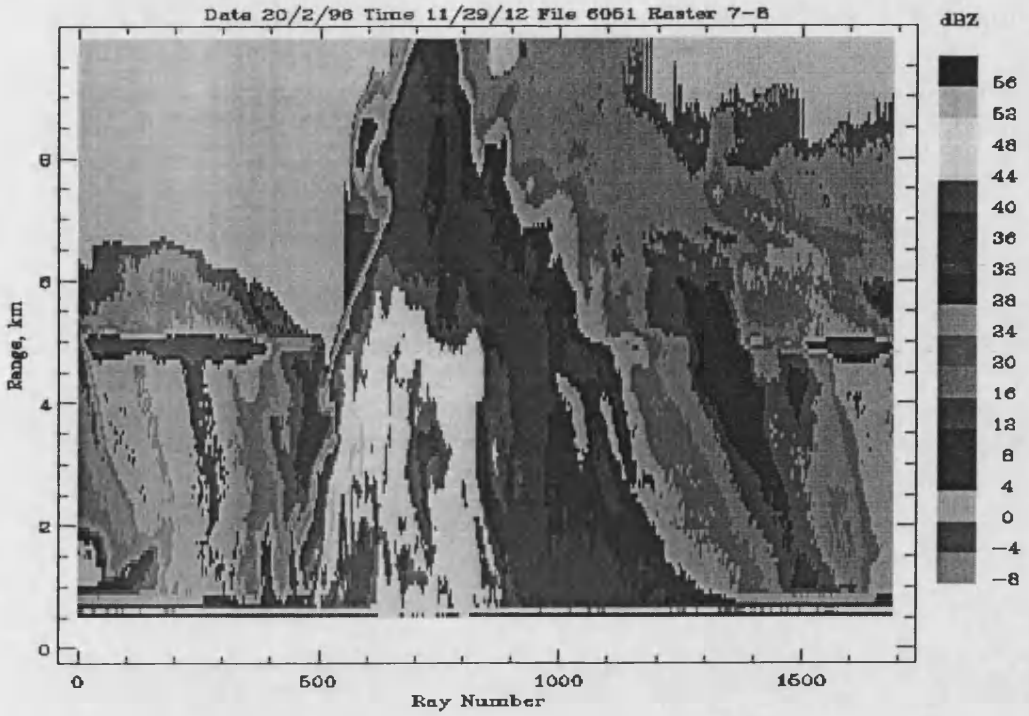

Figure 7.7: Convective event on 20/2/96

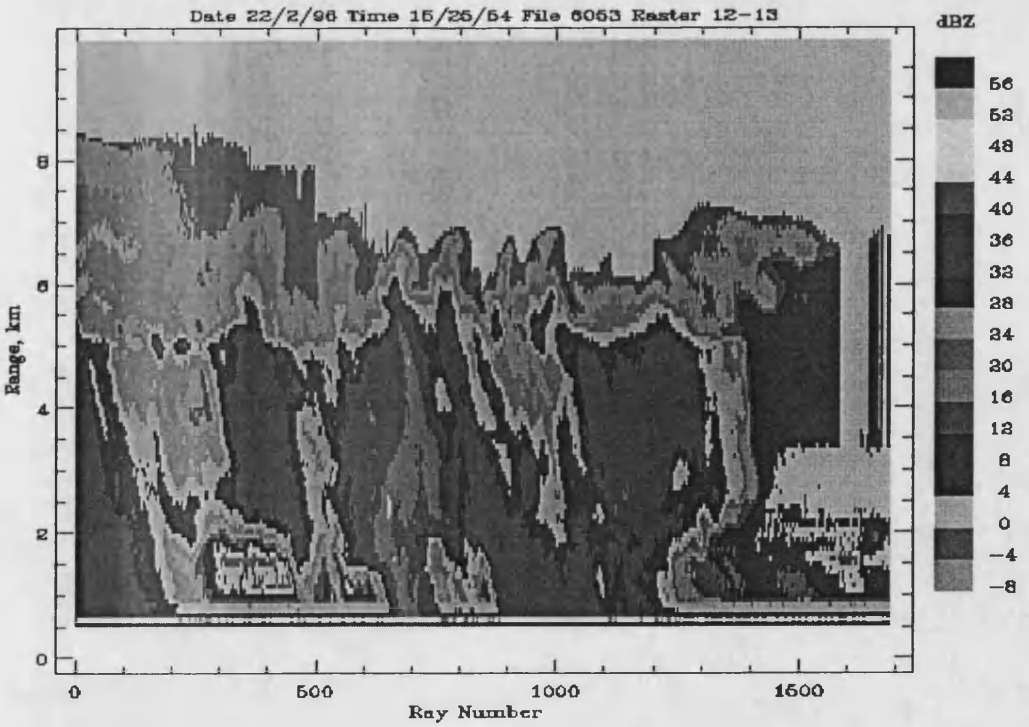

Figure 7.8: Convective event on 22/2/96

7.4 Comparison of Radar Observations with distrometer measurements

The accuracy of the radar calibration must be confirmed in order to substantiate the validity of the radar measurements for propagation studies such as prediction of rainfall rates and attenuation for Earth-space systems operating at higher frequencies. Since the co-located distrometer provided the drop size distribution measurements and the number of raindrops per unit time falling on it's sensor, such information could be used to calculate the expected S-band radar reflectivity. The radar is pointed at zenith therefore the concept of vertical and horizontal polarisation has no meaning. The co-polar reflectivity Z for the radar, determined from the horizontally polarised transmitted and received pulses is defined as [Goddard and Cherry, 1984; Doviak and Zrnic, 1993]

$$Z_{HH} = \frac{\lambda^4}{\pi^5 \left| \frac{(m^2-1)}{m^2+2} \right|^2} \times \sum N(D_i)\sigma_H(D_i)\delta D_i \qquad (7.1)$$

where λ is the wavelength assumed in the scattering cross section calculation. In our system the wavelength is equal to 10 cm and the coefficient m is the refractive index of water. By courtesy of Dr Robert Watson, University of Bath, we are allowed to use his numerical data of the scattering cross sections $\sigma_H(D_i)$ for horizontal polarisation at frequency of 3 GHz and temperature of 25 ° C.

The quantity of $N(D_i)\delta D_i$ in the above equation is given as follows

$$N(D_i)\delta D_i = \frac{n(D_i)}{(0.3v(D_i))} \qquad (7.2)$$

where $N(D_i)\delta D_i$ is the number of drops per cubic meter in the interval δD_i of the distrometer channel having arithmetic mean diameter D_i (mm) and $v(D_i)$ is the terminal velocity (m s^{-1}) of drops of diameter D_i

.

The co-polar reflectivity Z_{HH} can be expressed on a logarithmic scale in unit dBZ, which can be calculated from:

$$dBZ = 10\log Z_{HH} \tag{7.3}$$

With the assumption that the majority of raindrops fall in vertical direction, then it should be reasonable to expect good agreement between the distrometer derived reflectivity with the radar measurements. Figure 7.9 shows a radar profile of a convective event; where its time series comparison between the measure reflectivity at height of 1 km and the ground based distrometer inferred reflectivity is given in figure 7.10. Satisfactory good agreement is obtained when we adjusted the distrometer values by the time shift corresponding to the period during which the particles fall from 1 km to ground level. (95 s considering terminal velocity of ~9.5 ms^{-1})

With such agreement, this imply that the calibration for the radar system has been within its expected value based on testing previously in UK [Eastment, 1995] and further research for propagation studies of the system operating at other frequencies of interest can be carried out.

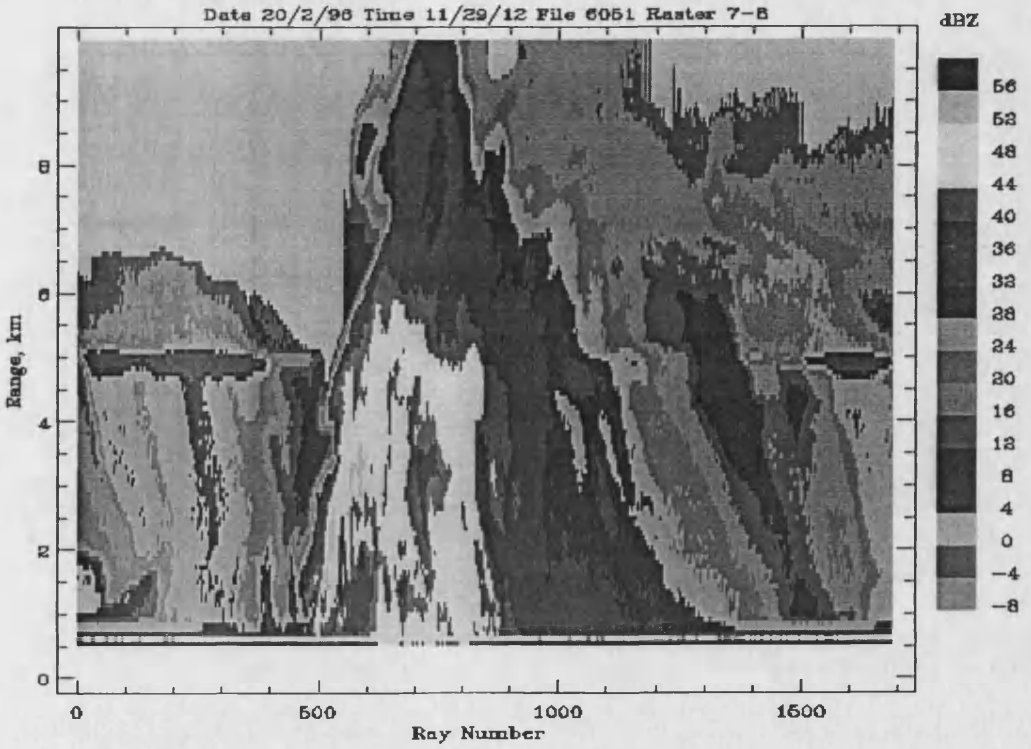

Figure 7.9: Papua New Guinea radar profile 20th February 1996.

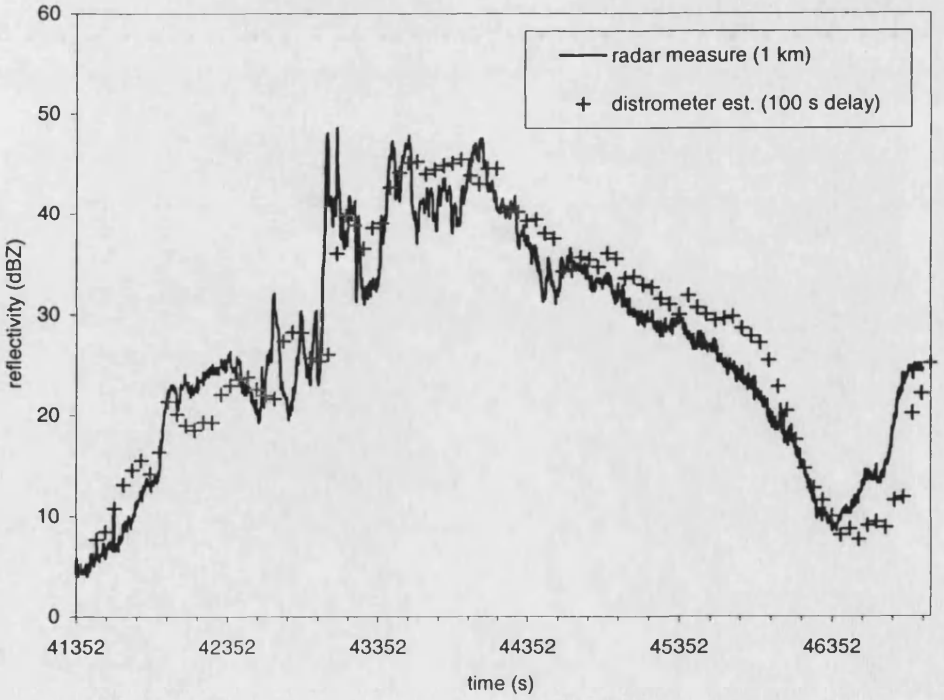

Figure 7.10: Time series comparison between the ground based distrometer and radar reflectivity 20th February 1996

7.5 Correlation of Rainfall Rate with Reflectivity

Radar measurements can be applied for estimating rainfall rate using the single parameter measurement of precipitation technique. The technique exploits the pre-determined rainfall rate versus reflectivity relationship (*R-Z* relationship) to convert radar reflectivity measurements to rainfall rates. Over the years, several different *R-Z* relationships have been developed and proposed. These are mostly empirical models that were developed using co-located and simultaneous rainfall rate measurements and radar reflectivity measurements.

There has been significant variability in the suggested models for estimating the rainfall rate from radar reflectivity measurements [Battan, 1973, Doviak, 1993]. It has been discussed that the propagation models may be site-specific and that they do not apply universally to different locations around the world [Sauvageot, 1992; Marshal Palmer 1948]. Additional distinction is that the models might depend on the type of rainfall, which commonly accepted to deviate considerably as from one specific region of the world to another. Hence, there is a necessity to develop a model that would best describe the *R-Z* relationship for measurements in tropical region.

Distrometer measurements of rainfall in PNG over a 6-months period were obtained, and the raindrop size distributions according to rainfall type have been characterised as detailed in previous chapter. It was discussed by investigators that the rain drop size distributions in the tropics are different from those summarised from other parts of the world. This could imply that the relationships by which the rainfall rate estimates are obtained from radar reflectivity measurements in the temperate region are very unlikely applicable to the tropics.

At 3 GHz, the Rayleigh scattering model may describe the radar scattering from rain. The wavelengths of microwave frequencies around S-band are larger compare to the diameters of the rain drops. The Rayleigh scattering model could be used with the

measured rain drop size distributions to estimate the reflectivity at the various rainfall rates. In our investigation, we employed Equation 7.1 to calculate the estimation of the radar reflectivity using the rain drop size distribution information. The rainfall rate is calculated using the size distribution information as given in Equation 6.4.

We processed more than 2000 convective and nearly 5000 stratiform profiles and employed these measurements in the tabulation for the best-fit relationships. Plots of reflectivity against rainfall rate for each rain type at selected frequencies can be observed in figures below. Table 7.1 furnishes the power law coefficients determined for the relevant best-fit Z-R relationships. The coefficient A and b for the relation $Z=AR^b$ obtained through research work then compared with other studies carried out in the tropical region.

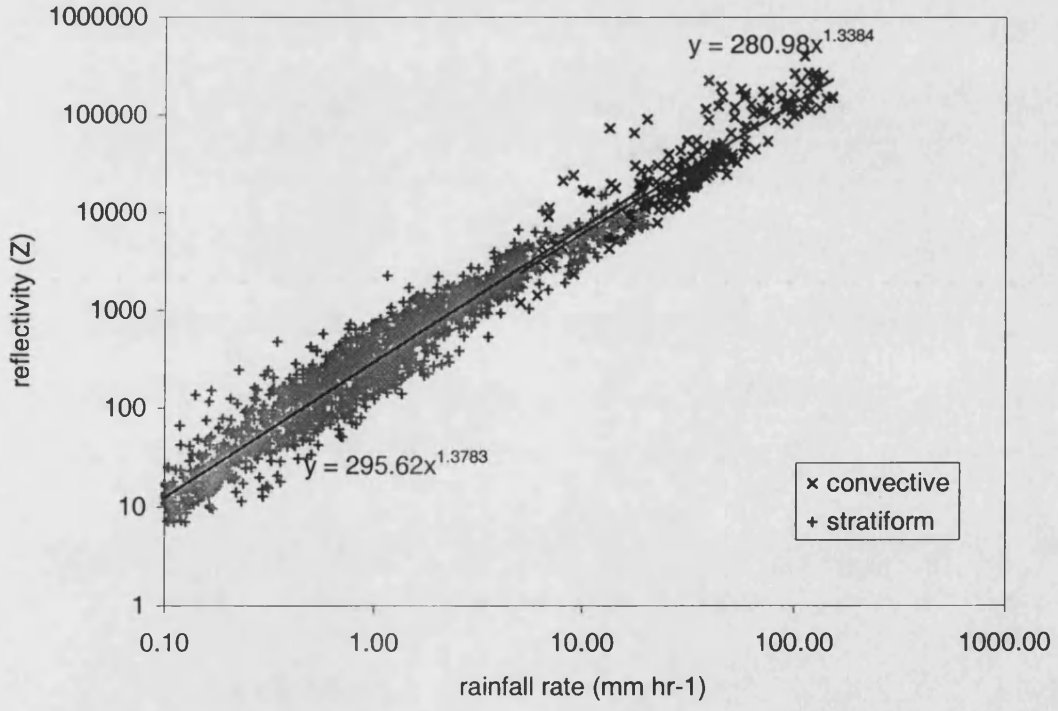

Figure 7.11: *Z-R* relationship for both convective and stratiform events

Coefficient values for stratiform events obtain from our analysis in the table above compare well with other studies carried out in the tropical region but those for convective differ significantly. We recognised that even if the actual drop size

distribution at two different locations were on average the same, there are other factors that could lead to different *R-Z* coefficients. As an example, we suspected that the number of sample involved and the derivation method of calculating the reflectivity value could have major influence on the proposed *R-Z* relationship.

	Convective		Stratiform	
	A	*b*	*A*	*b*
Papua New Guinea	281	1.31	296	1.38
PNG [Ladd *et al.*, 1997]	93	1.36	132	1.36
Singapore [Wilson and Tan, 2001]*	139	1.50	330	1.35
[Tokai and Short, 1996]	139	1.43	367	1.30

Table 7.1: Reflectivity-rainfall rates relationship coefficients for $Z=AR^b$ *results were derived using only major convective events logged in PNG

7.6 Propagation Effects at Higher Frequencies

The information provided by the radar can play important roles in studying the rain-induced propagation effects at high frequencies i.e., the K_u-band, K_a-band and V-band in the tropical region. For every radar reflectivity-height *Z(h)* profile measured at S-band, the path attenuation at frequency of interest can be derived using equation as follows [Thurai *et al.*, 1995; Eastment *et al.*, 1998]:

$$A = \left(\sum_{h=0}^{h_R} \alpha_R Z(h)^{\beta_R} dh \right) + \left(\sum_{h=h_R}^{h_m} \alpha_m Z(h)^{\beta_m} dh \right) \tag{7.4}$$

where *dh* is the height resolution of *Z(h)* profile, in our case 75 m, h_R and h_m are the heights of the rain and the melting layer respectively, αR and βR are the coefficients

required for attenuation scaling to frequency of interest and α_m and β_m are the corresponding coefficients in the melting layer.

Algorithm making used the radar properties can be developed to automatically detect the top and bottom of the melting layer providing the h_R and h_m in the above equation. The drop size distribution provided by a co-located distrometer can be used to estimate the rainfall rate, radar reflectivity and the specific attenuation at frequency of interest. The best fit α and β coefficients then could be derived from these data

.

In the next sections we present our findings in derivation of the best-fit relationship for propagation characteristics at 11, 22, and 38 GHz based on measurements conducted in tropical condition.

7.7 Assessment of Specific Attenuation – Rainfall Rate Relationship

Attenuation of electromagnetic waves by hydrometeors in the atmosphere may result from both absorption and scattering depending on the size, shape, and composition of the particles [Battan 1973]. Communication engineers and radar meteorologists have noticed that for a wide range of rainfall rates and rain types, a consistent relationships between specific attenuation of microwaves and the rainfall rate measured with rain gauges along the propagation path [Doviak, 1993]. The observations show that the specific attenuation, γ and rainfall rate, R are related by power law for a wide range of rainfall rates and rain types.

Given the scattering amplitude, the specific attenuation γ can be estimated using the known drop size distribution using the following formula [Cherry *et al.*, 1981; Goddard and Cherry, 1984]:

$$\gamma = 0.4343 N_0 \mathrm{Re}\left[\frac{2\pi}{k_0^2}\int_0^{D\max} S(D_i)\times\exp(-3.67 D_i / D_0) dD_i\right] \quad (7.5)$$

where N_0 is the number of drops per cubic meter $mm^{-1}m^{-3}$, D_0 is the median volume diameter (mm) and D_i is the diameter of a spherical drop equal in volume to the oblate drop, $k_0 = 2\pi/\lambda$ with λ the wavelength in (centimetres) of the attenuated transmission, and $S(D_i)$ is the forward scattering amplitude dependent on frequency, polarisation, and angle of incidence.

In rain, the number of drops per unit volume per unit interval of D_i can be expressed as:

$$N(D_i) = N_0 \exp(-3.67 D_i / D_o) \quad (7.6)$$

by substituting the above Equation 7.5 into Equation 7.4, the specific attenuation γ can be calculated using the know drop size distribution with the following expression:

$$\gamma = 0.4343 N_0 \mathrm{Re}\left[\frac{2\pi}{k_0^2}\sum S(D_i) N(D_i)\delta D_i\right] \quad (7.7)$$

where the quantity of $N(D_i)\delta D_i$ is the same as that for Equation 7.2. Again, by courtesy of Dr Robert Watson, we are provided with the numerical data of the forward scattering amplitude $S(D_i)$ at frequency of 11, 22 and 38GHz at temperature of 25 ° C.

Using the same stratiform and convective profiles as in previous section, the specific attenuation at 11, 22 and 38 GHz were calculated using the Equation 7.7 above. Figure 7.12, 7.13 and 7.14 show the specific attenuation versus the rainfall rate, both computed from the distrometer derived drop size distribution.

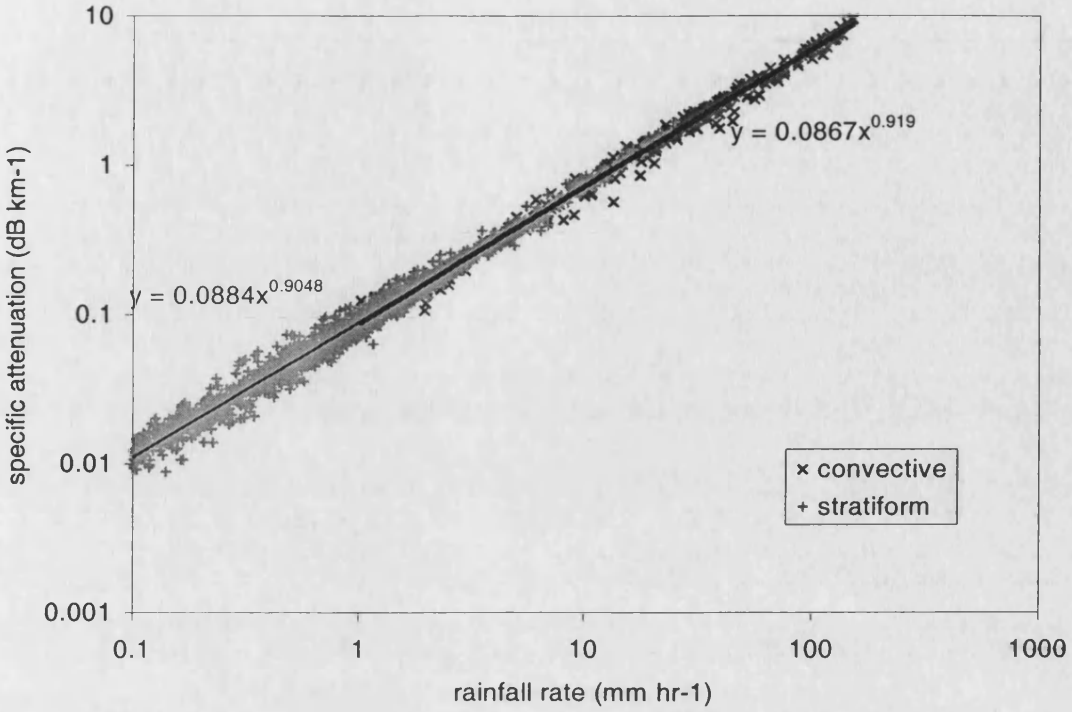

Figure 7.12: γ-R relationship for both convective and stratiform events at 11 GHz

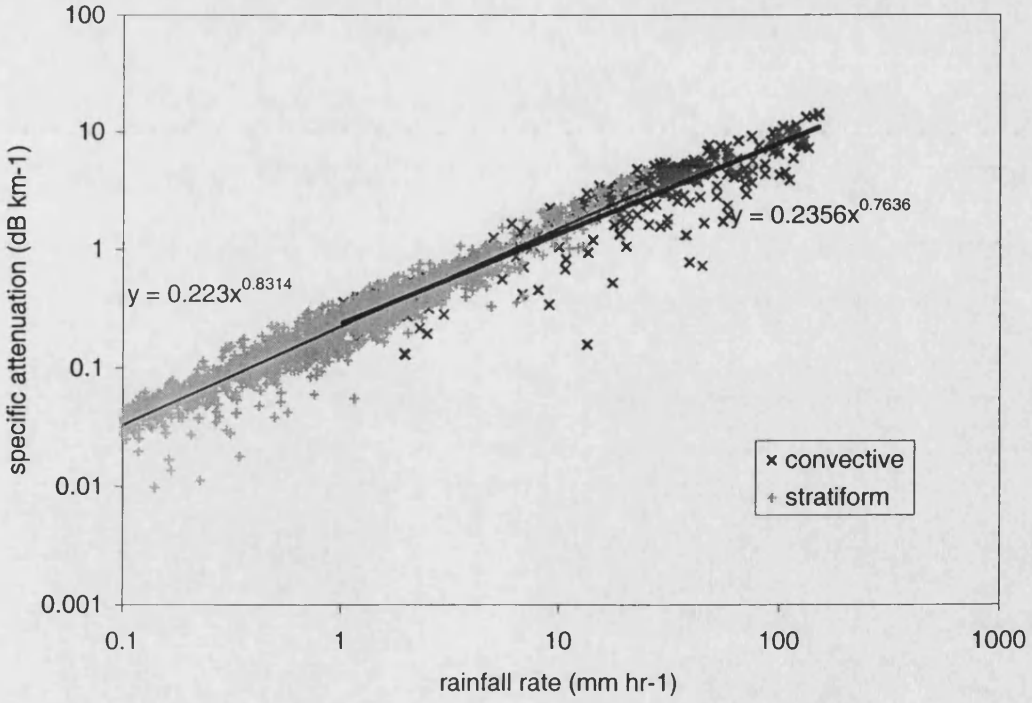

Figure 7.13: γ-*R* relationship for both convective and stratiform events at 22 GHz

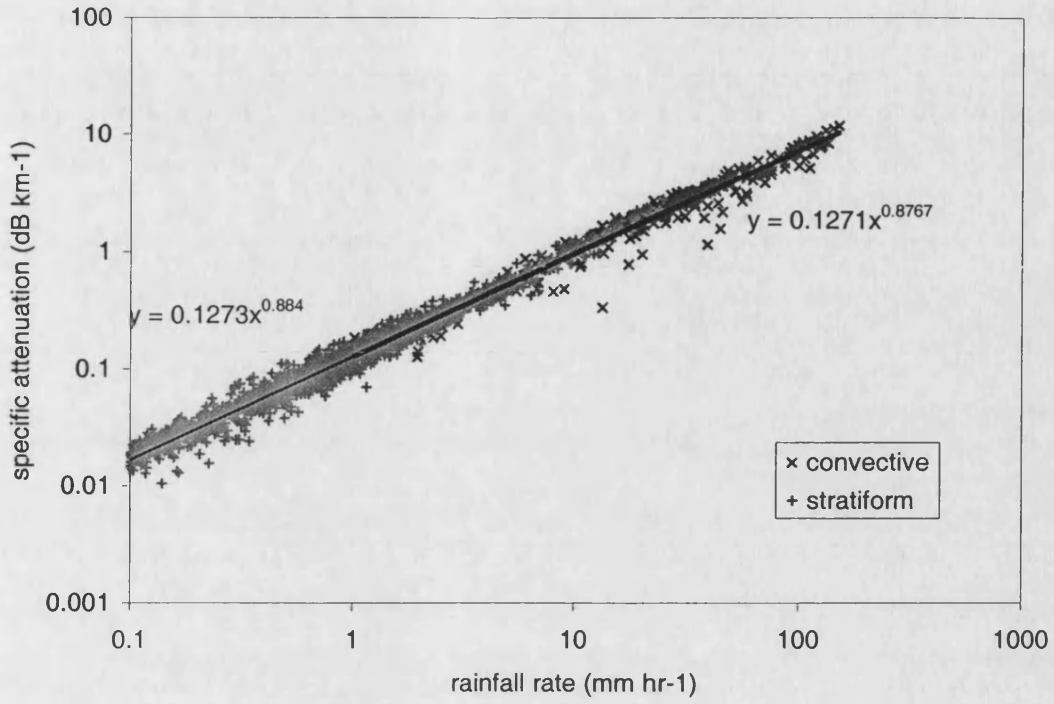

Figure 7.14: γ-R relationship for both convective and stratiform events at 38 GHz

Two parallel lines are obtained in each figure, which intercept the best-fit line. The power law coefficients for the best-fit relationships are included in Table 7.2 below.

	γ-R relationship			
	Convective		Stratiform	
	A	B	A	B
11 GHz	0.0867	0.9190	0.0088	0.9048
22 GHZ	0.2356	0.7636	0.2230	0.8314
38 GHz	0.1273	0.8767	0.1273	0.8840

Table 7.2: Specific attenuation-rainfall rates relationship coefficients for $\gamma=AR^b$

7.8 Assessment of Specific Attenuation – Reflectivity Relationship

Radar scans of rain event in PNG are used to characterise the rain type and the co-located distrometer measurements are utilised to ascertain the rain drop size

distributions. The rain drop size distributions are then applied to study the relationship between specific attenuation γ and the radar reflectivity. Using the measured rain drop size distributions and the appropriate scattering properties at frequencies of interest, the specific attenuation and the radar reflectivity is calculated at different rainfall rates.

The specific attenuation and reflectivity calculations are used to develop γ-*Z* model using standard regression analysis. Such model can be applied to estimate the specific attenuation using radar reflectivity from radar scans. The specific attenuation and reflectivity at 11, 22 and 38 GHz were acquired using the Equation 7.6 and Equation 7.1 respectively. Figure 7.15, 7.16 and 7.17 below show the scatter plots of specific attenuation versus reflectivity, which both calculated from the drop size distribution measurements. Two parallel lines are obtained in each figure, which intercept the best-fit line. The power law coefficients for the best-fit relationships are included in Table 7.3

	γ-Z relationship			
	Convective		Stratiform	
	A	*B*	*A*	*b*
11 GHz	0.0036	0.6147	0.2003	0.5961
22 GHZ	0.0071	0.5699	0.0048	0.5762
38 GHz	0.0277	0.4575	0.0111	0.5253

Table 7.3: Specific attenuation-rainfall rates relationship coefficients for $\gamma=AZ^b$

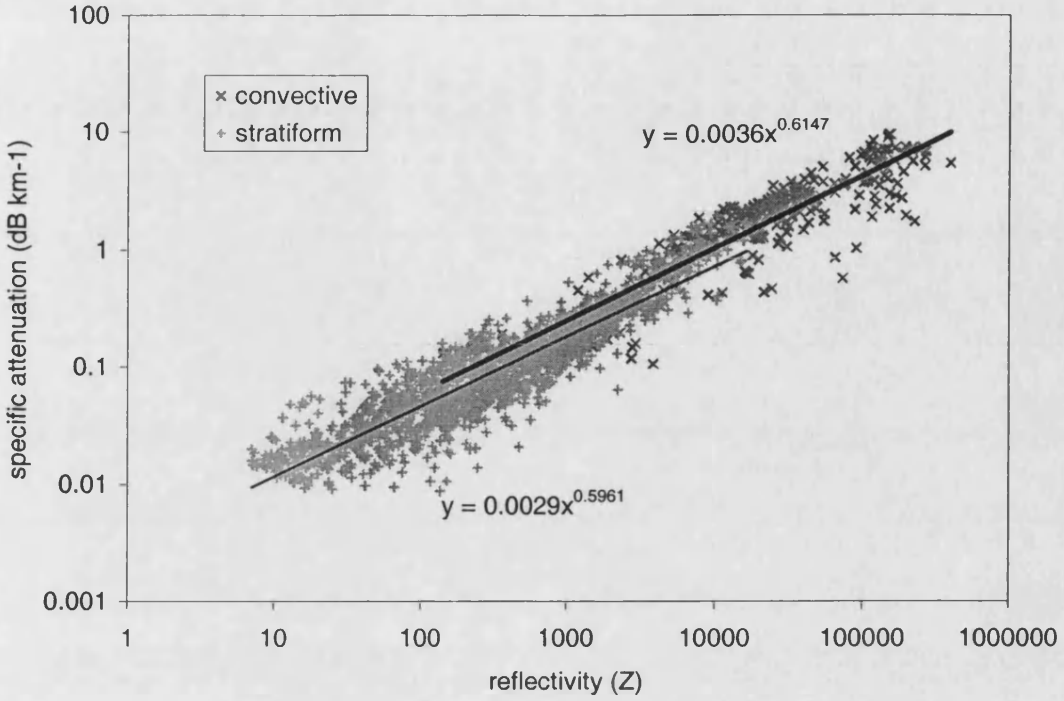

Figure 7.15: γ-*Z* relationship for both convective and stratiform events at 11 GHz

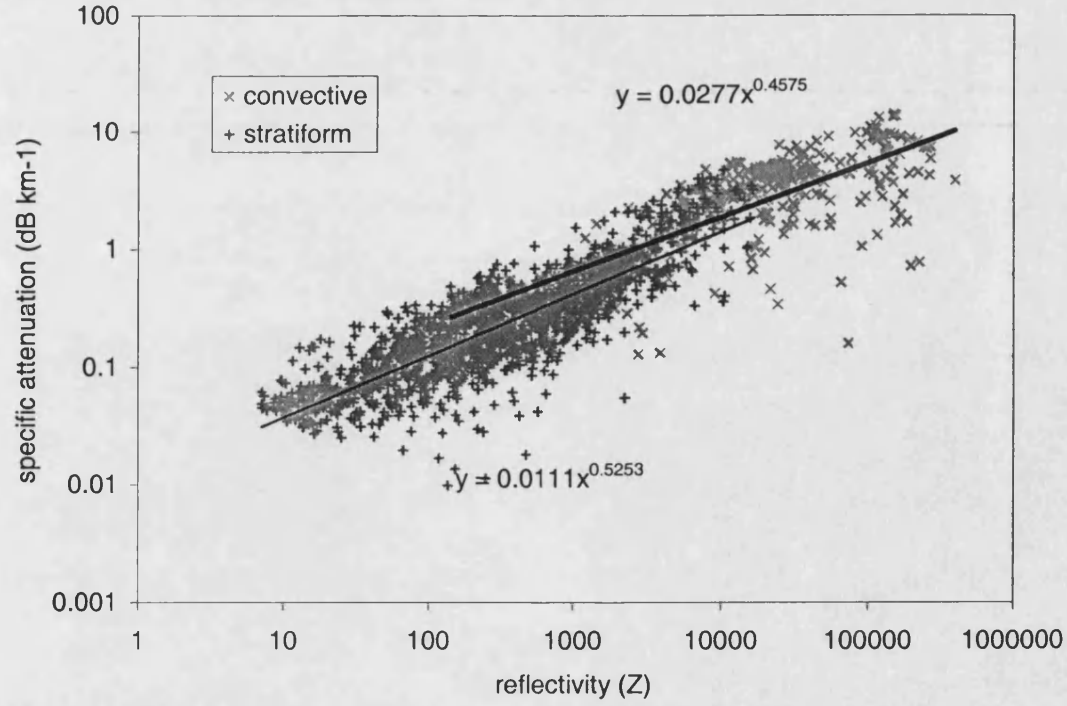

Figure 7.16: γ-Z relationship for both convective and stratiform events at 22 GHz

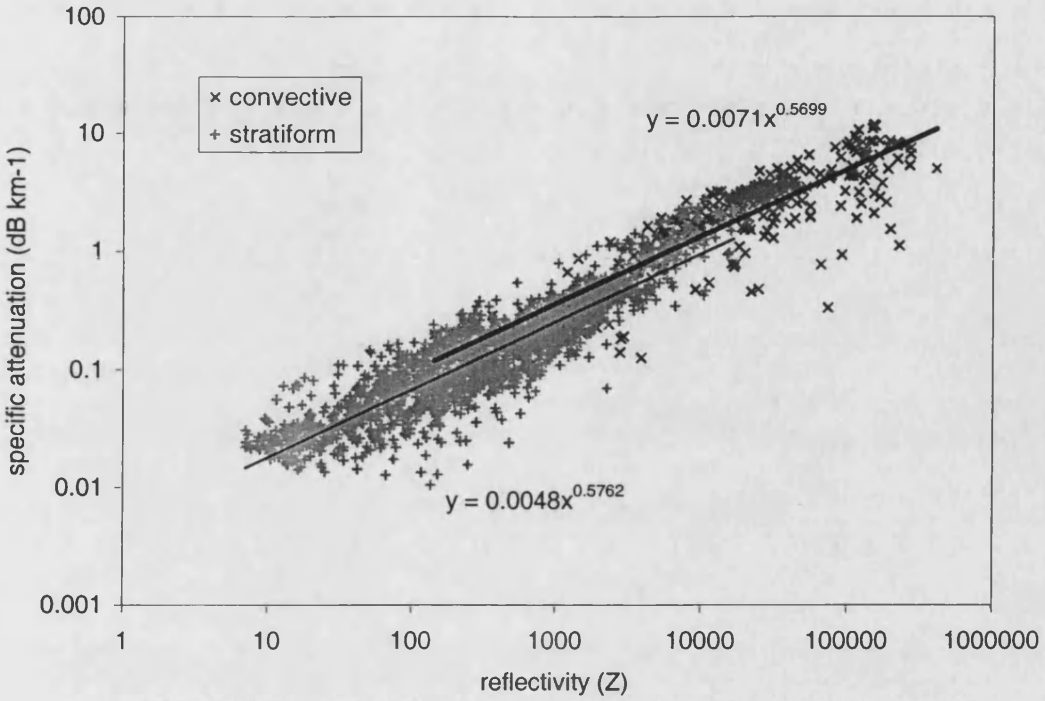

Figure 7.17: γ-Z relationship for both convective and stratiform events at 38 GHz

7.9 Radar Reflectivity Gradients

The co-polar reflectivity of the radar can be utilised to characterise the vertical variation of rain specific attenuation. This is because reflectivity is proportional to the back scattering properties of the hydrometeors in which the volume being detected.

It is normally assumed for practical calculations that the variation of reflectivity with height in the rain region of a precipitation process is height independent and in general, very small [Goldhirsh, 1979; Hall, 1978]. However, especially for high elevation angles; such small variation should be taken into consideration for an improved rain attenuation model [Crane, 1990]. Researchers have studied the climatology of vertical profiles of radar reflectivity and have listed several factors that influence this gradient. [Joss and Pittini, 1991; Joss and Waldvogel, 1989]. Among the factors are the growth or evaporation of precipitation and the air motion. Other investigators have also hypothesised that this variation with height can also be attributed to the variation of drop velocities with atmospheric pressure [Leitao and

Watson 1986]. This means, with assumption that vertical continuity of rainfall rate, larger particle concentrations are found near the ground than above.

Figure 7.19 and 7.20 below show vertical profile plots during stratiform and convective rain events. Reflectivity profiles in each rain classification seem to have a linear characteristic with height and after applying the regression method; straight lines such plotted on each figure can be approximated with equation:

$$Z = mh + c \tag{7.8}$$

where Z is given in dB, h in km and m and c are the linear coefficients.

For every selected profile, only values above a minimum and below a maximum threshold height have been utilised in our analysis to avoid sampling errors. The starting height for each range is the height defined by the minimum height not affected by the ground clutter. The maximum height has been taken 150 m (2 gates) below the detected rain height to ensure that all hydrometeors are in the liquid phase. Algorithm was developed in our program to automatically determine the appropriate heights for every profile.

The cumulative distribution of the reflectivity gradient for selected 6199 stratiform and 3011convective profiles investigated is shown in Figure 7.21. For both types of rain events, it can be observed that almost 70% of the times the radar reflectivity decreases with height. The median values for the reflectivity gradient cumulative distribution of stratiform and convective are –0.62 and -1.76 dB/km, respectively. In Table 7.4 below we compare our tropical results with values obtained in temperate climate.

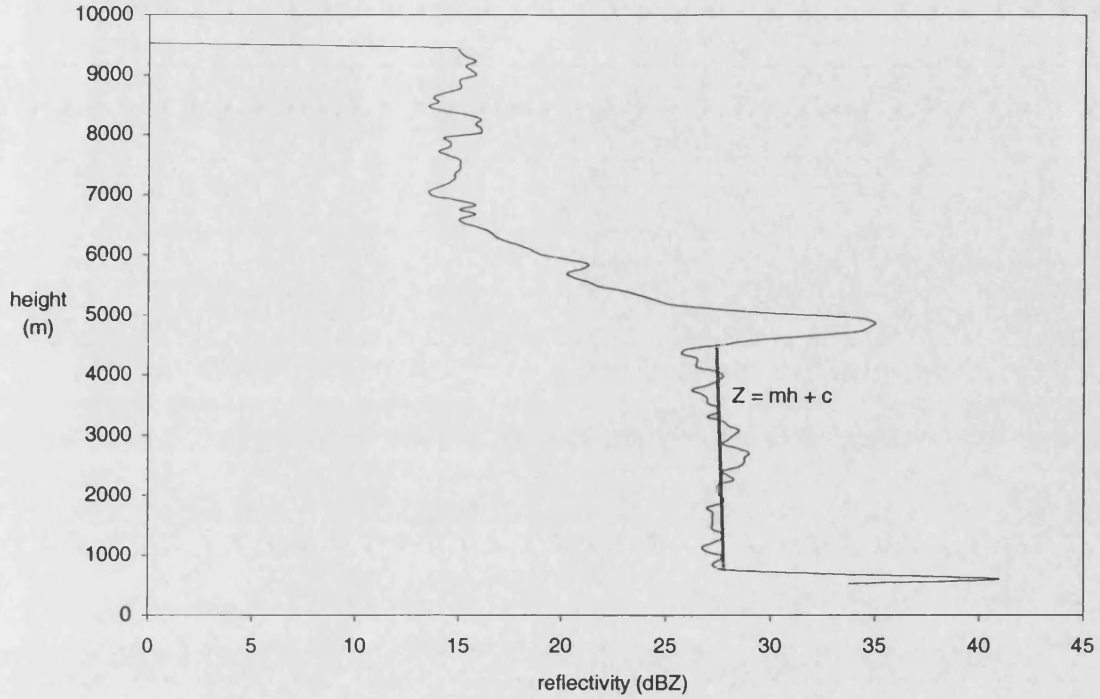

Figure 7.19: Vertical reflectivity profile during a stratiform event

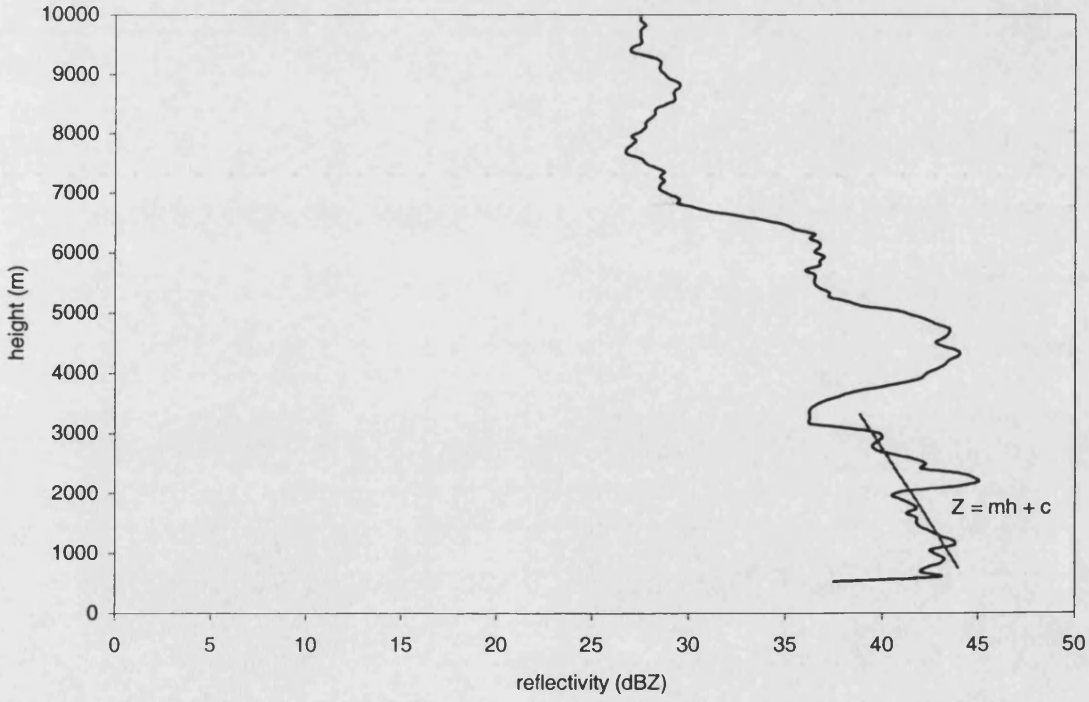

Figure 7.20: Vertical reflectivity profile during a convective event

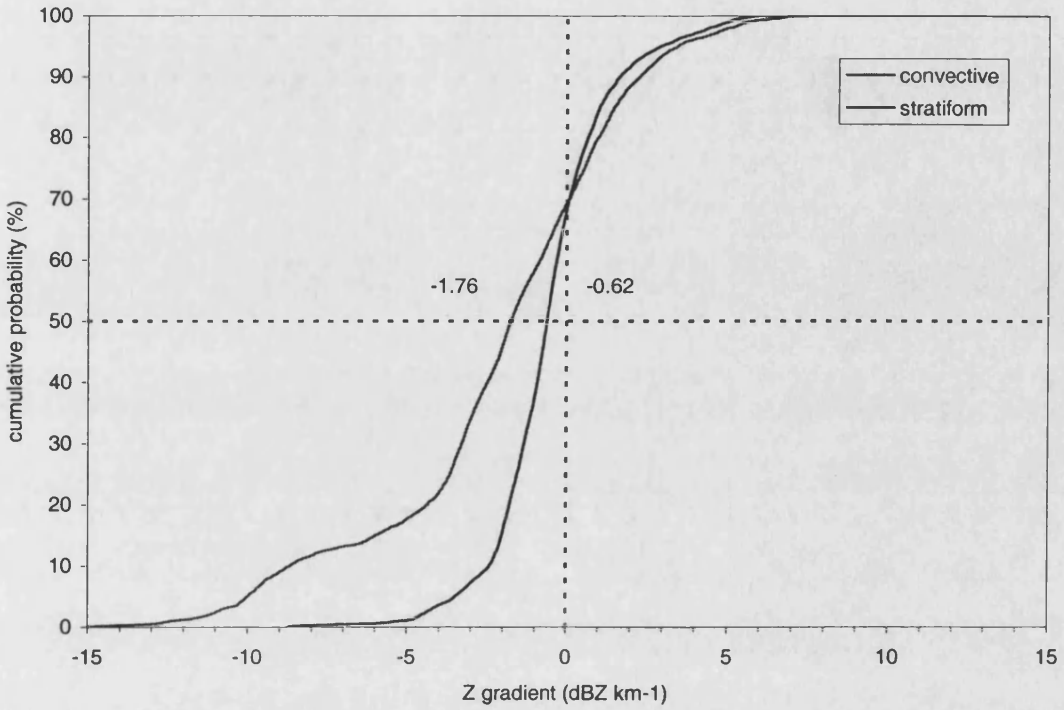

Figure 7.21: Cumulative distributions of reflectivity gradients

	Cumulative distribution median ($dBkm^{-1}$)	
	Stratiform	Convective
PNG	-0.62	-1.76
UK [Bandera *et al.*, 1999]	-0.47	-0.60

Table 7.4: Comparison of median cumulative distributions.

7.10 Vertical Attenuation correction factor

An accurate prediction of attenuation along a slant path should take into account the variability of specific attenuation in both the horizontal and vertical planes, since precipitation medium is inhomogeneous both directions [Radiocommunication Bureau, 1986]. For satellite communication systems using low elevation angles, the horizontal variability dominates over the vertical plane and so that it is common to assume the rain specific attenuation is constant with height. Simple use of cosecant law is used and the path attenuation is evaluated only from the horizontal projection in such cases [ITU-R P.618-5, 1997; Crane, 1980]. Yet on the other hand, most space

based telecommunication systems in the tropical region are or will be using high elevation angle slant paths.

In such condition the cosecant law cannot be applied completely because of the variability of specific attenuation coefficients with height [Bowthrope et al., 1990]. Therefore is is of great interest for an accurate modelling of vertical variation of precipitation to improve the prediction of attenuation along the slant path. Investigation and experiment involving vertical precipitation measurements are difficult to make, and the most appropriate instrument to interpret the vertical variability of rain is a radar system.

In the Rayleigh region, rain specific attenuation γ (dB km^{-1}) can be associated to reflectivity Z by the equation:

$$\gamma = AZ^b \tag{7.9}$$

where A and b are frequency dependent coefficients [Ulbrich, 1983]. ITU and many other investigators have adopted such approach for their rain attenuation models. By substituting Equation 7.9 into Equation 7.8, the specific attenuation can be represented by following expression:

$$\begin{aligned}
\gamma &= a10^{\frac{cbh}{10}} \cdot 10^{\frac{mbh}{10}} \\
&= a10^{\frac{cbh}{10}} \cdot \int_0^h 10^{\frac{mbx}{10}} dx \\
&= a10^{\frac{cbh}{10}} \cdot h\frac{1}{h}\int_0^h 10^{\frac{mbx}{10}} dx \\
&= A_{SVU} C_V
\end{aligned} \tag{7.8}$$

where

$$A_{SVU} = a10^{\frac{cbh}{10}} \cdot h \tag{7.9}$$

is the attenuation along the vertical path, with the assumption that a constant specific attenuation coefficient. Therefore C_V is the correction factor to the account for the vertical variability of the specific attenuation coefficient. The correction factor C_V can be written as:

$$C_V = \frac{1}{h}\int_0^h 10^{\frac{mbx}{10}} dx$$

$$= \frac{4.343}{mbh}\left(10^{\frac{mbh}{10}} - 1\right)$$

Using the median gradient values obtained for stratiform and convective rain types, combined with coefficients values of A and b from our previous analysis of γ-Z relationship (Table 7.3), the correction factors C_V for 11, 22, and 38 GHz are plotted in Figure 7.22 below. It can be observe that for the same operating frequency and height, the correction factor for stratiform rain is smaller compare to convective.

For comparison, we plotted the recommended correction factor in stratiform and convective rainstorm for temperate region [Bandera, 1999] against our correction factors that were derived from tropical measurements. We noticed that the tropical correction factors' values are smaller compare to those obtained for temperate climate

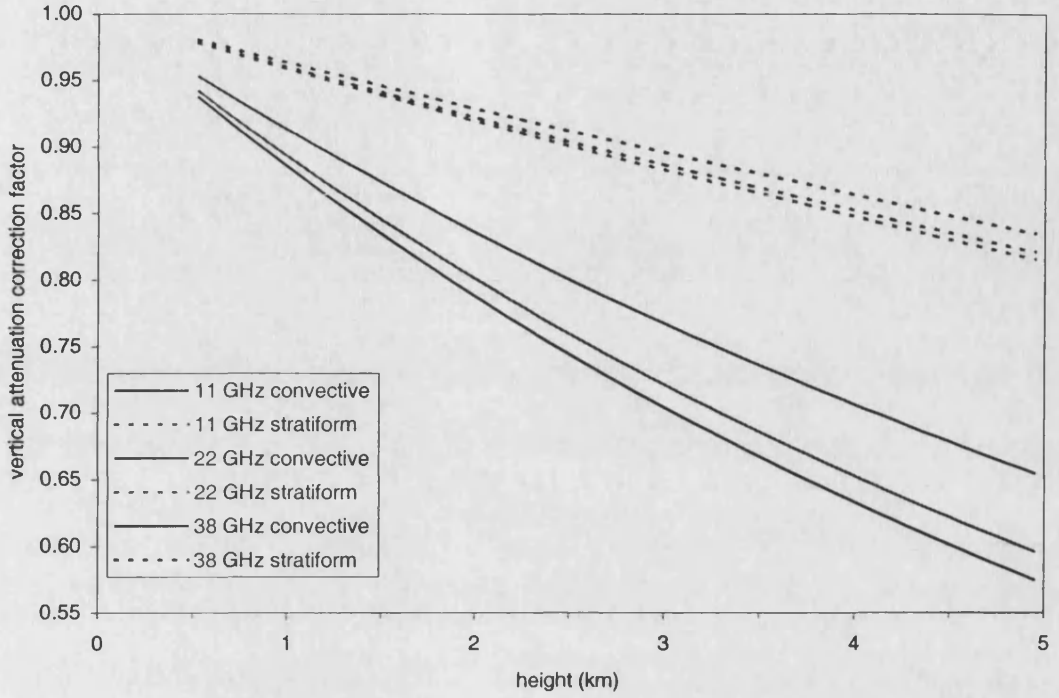

Figure 7.22: Tropical vertical attenuation correction factor in stratiform and convective rainstorms

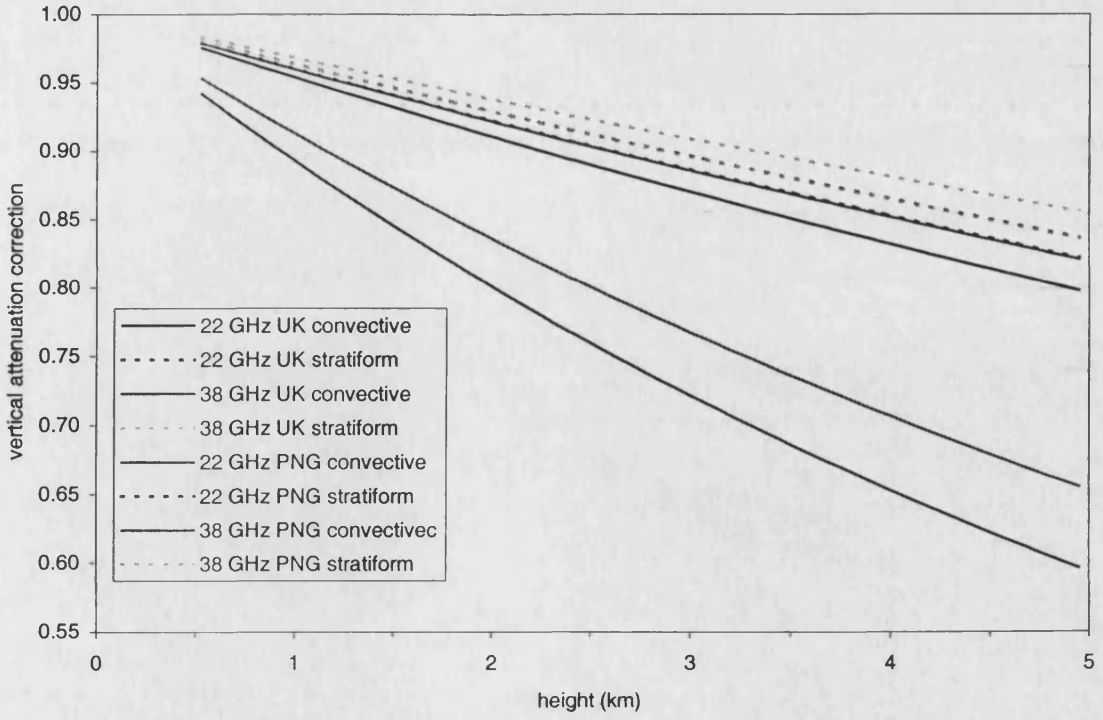

Figure 7.23: Comparison between tropical and temperate climate vertical attenuation correction factor in stratiform and convective rainstorms

7.11 Conclusion

The findings presented in this chapter have evaluated the radar measurements of various rain related parameters to simultaneous measurements by ground-based instruments. Precipitation characteristics for stratiform and convective event have been studied with a combination of a polarmetric 3-GHz radar and a co-located Joss distrometer. Good correlation between radar and distrometer measurements of reflectivity has been attained. Stratiform and convective events in PNG differ noticeably in their characteristics. The radar estimates of co-polar reflectivity, specific attenuation and rainfall rates using only the distrometer-derived measurements have been established. Coefficients relating specific attenuation-reflectivity relationship at various frequencies using the best-fit procedure have been obtained. All estimations of parameters involve direct measurements and no assumption was made concerning the drops size distribution.

Rain induced-attenuation correction factors to relate the variability of the rain specific attenuation has been investigated. The correction factor is a function depending on the frequency, type of rain, rain height and the median value of the radar reflectivity gradient. These factors were derived from a combination of radar measurements and a co-located Joss distrometer. The variation of reflectivity with height has been characterised by taking into account the vertical structure of precipitation in detail. From our finding we found that for recommended rain height of about 5 km in the tropics; correction factors have the average values of 0.85 and 0.67 for frequency range between 11 – 38 GHz in stratiform and convective rain respectively.

Chapter 8

Conclusion and Suggested Future Work

8.1 Conclusion

All the proceedings chapters of this thesis have a self-contained list of brief conclusions. The aim of this final chapter is to draw all the ideas contained within the research work together so that interrelationships can be clearly understood between each separate section.

Studies relating to the prediction of attenuation by rainfall in tropical climates have been presented in this thesis based on 20 months of attenuation and rainfall intensity measurements in Malaysia and 6 months of radar and distrometer data in Papua New Guinea. Monthly and annual statistics of attenuation have been presented for an 11-GHz satellite-Earth link operating in Malaysia. In this equatorial climate severe fading is observed with frequency typically more than 200 fades above the 10-dB threshold in a given year.

The attenuation data have been analysed to give new results on seasonal and diurnal distributions, fade and inter-fade durations and relationship to the worst month. It is argued that data such as these should be used in determining the likely user acceptance of the DTH and VSAT services. Pronounced diurnal variations with predominance of heavy rainstorms in afternoon and evening meaning that an additional fade margin should be included in for conventional television broadcast applications.

Conversion of rain rates with different integration times to that with 1-minute integration time has been investigated. Owing to the high rainfall rates encountered in

Malaysia, we conclude that the statistics of rainfall rates with variable integration time are very dependent on the integration time employed. Comparisons were made with available conversion models and significant differences can be observed. This may result at least in part from the different designs of rain gauges that have been used.

Developing appreciation for the variation of service quality over the monthly and diurnal period may also permit the service provider to change the dimensioning the link with the month or the season. This might be particularly valuable if the service provider is offering services to other country besides Malaysia, or over a very large country. For example the dry season in Malaysia (based one measurements at Bukit Jalil) is during the month of August and September and the worst time of the rain is between 4 pm to 8 pm. Changing the distribution of transmitted power in the spacecraft antenna to take into account the seasonal or monthly and diurnal variability would grant significant competitive advantage to the service provider.

The cumulative distributions of attenuation and rainfall rate collected in Malaysia appear to differ at specific percentages of time from those proposed in the ITU-R literatures. The attenuation and rainfall rates given in the most recent ITU-R recommendations show lower values than those measured. Specifically it would appear that the ITU-R 1995 Rec. 618-4 and ITU-R 1999 Rec. 618-6 do not give accurate predictions for rain attenuation on earth-Space links in tropical area such as Malaysia. The earlier ITU-R 1997 618-5 gave a reasonably good estimation.

Worst month statistics of rainfall rate and attenuation are normally very useful in designing high quality satellite communication networks in temperate climates since if average annual statistics alone are used, these values would be exceeded in a significant number of years. In this thesis it is experimentally verified that the power law with the ITU-R values of β and Q_1 can be used for estimating the worst-month statistics in Malaysia. New values for parameter Q_1 and β are proposed in order to obtain a better estimate for the worst-month statistics in Malaysia.

However it should be especially noted from this study that for equatorial climates with frequent fading throughout the year, the normal worst month fade criterion applied to satellite television networks (99% worst month availability) is not sufficient to ensure adequate annual availability as high as 99.7%. This is seen to be the case in Malaysia despite the seasonal influence of the Asia monsoon. These results also indicate that for point-to-point satellite K_u-band operation in Malaysia and other tropical regions, it may not be feasible to guarantee availability at 99.9% or above without an additional margin and / or the use of one or more techniques to alleviate the effects of rain attenuation.

The improvement from the use of time diversity at 11-GHz over the 20-month period has been measured for various diversity time spacings. It has been shown that a time diversity gain of between 4 to 10 dB can be obtained with delays of 5 to 30 min. This technique has relevance to time repeated video applications, and to data broadcast and multimedia applications.

Data from Lae in Papua New Guinea on rainfall rate and rain structure (radar data) have been analysed. Detected rain events have been separated into convective and stratiform rain based on observed structure. Rain drop size distributions for PNG have been expressed in terms of lognormal and gamma models. Comparisons between the PNG models and several other rain drop size distribution models proposed for tropical regions have been made. The results presented in this thesis indicate that the lognormal distribution is to be preferred

The thesis also investigated the vertical structure of rain using a meteorological radar in an attempt to see if this has a bearing on the problems at present in the latest ITU-R prediction techniques in which there are horizontal and vertical reduction factors. The main radar parameter utilised has been the reflectivity, but linear depolarisation ratio LDR was also available to determine the height of melting layer. In addition to

radar data, co-located distrometer measurements enabled the simulation of the performance of radio links operating at different frequencies.

Using the distrometer measurements, new coefficients relating specific attenuation and radar reflectivity with rainfall rates have been derived for frequencies of 11, 22 and 38 GHz for stratiform and convective rain. The vertical extent of rain and (closely related) the on-average vertical profile of attenuation have been investigated using the vertical range-gated radar returns. Vertical path reduction factors for stratiform and convective rain to account the vertical variability of rain specific attenuation with height have thus been derived which should improve rain attenuation predictions for communication system operating in the tropical regions. The new reduction factors are higher than those given in the latest ITU-R literature and should give a better agreement between measured and predicted values of attenuation.

8.2 Future Work

It is very likely that in the near future, satellite telecommunication systems will be capable of offering access to information of all types. Due to the congestion of the low bands of the spectrum, millimetre wavelengths will have to be considered in order to accommodate the demand for broadcast and data channels. However, at these frequencies the atmospheric attenuation in the tropics is much more severe and it is not all clear that sufficient margin can be found in these bands to give an acceptable grade of service.

While existing propagation models in the temperate regions are well established and are relatively reliable, there are no well-established approaches for tropical region in the millimetre frequency range. In order to give respond to this uncertainty, the research carried out in this thesis has been directed on the quantifying propagation characteristics. Enhanced water vapour content, cloud liquid water content and intense rain all present severe problems for the use of these bands.

Despite some advances in the recent years, ITU-R propagation prediction methods continue to lack of universal applicability, particularly in tropical areas. It is apparent that the latest ITU-R method seriously underestimates the measured attenuation. This could largely due to a shortage of measurement data for these regions of concerned. Hopefully this situation is changing in view of recent efforts to establish appropriate propagation experiments. Especially useful work to further radar measurements in conjunction with satellite beacons since the PNG data reported here worked for a very short period only (6 months).

Rainfall rate and rain height are widely employed in attenuation models to predict signal fading due to rain. Nevertheless, prediction models rarely differentiate among types of rain or include any seasonal and diurnal dependencies of these parameters despite being considered as factors that can greatly enhance the accuracy in rain attenuation estimates. In this work, the matters have been addressed by studying the correlation with specific attenuation and rainfall rates in stratiform and convective precipitation. Further information about the occurrence of each type of storm and statistics of its rain intensity are needed for an improved rain attenuation model. The initial evaluation of these two factors in PNG has revealed that stratiform precipitation is much more frequent than convective rain and dominates the low availability range statistics. This approach could be extended to include appropriate parameters based upon the type of rain in the propagation model.

Another aspect for further investigation is the modelling of attenuation in the melting layer. The radar parameter Doppler mean velocity, when combined with dBZ and *LDR* can act as sensitive indicator of bright band regions in stratiform and convective events. These facts add additional force to arguments for further radar measurement campaigns. Finally, given the adverse propagation characteristics in tropical regions, it is clearly evident that work to develop fade countermeasures should be undertaken. The studies reported in this thesis on time –diversity gain are just a start in this approach.

References

AJAYI, G.O (Editor) [1996] *URSI Handbook on Radiowave Propagation Related to Satellite Communications in Tropical and Subtropical Countries*, URSI publication

AJAYI, G.O., and OLSEN R.L. [1983] *Measurements and Analysis of Raindrop Size Distribution in South Western Nigeria*, Pro Proc. URSI comm. F 1983 Symposium, Louvain, Belgium

AJAYI, G.O., and OLSEN R.L. [1985] *Modelling of a Tropical Raindrop Size Distribution for Microwave and Millimetre Wave Applications*, Radio Science, vol.20, no. 2, March-April, pp.193-202. USA

ALLMAN, M., GLOVER, D., and SANCHEZ, L. [1999] *Enhancing TCP Over Satellite Channels using Standard Mechanisms*, RFC 2488, BCP 28, January.

ALLNUTT, J.E. [1989] *Chapter 4, Satellite-To-Ground Radiowave Propagation*, Peter Peregrinus, Ltd., London.

ALLNUTT, J.E., and ROGERS, D.V. [1990] *The INTELSAT Slant-Path Radiowave Propagation Experiments in Tropical Regions*, International Journal of Satellite Communications, vol.8, pp.181-186

BANDERA, J., PAPATSORIS, A.D., WATSON, P.A., TOZER, T.C., TAN, J. and GODDARD, J.W. [1999] *Vertical Path Reduction Factor for High Elevation Communication Systems*, Electronics Letters, vol.35, no.18, 2 Sept. 1999, pp.1584-5. Publisher: IEE, UK

BARRETT, E., and BAILEY, J. [1971] *Part 7, Weather and Climate*, The European Printing Corporation, Great Britain

BOSISIO, A.V., and RIVA, C. [1996] *Site Diversity Performance in 10/30 GHz Band: A Comparison Among Prediction Methods*, Electronics Letters, vol. 32, pp. 1760-1761

BOSTIAN, C., CHAN, V., HAGER, E.P., HELM, N., MAHLE, C., MILLER, E., PELTON, J.

[1993] *Chapter 4, New Markets and Policy Considerations*, Satellite Communications Systems and Technology NASA International Technology Research Institute

BOWTHROPE, B.J. ANDREWS, F.B., KIKKERT, C.J., and ARLETT, P.L. [1990] *Elevation Angle Dependence in Tropical Regions*, International Journal of Satellite Communication, vol. 8, no. 3, pp. 211-221

BRAND, E. [2000] *A Comparative Study of Techniques for Measuring Rainfall Rate and Accumulation*, AP 2000, Davos, Switzerland

BRUSSAARD, G. [1981] *Predicting of Attenuation Due to Rainfall on Earth-Space Links*, Radio Science, vol. 16, pp. 745-760

BRUSSARD, G. and WATSON, P.A. [1979] *Annual and Annual Worst Month Statistics of Fading on Earth-Satellite Path at 11.5 GHz*, Electronics Letters, vol. 14, pp. 278-280

BRUSSAARD, G., and WATSON, P.A. [1995], *Chapter 4, Atmospheric Modelling and Millimetre Wave Propagation*, Chapman & Hall, London

BURGUENO, A., AUSTIN, J., VILAR, E. and PUIGCERVER, M. [1987] *Analysis of moderate and intense rainfall rates continuously recorded over half of a century and influence on microwave communications planning and rain-rate data acquisition.* IEEE Transactions on Communications, vol. COM-35, no.4, pp.382-95

BURGUENO, A., PUIGCERVER, M., and VILAR, E. [1988] *Influence of Rain gauge Integration Time on Rain Rate Statistics Used in Microwave Communications*, Annales des Telecommunications - Annals of Telecommunications, vol. 43, pp.522-527

CAPSONI, C., MATRICCIANI, E., and MAURI, M. [1990] *SIRIO-OTS 12 GHz Orbital Diversity Experiment at Fucino*, IEEE Transactions on Antennas and Propagation, 1990, 777-782

CAPSONI, C., MATRICCIANI, E., and MAURI, M. [1996] *Application of Frequency Diversity for Dimensioning A K_a-Band Satellite System*, International Journal of Satellite Communications, vol. 14, pp. 53-62

CARASSA, F. and MATRICCIANI, E. [1988] *Frequency Diversity and Its Applications*, International Journal of Satellite Communications, vol. 6, pp. 313-322

CATALAN, C. [1999] *Comparison Between the Dynamics of Rainfall Rate and Attenuation: Correlation Factor and Fourier Analyses*, Internal Report 99/16, University of Portsmouth

CHERRY, S.M., GODDARD, J.W. and HALL, M.P.M. [1981] *The Use of Dual Polarisation Radar Data for Evaluation of Attenuation on Satellite-to-Earth Path.* Ann. Telecomm. Vol. 36 pp. 33-39

CRANE, R.K. [1980] *Prediction Of Attenuation By Rain*, IEEE Transactions on Communications, COM-28, pp. 1717-1733

CRANE, R.K. [1990] *Modelling Attenuation by Rain in Tropical Region*, International Journal of Satellite Communication, vol. 8, pp. 197-210

CRANE, R.K., and SHIEH, H.C. [1989] *A Two-component Rain Model for The Prediction of Site Diversity Improvement Performance*, Radio Science, vol.24, pp. 641-655

CURRIE, N.C., and BROWN, C.E. [1987] *Principles and Applications of Millimeter-Wave Radar*, Artech House, Massachusetts, USA

DALGLEISH, D.I. [1989] *Chapter 5, An Introduction to Satellite Communications*, Peter Peregrinus, London

De MAAGT, P.J.I., TOUW, S.I.E., DIJK, J., BRUSSAARD, G. and ALLNUTT, J.E. [1993b] *Diurnal Variation of 11.2 GHz Attenuation on Satellite Path in Indonesia*, Electronics Letters, vol. 29, pp. 2149-2150

De MIRANDA, E.C., PONTES, M.S., Da SILVA MELLO, L.A.R., and ALMEIDA, M.P. [1998] *Choice of Standard Medium Temperature for Tropical and Equatorial Climates: Comparison Between Radiometric and Satellite Beacon Attenuation Data on Two 12 GHz Links in Brazil* Electronics Letters, vol. 34, pp. 2002-2003

De MIRANDA, E., POMTES, M.S., Da SILVA MELLO, L.A.R., and SOUZA, R.S.I. [2000] *A Comprehensive Study of Slant Path Attenuation in Brazil – Second Part: Dynamic Statistics*, AP 2000, Davos, Switzerland

DISSANAYAKE, A., ALLNUTT, J., and HAIDARA, F. [1997] *A Prediction Model that*

Combines Rain Attenuation and Other Propagation Impairments Along Earth-Satellite Paths, IEEE Transactions on Antennas and Propagation, AP-45, pp. 1546-1558

DONALD, A.C. [1994] *Meteorology Today, An introduction to Weather, Climate and Environment*, West Publishing, Minnesota

DOVIAK, R.J., and ZRNIC, D.S [1993] 2nd Edition, *Doppler Radar and Weather Observation*, Academic Press, London

EASTMENT, J. [1999] *Polarimetric Doppler Radar*, PhD Thesis, University of Bradford, UK

EASTMENT, J.D., THURAI, M., LADD, D.N., AND MOORE, I.N. [1995] *A Vertically-Pointing Doppler Radar to Measure Precipitation Characteristics in The Tropics*, IEE Transactions on Geoscience and Remote Sensing, vol. 33, pp.1336-1340

EASTMENT, J.D., THURAI, M., LADD, D.N., AND MOORE, I.N. [1998], *Radiowave Propagation Research in The Tropics Using A Transportable Multiparameter Radar System*, Electronics & Communications Engineering Journal, vol. 10, pp. 4-16

FLAVIN, R.K. [1982] *Rain Attenuation Consideration for Satellite Paths in Australia*, Australian Telecommunication Research, vol. 16, pp. 11-24

FUKUCHI, H. [1992] *Slant Path Attenuation Analysis at 20 GHz for Time-Diversity Reception of Future Satellite Broadcasting*, U.R.S.I. Open Symposium, Wave Propagation and Remote Sensing, Univ. Bradford, pp. 6.5 Bradford, UK

FUKUCHI, H., WATSON, P.A., and ISMAIL, A.F. [2000] *Proposed Novel Attenuation Mitigation Technologies for Future Millimetre Wave Satellite Communications*, Proceedings of IEE/ EUREL International Conference on Antenna and Propagation, AP-2000, 2000

GARCIA LOPEZ, J.A., HERNANDO, J.M., and SELGA, J.M. [1988] *Simple Rain Attenuation Prediction Method for Satellite Radio Links*, IEE Transaction of Antenna and Propagation vol. 36 no. 3, pp.444-448

GLOAGUEN, V. and LAVERGNAT, J. [1995] *Rain Drop Size Distribution Near Paris*, Electronics Letters, vol. 31, pp. 405-406

GODDARD, J.W.F., and CHERRY, S.M. [1984] *The Ability of Dual-Polarisation Radar (Co-polar Linear) to Predict Rainfall rate and Microwave Attenuation*, Radio Science, vol. 19, pp. 201-208

GOLDHIRSH, J., and KATZ, I. [1979] *Useful Experimental Results for Earth-Satellite Rain Attenuation Modelling*, IEE Transaction on Antenna and Propagatoin 1979 vol. 27 pp. 413-415

GUNN, R., and KINZER, G.D. [1949] *The Terminal Velocity of Fall for Water Droplets in Stagnant Air*, Journal of Meteorology, vol. 6, pp. 243-248

HALL, M.P.M, and GODDARD, J.W.F. [1978] *Variation with Height of the Statistics of Radar Reflectivity due to Hydrometeors*, Electronics Letters, vol. 14, no. 17, pp. 224-225

HODGE, D.B. [1973] *The Characteristics Of Millimetre Wavelength Satellite- To-Ground Space Diversity Links*, IEE Conference Publication, vol. 98, pp. 28-32

HODGE, D.B [1974] *Path Diversity for Reception of Satellite Signals*, Journal of Research Atmosphere, vol. 8, pp. 443-449

HODGE, D.B. [*1982*] *An Improved Model for Diversity Gain on Earth-Space Propagation Paths*, Radio Science, vol. 17, no. 6, pp. 1393-1399, USA

HOUZE JR, R.A. [1981] *Structures Of Atmospheric Precipitation Systems: A Global Survey*, Radio Science, vol. 16, pp. 671-689

HUFFMAN, G.I., and NORMAN JR., G.A. [1988] *The Supercooled Warm Rain Process and the Specification of Freezing Precipitation*, Mon. Weather Review, vol.116, pp. 2172–2182

HUGHES, K.A. [1990] *CCIR Data for Slant-Path Propagation in Tropical Regions: A Critical Review*, International Journal of Satellite Communications, vol. 8, pp. 127-139

HULBERT, J. [1973] *Chapter 12, The World's Weather*, Pergamon Press, Oxford

IEEE STANDARD. 211-1977 [1977], *IEEE Standard Definitions of Terms for Radio Wave Propagation*, New York, August19

IPPOLITO, L.J. [1986] *Propagation in Satellite Communications*, Van Nostrand Reinhold, New York

JACKSON, I.J. [1989] *Climate, Water and Agriculture in the Tropics, Second Edition*, Longman Scientific & Technical, Essex, England

JASSAL, B., ARUN, S., VERMA, K. and SINGH, L.A.L [1994] *Rain Drop-Size Distribution and Attenuation for Indian Climate*, Indian Journal of Radio and Space Physics, vol. 23, Iss. 3, pp. 193-196

JIANG, H., SANO, M., and SEKINE, M. [1997] *Weibull Drop-size Rain Distribution and Application to Rain Attenuation*, IEE Proceedings – Microwaves, antennas and Propagation, vol. 144, pp. 197-200

JOHANNSEN, K.G. and CUEVAS, C. [1993] *Ku-Band Vs C-Band and Digital Vs. Analogue Television Transmission in Tropical Climate*, International Journal of Satellite Communications, vol. 11, pp. 119-143

JOSS, J., and PITTINI, A. [1991] *Climatologiy of Vertical Profiles of Radar Reflectivity*, Proceedings of 25th Conference on Radar Meteorology, pp. 828-831

JOSS, J., THAMS, J.C., and WALDVOGEL, A. [1968] *The Variation of Raindropsize Distribution at Lucarno*, Proceeding of International Conference on Cloud Physics, pp. 369-373 Toronto Ontario, Canada

JOSS, J. and WALDVOGEL, A. [1968] *The Variation of Raindrop Size Distributions at Locarno*, Proceeding Of the International Conference On Cloud Physics, Toronto, Canada, pp. 369-373

JOSS, J. and WALDVOGEL, A. [1989] *Precipitation and Vertical Reflectivity Correction*, Proceedings of 24th Conference on Radar Meteorology, pp. 682-688

JUY, M., MAUREL, R., ROORYCK, M., NUGROHO, J.A., and HARIMAN, T. [1990] *Monthly Distributions of Rain Rate and Attenuation Measured in Indonesia*, URSI Commission F Symposium on Regional Factors in Predicting Radiowave Attenuation Due to Rain, Rio de Janeiro, Brazil

KENDREW, W.G. [1922] *Chapter 23: South-east Asia and the East Indies, The climates of the Continents*, Oxford University Press, Oxford

KINGSLEY, S., and SHAUN Q. [1992] *Understanding Radar Systems*, McGraw-hill London, UK

LADD, D.N., WILSON, C.L., and THURAI M. [1997] *Radar Measurements from Papua*

New Guinea and Their Implications for TRMM PR Retrieval Algorithms. IGARSS'97, International Geoscience and Remote Sensing Symposium, Remote Sensing - A Scientific Vision for Sustainable Development IEEE, vol. 4, pp. 1648-1650 New York, NY, USA.

LAWS, J.O., and PARSON, D.A. [1943] *The Relation Of Raindrop Size To Intensity,* Transactions American Geophysics Union, vol. 24, pp.452-460

LEITAO, M.J., and WATSON, P.A. [1986] *Method for Prediction of Attenuation on Earth-Space Links Based on Radar Measurements of Physical Structure of Rainfall,* IEE Proceedings, vol. 133, pp. 429-440

LEKLA, R., LIM, S.L., WATCHA, J., and McCORMICK, K.S. [1995] *Rain Attenuation Measurements in South-East Asia,* Proceedings of URSI-F open symposium, Ahmedabad, India, pp. 241-244

LEKKLA, R., PRAPINMONGKOLKARN, P., and McCORMICK, K.S. [1998] *Analysis of Rain Intensity in Southeast Asia Over 3-Years,* Proceedings of URSI Commission F Open Symposium on CLIMPARA, pp. 1998, 223-226

LI, H.J., ZHANG, C.Q., LIAO, L., and ZHANG, G.F. [1987] *An Improved Model for the Prediction of Rain Attenuation Statistics,* Fifth International Conference on Antennas and Propagation (ICAP 87), vol. 2, pp. 226-2299 London, UK

LIN, K.T., ZAKS, C., DISSANAYAKE, A.W., and ALLNUTT, J.E. [1993] *Results of an Experiment to Demonstrate the Effectiveness of Open-Loop Power Control for K_u-band Satellite Links,* Proceedings of 8th International Conference on Antennas and Propagation, pp. 202-205

LIST, R., HUDAK, D., NISSEN, R., and KANG, T.S. [1988] *Results from Warm Rain Studies in Penang Malaysia,* Proceedings 10th International Cloud Physics Conference, Bad Homburg, FRG, 15-20 August, vol. 2, pp. 446-448

LONG, M.E. [1999] *The World of Satellite TV, 9th Edition,* The book Publishing, Tennessee, USA

MAITRA, A. [2000] *Three-Parameter Raindrop Size Distribution Modelling at a Tropical Location,* Electronics Letters, vol. 36, no. 10, pp. 906-907 Publisher: IEE, UK

MANABE, T., IHARA, T., AWAKA, J and FURUHAMA, Y. [1987] *The Relationship of*

Rain Drop Size Distribution to Attenuation Experienced at 50, 80, 140, And 240 GHz, IEEE Transactions on Antennas and Propagation, 1987, pp. 1326-1330

MARCIEL, L.R. and ASSIS, M.S. [1990] *Tropical Rainfall Drop Size Distribution*, International Journal of Satellite Communications, vol. 8, pp. 181-186

MARSHALL, J.S., and PALMER, W. Mck. [1976] *The Distribution Of Raindrops With Size*, Journal Meteorology, vol. 5, pp. 16-166

MATRICCIANI, E. [1997] *Prediction of Orbital Diversity Performance in Satellite Communication Systems Affected by Rain Attenuation*, International Journal of Satellite Communications, vol. 15, pp. 45-50

MENDENHALL, W., and SINCICH, T. [1988] *2nd ed. Statistics for the Engineering and Computer Sciences*, Dellen Publishing Co., USA

MILLER, I., and FREUND, J.E. [1985] *3rd Edition, Probability and Statistics for Engineers*, Prentice-Hall New Jersey

MITRA, A.P., REDDY, B.M., RADICELLA, S.M., OYINLOYE, J.O and FENG, S. (Editors) [1987] *URSI Hand Book on Radio Propagation for Tropical and Subtropical Countries*, URSI Publication

MONTANARI, C., VILAR, E., LORENTE, REDANO, A., CODINA, B., PONTES, M.S., and SILVA MELLO, L.A.R. [1996] *Comparative Measurements Between Impact and Optical Distrometers – Effects on Microwave Specific Attenuation*, Proceedings of "Climatic Parameters in Radiowave Propagation Prediction (CLIMPARA 960 URSI Commission F Workshop

MOUPFOUMA, F. [1987] *Rain Induced Attenuation Prediction Model for Terrestrial and Satellite-Earth Microwave Links*, Annual Telecommunications, vol. 42, no. 9-10, pp.539-550

MOUPFOUMA, F. [1997] *A New Theoretical Formulation for Calculation of the Specific Attenuation Due to Precipitation Particles on Terrestrial and Satellite Radio Links*, International Journal of Satellite Communications, vol. 15, pp. 89-99

MURAKAMI, M., MATSUO, T., MIZUNO, H., and YAMADA, Y. [1994] *Mesoscale and*

Microscale Structures of Snow Clouds over the Sea of Japan Part I: Evolution of Microphysical Structures in Short-lived Convective Snow Clouds, Journal of Meteorology Society, Japan, vol. 72, no. 5, pp. 671-694

NIEUWOLT, S. [1981] *Chapter 1, The Climate Continental Southeast Asia*, Elsevier Scientific, Amsterdam

OGUCHI, T. [1983] *Electromagnetic Wave Propagation and Scattering in Rain and Other Hydrometeors*, Proceedings of the IEEE, vol. 71, pp. 1029-1078

OLSEN, R.L., ROGERS, D.V., and HODGE, D.B. [1978] *The aR^b Relation in the Calculation of Rain Attenuation*, IEEE Transactions on Antennas and Propagation, AP-26, 1978, pp. 318-329

ONG, J.T., TIMOTHY, K.I., CHOO, E.B.L., and CARRON, W.L. [2000] *Effective Rain Height Statistics for Slant Path Attenuation Prediction in Singapore*, Electronics Letters, vol.36, no. 7, pp. 661-663. Publisher: IEE, UK.

ONG, J.T., and SHAN, Y.Y. [1997] *Rain Drop Size Distribution Models for Singapore – Comparison with Results from Different Regions*, Proceedings of the 10th International Conference on Antennas and Propagation (ICAP'97), p.p. 2.281-2.285, Edinburgh UK

ONG, J.T., and ZHU, C.N. [1997] *Slant Path Attenuation at 11 GHz in Singapore*, Electronics Letters, vol. 33, pp. 178-179

ONG, J.T., ZHU, C.N., and LEE, Y.K. [1997] *Ku-Band Satellite Beacon Attenuation and Rain Rate Measurements in Singapore Comparison with ITU-R Models*. 10th IEE International Conference on Antennas and Propagation, Part 2, vol.2, pp. 153-156, London, UK

PAN, Q.W. and ALLNUTT, J.E. [2001] *Some Second Order K_u-band Site Diversity Results on a High Elevation Angle Path in a Rainy Tropical*, 11th International Conference on Antennas and Propagation IEE, part 2, vol.2. London, UK, pp. 551-555

PAN, Q.W., and BRYANT, G.H. [1992] *Results of 12 GHz Propagation Measurements in Lae (PNG)*, Electronics Letters, vol. 28, pp. 2022-2024

PAN, Q.W., and BRYANT, G.H. [1994] *Effective Rain-Cell Diameters and Rain-Column*

Heights in the Tropics, Electronics Letters, vol. 30, pp. 1800-1802

PRATT, T., and BOSTIAN, C.W. [1986] *Satellite Communications*, John Wiley & Sons, New York.

PRENTISS, S. [1987] *Satellite Communications*, Tab Books, United States

PRITCHARD, W.L., and SCIULLI, J.A. [1986] *Satellite Communication Systems Engineering*, Prentice Hall, New Jersey, USA

PRUPPACHER, H.R., and BEARD, K.V. [1970] *A Wind-Tunnel Investigation of the Internal Circulation and Shape of Water Drops Falling at Terminal Velocity in Air*, Quarterly Journal Royal Meteorology Society, vol. 96, pp. 247-256

PRUPPACHER, H.R. and PITTER, R.L. [1971] *Semi-Empirical Determination of the Shape of Cloud and Raindrops*, Journal of Atmospheric Science, vol. 28, pp. 86-94

READ, W.H. and YOUTIE, J.L. [1996] *Telecommunications Strategy for Economic Development*, Praeger Publishers, Connecticut

RECOMMENDATION ITU-R PN.310-9 [1994] *Definition of Terms Relating to Propagation in Non-Ionised Media.*

RECOMMENDATION ITU-R P.581-2 [1990] *The Concept of Worst Month*

RECOMMENDATION ITU-R P.618-4 [1995] *Propagation Data and Prediction Methods Required for the Design of Earth-Space Telecommunication Systems*

RECOMMENDATION ITU-R P.618-5 [1997] *Propagation Data and Prediction Methods Required for the Design of Earth-Space Telecommunication Systems*

RECOMMENDATION ITU-R P.618-6 [1999] *Propagation Data and Prediction Methods Required for the Design of Earth-Space Telecommunication Systems*

RECOMMENDATION ITU-R P.679-2 [1999] *Propagation Data Required for the Design of Broadcasting-Satellite Systems*

RECOMMENDATION ITU-R P.837-1 [1994] *Characteristics of Precipitation for Propagation Modelling*

RECOMMENDATION ITU-R P.837-2 [1999] *Characteristics of Precipitation for Propagation Modelling*

RECOMMENDATION ITU-R P.838 [1992] *Specific Attenuation Model for Rain for Use in*

Prediction Methods

RECOMMENDATION ITU-R P.839-2 [1997] *Rain Height Model for Prediction Methods*

RECOMMENDATION ITU-R P. 841[1992] *Conversion of Annual Statistics to Worst-Month Statistics*

RADIOCOMMUNICATION BUREAU [1996] *Handbook on Radiometeorology*, Geneva

RILEY, D., and SPOLTON, L. [1974] *Part 3, World Weather and Climate*, Cambridge University Press, London

ROGERS, D.V., and OLSEN, R.L. [1976] *Calculation of Radiowave Attenuation Due to Rain at Frequencies Up to 1000 GHz*, CRC report No. 1299. Communication Research centre, Department of Communications, Ottawa, Canada

RUCKER, F. [1993] *Frequency and Attenuation Dependent Fade Slope Statistics*, Electronics Letters, vol. 29, pp. 774-776

SALONEN, E., KARHU, S., JOKELA, P., ZHANG, W., UPPALA, S, AULAMO, H., and SARKKULA, S. [1990] *Study of Propagation Phenomena for Low Availabilities*, ESA Contract Report 8025/88/NL/PR

SAVAGEOT, H. [1992], *Radar Meteorology*, Artech House, Massachusetts, USA

SCHWARTZ, M. [1996] *Chapter 10, Communication Systems and Techniques*, IEEE Press

SEGAL, B. [1986] *The Influence Of Rain gauge Integration Time on Measured Rainfall-Intensity Distribution Functions*, Journal of atmospheric and Oceanic Technology, pp. 662-671

SHAN, Y.Y, [1996] *Study On Rain Attenuation Effects on Microwave Signals*, M.Eng. Thesis, Nanyang Technology, University, Singapore 1996

SOONG, T.T. [1981] *Probabilistic Modelling and Analysis in Science and Engineering*, John Wiley and Sons, USA

SUTCLIFFE, R.C. [1966] *Chapter 6,Weather and Climate*, Weidenfeld and Nicolson, London.

THAREK, A.R., and DIN, J. [1992] *Rainfall Drop Size Distribution Measurements in Malaysia*, Proceedings URSI comm. F 1992 Symposium Wave Propagation and Remote Sensing, pp. 1.2.1-1.2.5 Ravenscar, North Yorkshire, UK

THENAKIS, E.F. [1984] *Manual of Satellite Communications*, McGraw-Hill, New York

THE WORLD BOOK ENCYCLOPAEDIA™ [2000], *The World Book Encyclopaedia Millennium 2000 Edition*, World Book, Chicago

THURAI, M., EASTMENT, J.D., LADD, D.N. and MOORE, I.N. [1995] *A Vertically-Pointing Doppler Radar to Study the Precipitation Characteristics in the Tropics*. International Geoscience and Remote Sensing Symposium, IGARSS '95. Quantitative Remote Sensing for Science and Applications IEEE. Part vol.3, 1995, pp.1669 vol.3. New York, NY, USA.

TIMOTHY, K.I., SHARMA, S., DEVI, M. and BARBARA, A.K. [1995] *Tropical Raindrop Size Distribution (RSD): Prediction and Modelling its Effects on Microwave Propagation*, Proceedings of 9th International Conference on Antennas and Propagation, pp.244248, Eindhoven, The Netherlands

TREWARTHA, G.T., and HORN, L.H. [1980] *An Introduction To Climate*, McGraw-Hill Inc, United States

TRI, T. [1990] *Digital Satellite Communication*, McGraw-Hill, New Jersey

TWI SYSTEM INC. [1996] *User's Guide ORG-115-DA Optical Precipitation Sensor, Rain Rate Measurement System Manual*, Non-Governmental Documents, Santa Clara

ULBRICH, C.W. [1983] *Natural Variations in the Analytical Form of the Rain Drop Size Distribution*, Journal of Climatology and Applied Meteorology, vol. 22, pp. 1764-1775

VILAR, E., MONTANARI, C., PONTES, M.S., SILVA MELLO, L.A.R., LORENTE, J., and CODINA, B. [1997] *Scattering and Extinction: Dependence Upon Raindrop Size Distribution in Temperate (Barcelona) and Tropical (Belem) Regions*. Tenth International Conference on Antennas and Propagation, IEE, vol. 2, pp. 230-233, London, UK

WILIAMSON, M. [1990] *The Communications Satellite*, Adam Hilger, Bristol, UK

WATSON, P.A. [1997] *Effect of Rain on SHF/EHF Terrestrial Systems*, Radio Propagation Prediction IDGS Lectures

WATSON, P.A. and ALLNUTT, J.E. [1998] *Chapter 7, VSAT Book*, University of York

WATSON, P.A., ISMAIL, A.F., SENG, P.K., JA, Y.Y., KAMARUDDIN, H.S., EASTMENT, J., and THURAI, M. [1998] *Investigation on Rain Fading and Possible Countermeasures on Satellite-Earth Links in Tropical Climates*, Proceedings URSI comm. F Symposium Wave Propagation and Remote Sensing, pp. 1.3-1.7, Portugal

WITTERNIGG, N., RANDEA, W.L., RIEDLER, W., KUBISTA, E., ARBERSSER-RASTBURG, B. and ALLNUTT, J.E. [1993] *Quadruple Site Diversity In Austria Using 12 GHz Radiometers*, IEE Proceedings, vol. 140

WOOD, J. [1994] *Satellite Communications Pocket Book*, Newnes Butterworth-Heinemann, Oxford.

YUSOF, M.A., YUSOFF, M.M.M., and HASSAN, S.I.S. [1990] *Recommended Conversion Factor for Malaysia Based on One Year Measured Rainfall Data*, Proc. Com. F. URSI, pp. 53-55.

ZAINAL, A.R., GLOVER, I.A., WATSON, P.A., and HASSAN, S.I.S. [1993] *Rain Attenuation Measurements at 6.75 GHz In Malaysia*, Proceeding SICON, pp. 573-577

Appendixes

Appendix A – Measured Distribution for Stratiform Events

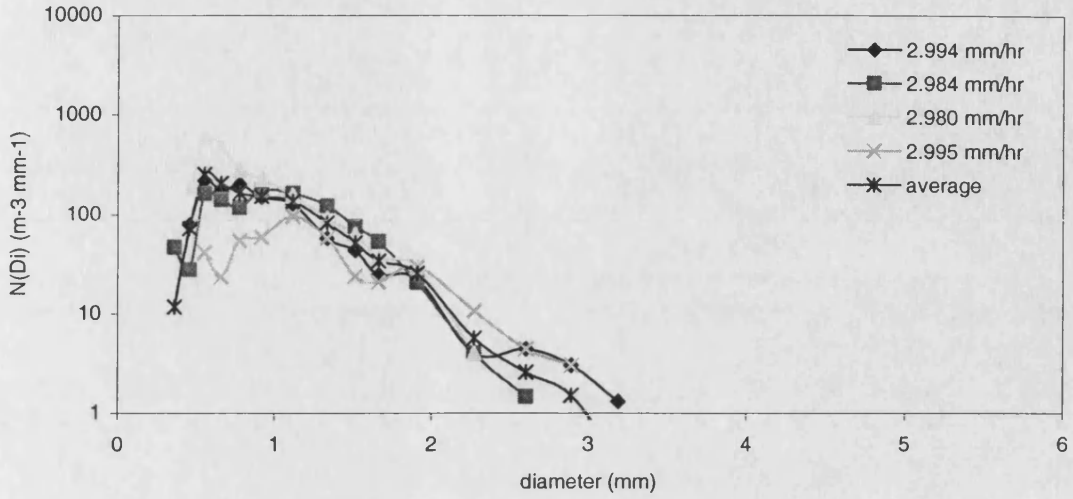

Figure A.1: Measured distributions for stratiform rainfall rates at ~ 3.0 mm hr^{-1}

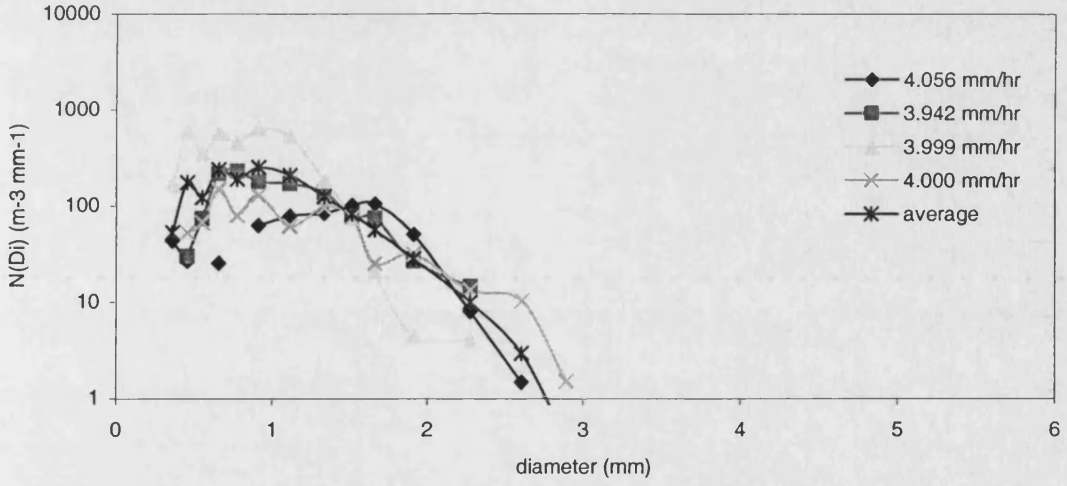

Figure A2: Measured distributions for stratiform rainfall rates at ~ 4.0 mm hr^{-1}

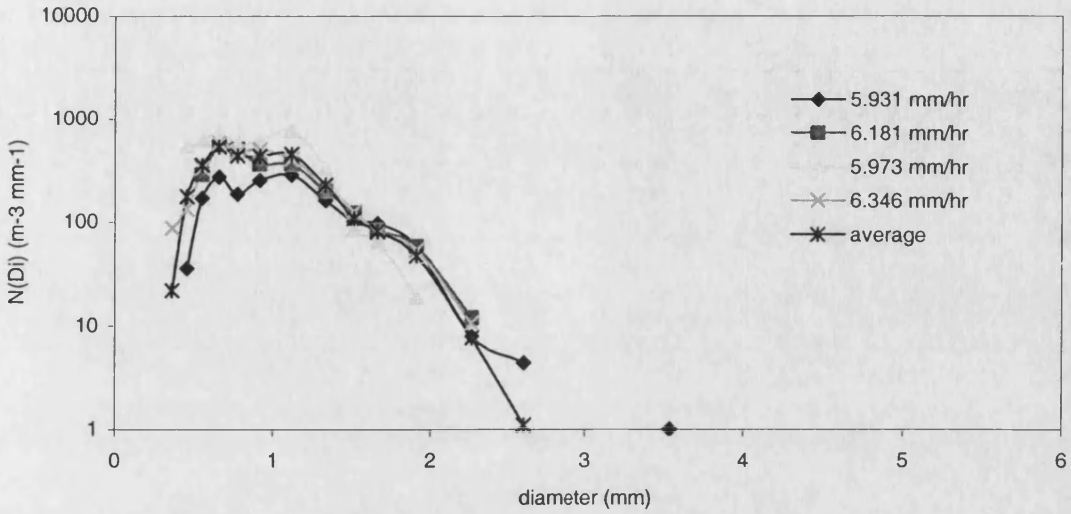

Figure A.3: Measured distributions for stratiform rainfall rates at ~ 6.0 mm hr^{-1}

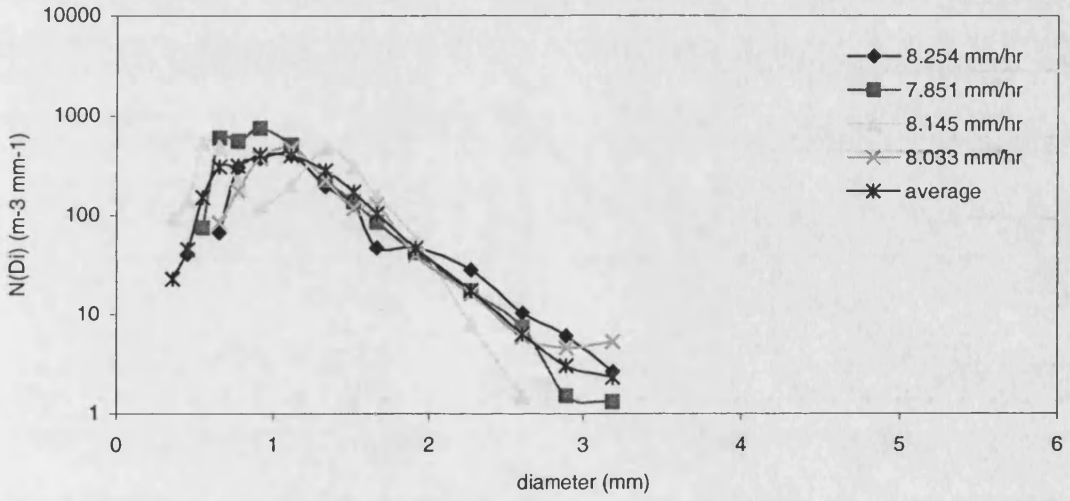

Figure A.4: Measured distributions for stratiform rainfall rates at ~ 8.0 mm hr^{-1}

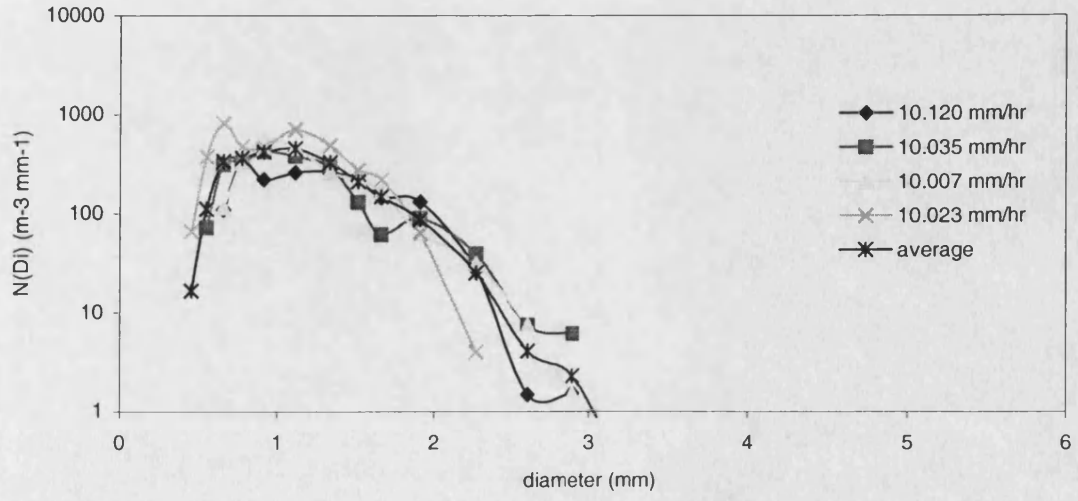

Figure A.5: Measured distributions for stratiform rainfall rates at ~ 10.0 mm hr^{-1}

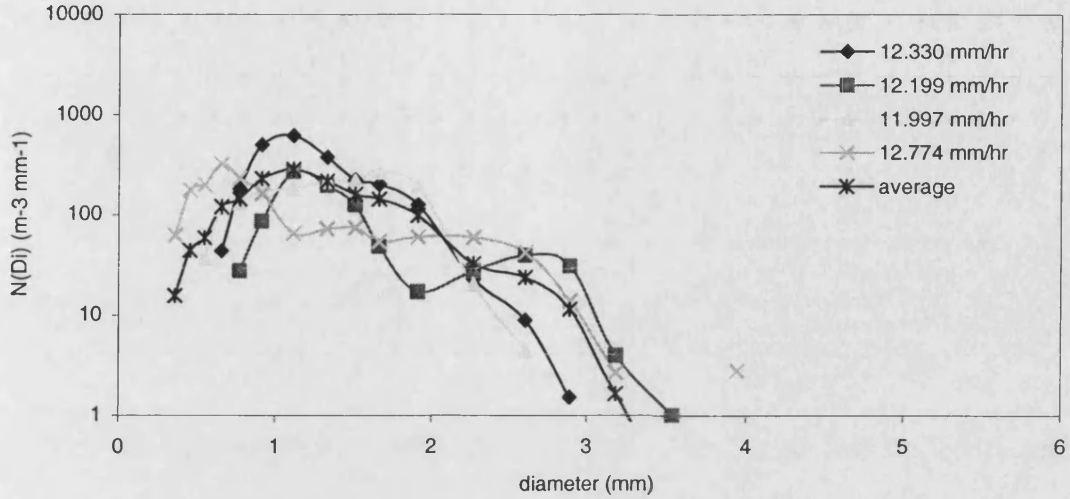

Figure A.6: Measured distributions for stratiform rainfall rates at ~ 12.0 mm hr^{-1}

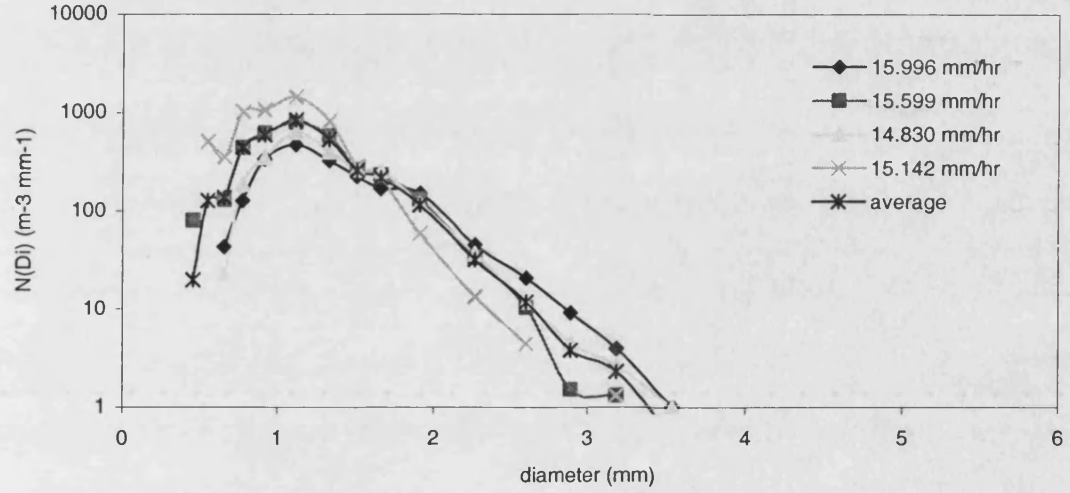

Figure A.7: Measured distributions for stratiform rainfall rates at ~ 15.0 mm hr^{-1}

Appendix B – Measured Distribution for Convective Events

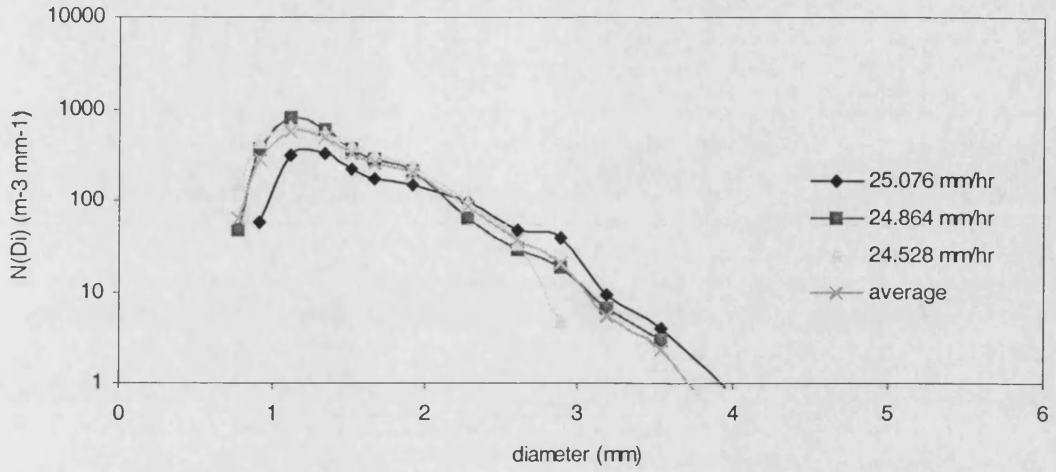

Figure B.1: Measured distributions for convective rainfall rates at ~ 25.0 mm hr^{-1}

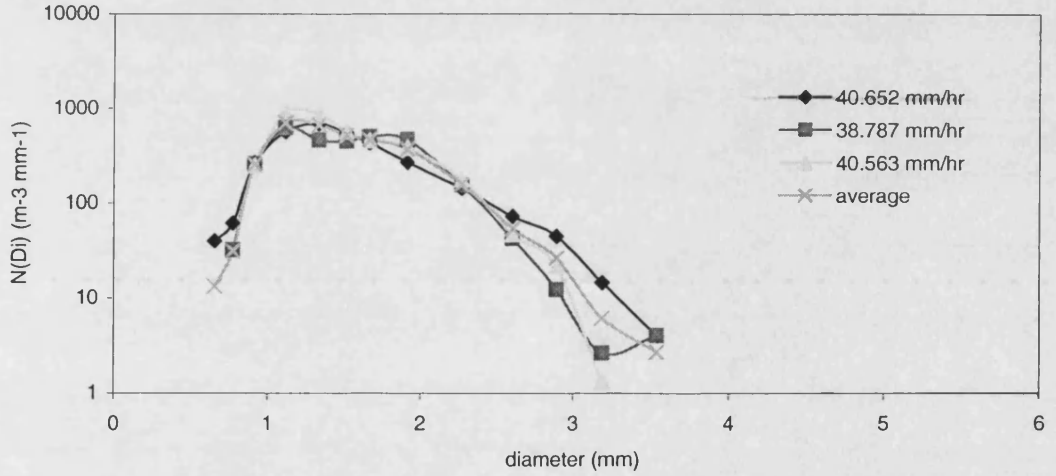

Figure B.2 Measured distributions for convective rainfall rates at ~ 40.0 mm hr^{-1}

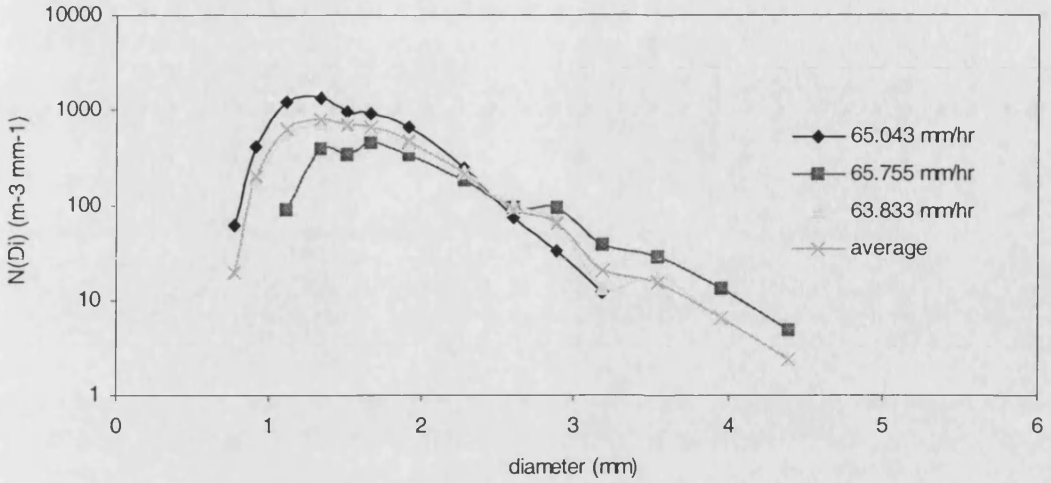

Figure B.3 Measured distributions for convective rainfall rates at ~ 65.0 mm hr^{-1}

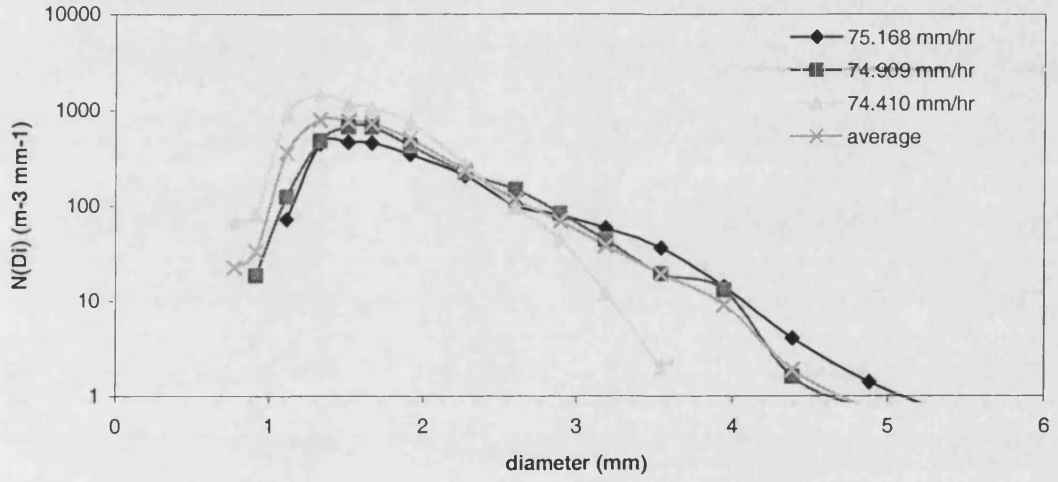

Figure B.4: Measured distributions for convective rainfall rates at ~ 75.0 mm hr^{-1}

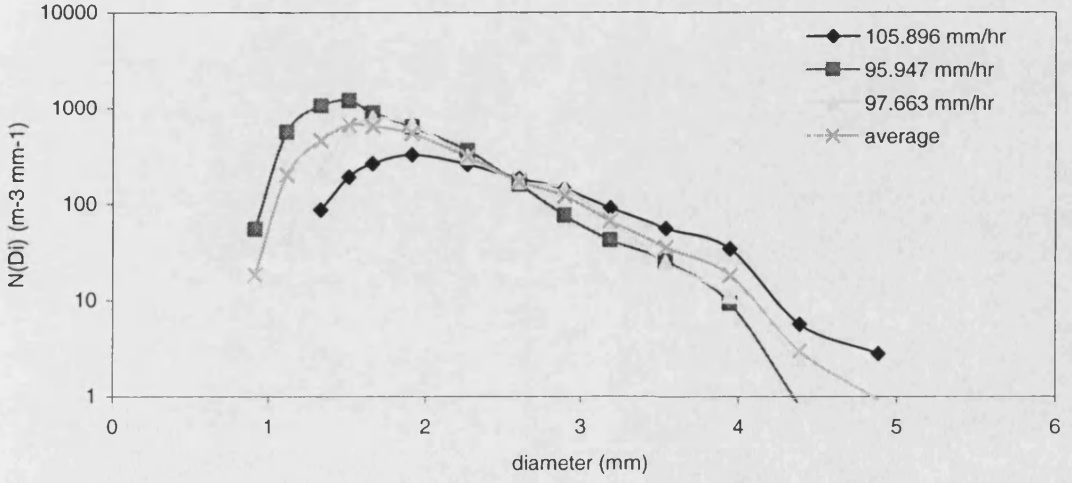

Figure B.5: Measured distributions for convective rainfall rates at ~ 100.0 mm hr^{-1}

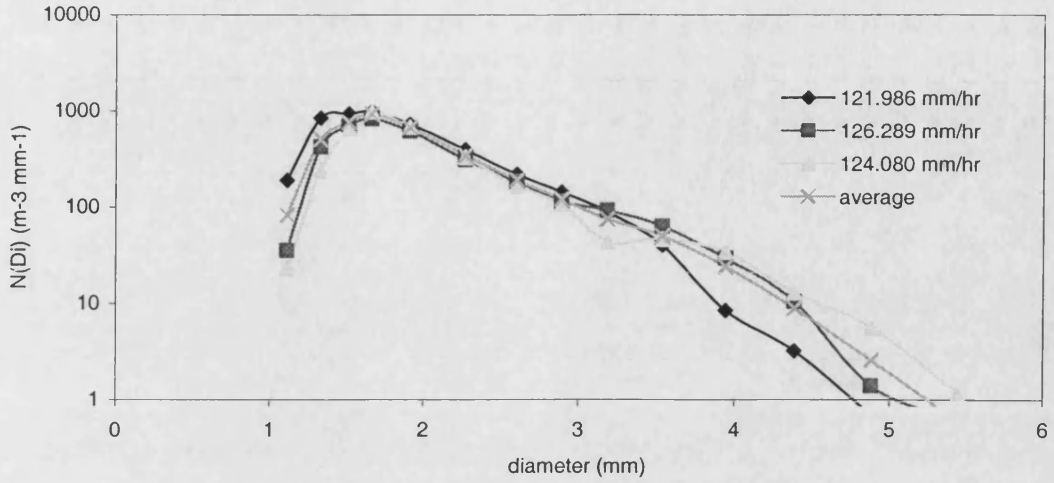

Figure B.6: Measured distributions for convective rainfall rates at ~ 125.0 mm hr-

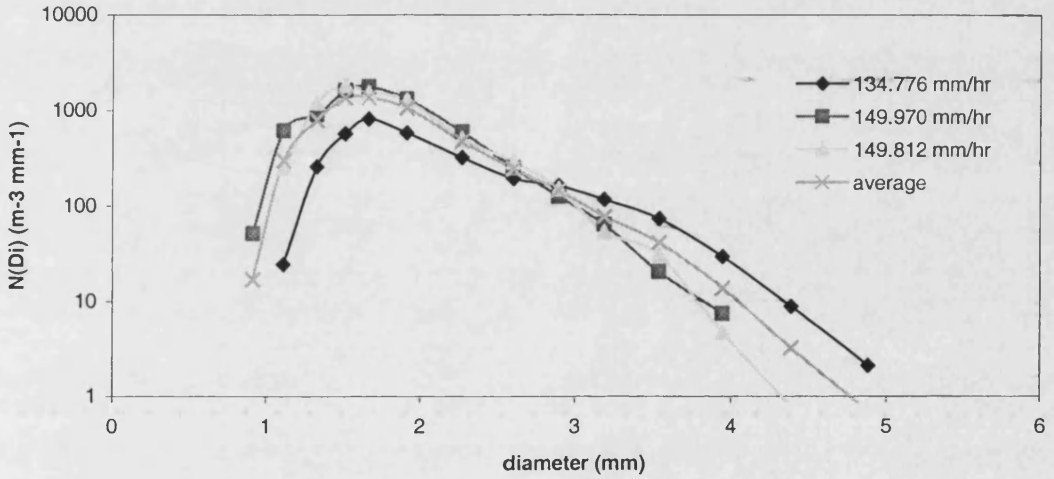

Figure B.7: Measured distributions for convective rainfall rates at ~ 145.0 mm hr^{-1}

Appendix C - Special Equations for Distrometer Data

For the PNG distrometer data, the diameters of raindrops are divided into 20 channels. Defining $N_i(D_i)$ as the expression of the drop size distribution representing each value in channel i, $N_i(D_i)$ then can be calculated from the distrometer data $n(D_i)$ using the following expression:

$$N_i(D_i) = \frac{n(D_i)}{v(D_i)\times 0.3\times \Delta D_i} \qquad \text{(C.1)}$$

The parameter N_t in the lognormal function is the total number of rain drops in a cubic metre. Therefore for the 20-channel data, the parameter of the lognormal function can then be calculated using the expression:

$$N_t = \sum_{i=1}^{20} N_i(D_i)\Delta D_i \qquad \text{(C.2)}$$

$$= \sum_{i=1}^{20} \frac{n(D_i)}{v(D_i)\times 0.3\times \Delta D_i}\Delta D_i$$

$$= \frac{1}{0.3}\sum_{i=1}^{20} \frac{n(D_i)}{v(D_i)}$$

All coefficients have the same definition as previously defined in Equation 6.3 where $n(D_i)$ is the number of drops falling in channel i and $v(D_i)$ is the terminal velocity of drops D_i.

The special equation to estimate the other parameters μ and σ for the lognormal function using the method of maximum likelihood for 20-channel data are given as:

$$\hat{\mu} = \sum_{i=1}^{20} \frac{N_i(D_i)\Delta D_i}{N_t} \ln D_i$$

$$= \frac{1}{3}\sum_{i=1}^{20}\frac{n(D_i)}{N_t v(D_i)}\ln D_i \qquad \text{(C.3)}$$

$$\hat{\sigma} = \sum_{i=1}^{20}\frac{N_i(D_i)\Delta D_i}{N_t}(\ln D_i - \hat{\mu})^2$$

$$= \frac{1}{3}\sum_{i=1}^{20}\frac{n(D_i)}{N_t v(D_i)}(\ln D_i - \hat{\mu})^2 \qquad \text{(C.4)}$$

where $N_i(D_i)\Delta D_i$ in both equations is the number of drops in channel i per cubic metre. The estimates from the methods of moments are obtained from equating a sufficient number of the measured moments to corresponding theoretical moments [Ajayi and Olsen, 1983]. The special equation to determine the experimental kth moment suitable for distrometer data it is given as:

$$M_k = \sum_{i=1}^{20} D_i^{\,k} N_i(D_i)\Delta D_i$$

$$= \frac{1}{3}\sum_{i=1}^{20}\frac{n(D_i)}{v(D_i)}D_i^{\,k} \qquad \text{(C.6)}$$

The equation to calculate the parameters μ and σ estimated using method of moments for the lognormal function are expressed as follows:

$$\hat{\mu} = \frac{1}{l-k}\left[\frac{1}{l}\ln\frac{M_k}{N_t} - \frac{k}{l}\ln\frac{M_l}{N_t}\right] \qquad \text{(C.7)}$$

$$\hat{\sigma} = \frac{2}{l-k}\left[\frac{1}{l}\ln\frac{M_l}{N_t} - \frac{1}{k}\ln\frac{M_k}{N_t}\right] \qquad \text{(C.8)}$$

where $k \geq 1$, $l \geq 1$ and $k \# 1$.

The maximum likelihood estimators do not exist for the gamma model. The moment estimators for the three parameters can be computed from measured data using the

Equation C.6 above for M_k. The associated equations for parameters p, Λ_2 and Λ_1 are given as:

$$\eta_{k,k-1} = \frac{M_k}{l-k} \tag{C.9}$$

$$p = \frac{k\eta_{m,m-1} - m\eta_{k,k-1}}{\eta_{k,k-1} - \eta_{m,m-1}} \tag{C.10}$$

$$\Lambda_2 = \frac{k-m}{\eta_{k,k-1} - \eta_{m,m-1}} \tag{C.11}$$

where $k \geq 1$, $m \geq 1$, $k \neq m$, and

$$\frac{1}{\Lambda_1} = \frac{1}{M_k - M_m}\left[\frac{\Gamma(p+k+1)}{\Lambda_2^{\,p+k+1}} - \frac{\Gamma(p+m+1)}{\Lambda_2^{\,p+m+1}}\right]$$

$$\therefore \Lambda_1 = \frac{M_k - M_m}{\left[\frac{\Gamma(p+k+1)}{\Lambda_2^{\,p+k+1}} - \frac{\Gamma(p+m+1)}{\Lambda_2^{\,p+m+1}}\right]} \tag{C.12}$$

where $m = 0, 1, 2, , k > m$.

Appendix D – Comparison between various lognormal distributions with measured data distribution for stratiform rainfall rates

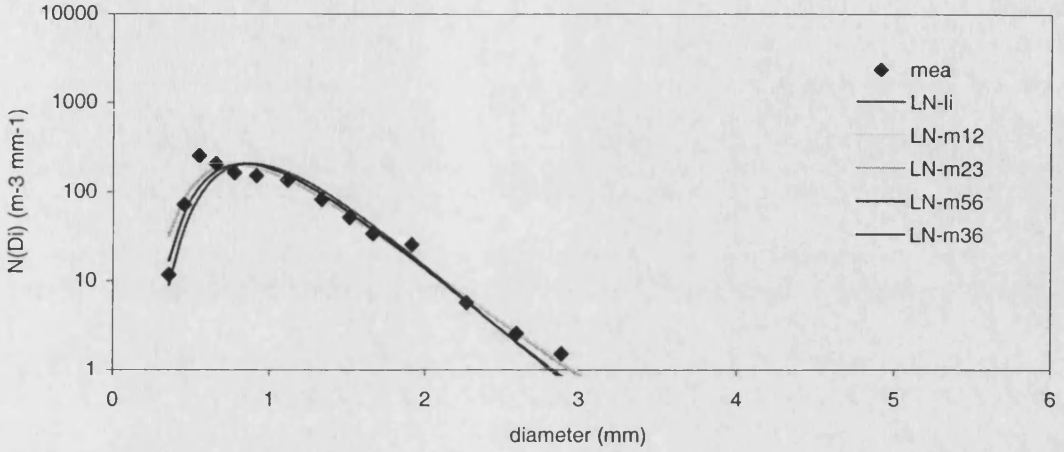

Figure D.1: Comparison between various lognormal distributions with measured data distribution for stratiform rainfall rate of 3.0 mm hr^{-1}

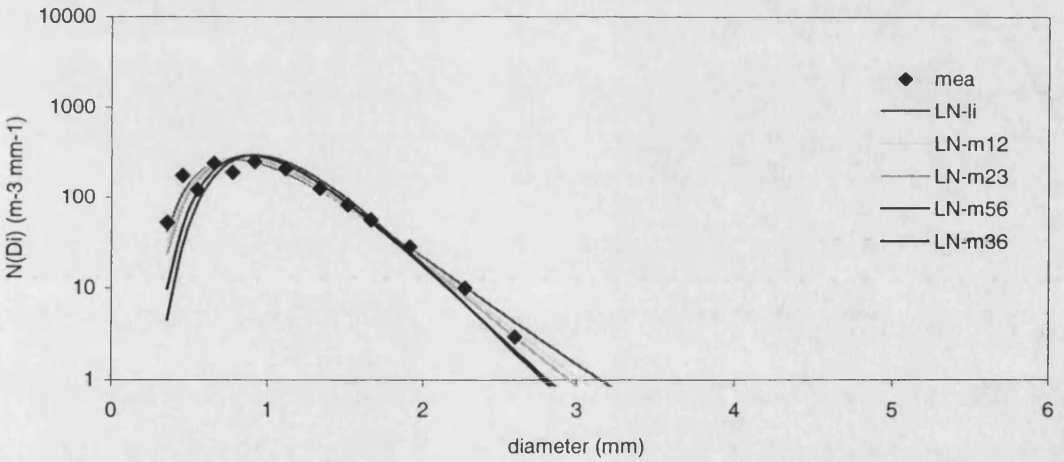

Figure D.2: Comparison between various lognormal distributions with measured data distribution for stratiform rainfall rate of 4.0 mm hr^{-1}

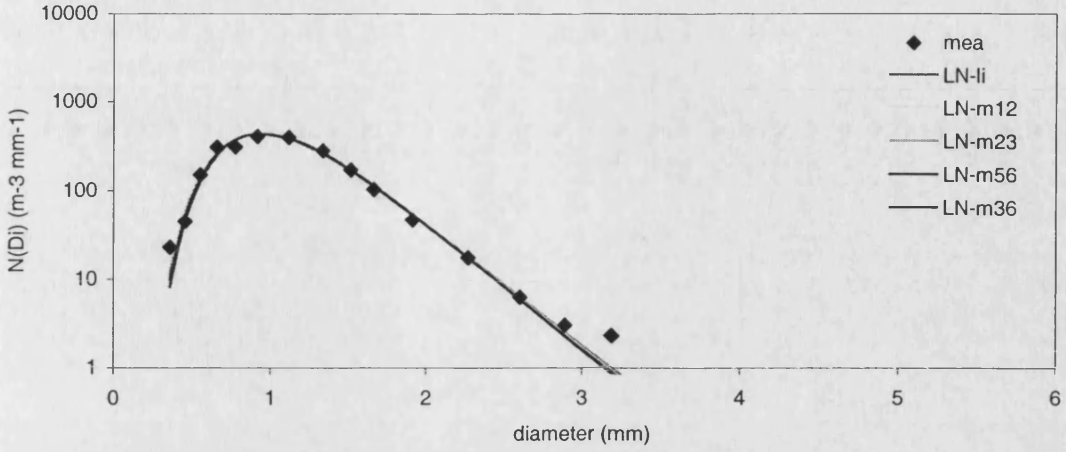

Figure D.3: Comparison between various lognormal distributions with measured data distribution for stratiform rainfall rate of 6.1 mm hr^{-1}

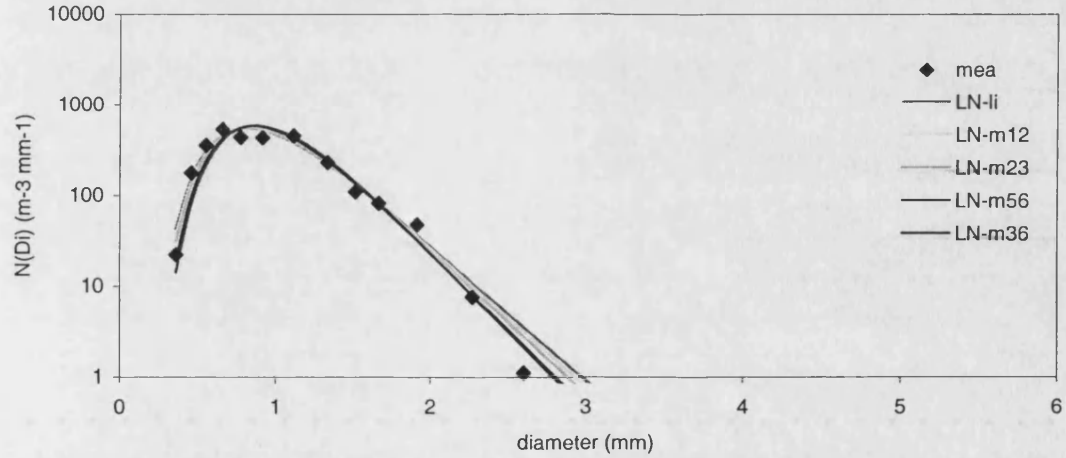

Figure D.4 Comparison between various lognormal distributions with measured data distribution for stratiform rainfall rate of 8.0 mm hr^{-1}.

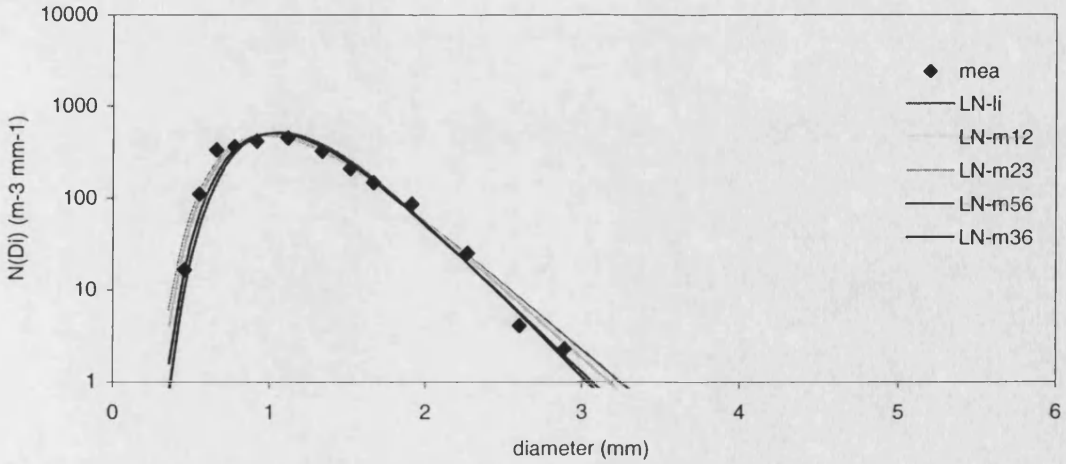

Figure D.5 Comparison between various lognormal distributions with measured data distribution for stratiform rainfall rate of 10.0 mm hr^{-1}.

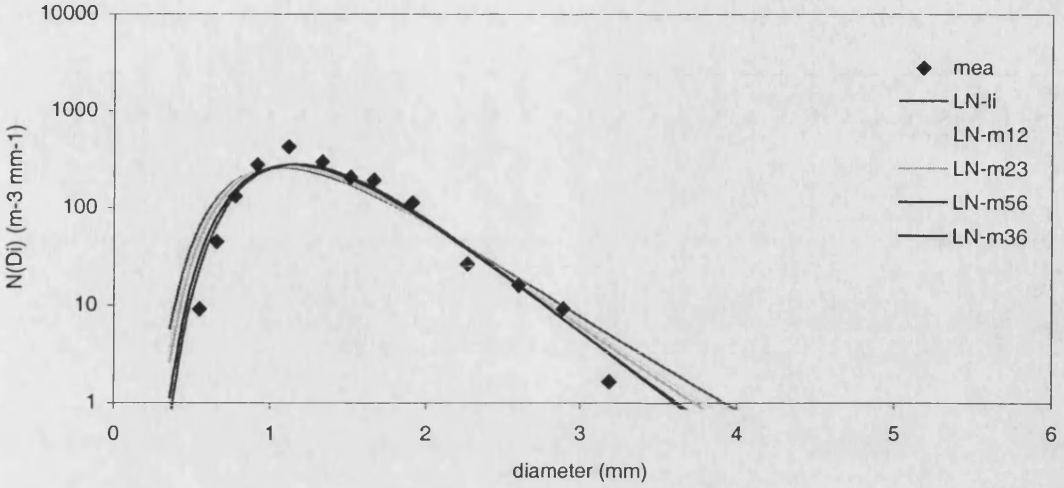

Figure D.6 Comparison between various lognormal distributions with measured data distribution for stratiform rainfall rate of 12.3 mm hr^{-1}.

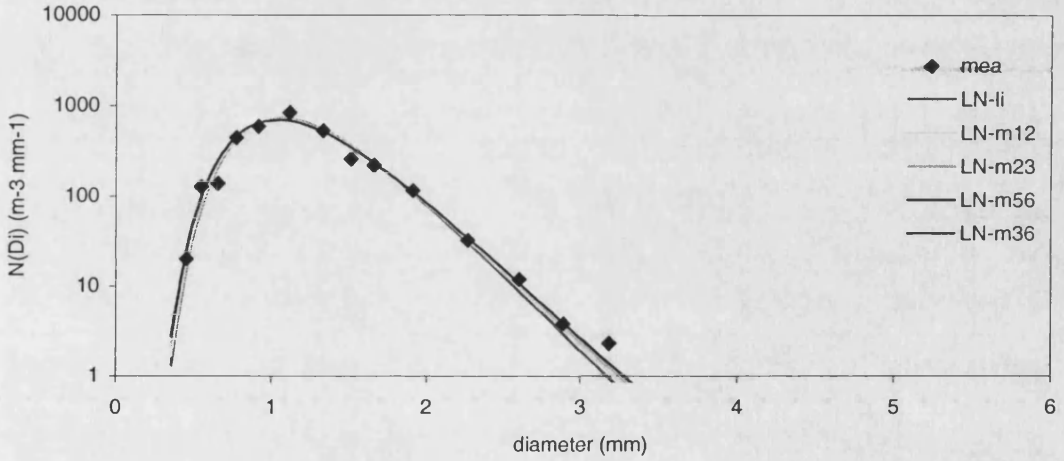

Figure D.7: Comparison between various lognormal distributions with measured data distribution for stratiform rainfall rate of 15.4 mm hr^{-1}.

Appendix E – Comparison between various gamma distributions with measured data distribution for stratiform rainfall rates

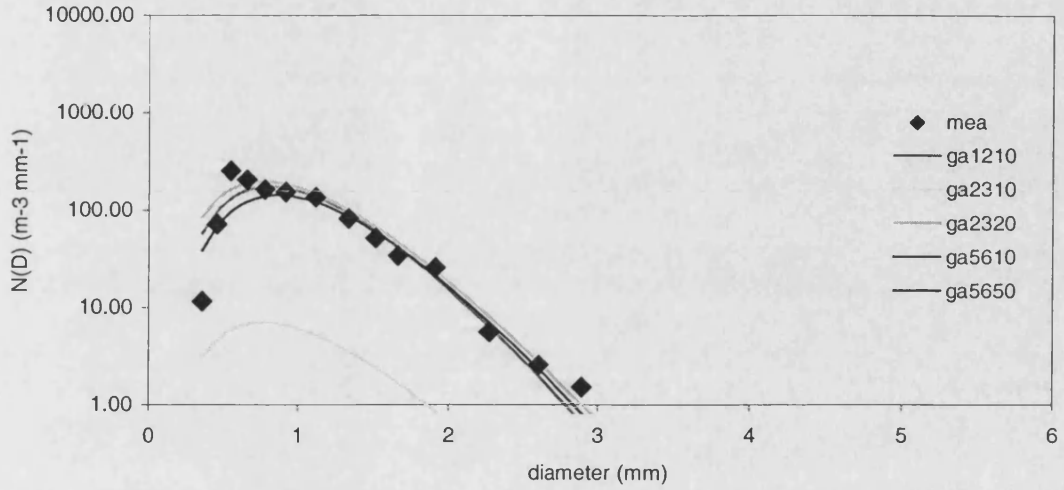

Figure E.1: Comparison between various gamma distributions with measured data distribution for stratiform rainfall rate of 3.0 mm hr^{-1}.

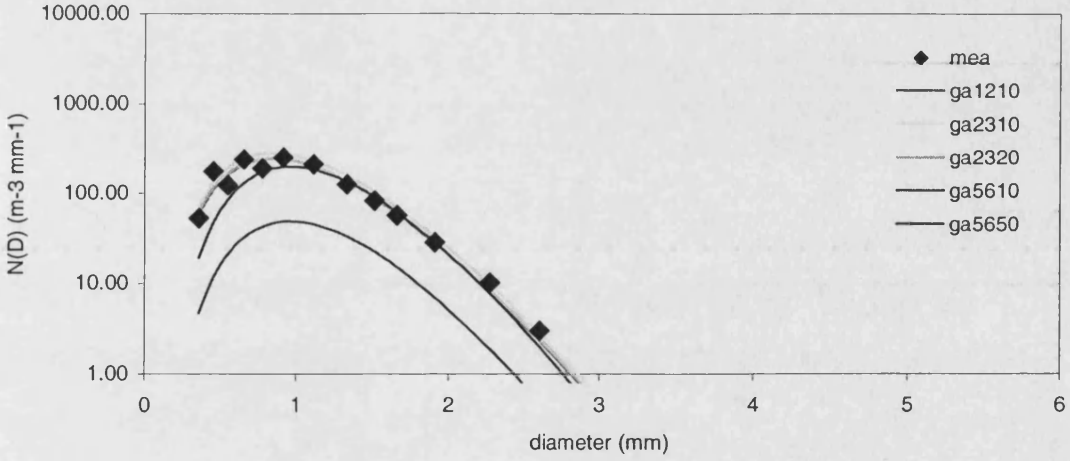

Figure E.2: Comparison between various gamma distributions with measured data distribution for stratiform rainfall rate of 4.0 mm hr^{-1}.

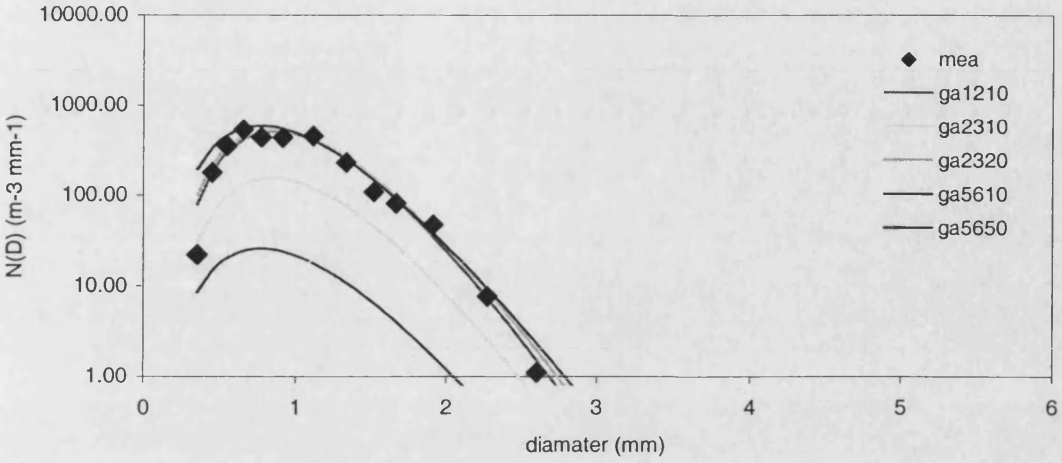

Figure E.3: Comparison between various gamma distributions with measured data distribution for stratiform rainfall rate of 6.1 mm hr^{-1}.

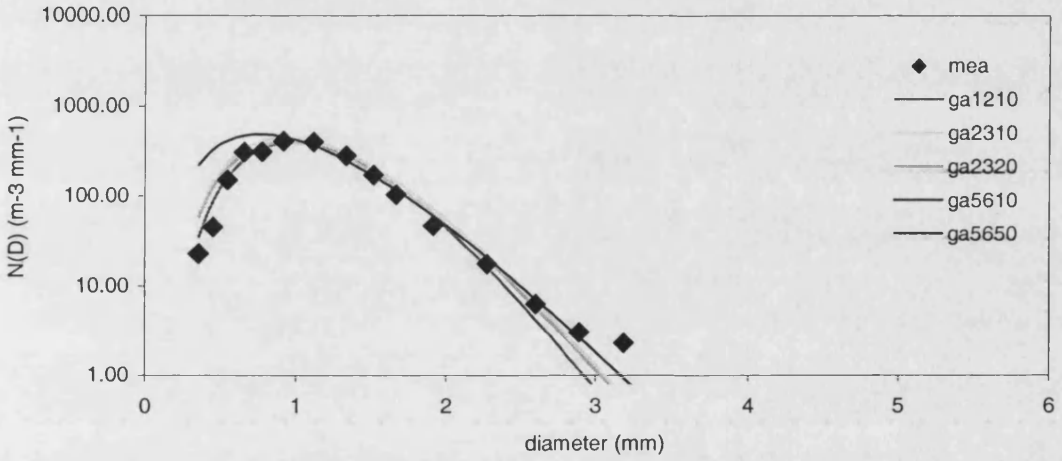

Figure E.4: Comparison between various gamma distributions with measured data distribution for stratiform rainfall rate of 8.0 mm hr^{-1}.

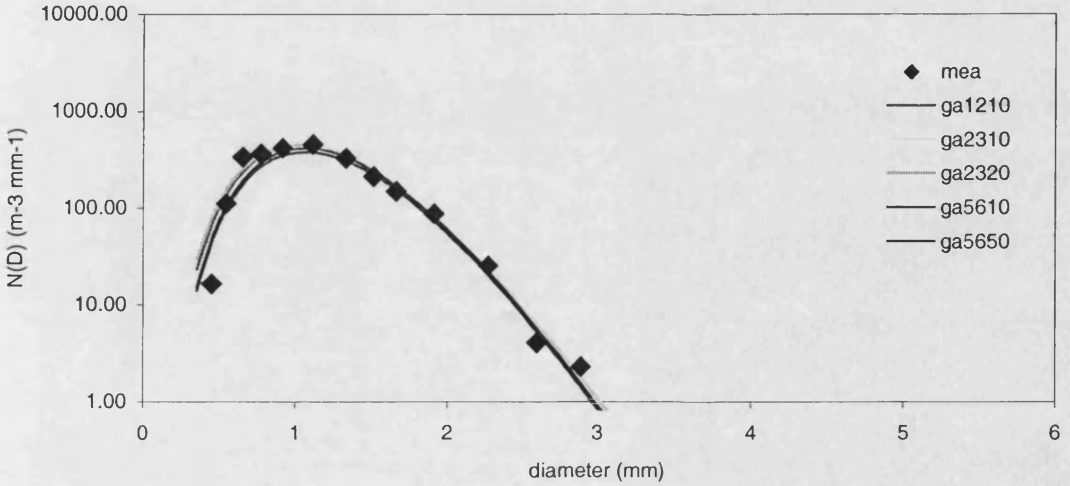

Figure E.5: Comparison between various gamma distributions with measured data distribution for stratiform rainfall rate of 10.0 mm hr^{-1}.

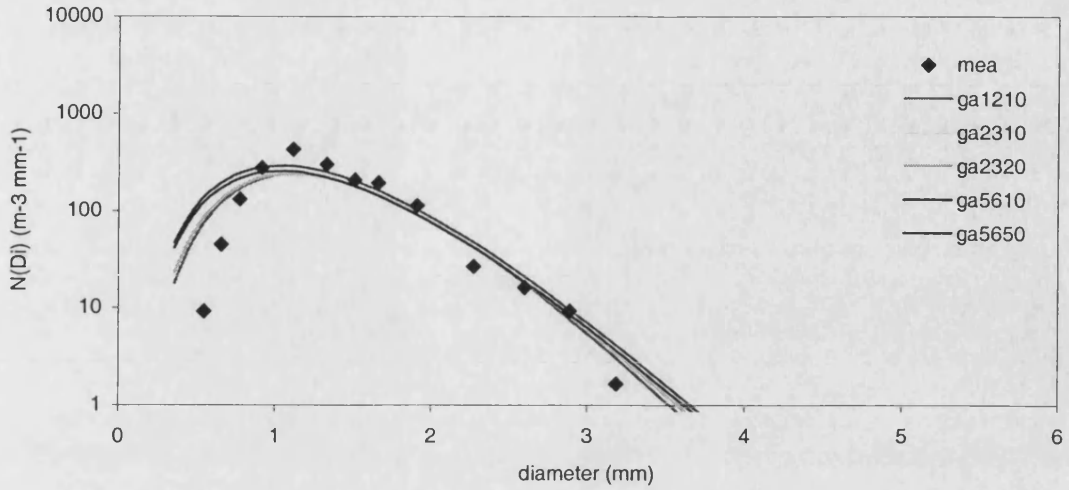

Figure E.6: Comparison between various gamma distributions with measured data distribution for stratiform rainfall rate of 12.3 mm hr^{-1}.

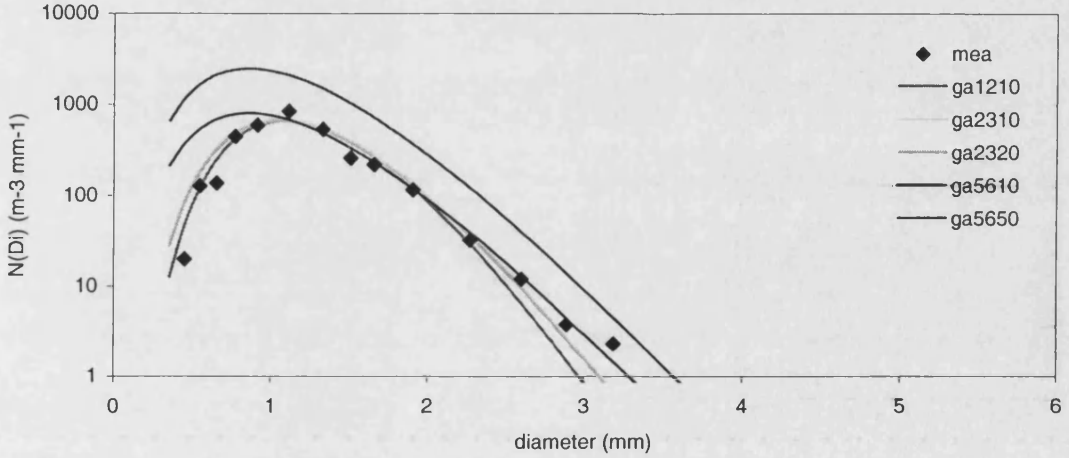

Figure E.7: Comparison between various gamma distributions with measured data distribution for stratiform rainfall rate of 15.4 mm hr^{-1}.

Appendix F – Comparison between various lognormal distributions with measured data distribution for convective rainfall rates

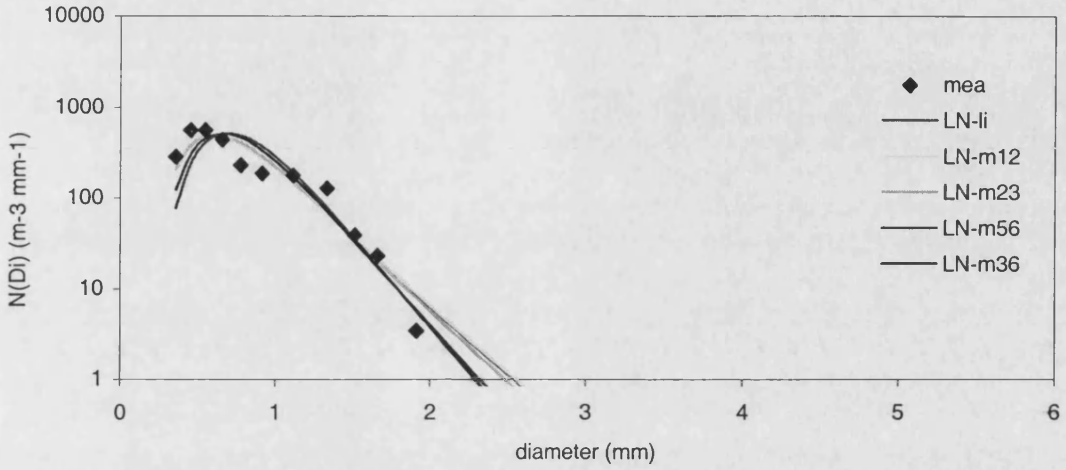

Figure F.1: Comparison between various lognormal distributions with measured data distribution for convective rain fall rate of 24.8 mm hr^{-1}

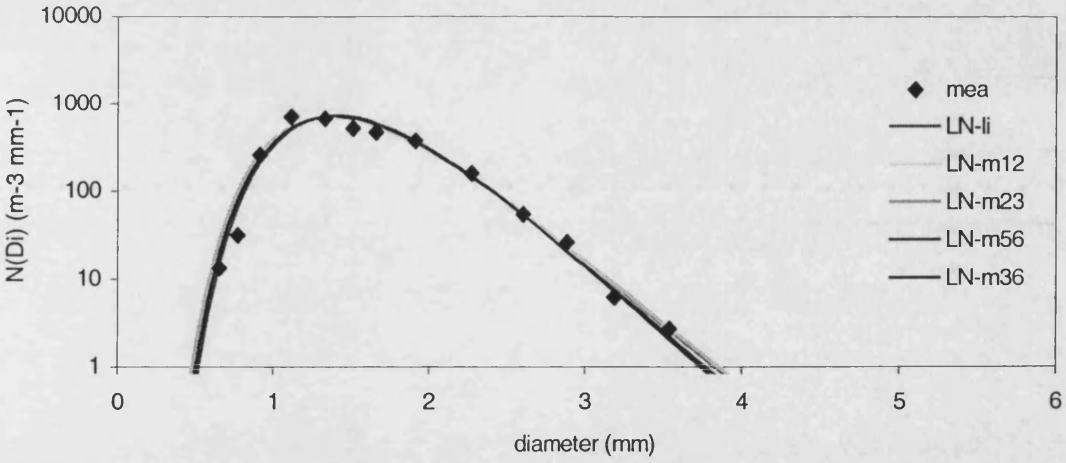

Figure F.2: Comparison between various lognormal distributions with measured data distribution for convective rain fall rate of 40.0 mm hr^{-1}

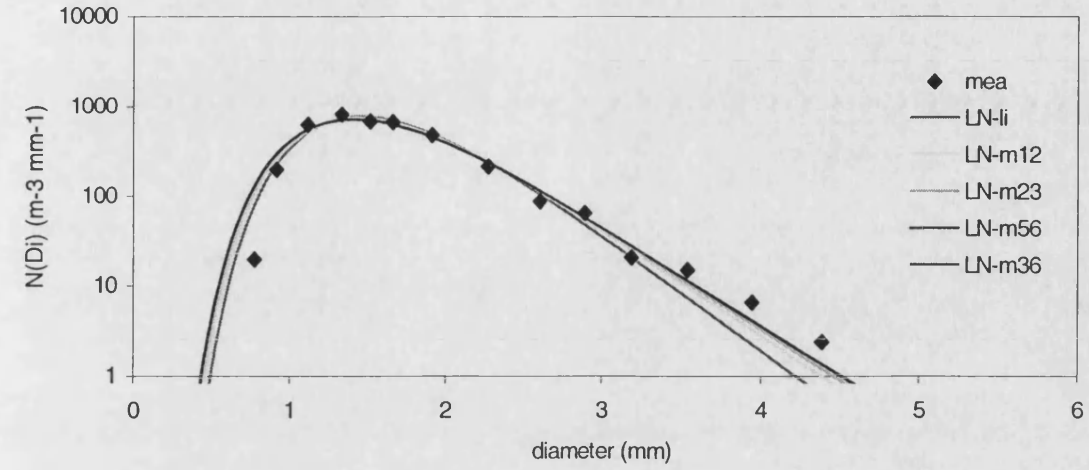

Figure F.3: Comparison between various lognormal distributions with measured data distribution for convective rain fall rate of 64.9 mm hr^{-1}

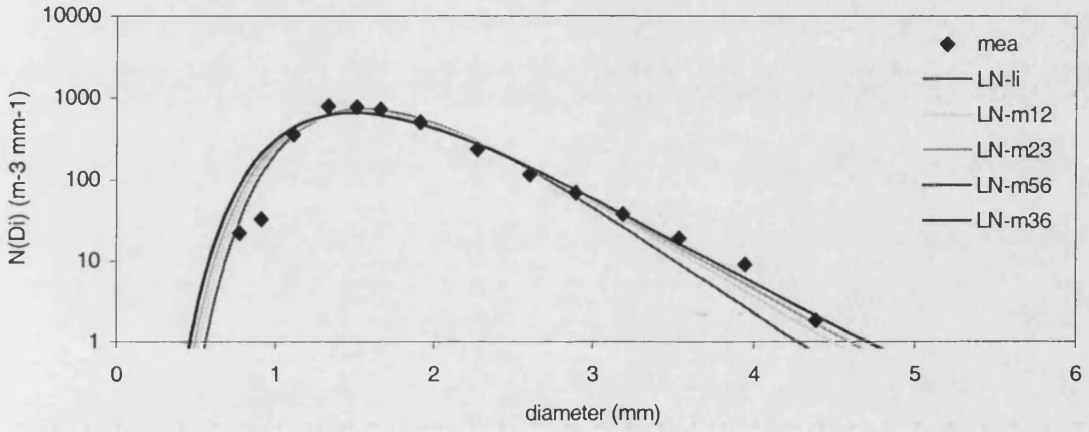

Figure F.4: Comparison between various lognormal distributions with measured data distribution for convective rain fall rate of 74.8 mm hr^{-1}

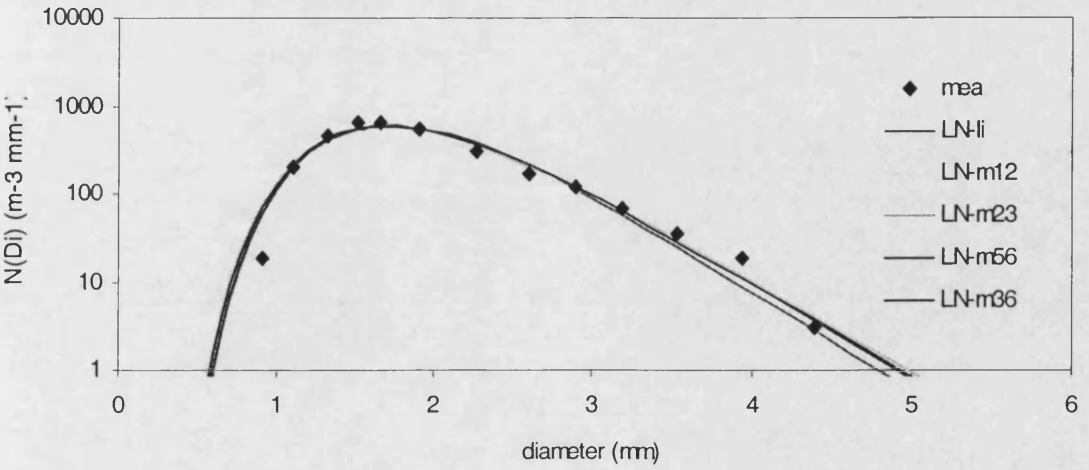

Figure F.5: Comparison between various lognormal distributions with measured data distribution for convective rain fall rate of 99.8 mm hr^{-1}

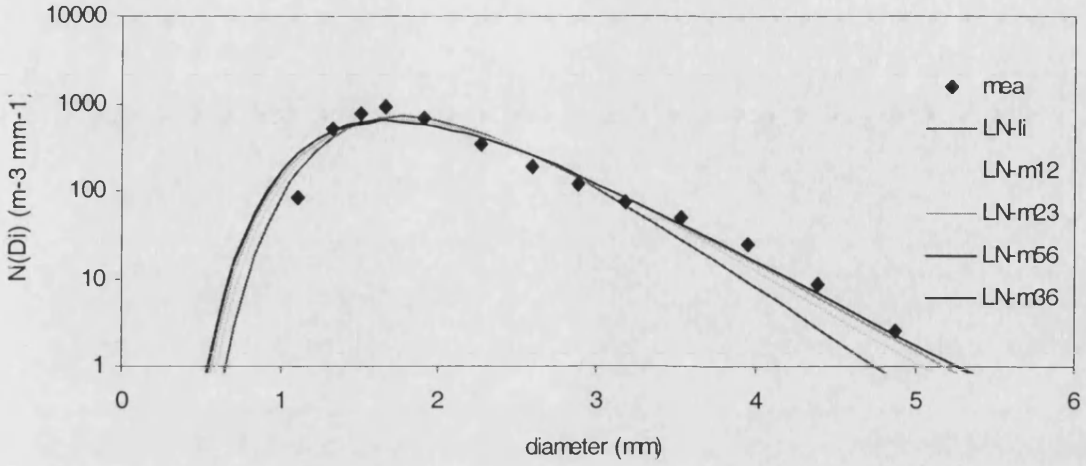

Figure F.6: Comparison between various lognormal distributions with measured data distribution for convective rain fall rate of 124.1 mm hr^{-1}

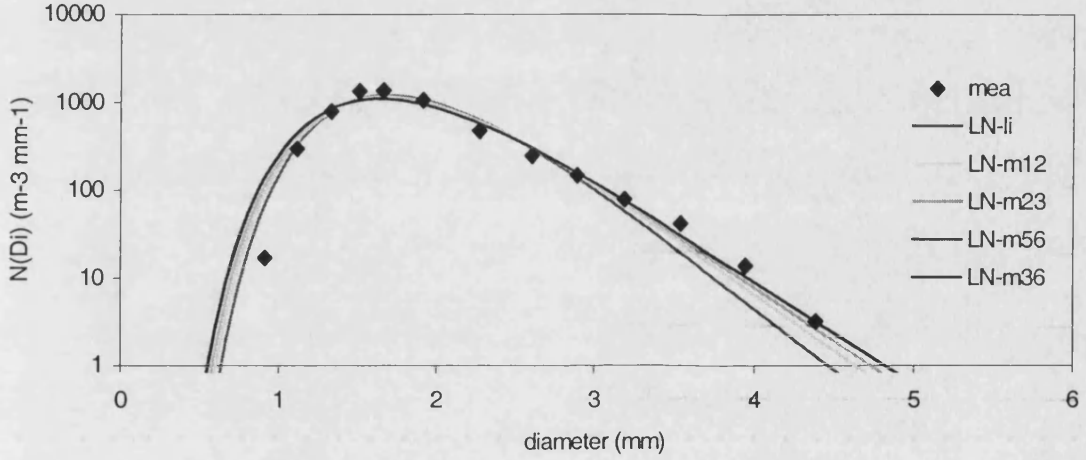

Figure F.7: Comparison between various lognormal distributions with measured data distribution for convective rain fall rate of 144.8 mm hr^{-1}

Appendix G – Comparison between various gamma distributions with measured data distribution for convective rainfall rates

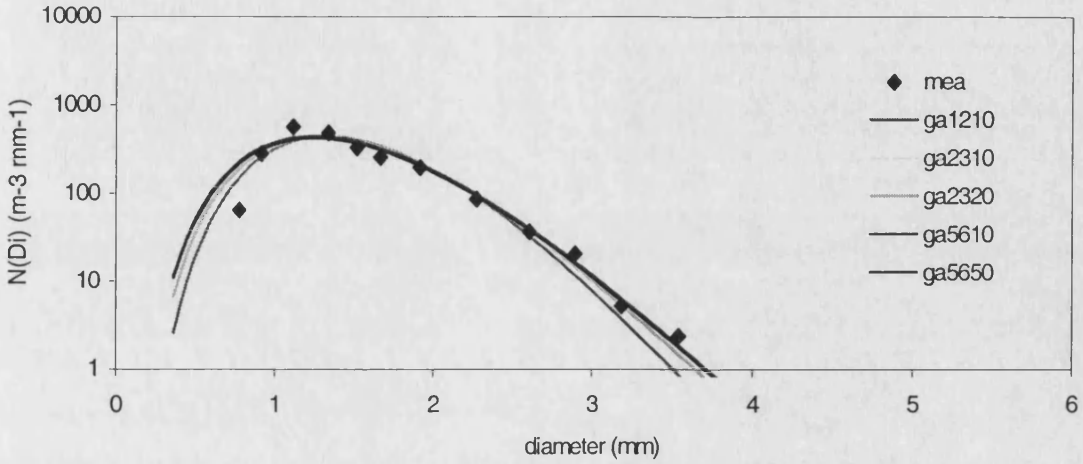

Figure G.1: Comparison between various gamma distributions with measured data distribution for convective rainfall rate of 24.8 mm hr^{-1}.

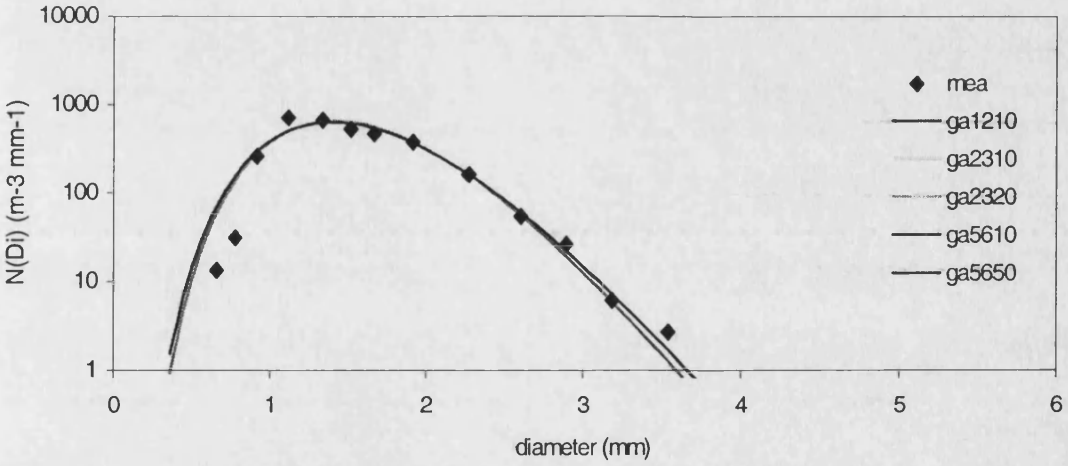

Figure G.2: Comparison between various gamma distributions with measured data distribution for convective rainfall rate of 40.0 mm hr^{-1}.

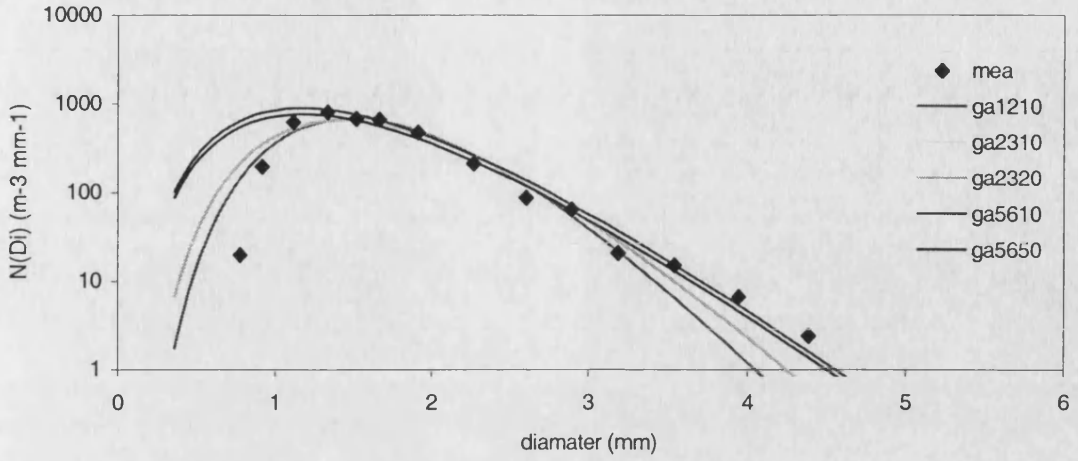

Figure G.3: Comparison between various gamma distributions with measured data distribution for convective rainfall rate of 64.9 mm hr^{-1}.

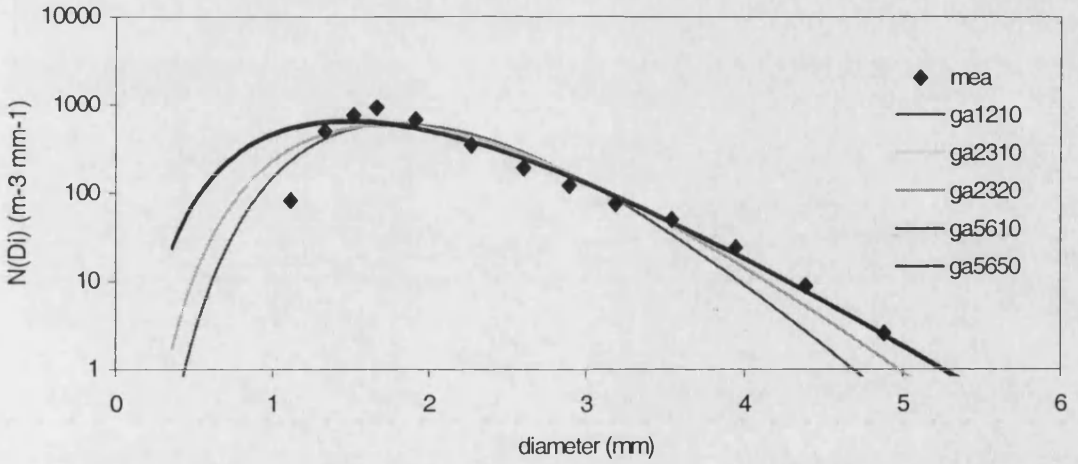

Figure G.4: Comparison between various gamma distributions with measured data distribution for convective rainfall rate of 74.8 mm hr^{-1}.

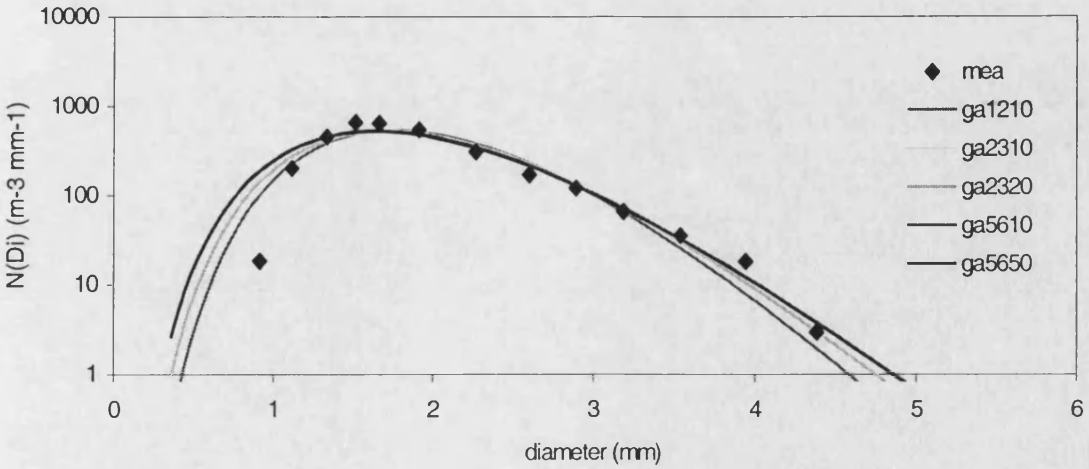

Figure G.5: Comparison between various gamma distributions with measured data distribution for convective rainfall rate of 99.8 mm hr^{-1}.

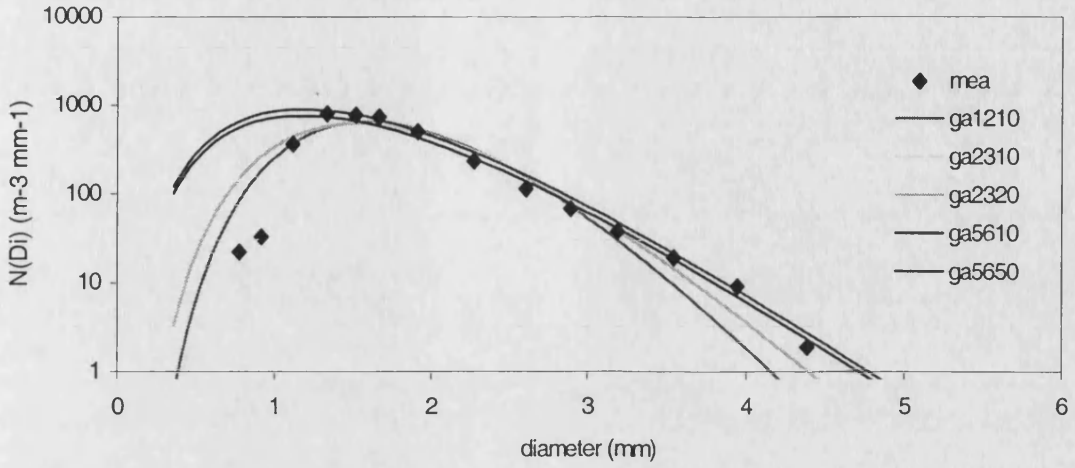

Figure G.6: Comparison between various gamma distributions with measured data distribution for convective rainfall rate of 124.1 mm hr^{-1}.

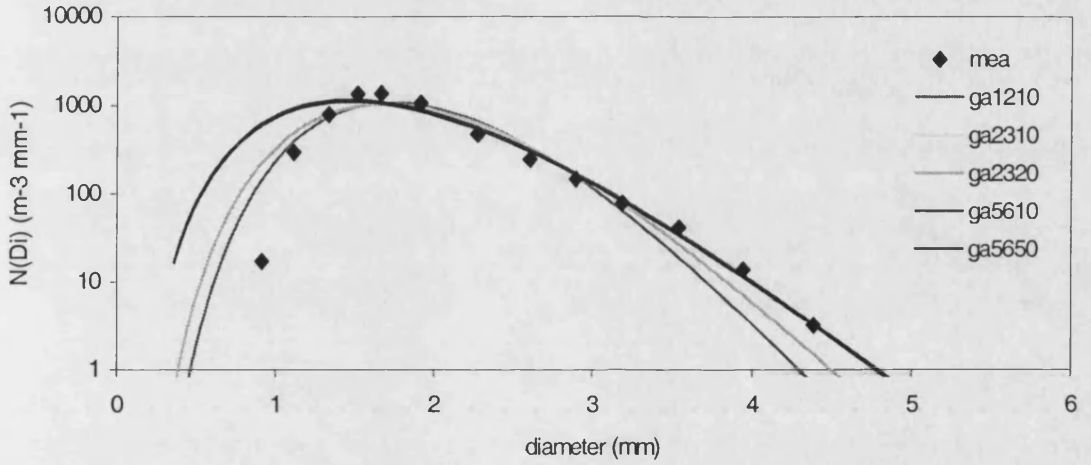

Figure G.7: Comparison between various gamma distributions with measured data distribution for convective rainfall rate of 144.8 mm hr^{-1}.

Appendix H – Comparison between various generalised lognormal distributions with measured data distribution for stratiform rainfall rates

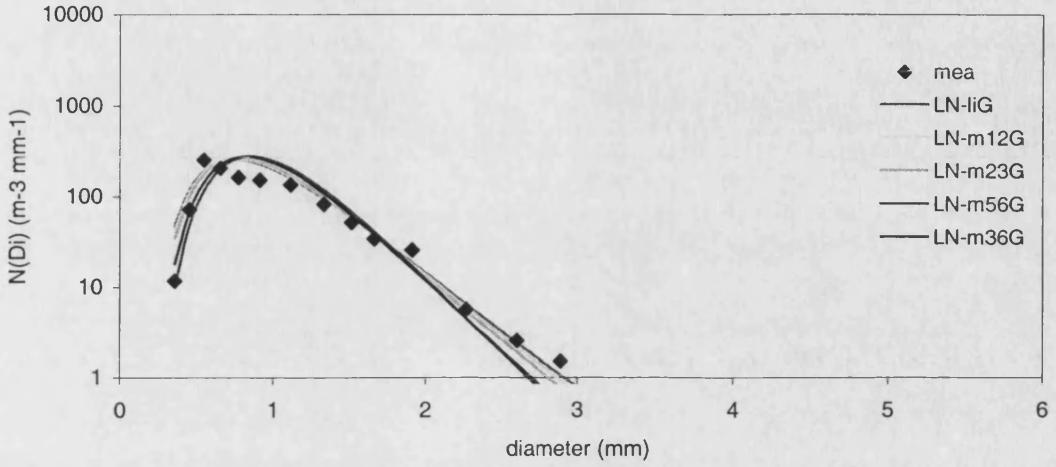

Figure H.1: Comparison between various generalised lognormal distributions with measured data distribution for stratiform rainfall rate of 3.0 mm hr^{-1}.

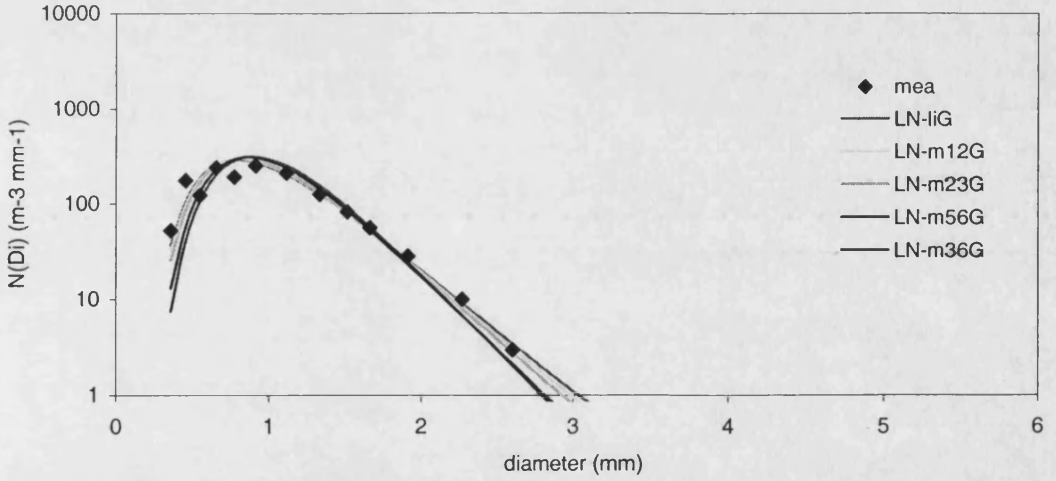

Figure H.2: Comparison between various generalised lognormal distributions with measured data distribution for stratiform rainfall rate of 4.0 mm hr^{-1}.

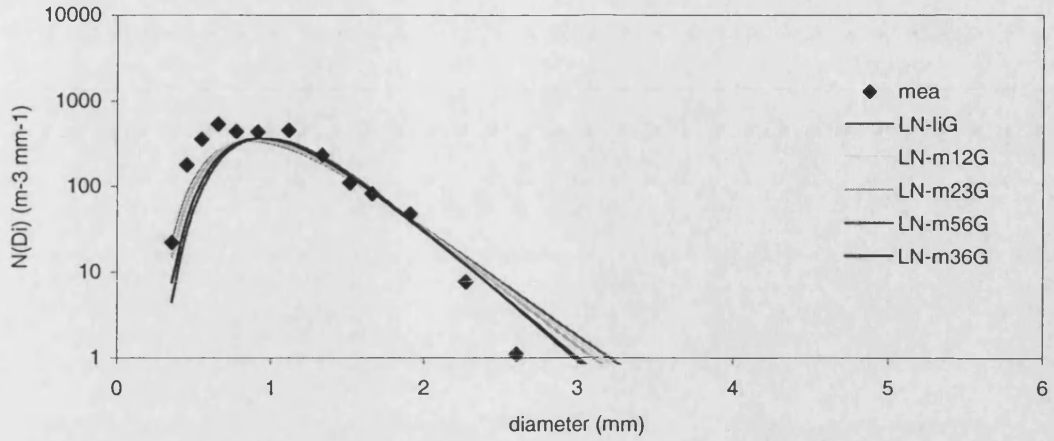

Figure H.3: Comparison between various generalised lognormal distributions with measured data distribution for stratiform rainfall rate of 6.1 mm hr^{-1}.

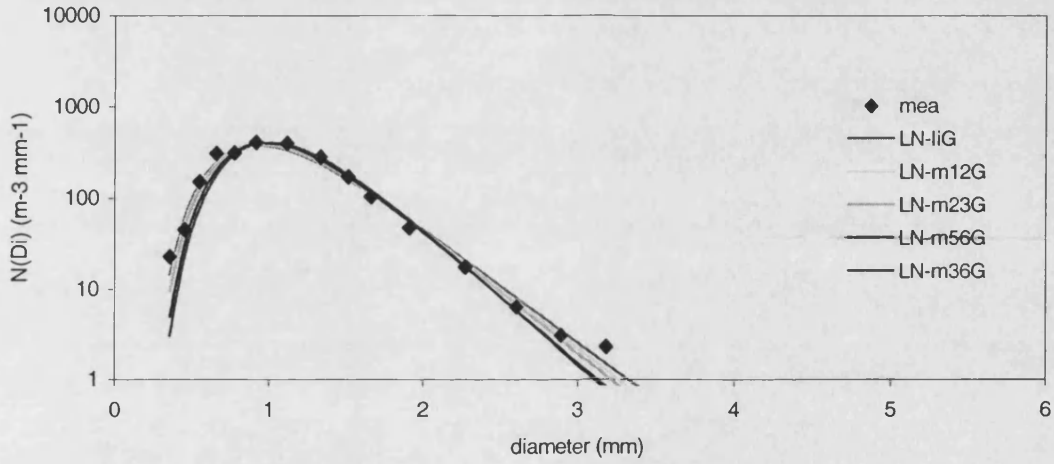

Figure H.4 Comparison between various generalised lognormal distributions with measured data distribution for stratiform rainfall rate of 8.0 mm hr^{-1}.

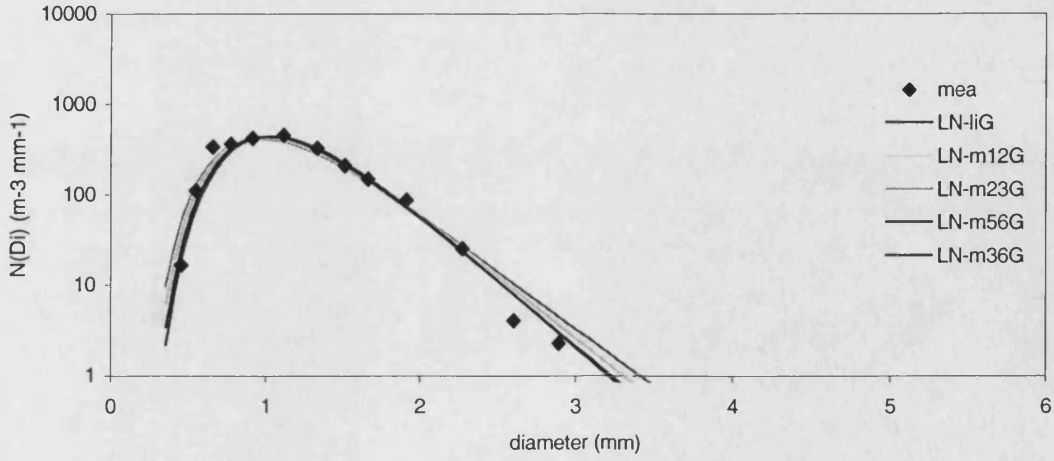

Figure H.5: Comparison between various generalised lognormal distributions with measured data distribution for stratiform rainfall rate of 10.0 mm hr^{-1}.

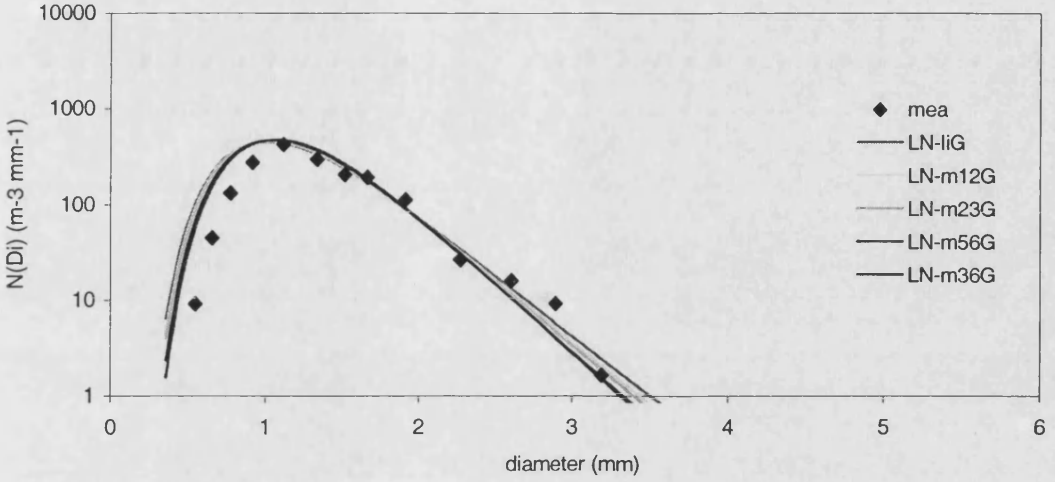

Figure H.6: Comparison between various generalised lognormal distributions with measured data distribution for stratiform rainfall rate of 12.3 mm hr^{-1}.

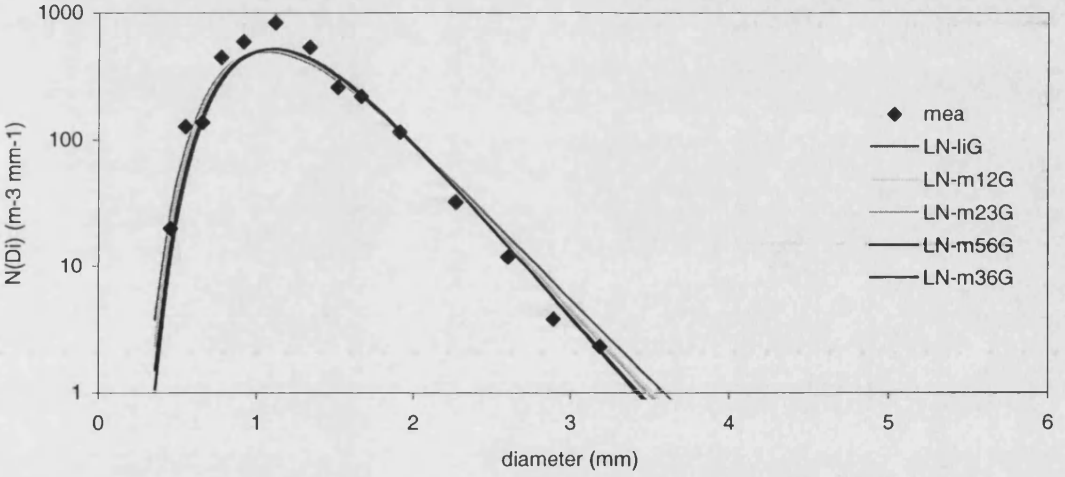

FigureH.7: Comparison between various generalised lognormal distributions with measured data distribution for stratiform rainfall rate of 15.4 mm hr^{-1}.

Appendix I – Comparison between various generalised gamma distributions with measured data distribution for stratiform rainfall rates

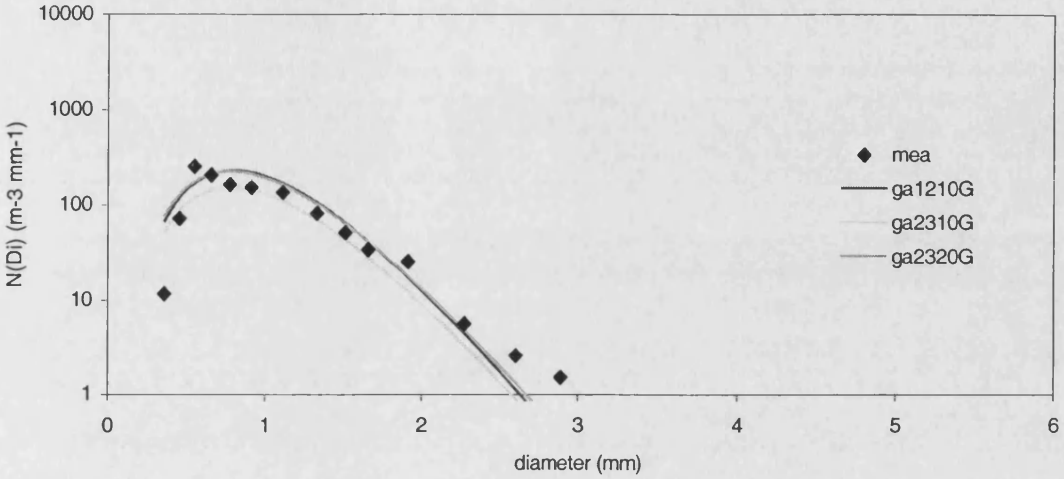

Figure I.1: Comparison between various generalised gamma distributions with measured data distribution for stratiform rainfall rate of 3.0 mm hr^{-1}.

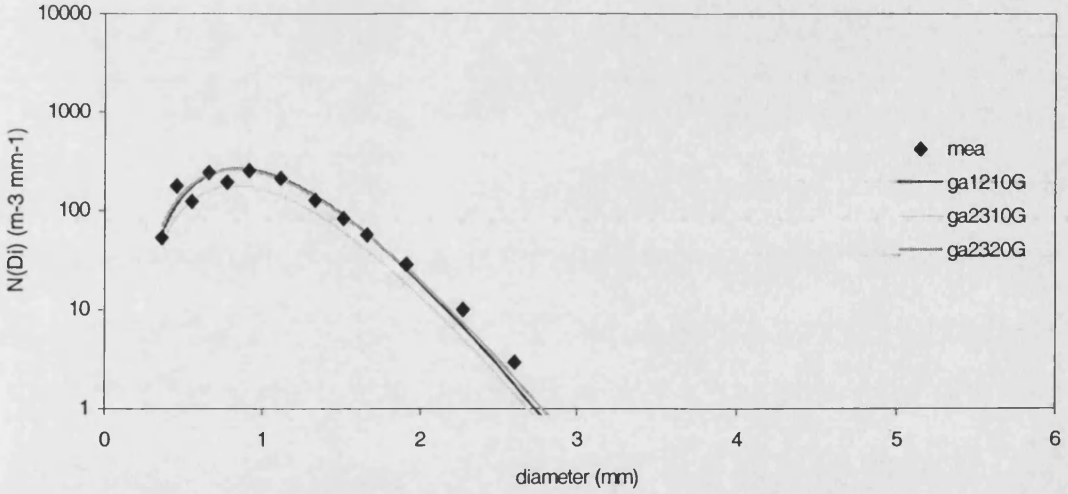

Figure I.2: Comparison between various generalised gamma distributions with measured data distribution for stratiform rainfall rate of 4.0 mm hr^{-1}.

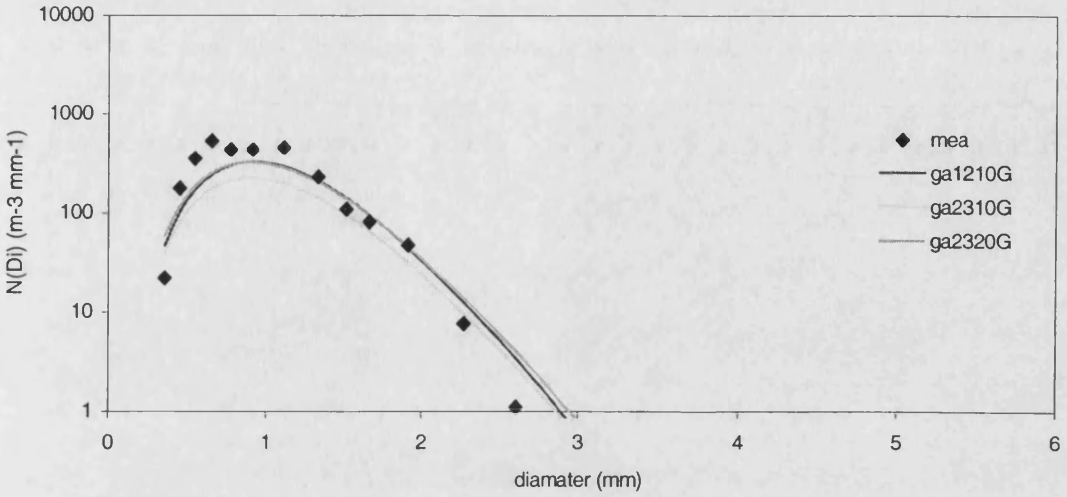

Figure I.3: Comparison between various generalised gamma distributions with measured data distribution for stratiform rainfall rate of 6.0 mm hr^{-1}.

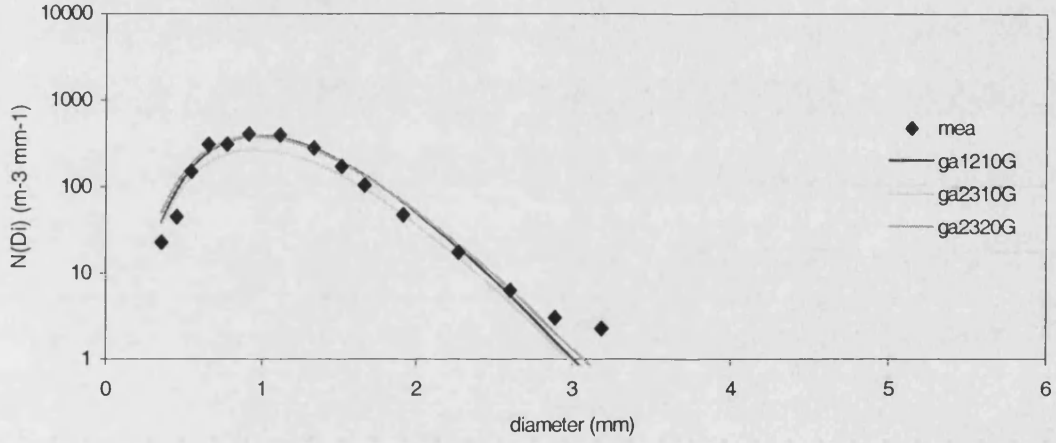

Figure I.4: Comparison between various generalised gamma distributions with measured data distribution for stratiform rainfall rate of 8.0 mm hr^{-1}.

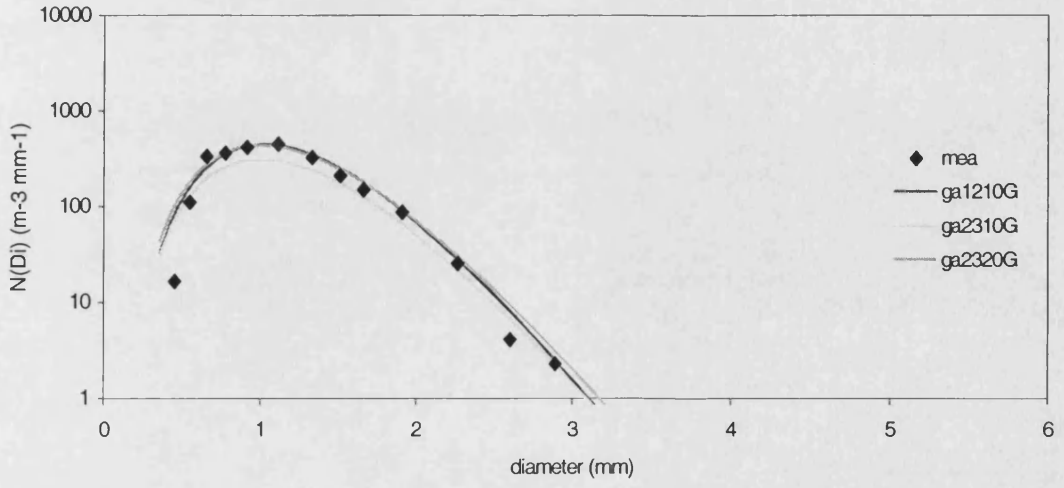

Figure I.5: Comparison between various generalised gamma distributions with measured data distribution for stratiform rainfall rate of 10.0 mm hr^{-1}.

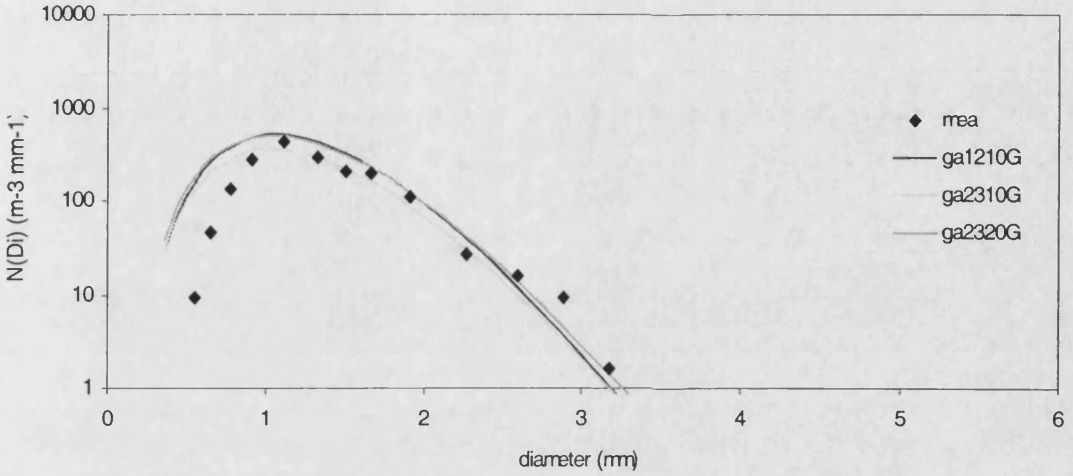

Figure I.6 Comparison between various generalised gamma distributions with measured data distribution for stratiform rainfall rate of 12.0 mm hr^{-1}.

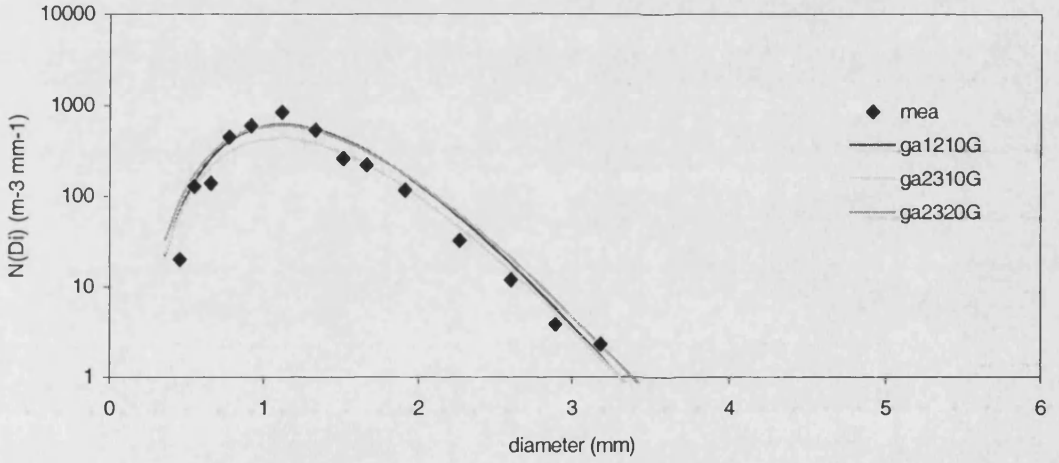

Figure I.7 Comparison between various generalised gamma distributions with measured data distribution for stratiform rainfall rate of 15.0 mm hr^{-1}.

Appendix J – Comparison between various generalised lognormal distributions with measured data distribution for convective rainfall rates

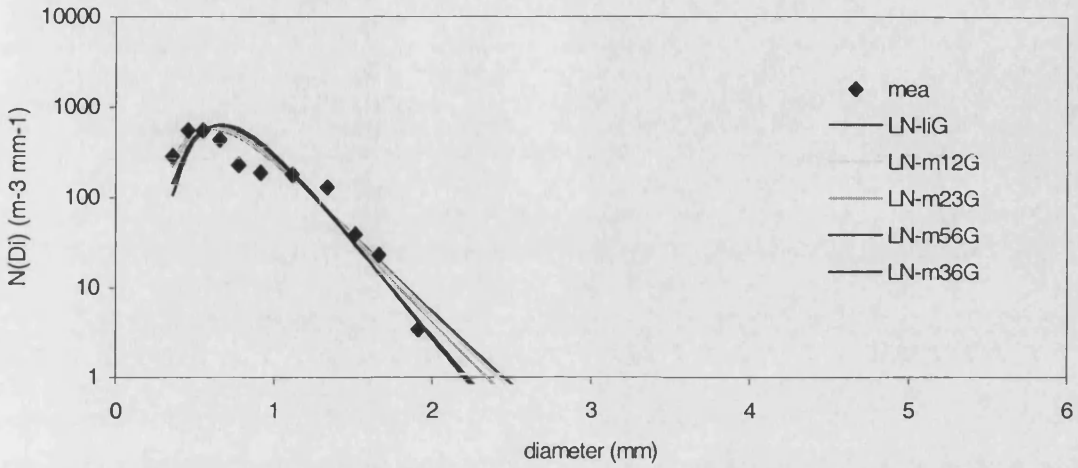

Figure J.1: Comparison between various generalised lognormal distributions with measured data distribution for convective rainfall rate of 24.8 mm hr^{-1}

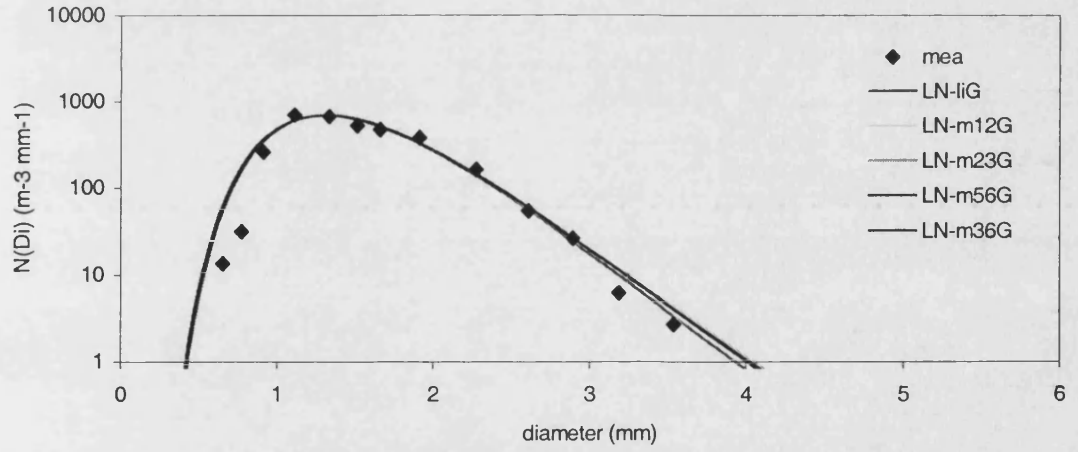

Figure J.2: Comparison between various generalised lognormal distributions with measured data distribution for convective rainfall rate of 40.0 mm hr^{-1}

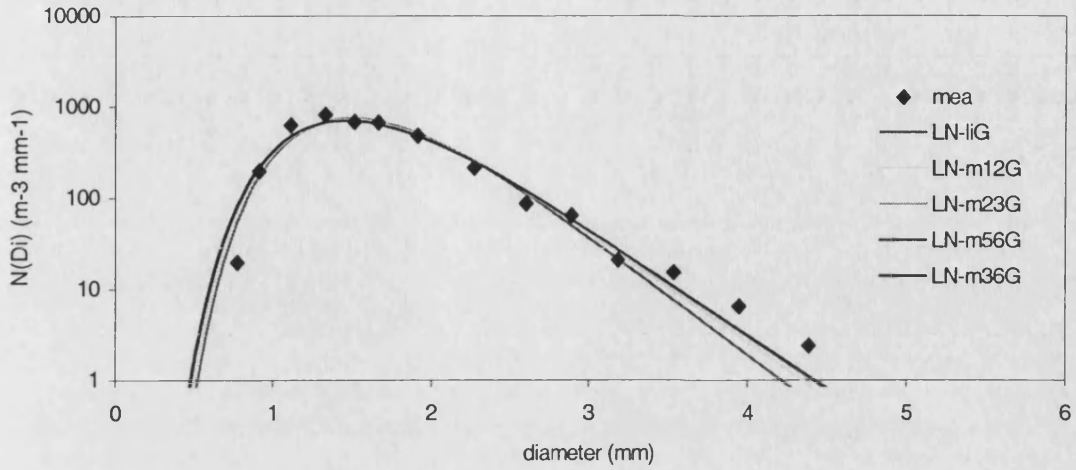

Figure J.3: Comparison between various generalised lognormal distributions with measured data distribution for convective rainfall rate of 64.9 mm hr^{-1}

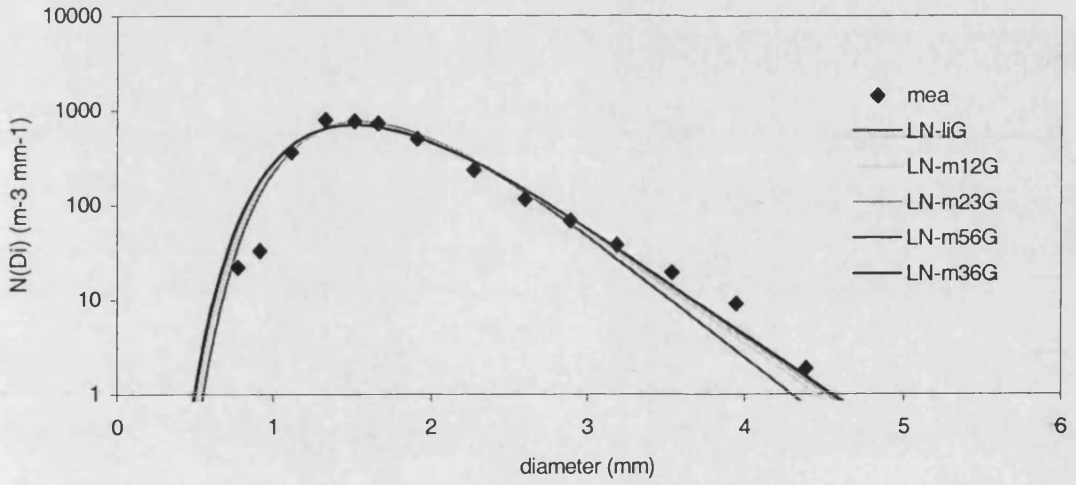

Figure J.4: Comparison between various generalised lognormal distributions with measured data distribution for convective rainfall rate of 74.8 mm hr^{-1}

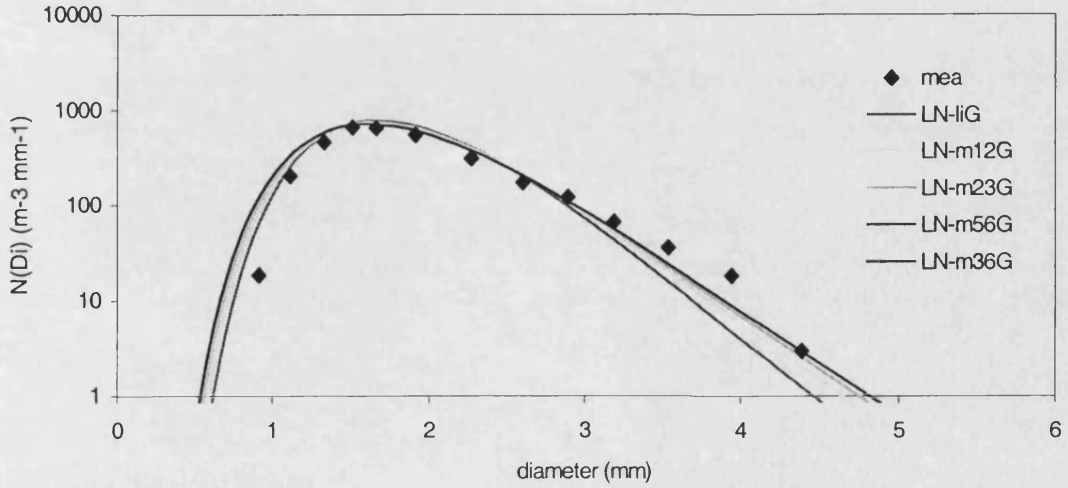

Figure J.5: Comparison between various generalised lognormal distributions with measured data distribution for convective rainfall rate of 99.8 mm hr^{-1}

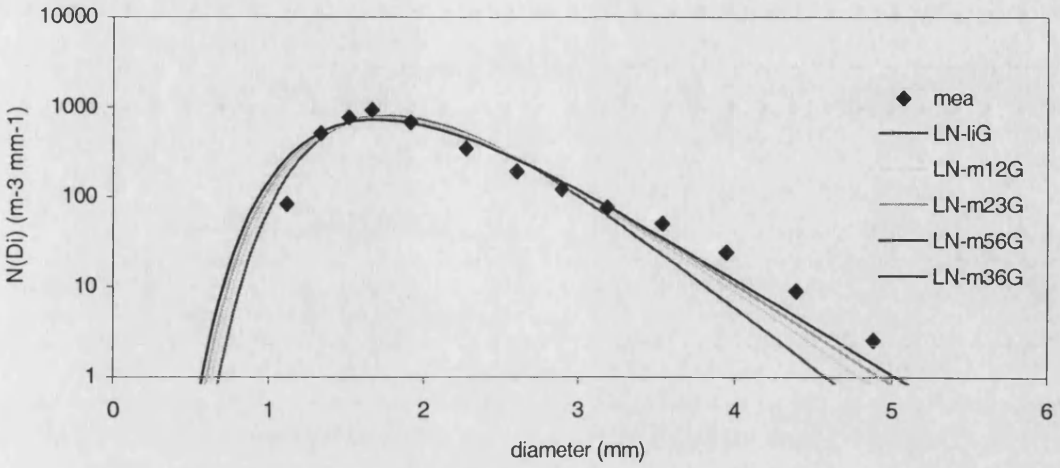

Figure J.6: Comparison between various generalised lognormal distributions with measured data distribution for convective rainfall rate of 124.1 mm hr^{-1}

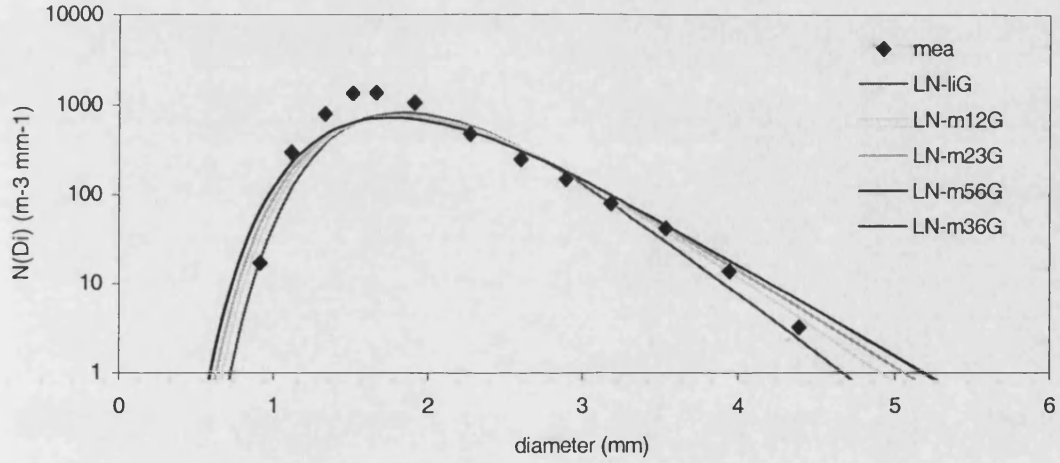

Figure J.7: Comparison between various generalised lognormal distributions with measured data distribution for convective rainfall rate of 144.8 mm hr^{-1}

Appendix K – Comparison between various gamma distributions with measured data distribution for convective rainfall rates

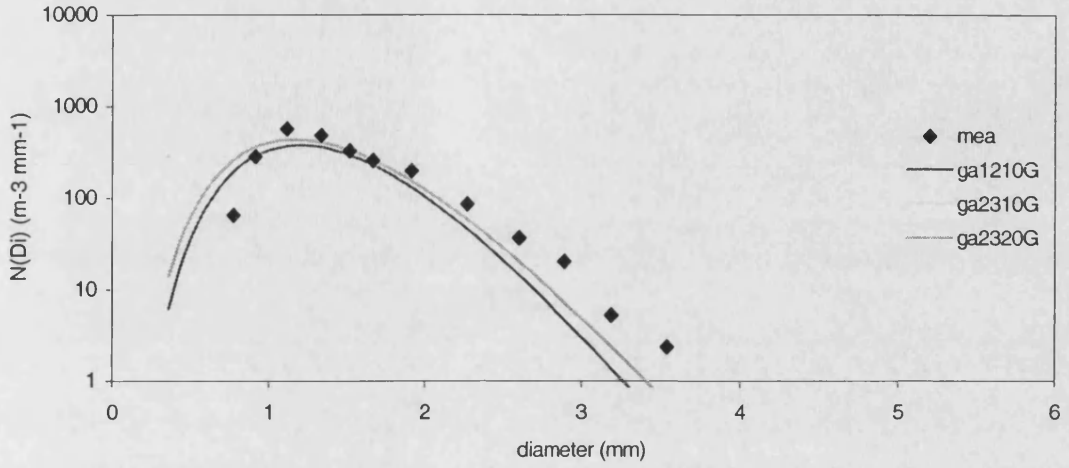

Figure K.1: Comparison between various generalised gamma distributions with measured data distribution for convective rainfall rate of 24.8 mm hr^{-1}.

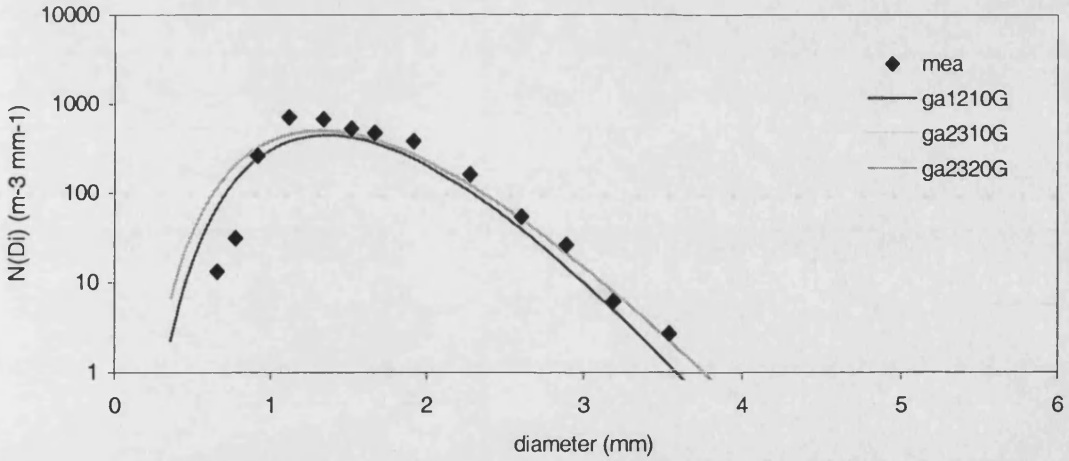

Figure K.2: Comparison between various generalised gamma distributions with measured data distribution for convective rainfall rate of 40.0 mm hr^{-1}.

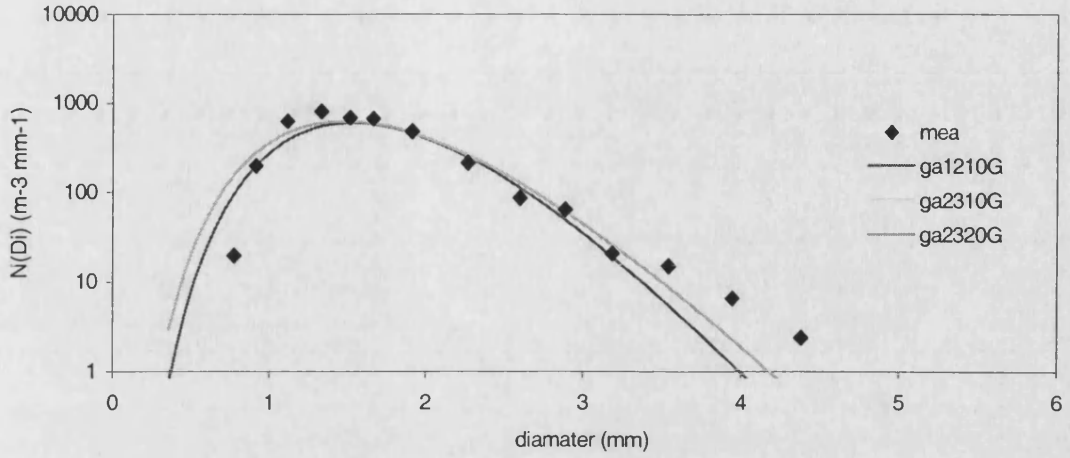

Figure K.3: Comparison between various generalised gamma distributions with measured data distribution for convective rainfall rate of 64.9 mm hr^{-1}.

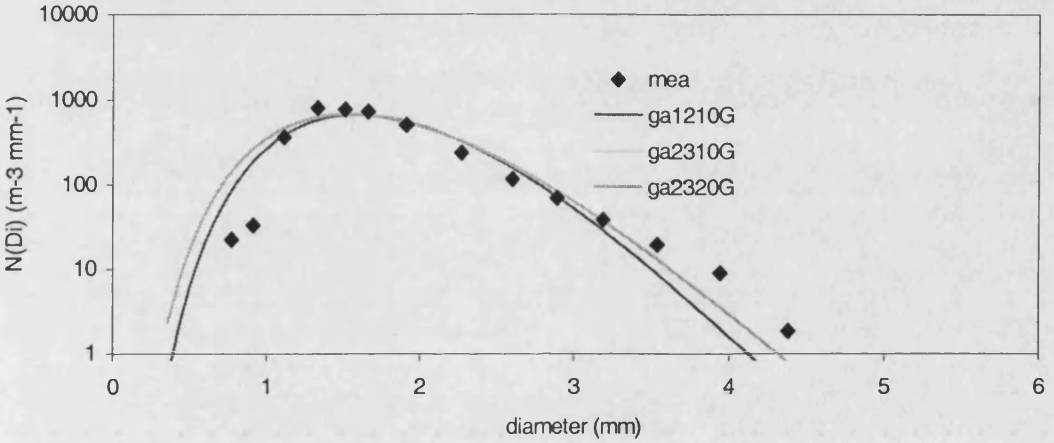

Figure K.4: Comparison between various generalised gamma distributions with measured data distribution for convective rainfall rate of 74.8 mm hr^{-1}.

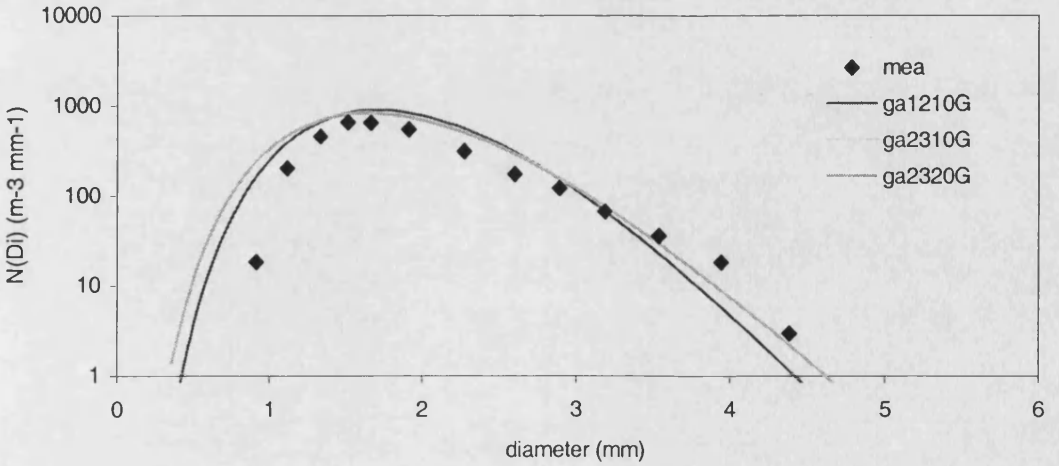

Figure K.5: Comparison between various generalised gamma distributions with measured data distribution for convective rainfall rate of 99.8 mm hr^{-1}.

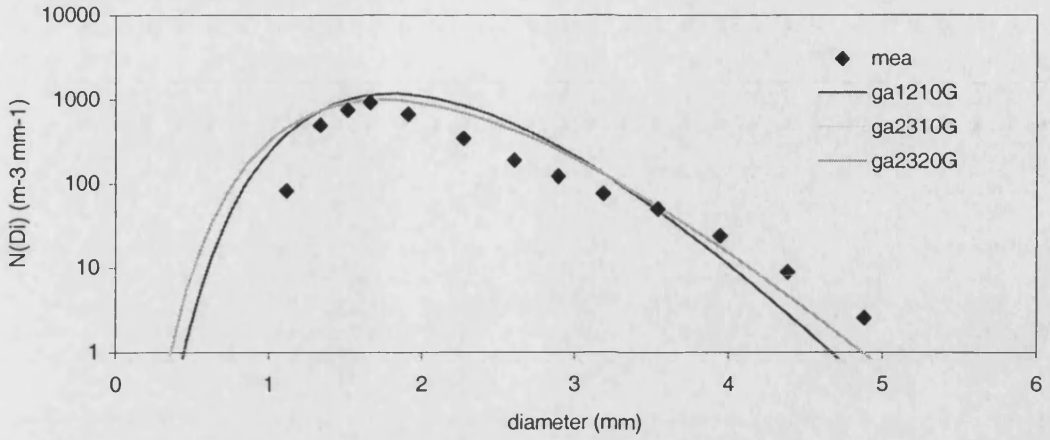

Figure K.6: Comparison between various generalised gamma distributions with measured data distribution for convective rainfall rate of 124.1 mm hr^{-1}.

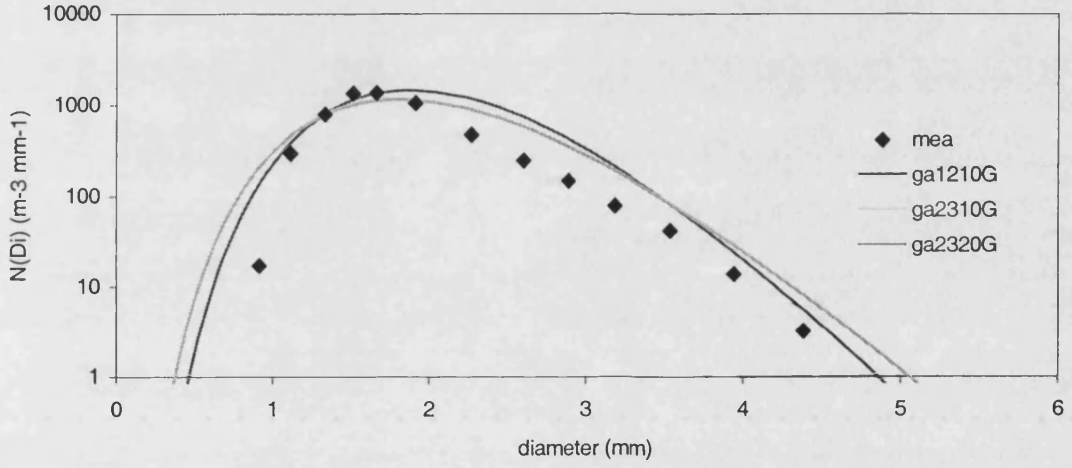

Figure K.7: Comparison between various generalised gamma distributions with measured data distribution for convective rainfall rate of 144.8 mm hr^{-1}.

Appendix L - Radar scans according to classification

File number	Data	Radar Raster	Event	Radar Start
		Number		Times
5335	01/12/95		Nothing	
5336	02/12/95	1 to 12	Nothing	
		13	Convective	10:43:05
		14	Weak convective	11:29:42
		15	Mixed	12:18:30
		18	Weak stratiform	13:05:06
		17	Stratiform	13:53:54
		18	Stratiform	14:40:35
		19	Stratiform	15:29:27
		20	Stratiform	16:16:06
		21 to 28	Nothing	
5338	04/12/95	16 to 34	Nothing	
5339	05/12/95	1 to 19	Nothing	
5340	06/12/96	3	Nothing	
		4	Weak stratiform	
		5	Weak stratiform	
		8	Weak stratiform	
		7	Stratiform	11:45:48
		8	Weak stratiform	
		9 to 19	Nothing	
5341	07/12/95	1 to 3	Nothing	
		4	Convective	12:18:04
		5	Weak convective	13:07:29
		8	Weak stratiform	13:56:55
		7	Weak stratiform	14:46:20
		8 to 17	Nothing	
5342	08/12/95	1 to 4	Nothing	
		5	Mixed	
		8	Weak stratiform	10:50:57
		7	Stratiform	11:40:27
		8	Stratiform	1229:56
		9	Stratiform	13:19:24
		10	Stratiform	14:08:53
		11	Stratiform	14:58:22
		12 to 20	Nothing	
5343	09/12/95	1	Mixed	09:49:32
		2	Weak convective	10:36:01
		3	Weak convective	1123:30
		4	Mixed	12:08:58
		5	Convective	12:55:27
		8	Mixed	13:41:55
		7	Stratiform	14:28:24
		8	Stratiform	15:14:52
		9	Stratiform	16:01:21
		10	Weak stratiform	16:47:50
		11 to 16	Nothing	
5344	10/12/95	1 to 6	Nothing	
		7	Stratiform	
		8 to 21	Nothing	
5345	11/12/95	1 to 4	Nothing	
		5	Convective	10:35:57
		8	Convective	1122:25
		7	Mixed	12:08:54
		8	Mixed	12:55:23
		9	Stratiform	13:41:51
		10	Weak stratiform	14:28:20
		11	Stratiform	15:14:49
		12	Stratiform	16:01:18
		13	Weak stratiform	16:47:46
		14	Weak stratiform	
		15 to 19	Nothing	
5346	12/12195	2 to 18	Nothing	
5347	13/12/95	1 to 3	Nothing	
		4	Mixed	09:05:43
		5	Mixed	09:52:12
		6	Mixed	10:38:41
		7	Weak stratiform	11:25:09
		8	Weak stratiform	
		9	Weak stratiform	
		10	Wok stratiform	

		11	Weak stratiform	
		12 to 20	Nothing	
5348	14/12/95	1 to 8	Nothing	
		9	Mixed	
		10	Mixed	
		11	Weak stratiform	
		12	Mixed	
		13 to 21	Nothing	
5349	15/12/95	1105	Nothing	
		6	Convective	10:22:27
		7	Convective	11:08:59
		8	Mixed	11:55:31
		9 to 21	Nothing	
5350	16/12/95	3 to12	Nothing	
		13	Mixed	
		14	Convective	15:02:44
		15	Mixed	15:49:15
		16	Stratiform	16:35:47
		17	Stratiform	17:22:19
		18	Weak stratiform	18:08:51
		19 to 23	Nothing	
5351	17/12/95	1 to 18	Nothing	
5352	18/12/95	7 to 20	Nothing	
5353	19/12/95	1 t09	Nothing	
		10	Weak convective	
5354	20/12/95	1	stratiform	07:03:20
		2	stratiform	07:49:55
		3	stratiform	08:36:29
		4	Nothing	
		5	Weak stratiform	
		6	Weak stratiform	
		7 to 8	Nothing	
		9	W convective	13:15:54
		10	Weak convective	14:02:29
		11	Weak stratiform	14:49:04
		12 to 21	Nothing	
5355	21/12/95	4 to 11	Nothing	
5356	22/12/95	1 to 14	Nothing	
5361	27/12/95	1 to 17	Nothing	
5363	29/12/95	1 to 6	Nothing	
		7	Weak stratiform	
		8	Weak stratiform	
		9 to 25	Nothing	
5365	31/12/95	1 to 27	Nothing	
	04/01/96	28	Convective	09:16:14
		29	Weak convective	10:02:47
		30 to 45	Nothing	
	05/01/96	46 to 48	Nothing	
		49	Stratiform	10:11:32
		50 to 51	Nothing	
		52	Convective	12:31:17
		53	Weak convective	13:17:52
		54	Weak stratiform	14:04:27
		55	Stratiform	14:51:02
		56	Stratiform	15:37:37
		57	Stratiform	16:24:13
		58	Weak stratiform	17:10:47
		59	Nothing	
		60	Weak stratiform	18:43:58
		61	Weak stratiform	19:30:33
		62	Weak stratiform	20:17:08
		63	Weak stratiform	21:03:43
		64 to 70	Nothing	
	07/01/96	71 to 90	Nothing	
	08/01/96	91 to 93	Nothing	
		94	Stratiform	09:31:06
		95	Stratiform	10:17:41
		96	Stratiform	11:04:16
		97 to 99	Nothing	
6008	08/01/96	3 to 12	Nothing	
	09/01/96	13 to 14	Nothing	
		15	Weak convective	
		16 to 17	Nothing	
	15/01/96	18 to 24	Nothing	
		25	Weak convective	12:20:51
		28	Convective	13:07:26
		27	Mixed	13:54:01
		28	Stratiform	14:40:36
		29	Stratiform	15:27:15
		30	Stratiform	16:13:53

		31	Stratiform	
		32	Stratiform	
		33	Weak stratiform	
		34	Weak stratiform	
		35 to 37	Nothing	
	16/01/96	38	Nothing	
		39	Weak stratiform	09:07:31
		40	Weak stratiform	09:54:10
		41	Weak stratiform	10:40:48
		42	Weak stratiform	11:27:27
		43	Weak stratiform	12:14:05
		44	Weak stratiform	13:00:43
		45	Weak stratiform	13:47:22
		48	Mixed	14:34:00
		47 to 52	Nothing	
	17/01/96	56 to 77	Nothing	
6012	18/01/96	77 to 95	Nothing	
	19101/96	96 to 99	Nothing	
6013	19/01/96	1 to 17	Nothing	
	20/01/96	18 to 37	Nothing	
	21/01/96	38 to 56	Nothing	
	22/01/96	57 to 65	Nothing	
		68	Mixed	
		87	Mixed	
		68 to 76	Nothing	
	23/01/96	77 to 86	Nothing	
		87	Convective	14:28:40
		88	Weak convective	15:15:15
		89 to 97	Nothing	
	24/01/96	98 to 100	Nothing	
6018	24/01/96	1 t05	Nothing	
		8	Mixed	13:03:14
		7	Mixed	13:49:49
		8 to 18	Nothing	
	25/01/96	19 to 21	Nothing	
		22	Weak stratiform	09:39:22
		23 to 24	Nothing	
		25	Convective	11:59:14
		26	Mixed	12:45:48
		27	Convective	13:32:27
		28	Convective	14:19:06
		29	Mixed	15:05:44
		30	Weak stratiform	15:52:19
		31 to 39	Nothing	
	26/01/96	41 to 63	Nothing	
	27/01/96	64 to 84	Nothing	
	28/01/96	85 to 100	Nothing	
6028	28/01/96	1 to 2	Nothing	
	29/01/96	3	Very weak stratiform	
		4	Very weak stratiform	
		5	Very weak stratiform	
		6	Very weak stratiform	
		7 to 21	Nothing	
	30/01/96	22 to 40	Nothing	
	31/01/96	41 to 46	Nothing	
		47	Mixed	
		48	Mixed	13:35:47
		49	Weak stratiform	14:22:29
		50	Stratiform	15:09:11
		51	Stratiform	15:55:53
		52	stratiform	16:42:34
		63 to 59	Nothing	
	01/02/96	60 to 62	Nothing	
		63	Weak stratiform	
		64	Weak stratiform	
		65	Weak stratiform	
		66 to 78	Nothing	
		79	Mixed	
		80	Stratiform	
		81 to 83	Nothing	
	02/02/96	84 to 89	Nothing	
		94	Mixed	15:50:40
		95	Weak convective	16:37:15
		98	Mixed	17:23:51
		97	Weak stratiform	18:10:29
		98	Weak stratiform	18:57:03
		99	Weak stratiform	19:43:39
		100	Nothing	
6033	02/02/96	1 to 4	Nothing	
	03/02/96	5 to 22	Nothing	

	04/02/96	23 to 40	Nothing	
	05/02/96	41 to 59	Nothing	
6037	06/02/96	1 to 21	Nothing	
6038	07/02/96	1 to 20	Nothing	
6039	08/02/96	1 to 20		
	09/02/96	1	Weak stratiform	
		2	Mixed	
		4 to 24	Nothing	
6041	10/02/96	1 to 20	Nothing	
6042	11/02/96	1 to 17	Nothing	
6043	12/02/96	1 to 5	Nothing	
		6	Wok convective	
		7	Weak convective	
		8	Weak convective	
		9	Weak convective	
		10	Weak convective	
		11 to 19	Nothing	
6044	13/02/96	1 to 8	Nothing	
		9	Weak convective	
		10	Weak stratiform	
		11	Weak stratiform	
		12	Weak stratiform	
		13 to 21	Nothing	
6045	14/02/96	1 to 7	Nothing	
		8	Weak convective	
		9	Weak convective	
		10 to 21	Nothing	
6046	15/02/96	1 to 23	Nothing	
6047	16/02/96	1 to 24	Nothing	
6049	18/02/96	1	Stratiform	
		2	Stratiform	
		3 to 22	Nothing	
6050	19/02/96	1 to 23	Nothing	
6051	20/02/96	1 to 6	Nothing	
		7	Stratiform to convective	11:29:12
		8	Convective to stratiform	12:15:54
		9	Stratiform	13:02:35
		10	Stratiform	13:49:17
		11	Weak stratiform	14:35:59
		13 to 21	Nothing	
6052	21/02/96	4 to 8	Nothing	
		9	Stratiform	
		10	Weak stratiform	
		11 to 21	Nothing	
6053	22/02/96	1 t09	Nothing	
		10	Mixed	13:5229
		11	Mixed	14:39:13
		12	Mixed	15:25:54
		13	Mixed	16:12:36
		14 to 20	Nothing	
6054	23/02/96	1 to 5	Nothing	
		6	Convective	10:35:15
		7	Convective	11:21:56
		8	Convective	12:08:38
		9	Stratiform	12:55:19
		10	Stratiform	13:42:01
		11	Nothing	
		12	Mixed	
		13 to 22	Nothing	
6056	25/02/96	1 to 4	Nothing	
		5	Mixed	
		6	Mixed	
		8 to 18	Nothing	
6057	26/02/96	1 to 23	No i	
	27/02/96	24 to 44	Nothing	
	28/02/96	45 to 48	Nothing	
		49	Weak convective	
		50	Weak convective	
		51 to 69	Nothing	
	01/03/96	70	Stratiform	03:52:54
		71	Weak stratiform	04:39:31
		72	Weak stratiform	05:26:07
		73	Weak stratiform	06:12:45
		74	Weak stratiform	06:59:23
		75	W stratiform	07:45:59
		76	Weak stratiform	08:32:37
		77	Weak stratiform	
		78 to 93	Nothing	
	02/03/96	94 to 99	Nothing	
6058	02/03/96	1	Stratiform	12:39:51

		2	Stratiform	13:26:29
		3	Stratiform	14:13:08
		4	Stratiform	14:59:46
		5	Stratiform	15:46:25
		6	Stratiform	16:33:03
		7 to 17	Nothing	
	06/03/96	18	Weak stratiform	06:12:33
		19	Weak stratiform	06:59:10
		20 to 38	Nothing	
	07/03/96	39 to 59	Nothing	
	08/03/96	60 to 81	Nothing	
	09/03/96	82 to 89	Nothing	
		90 0	Weak stratiform	
		91	Weak stratiform	
		92 to 100	Nothing	
6059	09/03/96	1 to 5	Nothing	
	12/03/96	6 to 15	Nothing	
		16	Weak convective	
		17 to 27	Nothing	
6060	16/03/96	1 to 9	Nothing	
	19/03/96	10 to 28	Nothing	
	20/03/96	29 to 49	Nothing	
	21/03/96	50 to 68	Nothing	
	23/03/96	69 to 70	Nothing	
		71	Convective	
		72	Convective	
		73	Stratiform	
		74	Stratiform	
		75 to 91	Nothing	
	25/03/96	92 to 99	Nothing	
6061	25/03/96	1 to 10	Nothing	
	27/03/96	11 to 17	Nothing	
		18	Weak convective	13:27:26
		19	Weak stratiform	14:14:09
		20	Weak stratiform	15:00:53
		21	Nothing	
		22	Weak convective	16:34:11
		23	Nothing	
		-26	Stratiform	18:54:21
		27 to 29	Nothing	-
	29/03/96	30 to 33	Nothing	
		34	Mixed	09:18:58
		35	Weak stratiform	10:05:39
		36 to 37	Nothing	
		38	Stratiform	12:25:44
		39	Stratiform	13:12:25
		40	Mixed	13:59:08
		41	Stratiform	14:45:49
		42 to 50	Nothing	
	30/03/96	51 to 71	Nothing	
		72	Stratiform	
		73	Nothing	
		74	Weak stratiform	
	02/04/96	75	Stratiform	
		76	Stratiform	
		77	Stratiform	
		78	Stratiform	
		79 to 99	Nothing	
6062	04/04/96	2	Weak atra0fortn	
		3	Weak stratiform	
		4 to 5	Nothing	
		6	Weak stratiform	
		7	Weak stratiform	
		8 to 27	Nothing	
	05/04/96	28	Stratiform	
	28/06/96	35 to 67	Nothing	
	29/06/96	68 to 69	Nothing	
		70 0	Week stratiform	
		71	Weak stratiform	
		72	Mixed	
		73	Mixed	
		74 to 89 9	Nothing	
	02/07/96	90	Nothing	
		91	Weak stratiform	
		92 to 93	Nothing	
6183	09/07/96	8 to 13	Nothing	
	10/07/96	14 to 28	Nothing	

Appendix M – Publications

ISMAIL, A.F. and WATSON P.A. [2000] *Characteristics of Fading and Fade Countermeasures on a Satellite-Earth Link operating in an Equatorial Climate, with Reference to Broadcast Applications*, IEE Proceedings on Antennas and Propagation, vol. 147, no. 5, pp. 369-373

FUKUCHI, H., WATSON, P.A., and ISMAIL, A.F. [2000] *Proposed Novel Attenuation Mitigation Technologies for Future Millimetre Wave Satellite Communications*, Proceedings of IEE/ EUREL International Conference on Antenna and Propagation, AP-2000, 2000

WATSON, P.A., ISMAIL, A.F., SENG, P.K., JA, Y.Y., KAMARUDDIN, H.S., EASTMENT, J., and THURAI, M. [1998] *Investigation on Rain Fading and Possible Countermeasures on Satellite-Earth Links in Tropical Climates*, Proceedings URSI comm. F Symposium Wave Propagation and Remote Sensing, pp. 1.3-1.7, Portugal

Characteristics of fading and fade countermeasures on a satellite-Earth link operating in an equatorial climate, with reference to broadcast applications

A.F.Ismail and P.A.Watson

Abstract: Measurements of 12 GHz attenuation, using a satellite beacon receiver, are reported for a station in Malaysia, in one of the most extreme climates with regard to rainfall intensity. The data are analysed, with particular reference to broadcast applications, including data broadcast, multi-media, and time-repeated video applications. Of particular interest is the performance of time diversity, which is characterised with delays between 1 and 60 min. An empirical relationship is proposed, enabling time-diversity gain to be determined as a function of delay. Consideration is given to diurnal variations of attenuation and the additional margin necessary if good performance is to be maintained in peak broadcast hours. The relationship between the annual cumulative statistics of attenuation and the worst month attenuation is also investigated. In such an equatorial climate, with frequent fading throughout the year, it is seen that the worst-month criterion may not be such a useful or necessary measure as in other climates. The problem of prediction of attenuation is addressed using locally collected rain intensity data, and it is seen that further knowledge of rain structure is necessary to improve the quality of predictions.

1 Introduction

Satellite-Earth links using geostationary satellites have an important and developing role in supporting broadcast applications, including conventional TV broadcast, data broadcast and multi-media applications operating with a low data rate return path. Video coding standards, especially MPEG-2, have had a major impact on system design, enabling a few hundred digital TV channels to be carried on a single spacecraft, and opening up transponder capacity for a range of broadcast applications [1–4].

As a consequence of transmitter power limitations, coverage requirements and practical considerations for Earth station antennas, it is difficult to include fade margins of more than approximately 10dB in typical down-link budgets for broadcast systems. Such fades are encountered frequently in equatorial and tropical climates for links operating at 12GHz and above, and in typical European mid-latitude climates for links operating at 20GHz and above.

The availabilities relevant to broadcast down-links are usually considered to be in the range 99.5–99.9% of the average year, combined with a worst-month criterion. For the latter, the ITU-R recommends 99% of the worst-month [5], but this criterion is based on certain modelling assumptions that are climate-specific. In addition, since peak conventional TV broadcast hours occur typically in the late afternoon and evening, diurnal effects on fading must be considered, rather than just the average year or average worst-month figures.

For up-links, availabilities of 99.99% of the average year and 99.93% of the worst month are pertinent. Thus, the satellite beacon data presented here may be scaled, using appropriate coefficients [6], to predict up-link performance and determine the need for appropriate countermeasures. Currently, satellite broadcast applications use down-link frequencies near 12GHz. As new applications are found that exploit the point-to-area characteristic of the satellite path (such as data broadcasting and multi-media applications), pressure for improved availability using the existing bands in tropical regions, and interest in exploiting higher bands in less severe rain climates, will increase. It is in these two contexts that fade countermeasures, such as time diversity, should have an important role.

2 Use of fade countermeasures

At least three fade countermeasure techniques have potential importance to the physical link on a satellite broadcast system: power control, space diversity and time diversity. Power control [7] and space diversity [8] are well known techniques for application to broadcast up-links. Time diversity is a new technique especially relevant to satellite down-links [9, 10], but also relevant to systems with radio-return paths [3, 4].

Time diversity can be applied in video-on-demand applications with time-delayed programme repeats. It is also directly relevant to data broadcast and multi-media applications [4]. In this paper, we focus on time-diversity countermeasures. However, the presented data, using a satellite beacon receiver with a fade margin in excess of 35dB, can also be applied if required to deduce the performance of other techniques, using appropriate modelling assumptions.

IEE Proceedings online no. 20000704

DOI: 10.1049/ip-map:20000704

Paper first received 18th February and in revised form 12th June 2000

The authors are with the Department of Electronic and Electrical Engineering, University of Bath, Claverton Down, Bath BA2 7AY, UK

Table 1: Comparison of measured annual cumulative statistics of slant path attenuation measured in equatorial climates

Site	Elevation, deg.	Period of measurement	Instrument type	Attenuation exceeded for specified % times		
				0.3%	0.1%	0.01%
Malaysia	77.4	Aug 96–Mar. 98, weighted to 2 years	beacon receiver	6.5	12.5	26.2
Singapore [18]	42.9	Nov. 1992–April 1994	beacon receiver	6.2	13.4	32.0
Singapore [17]	39.4	Mar 92–Feb 93 Mar 93– Feb 94 Mar 94–Feb 95	radiometer	5.7 6.5 6.5	not available	not available
Surabaya, Indonesia [19]	20	Apr 92–Mar 93 Apr 93–Mar 94	beacon and radiometer	8.4 7.7	16.1 14.5	not available
Papua New Guinea [20]	72.8	Feb 91–Jan 92	beacon	not available	6.0	16.4
Belem, Brazil [21]	89	1 year during 1996/7	beacon and radiometer	4.5	9.0	22.0

3 Fading from rainfall in equatorial and tropical regions

Tropical climates are defined as possessing a dry season (2 months with < 50mm total rain), whereas equatorial climates have no dry season and exhibit very small seasonal differences in temperature [11]. The climate of peninsula Malaysia is clearly in the equatorial category. Although there are pronounced seasonal variations in rainfall owing to the influence of the system of Asian monsoons [11], there is no dry season.

There is still a paucity of attenuation data for equatorial and tropical regions, especially using satellite beacon receivers rather than radiometers [12]. The latter suffer from saturation at approximately 12dB attenuation, and hence the inability in these climates to characterise the lower range of exceedances, i.e. below ~0.03% of the year (Table 1). Radiometric studies have been reported from Africa [13, 14], Brazil [15], Hong Kong [16], Thailand and Singapore [17].

Only a very limited range of measurements with satellite beacons have been reported in equatorial and tropical regions [18–22], although in some cases the data sets have been extended by combining beacon data with radiometer data.

Models for the prediction of attenuation in tropical regions are still the subject of development and study, especially in relation to the vertical and horizontal structure of rain [23, 24]. A common feature of tropical satellite link geometry using geostationary satellites with restricted coverage (as in broadcast systems) is the relatively high angle of elevation encountered. As a consequence, it has been conjectured that the columnar structures seen on a short time scale within rainstorms may have an influence on the dynamics of fading [23].

4 Measurement details

Attenuation data were collected in association with the Malaysian MEASAT broadcast satellite, operated by the All Asia Broadcast Centre, with a 12GHz beacon receiving station located near Kuala Lumpur (101.42° E and 3.08° N), giving an elevation of 77.43°. The measurements experienced very little equipment down-time; this was concentrated in a single 4-day period during which unexceptional weather conditions were observed.

An optical rain gauge was used located at the receiving site, and data from both instruments were supplied in the form of time series with 10 s sampling interval. Fig. 1 illustrates a typical record. Note that, with a single rain gauge at the receiving end of a satellite-Earth link, time offsets occur between the rain intensity measured on the gauge and the attenuation on the path. This relates to the path geometry, the fall velocity of drops and the horizontal fine-scale structure of rain.

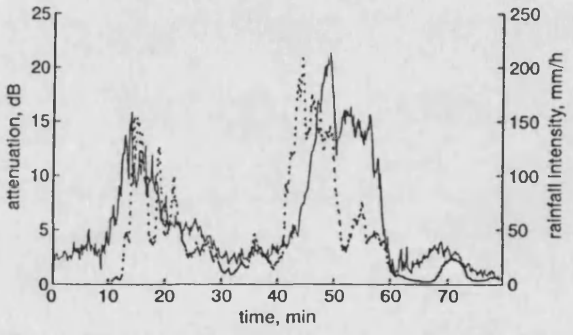

Fig. 1 *Typical time-series record of attenuation (——) and rainfall intensity (– – –)*

A rain height of typically 5km combined, in our case, with a relatively high elevation gives an interest in a radio path extending horizontally to approximately 1 km. Raindrops falling from half the maximum rain height still take several minutes to reach the ground. In addition, a storm cell passing at right angles to the edge of the radio link may deposit in the rain gauge but not show much attenuation on the slant path. When comparisons are made on the basis of cumulative statistics, such offsets are not important.

20 months of data were recorded in total, permitting the study of annual, seasonal and diurnal effects and an evaluation of time-diversity performance. As a consequence of our knowledge of the seasonal effects (see below), we are able to present annual statistics making full use of the 20-month record.

5 Cumulative distributions of attenuation

5.1 Monthly distributions and seasonal effects

Fig. 2 shows histograms of fading on a monthly basis for the 20-month period from August 1996 to March 1998. The numbers of fades equal to or exceeding 10dB in each month (with a duration equal to or greater than 10s) are noted on each column. The monsoon winds reverse in March/April and September/October each year, during which periods there is increased convective activity, causing

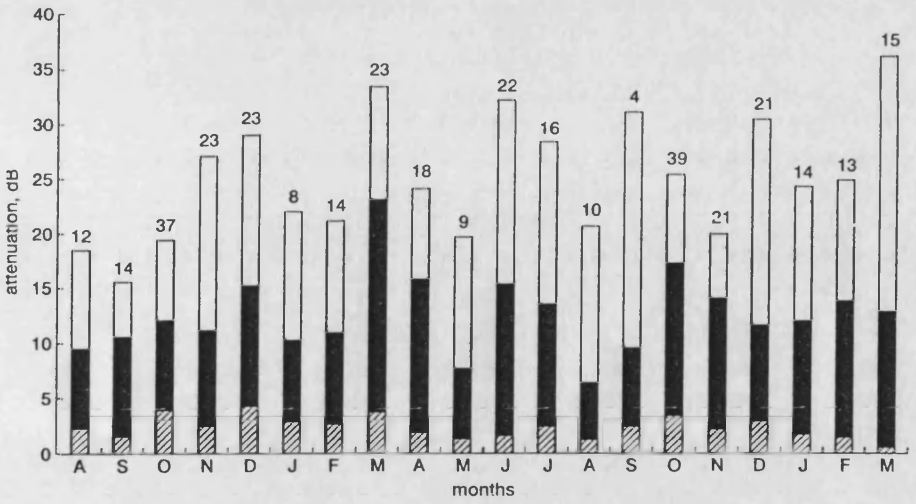

Fig. 2 *Histograms of attenuation exceeded for 1%, 0.1% and 0.01% of each month from August 1996 to March 1998*
Numbers at top of each column = number of fades in excess of 10dB
□ 0.01%
■ 0.10%
■ 1%

the most extreme rainfalls. However, it is noted that in this climate significant rainfall and fading occur each month, with 10dB fades occurring between 5 and 26 times for every month of the year.

5.2 Annual cumulative distributions of attenuation

As a consequence of the seasonality observed in Fig. 2, we have presented annual cumulative statistics (Fig. 3) for the period August 1996–July 1997 and an extrapolated two-year period, placing double weight on the months April–July. We believe that this extracts the maximum value from the data, especially as the two worst months are included; in this climate these correspond closely to the calendar months of March 1996 and March 1997.

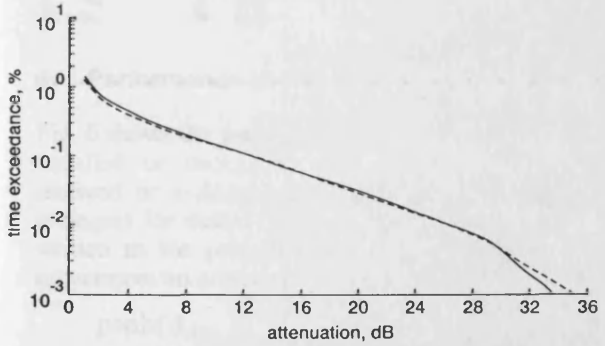

Fig. 3 *Cumulative statistics of attenuation for August 1996–July 1997 (——) and extrapolated two-year period (– – –)*

We note from Fig. 3 the remarkably low year-to-year variability of the annual cumulative distributions for the two years over the 0.1% to 0.01% exceedance range. This may be a coincidence, with only two years of data, but may also relate to the frequency of fades in this (equatorial) climate; approximately in excess of 200 fades per year at the 10dB threshold. We emphasise that this is not an artefact of the 4-month data overlap between the two years since if we plot only the 8 months available for each of the two consecutive years, we see even less variability than between the annual curves.

The attenuations exceeded for 0.3%, 0.1% and 0.01% of the average year are compared in Table 1 with other data from sites in equatorial climates. To make comparisons between these data, the differing elevation angles need to be taken into account, although we hesitate to undertake this process without further information on the structure of rain in tropical and equatorial regions. The data from Pan and Bryant [20] in Papua New Guinea and Couto de Miranda *et al.* [21] in Belem, Brazil, both in equatorial regions, show considerably less fading than those for South-East Asia. With the variety of rain climates to be characterised, considerably more data are thus required for the development of satisfactory physically based models for prediction.

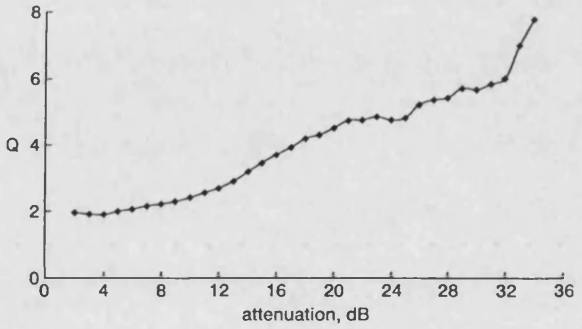

Fig. 4 *Ratio of exceedances between average year and average worst month (Q) as function of attenuation*

5.3 Worst-month attenuation statistics

There is a clear calendar worst month (March) for all monthly exceedances < 0.7%, owing to the pronounced seasonality of the climate, despite the fact that there is significant fading in all other months. Nevertheless, the ratio of exceedances between the average year and the average worst month (Q) [25] varies from 2 to 4.5 over the 6–20dB attenuation range (Fig. 4). We note, in particular, that the attenuation exceeded for 1% of the worst month is just 4dB. If such a margin was adopted for this equatorial climate, an annual availability of just 99.5% of the year would be achieved. Hence the conventional worst-month criterion for broadcast down-links (99% availability [5]) is not appropriate as the sole criterion for equatorial climates, which experience such frequent fading.

5.4 Diurnal variations

Cumulative distributions of attenuation have been calculated in 4-hour periods throughout the day and compared to the annual statistics (Fig. 5). Quite clearly the worst periods for fading in this climate are in the late afternoon and

evening. An extra fade margin of ~3.5dB is required from noon to midnight to achieve the same availability as observed on an average annual basis.

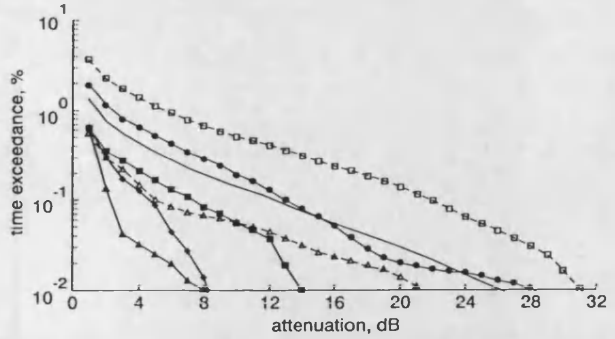

Fig.5 *Cumulative distributions of attenuation calculated in 4-hour periods throughout the day and compared to average annual statistic*
■ 00:00–04:00 □ 16:00–20:00
▲ 04:00–08:00 △ 20:00–24:00
◆ 08:00–12:00 —— 08/96–07/97
● 12:00–16:00

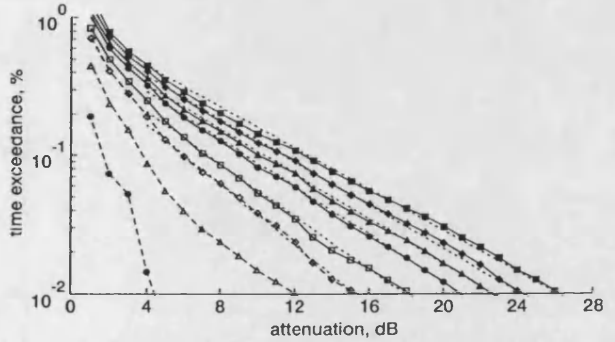

Fig.6 *Percentage time given attenuation exceeded with time diversity for delays in range 1–60 min*
Ideal diversity assumed, with full recovery in inter-fade interval; dashed curves without markers = fitted exponential distributions
■ 0m □ 10m
◆ 1m ◇ 15m
▲ 3m △ 30m
● 5m ● 60m

6 Performance of time diversity

Fig. 6 shows the percentage time that a given attenuation is equalled or exceeded, using either the instantaneously received or a Δt-minute delayed signal (whichever is the stronger) for delays in the range 1–60 min. This may be written as the probability that the diversity combination experiences an attenuation greater than A:

$$\text{prob}(A_{div} \geq A) = 1 - P[(A_o \text{ or } A_\Delta) < A]$$

We may thus define the time-diversity gain (in dB) for a specified exceedance probability (p) as A_p (non-diversity) – A_p (diversity).

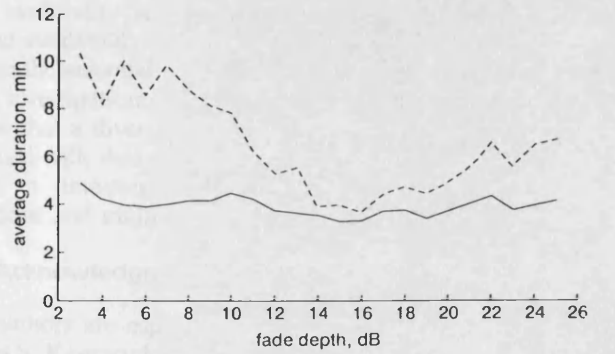

Fig.7 *Average fade duration (——) and inter-fade interval (– – –) as function of fade depth*

Ideal selection time diversity is assumed with full recovery in the inter-fade interval. The observed time-diversity performance is in keeping with the measured average fade duration for all fades lasting 10s or more (~4 min, independent of threshold over a wide range), as illustrated in Fig. 7. The variation of inter-fade interval with fade depth is shown in Fig. 7. Note that this lies between 8 and 4 min for fades above the 10dB fade threshold. Considering practical intervals for time-repeated material (15–30 min) leads to the conclusion that a recovery strategy must operate with a frame length considerably less than the repeat period.

For attenuations > 4dB, the cumulative distributions with or without time diversity may be represented (through least squares fitting) by exponential distributions of the form

$$P(A) = \beta \exp(-\alpha A)$$

α and β are given in Table 2, but may be determined (within an error of ±0.34dB) as a function of delay (Δt) from

$$\alpha = 0.005\Delta t + 0.1726$$
$$\beta = -0.0224\Delta t + 0.7575$$

Evidently, there is significant and increasing diversity gain for delays between 1 and 30 min, but above 30 min delay proportionately less gain is seen per unit of delay. Diversity gain at the 0.1% exceedance threshold varies between 4dB (5 min delay) and 10dB (30 min delay). Fukuchi *et al.* [9, 10], working in mid-latitudes (Japan), showed similar overall trends, but with much lower fades, in not such a severe rain climate.

Table 2: Coefficients for exponential approximations to time-diversity gain relationships (Fig. 6)

Delay, min	α	β
0	0.1715	0.8807
1	0.1793	0.7611
3	0.1866	0.6828
5	0.1982	0.6372
10	0.2181	0.4950
15	0.2499	0.4494
30	0.2801	0.2654

7 Prediction of attenuation by rain

The effective height of rain is an important factor in attenuation prediction for satellite-Earth links. For Malaysia and much of the tropical region, this is believed to lie on average at ~5km altitude [6, 26]. Using local (concurrently measured) rainfall data (Fig. 8) and applying them to the prediction of attenuation using the ITU-R procedure P618-5 [6], in which a fixed rain height of 5km is taken, gives good agreement in the 0.1–0.01% exceedance range (Fig. 9). Predictions based on the ITU-R climate P are also included for comparison. For exceedances below 0.01%, the data sample is too small (20 months) to be able to draw conclusions.

Note that attempts to include both vertical and horizontal reduction factors, as in ITU-R 618-6 [6], do not appear to be satisfactory (see Fig. 9). Further improvements to the prediction of attenuation in equatorial climates probably lie in the refinement of the rain height model as a result of radar studies [26] and the inclusion of a more physically based horizontal reduction factor or point-to-path transfor-

mation [24, 27]. The time offsets frequently seen in these data when comparing individual rain and attenuation time series (as in Fig. 1) are taken as further evidence of the fine-scale columnar structure of rain, as observed by Bryant *et al.* [23].

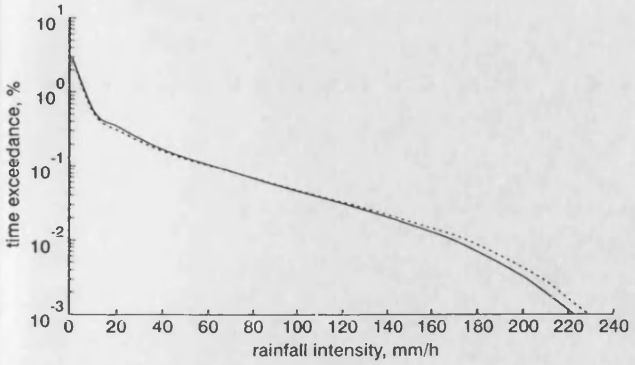

Fig. 8 *Cumulative statistics of rainfall intensity for August 1996–July 1997 (———) and extrapolated two-year period (– – –)*
Measurements taken on optical rain gauge

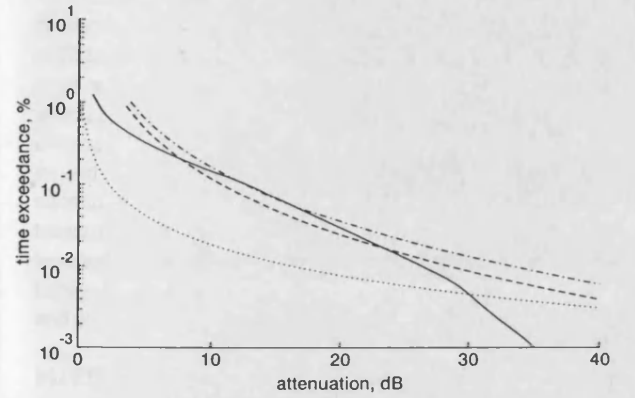

Fig. 9 *Measured and predicted statistics of attenuation for extrapolated two-year period using various methods for prediction*
——— measured data; predictions based upon ITU 618-5 model with local rain data (— · —); same model with ITU-R climate P rain statistics (– – –); ITU-R 618-6 model (·····) which includes vertical and horizontal reduction factors

8 Conclusions

Monthly and annual statistics of attenuation have been presented for a 12GHz satellite-Earth link operating in Malaysia. As expected in this equatorial climate, frequent severe fading is observed, with typically more than 200 fades above the 10dB threshold in a given year. Pronounced diurnal variations, with a preponderance of rainstorms in the afternoon and evening, mean that an additional fade margin of approximately 3.5dB should be included for conventional TV broadcast applications.

For equatorial climates with frequent fading throughout the year, we conclude that a worst-month fade criterion of 99% availability is not sufficient to ensure an adequate annual availability. This is seen to be the case in Malaysia despite the seasonal influences of the Asian monsoon.

An investigation of the performance of time diversity has shown that a diversity gain of between 4 and 10dB can be obtained with delays of 5–30 min. The technique has relevance to time-repeated video applications, and to data broadcast and multi-media applications.

9 Acknowledgments

The authors are especially grateful to P.K. Seng, Y.Y. Ja and H.S. Kamaruddin, All Asia Broadcast Centre, Malaysia, for the supply of data to make this study possible.

10 References

1 HAINES, P.: 'Multi-media services and digital television by satellite'. Proceedings of IEE colloquium 1999/111, London, Oct. 1999
2 International Standards Organisation: 'Generic coding of moving pictures and associated audio information'. MPEG-2 ISO/IEC 13818-1, 1996
3 WREDE, D.: 'Astra broadband interactive system; a Ka band return path for IP connectivity'. Proceedings of IEE colloquium, London, Oct. 1999, pp. 2/1–2/6
4 PAGE, A., and WATSON, P.A.: 'Use of V-band in multimedia messaging services via geostationary satellites'. Proceedings of IEE/Eurel international conference on *Antennas and propagation*, AP-2000, 2000,
5 ITU-R Recommendation P.679-1: 'Propagation data required for the design of satellite broadcast systems'. ITU, Radio-Communications Bureau, Geneva
6 ITU-R Recommendations P.618-5 and P.618-6: 'Propagation data required for the design of Earth-space telecommunications systems'. ITU, Radio Communications Bureau, Geneva
7 LIN, K.T., ZAKS, C., DISSANANYAKE, A.W., and ALLNUTT, J.E.: 'Results of an experiment to demonstrate the effectiveness of open-loop power control for Ku-band satellite links'. Proceedings of 8th international conference on *Antennas and propagation*, 1993, pp. 202–205 (IEE Conf. Pub. 370)
8 HOAGE, D.B.: 'An improved model for diversity gain on Earth-space propagation paths', *Radio Sci.*, 1982, **17**, pp. 1393–1399
9 FUKUCHI, H.: 'Slant path attenuation analysis at 20 GHz for time-diversity reception in future satellite broadcasting'. Proceedings of URSI-F international open symposium, Scarborough, UK, 1992, pp. 6.5.1–6.5.4
10 FUKUCHI, H., WATSON, P.A., and ISMAIL, F.: 'Proposed novel attenuation mitigation technologies for future millimetre-wave satellite communications'. Proceedings of IEE/Eurel international conference on *Antennas and propagation*, AP-2000, 2000,
11 NIEUWOLT, S.: 'The climates of continental South-East Asia' (Elsevier, Amsterdam, 1981), pp. 1–66
12 ALLNUTT, J.E., and RODGERS, D.V.: 'The INTELSAT slant-path radiowave propagation experiments in tropical regions', *Int. J. Satellite Commun.*, 1990, **8**, pp. 121–125
13 ALLNUTT, J.E., and HAIDRA, F.: 'Ku-band diurnal rain fade statistics from three, two-year, Earth-space experiments in equatorial Africa'. Proceedings of URSI-F open symposium, CLIMPARA'98, Ottawa, 1998, pp. 159–162
14 McCARTHY, D.K., ALLNUTT, J.E., SALAZAR, W.E., WANMI, F., TCHINDA, M., NDINAYA, T.D.G., and ZAKS, C.: 'Results of 11.6 GHz radiometric experiments in Cameroon: second year', *Electron. Lett.*, 1994, **30**, (B), pp. 1449–1450
15 PONTES, M.S., SILVA MELLO, L.A.R., and MIGLIORA, C.G.S.: 'Ku-band slant-path radiometeric measurements at three locations in Brazil', *Int. J. Satellite Commun.*, 1990, **8**, pp. 239–249
16 ALLNUTT, J.E., and UPTON, S.A.J.: 'Results of a 12 GHz radiometric experiment in Hong-Kong', *Electron. Lett.*, 1985, **21**, (5), pp. 1217–1219
17 LEKKLA, R., LIM, S.L., WACHJA, J., and McCORMICK, K.S.: 'Rain attenuation measurements in South-East Asia'. Proceedings of URSI-F open symposium, Ahmedabad, India, 1995, pp. 241–244
18 ONG, J.T., and ZHU, C.N.: 'Slant path attenuation at 11 GHz in Singapore', *Electron. Lett.*, 1997, **33**, (13), pp. 1178–1179
19 MAAGT, P.J.I., TOUW, S.I.E., DIJK, W., BRUSSAARD, G., and ALLNUTT, J.E.: 'Results of 12 GHz propagation experiments in Indonesia', *Electron. Lett.*, 1993, **29**, (22), pp. 1988–1990
20 PAN, Q.W., and BRYANT, G.H.: 'Results of 12 GHz propagation measurements in Lae (PNG)', *Electron. Lett.*, 1992, **28**, (21), pp. 2022–2024
21 COUTO DE MIRANDA, E., PONTES, M.S., DA SILVA MELLO, L.A.R., and ALMEIDA, M.P.: 'Choice of standard medium temperature for tropical and equatorial climates: comparison between radiometric and satellite beacon attenuation data on two 12 GHz links in Brazil', *Electron. Lett.*, 1998, **34**, (21), pp. 2002–2003
22 DISSANAYAKE, A.W., McCARTHY, D.K., ALLNUTT, J.E., SHEPHERD, R., and ARBESSER-RASTBURG, B.: '11.6GHz rain attenuation measurements in Peru', *Int. J. Satellite Commun.*, 1990, **8**, (3), pp. 229–237
23 BRYANT, G.H., ADIMULA, I.A., and RIVA, C.: 'Rain cell diameters and heights'. Proceedings of URSI-F open symposium, Aveiro, Portugal, 1998, pp. 16–19
24 LEITAO, M.J., and WATSON, P.A.: 'Method for prediction of attenuation on Earth-space links based on radar measurements of the physical structure of rainfall', *IEE Proc.-F*, 1986, **133**, (4), pp. 429–440
25 BRUSSAARD, G., and WATSON, P.A.: 'Annual and annual-worst-month statistics of fading on Earth-satellite paths at 11.5 GHz', *Electron. Lett.*, 1978, **14**, (9), pp. 278–280
26 EASTMENT, J.D., THURAI, M., LADD, D.N., and MOORE, I.N.: 'Radiowave propagation research in the tropics using a transportable multi-parameter radar system', *Electron. Commun. Eng. J.*, 1998, **10**, (1), pp. 4–16
27 GODDARD, J.W.F., and THURAI, M.: 'Radar-derived path reduction factors for terrestrial systems'. Proceedings of IEE international conference on *Antennas and propagation*, 1997, pp. 2.218–2.221 (Conf. Pub. 436)

PROPOSAL OF NOVEL ATTENUATION MITIGATION TECHNOLOGIES FOR FUTURE MILLIMETER-WAVE SATELLITE COMMUNICATIONS

Hajime Fukuchi[(1)], Peter A. Watson[(2)] and Ahmad F. Ismail[(2)]

[(1)]Communications Research Laboratory
588-2 Iwaoka, Kobe, Hyogo 651-2492, Japan
E-mail: fuku@crl.go.jp

[(2)]University of Bath, Department of Electronic and Electrical Engineering
Claverton Down, Bath BA2 7AY, UK
E-mail: p.a.watson@bath.ac.uk and A.F.Ismail@bath.ac.uk

INTRODUCTION

To realize large-capacity millimeter wave satellite telecommunication system, development of mitigation technologies of performance degradation due to rain attenuation is very important. Several technologies have been proposed and some of them are practically used, such as a site diversity method. In future, novel mitigation technologies will be needed to cope with large attenuation events. As some examples of such novel technologies, those which make use of space-and-time correlation properties of rain are proposed. They are an adaptive satellite power control and a macroscopic time diversity methods. The former method makes use of the natural characteristics that intense rain is confined in a small region and the latter makes use of that rain never lasts forever. Although both technologies can not be fully realized by current level of related technologies such as satellite hardware or ground-receiver, strong needs of large-capacity transmission in satellite communication system will make it possible in future. Recent rapid progress of computer technology including CPU-power and memory-capacity helps our proposals. In this paper, principles of these mitigation technologies are proposed and quantitative evaluation of these methods are shown based on long-term measured rain and attenuation data.

MITIGATION TECHNOLOGIES

Several attenuation mitigation technologies for satellite communication are summarized in Table 1. So far we have only used Static-methods, up-link power control and site-diversity method as rain-countermeasure. For future high-capacity and reliable satellite communication systems we should make use of other Adaptive-methods, Diversity-methods or combination of the methods in Table 1 considering features of their services. In the following sections we discuss time diversity method and adaptive satellite power control method.

Table 1. Rain attenuation mitigation technologies

Mitigation Technology	Principle and Feature	Examples
Static-method	- To add rain-margin into link budget - To prepare several transmission channels with different robustness against attenuation - Resource waste in large attenuation	- Ground-station and Satellite EIRP margin addition - Hierarchical coding and modulation
Adaptive-method (Dynamic-method)	- Link resources such as power are adaptively controlled. - Useful for point-to-point system	- Up-link power control - **Satellite power control** - Bandwidth control(Including Burst transmission)
Diversity-method	- To prepare several transmission channels with low attenuation correlation and to select or to combine the signal for best reception condition - Useful for large attenuation situation	- Site Diversity - Frequency Diversity - Orbit or satellite Diversity - **Time Diversity**

USE OF TIME DIVERSITY

Most simple time diversity scheme can be realized by transmitting information several times with certain time delays. The receiver accumulates information obtained in better receiving condition with help of sophisticated memory function in the receiver. The advent of digital broadcasting via satellite, with its efficient use of radio spectrum and transponder capacity, means that we can now consider using this technique [1,2] for exploiting regions of the radio spectrum which hitherto might be considered to be difficult to use in certain regions of the world for broadcast related applications. The availability of high capacity low-cost computer hard disk memory also encourages us in that approach.

Two areas of application are obvious (a) near real-time video-on-demand and (b) data broadcasting for asymmetric channels (e.g. IP-type applications making extensive use of local cache memory in services such as home shopping). The latter application inherently includes time-diversity, but the former application would entail duplicate transmission of video-on-demand channels with a suitable time delay.

Measurements in Malaysia

Malaysia lies in one of the worlds most extreme rain climates in terms of the frequency of intense rains (in or near to the ITU-R climatic zone P). Rainfall intensities of ~ 70 and 150 mm/hr are exceeded for 0.1 and 0.01% of the average year respectively. Fig. 1 shows the annual fading cumulative distribution for a period of August 1996 to March 1998 (20 months) for a 12 GHz slant path as observed using the Malaysian Mesat satellite for a site near Kuala Lumpur. Mesat is at 91.5° E and the resulting elevation angle was 77.4°. Although the data cover 20 months, in order to be more representative of seasonality, they have been weighted to cover 24 months by duplicating the missing 4 months data in the second year. It is seen that the attenuation thresholds exceeded for 0.1 and 0.01% of the average year are 12 dB and 26 dB respectively. There are also diurnal dependencies which must be taken into account [2], which unfortunately degrade the link margin during peak broadcasting hours by a further 3-dB.

The corresponding fade durations and interfade intervals as a function of fade depth for the same set of data are given in Fig. 2. As seen in data for other locations [3] the average fade duration is almost independent of fade-depth. Evidently for successful time diversity operation in this type of climate we must be using delays in excess of 4 minutes. With a delay of 5 minutes a time diversity improvement of 5dB is available at the 0.1% exceedance threshold, which could be of significance in broadcast applications.

Fig.1 Attenuation and time-diversity performance for various delays
(12 GHz data for Earth-satellite link in Malaysia)

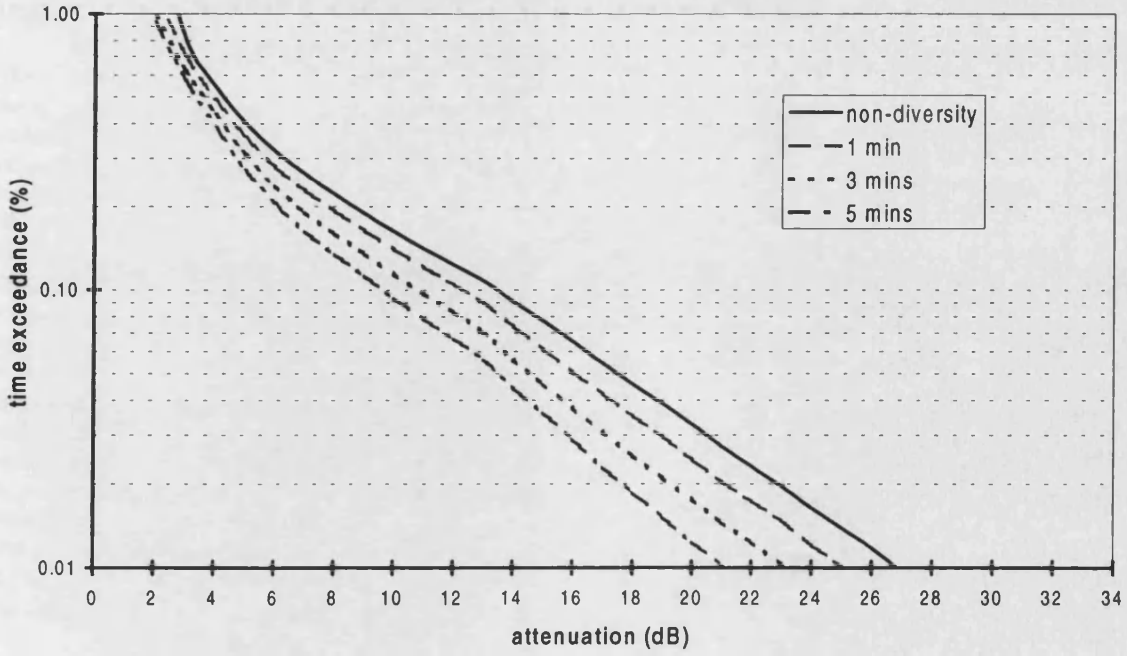

Fig.2 Average fade duration and interfade interval for 12 GHz link

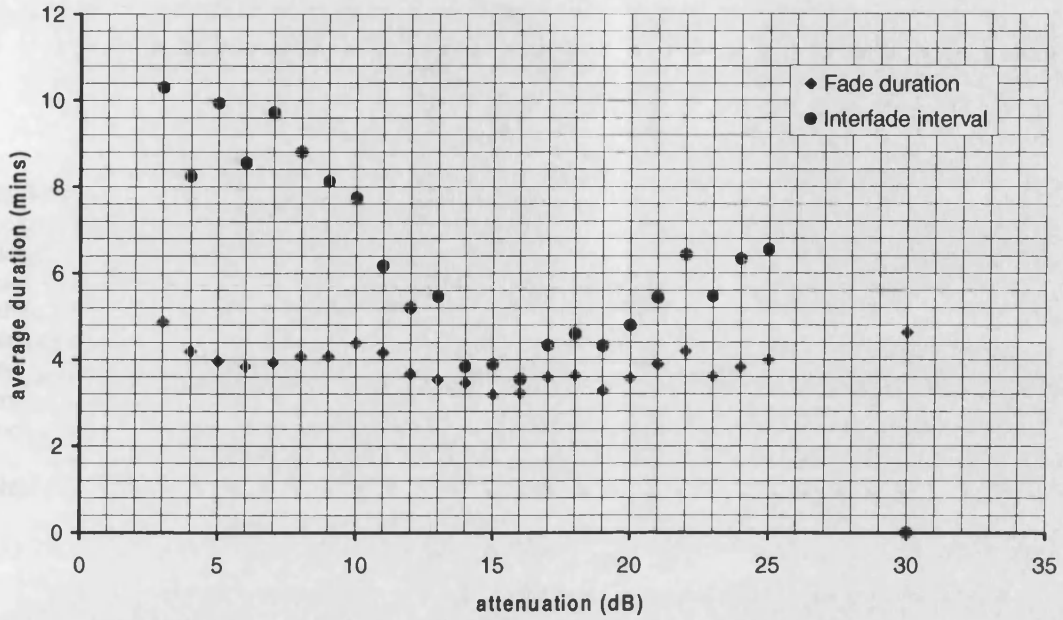

Measurements in Japan

Fig.3 shows the yearly attenuation statistics with no-diversity and the effective yearly statistics with time-diversity. These results were based on slant path attenuation data at 19.5GHz and at an elevation angle of 48degrees measured over 8years at Kashima, Japan. This figure was derived under assumptions that the program was transmitted twice with time delay, Td, and the program information was accumulated using lower attenuation situation. This figure shows that drastic effective attenuation reduction as Td increases. Even several minutes delay, we can expect large diversity-gain especially in small time-exceedance region and also expect link performance improvement with a combination of the conventional Static-method in Table 1. This method is quite suitable for satellite broadcasting application even in future 40 and 80 GHz band.

USE OF ADAPTIVE SATELLITE POWER CONTROL

This method uses multi-beam satellite antenna and power allocated to each beam is adaptively controlled according to the rain attenuation observed in each beam coverage area. It is supposed that in each coverage at least 1 attenuation-monitor station is available as shown in Fig.4. This method will be most suitable for community reception system which uses previous monitor station as a head-end station. If the satellite hardware can control the satellite power continuously, this method compensates rain-attenuation at monitor station perfectly within a range of satellite power capability and rapidness of attenuation time series in feedback time-period. It is interested that attenuation compensation effect at other places with certain separation distance with the monitor station. To analyze the above effect quantitatively, spatial rain correlation properties are useful[4]. Once the 2-dimendional probability

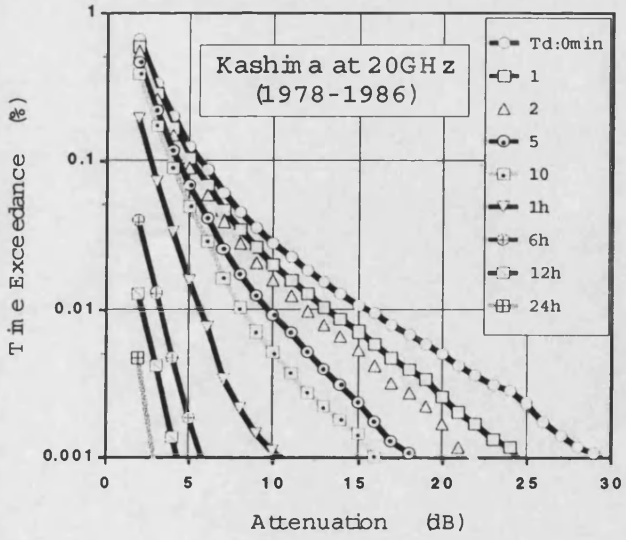

Fig3 Time-diversity performance for various delays
(20GHz data for Earth-satellite link in Japan)

distribution of attenuation at two sites $p(A_1,A_2)$ is obtained according to the procedure in [4], the effective cumulative distribution of attenuation at site-2, a_{2e}, can be derived from the following equation when the satellite power is controlled according to the attenuation at site-1:

$$P(a_{2e} \geq X) = \int_0^{\infty} \int_{A1+X}^{\infty} p(A_1, A_2)\, dA_2\, dA_1 \qquad (1)$$

In the probability distribution, p, correlation coefficient of attenuations at 2-sites is needed. As an example of the correlation properties, Fig.5 shows those analyzed with long-term rain data in UK(PEPR data) and Japan(AMeDAS data). In Japanese data, there is little difference between northern and southern part in contrast to the large difference in rain cumulative distributions. Fig.6 shows an example of power control effect analysis using (1). In this figure, effective attenuation statistics with no power control situation is shown by a solid line, and those in power control situations are shown by dotted lines with correlation parameter rho. This figure shows that there is little improvement at the place with no rain-correlation (rho=0) with the monitor station. As a correlation coefficient larger than 0.5 corresponds to the mutual distance about less than 10km, the benefit of the method may be confined to the area near the monitor station.

REFERENCES

[1] H. Fukuchi, "Slant path attenuation analysis at 20 GHz for time diversity reception of future satellite broadcasting" *URSI-F Open Symposium, Ravenscar, UK,* Proc. pp 6.5.1- 6.5.4, June, 1992

[2] P.A. Watson, A.F. Ismail , P.K. Seng, Y.Y. Ja , H.S. Kamaruddin, J.D. Eastment and M. Thurai, "Investigation of rain fading and possible countermeasures on satellite-Earth links in tropical climates" *URSI-F Open Symposium, Aveiro, Portugal,* pp 3 – 7, Sept. 1998

[3] ITU-R *Handbook on Radiowave Propagation Information for Predictions for Earth-to-Space Path Communications* Radiocommunications Bureau, Geneva, 1996

[4]H.Fukuchi, "Correlation properties of rainfall rates in th 88, 1988.

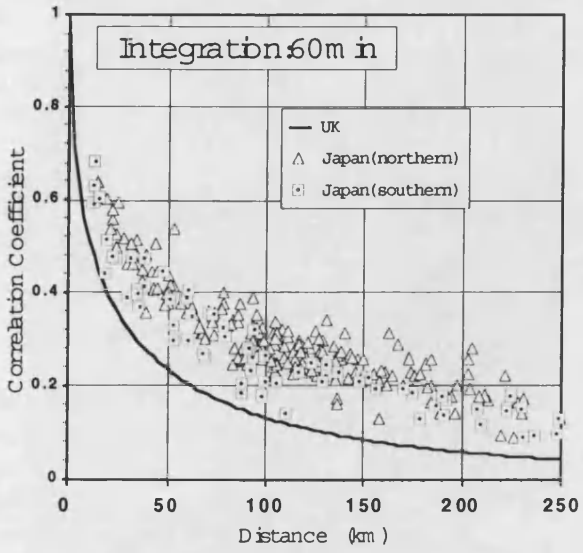

Fig5 Spatial correlation properties of rain

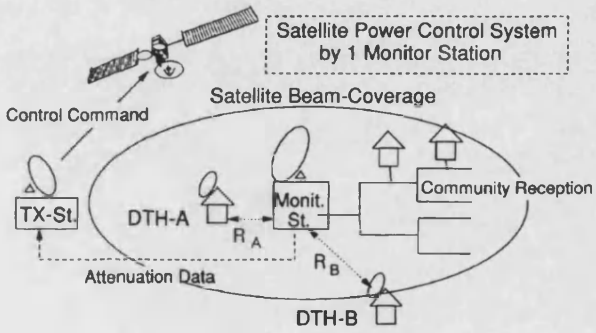

Fig.4 1-Moniter-station model for satellite power control

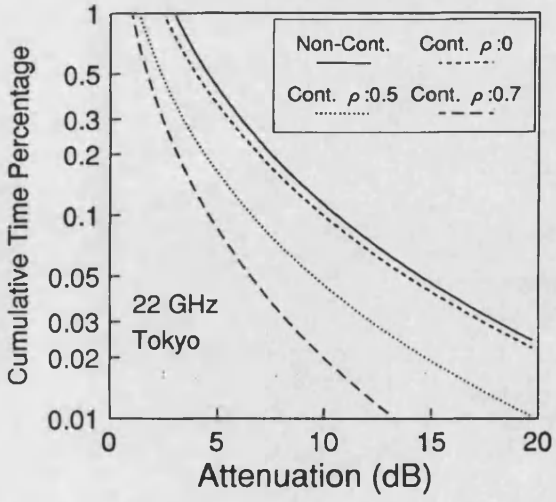

Fig.6 Effective attenuation statistics with satellite power control method

Investigation of Rain Fading and Possible Countermeasures on Satellite-Earth Links in Tropical Climates

P.A. Watson[1] and A.F. Ismail[2]
University of York, Department of Electronics, Heslington, York, YO1 5DD United Kingdom

P.K. Seng[3], Y.Y. Ja[4] and H.S. Kamaruddin[5]
All Asia Broadcast Centre, Technology Park Malaysia
Lebuhraya Puchong - Sungai Besi, Bukit Jalil, 57000 Kuala Lumpur, Malaysia

J.D. Eastment[6]
Rutherford Appleton Laboratory, Chilton, Didcot, Oxon OX11 0QX, United Kingdom

M. Thurai[7]
Radiocommunications Agency, New King's Beam House, 22 Upper Ground, London, SE1 9SA, United Kingdom
(on leave from: Rutherford Appleton Laboratory, Chilton, Didcot, Oxon OX11 0QX, United Kingdom)

1: Tel: +44-1904-432338, Fax: +44-1904-432335, email: paw@ohm.york.ac.uk
2: Tel: +44-1904-432415, Fax: +44-1904-432335, email: afi100@ohm.york.ac.uk
3: Tel: +60-3-5836688 Ext 6818, Fax: +60-3-5838009, email: kee-seng_poh@astro.com.my
4: Tel: +60-3-5836688 Ext 6811, Fax: +60-3-5836868, email: hafi_kamarudin@astro.com.my
5: Tel: +60-3-5836688 Ext 6811, Fax: +60-3-5836868, email: yap-ja_yan@astro.com.my
6: Tel: +44-1235-446546, Fax: +44-1235-446140, email: J.D.Eastment@rl.ac.uk
7: Tel: +44-0171-2110038, Fax: +44-0171-2110053, email: thuraim@ra.gtnet.gov.uk

Abstract

This paper is concerned with the prediction of attenuation caused by rainfall in tropical climates, and the possible use of time diversity as a fade countermeasure. Data from two regions are examined namely Malaysia and Papua New Guinea. In Malaysia we are able to compare measured attenuation data against predictions from rain and can draw conclusions on the possible performance of time-diversity as a fade countermeasure. In PNG we have direct evidence from a radar on rain height in conjunction with a beacon receiver and can thus also attempt to draw conclusions on the efficacy of the current prediction models, especially in relation to rain height.

Keywords: tropical climates; rainfall rates; attenuation

1. Introduction

The intensity of tropical rain climates and the vertical extent of rain in tropical climates ensure that quite significant fading is present on satellite radio links operating in the 11 - 14 GHz bands. The demand for radio spectrum in tropical regions, will no doubt increase in future, as it will in other regions, but in the tropics there may be fundamental limitations on the exploitation of bands above 20 GHz, making the accurate modelling and prediction of attenuation from rainfall an important issue. In addition, the seasonal and diurnal variations of attenuation from rain may have an important bearing on particular applications. (For example, a satellite broadcast system may find greatest viewer demand during the late afternoon and evening hours, times in some climates when the highest rainfalls occur.)

One year of observations of attenuation during rainfall from a 12 GHz satellite beacon measurement associated with the Malaysian MEASAT broadcasting satellite are used firstly with simultaneously gathered raingauge data to enable comparisons to be made with predicted models for annual cumulative statistics. We then investigate seasonal and diurnal variability, considering their importance for the prediction of annual statistics and for systems design.

Further evidence on the modelling of rain attenuation in tropical regions will be drawn from the RAL zenith pointing radar system which has been operated in Papua New Guinea [1] and the potential contribution of further studies using this and other radars will be assessed. Finally, in view of the extreme rainfall climates experienced in tropical regions, the possible use of time-diversity fade countermeasure techniques will be investigated using the MEASAT beacon data. Such techniques are relevant to messaging, retrieval and distribution applications, including broadcasting.

2. Attenuation in Tropical Rainfall: A Brief Overview

2.1 Rain climates and cumulative distributions of rain intensity

The variety of tropical rain types arises from the effects of the inter-tropical convergence zone, its north-south migration with season, combined with a secondary circulation overland, influenced by topography and surface heating (which results in the monsoons). The scarcity of long-record rain intensity data for the tropics has, in the past, lead to the association of climatically similar regions into rain climate zones [2] permitting (with some success, as will be seen later) the pooling of data, to overcome problems of year-to-year variability. More recently, global rain intensity mapping has been developed using 15 years of assimilated precipitation forecast data [3]. Both of these approaches require testing and development against high quality "ground truth" data.

A striking variety of diurnal and seasonal characteristics is evident in tropical rain, linked to the generation mechanisms (for example see [4,5 and 6]). Such variations can have a profound effect on the performance of communications systems and are not visible either in the ITU-R rain climates or (as yet) have not been extracted from the precipitation forecast data. A number of authors [7,8,9] have commented on the occurrence of "breakpoints" in tropical annual cumulative distributions of rain intensity and attenuation, near the 0.01% exceedance value. Explanations have been given in terms of the occurrence of various rain types and rain structures.

As a result the cumulative statistics often do not follow a simple lognormal distribution particularly well, though more generalised forms such as the gamma and Weibull distributions can be used [10]. The exponential distribution (a special case of the Weibull distribution) has been seen to fit quite well to data from 4 locations in Southeast Asia [5]. However, the importance of using long data records is emphasised before drawing conclusions in this context. As tools for investigation of the "breakpoint" phenomenon, we consider the classification and separate investigation of rain types occurring with season and time of day to be of value, and also the study of rain structure using radar. These are two of the main interests for our study.

2.2 Attenuation prediction models

Here the complications relate to rain type, rain height, vertical and horizontal structure and drop-size distribution. In many tropical climates, convective rain dominates, but radar evidence clearly indicates that in some tropical regions stratiform rain exists on a significant scale [11].

Also of significance is the fact that many tropical sites operating to GEO satellites do so at relatively high elevations, possibly giving more importance to rain structure models such as those proposed from observations in Papua New Guinea [12]. Studies on the use of the simple cosecant law for elevation scaling in rain has also pointed to the inadequacy of this approach at high elevations [13]. Until we have better knowledge of rain structures occurring in the various tropical climates, we continue to use the ITU-R "reduction factor" approach, despite its potential shortcomings.

The current ITU-R rain height model, though appropriate in certain regions is, one suspects, too simple and should in some regions take seasonal effects into account. The convective and stratiform rain types observed for example in Papua New Guinea [11] show quite different rain heights, which, for convective rains, can reach at least 7 km.

Further evidence on tropical rain structures and heights should emerge from the TRMM mission [16] especially if such observations can be combined with ground based measurements [1,11].

Some reports have been given on the rain drop-size distributions in tropical regions, however attenuation in the frequency range 10 to 30 GHz shows minimal variation with drop-size [17].

3. Measurement and Prediction of Annual Attenuation Cumulative Distributions

The MEASAT beacon receiving station, operated by the All Asia Broadcast Centre, is located at Bukit Jalil, Kuala Lumpur (101.42° E and 3.08° N) giving an elevation angle of 77.43°. A 13 m diameter, Cassegrain mounted paraboloidal antenna (vertically polarised) was used. A comparison of time-series of attenuation and rainfall rate for the 15 most significant events (see Fig. 1 for a typical example) especially in the tails of events, illustrated that problems with rain water falling on the antenna were minimal.

Fig. 1: Event on July 04, 1997; 17:37:34

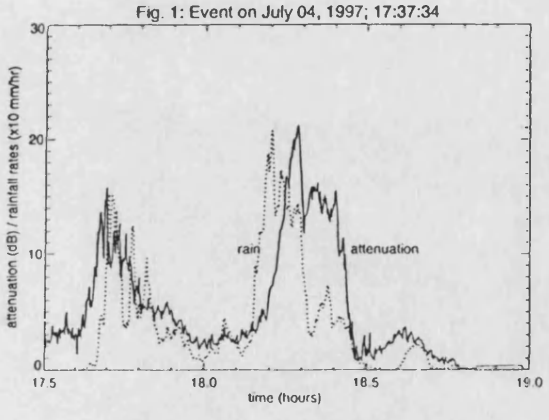

Measured annual cumulative distributions of attenuation are compared with predicted values using the latest ITU-R method [14] using (a) local rain data and (b) ITU-R climate P. Fig. 2 shows the results. It is

noted in particular that much better agreement between predicted and measured data is found with the new rain height model given in reference [14] than with that given in ITU-R 618-4 [15]. By implication the effective rain height for much of the time for in Malaysia is ~ 5km.

Fig. 2: Measured and Predicted Attenuation by Rain (a)

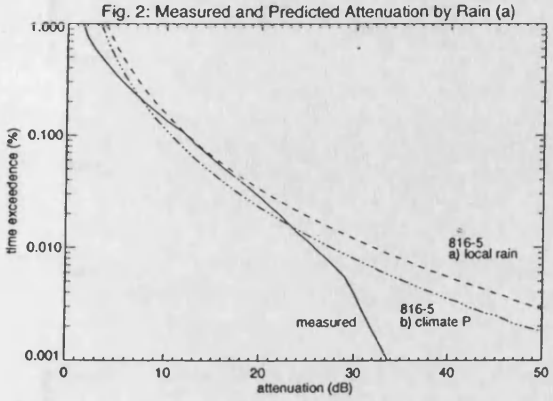

We note additionally the presence of a change of slope or "breakpoint" in the rain intensity statistics near 150 mm/hr (see Fig. 3). Any questions that the effect might relate to the performance of the raingauge seem to be answered by the knowledge that an optical "scintillation" type of raingauge was used. However, the question of the year-to-year variability of the cumulative distribution in the tail below 0.01% of time needs to be resolved by examining further annual data. It should be noted that fitting an exponential line of the form given in [6] gives a curve close to ITU-R climate P.

Fig. 3: Rainfall Rate Distribution

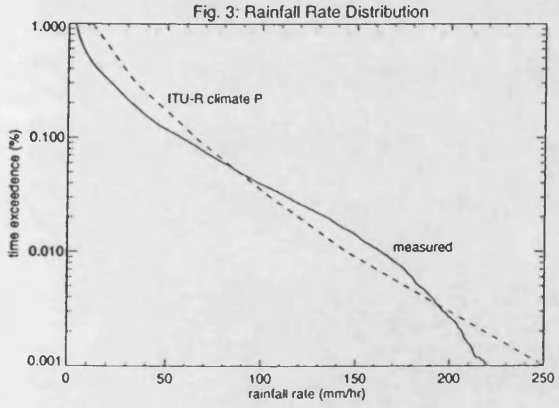

The breakpoint effect (whether a feature of this year's data alone or a longer term effect) leads inevitably to an overestimate of attenuation at the higher rain rates when using the simple ITU-R method, which extrapolates from the 0.01% value. A possible simple improvement to the model might be to use local rain data for all points above 150 mm/hr together with the ITU-R reduction factor (it is fixed above 100 mm/hr). Fig. 4 illustrates the application of this technique, which is seen to give a slight improvement, but still leaves an overestimation. An adequate physical explanation here is sought, but the occurrence of rain in high intensity narrow shafts (as observed by Bryant, [9]) may have a bearing. The radar data from PNG should be relevant here. Also the question of the limited spatial sampling of raingauge in relation to the radio link must be born in mind. For that reason we prefer to wait for at least another year's data before drawing any conclusions

Fig. 4: Measured and Predicted Attenuation by Rain (b)

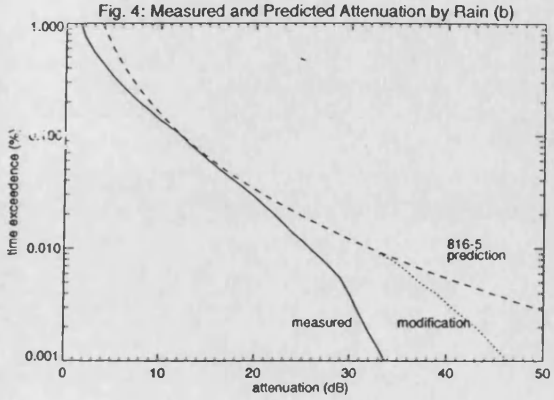

4. Seasonal and Diurnal Effects Observed in Malaysia

Fig. 5 illustrates the diurnal variation of attenuation throughout a year. Evidently there is a pronounced tendency at this location for severe fades to occur in the afternoon and evening, which has implications on the availability required for broadcast systems.

Fig.5: Distributions of Attenuation; Annual C.D. (solid line) Compared to Annual C.Ds. for Specific Hour of Day

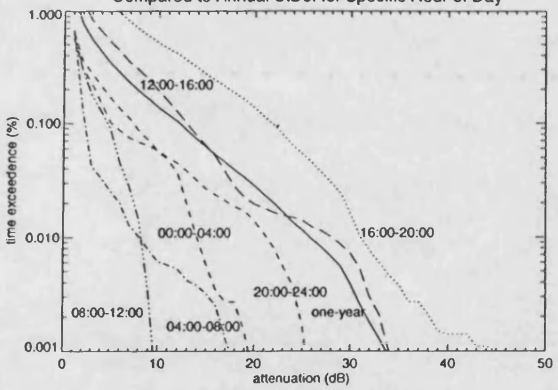

From one year's data we cannot yet comment on the long-term seasonal effects, nevertheless the monthly distributions are shown in Fig 6 and Fig 7. Most locations in Malaysia will show some seasonality from the effects of the south-west monsoon seen in the higher rainfall intensities in March/April. This type of seasonal behaviour has also been reported for Singapore [4]. The seasonal and diurnal patterns we observed indicate strong convective activity in the late afternoons, throughout the year, plus the influence of a relatively weak monsoon during March and April.

Fig 6: Monthly Distributions of Attenuation (Aug 96-Jan 97)

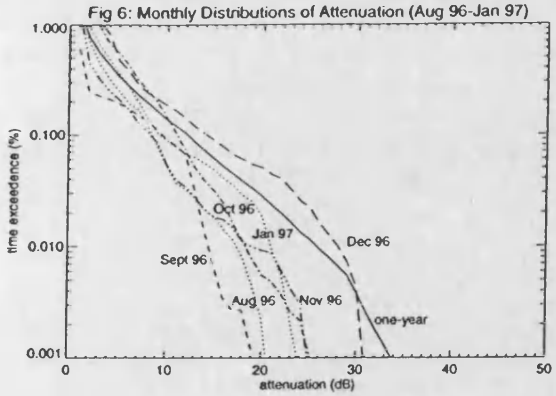

Fig. 7: Monthly Distributions of Attenuation (Feb 97-July 97)

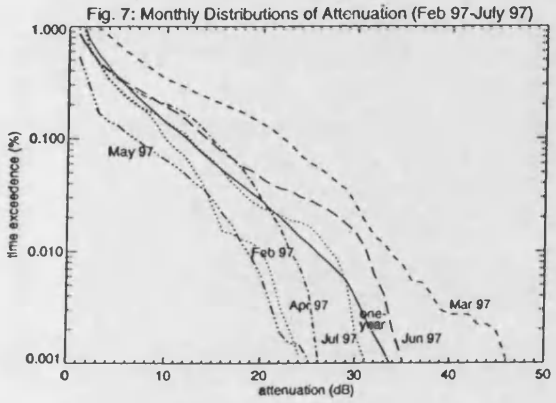

5. Radar Observations of Rain Height in Papua New Guinea

The vertically pointing Z/LDR radar with Doppler capability was operated in PNG for 6 months, during which time more than 50 rain events were recorded. These data have only been subject to preliminary analysis, but particularly pertinent to rain attenuation modelling are initial findings on rain height. Linear depolarisation ratio (LDR) is an excellent indicator of the boundary between rain and ice populations, evidence for the presence of which is clearly seen in both stratiform and convective structures (see Figs 8 and 9).

Fig. 8: PNG Stratiform Event 9/12/95, Start time; 14:28:24

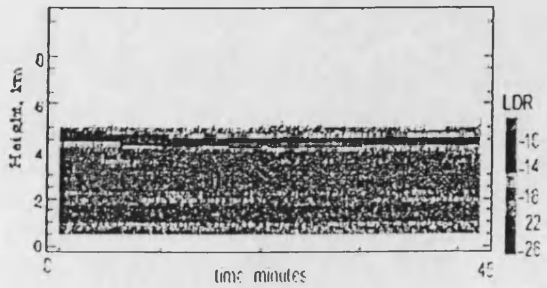

Fig. 9: PNG Convective Event 1/12/95 Start time; 10:35:57

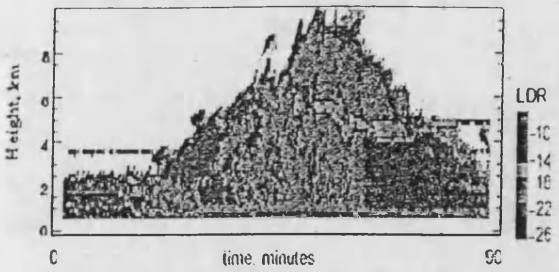

The typical convective event (Fig. 9) shows clear evidence of melting in the LDR returns from about minute 40, when a melting layer develops at approximately 7 km altitude and gradually descends to about 4 km over the next 20 minutes.Quite clearly, different rain heights apply for the two examples shown. The variation of melting layer height for all events over the 6 month period is shown in Fig. 10.

Fig.10: Melting Layer Distribution For Stratiform and Convective Events, over 6 month period

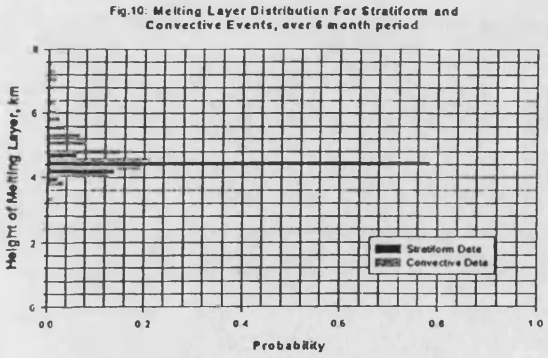

6. Investigation of Performance of Time Diversity as Fade Countermeasure

Uplink fading on satellite broadcast systems can be counteracted by the use of space diversity or uplink power control. The MEASAT earth station uses the latter. Time diversity represents a technique that might have potential for the use on the downlink, building in memory and switches into domestic receivers. Here we investigate the time diversity spacing necessary to achieve a significant improvement in availability.

Plots with and without time diversity gain are shown in Fig. 11 and Fig. 12 for diversity interval of 3 and 5 minutes. For 5 minutes interval we note from Fig. 12, diversity gains of 3.5 dB and 5.3 dB for 99.9% and 99.99% availabilities. At 10 dB attenuation the diversity improvement is a factor of 2. At present, we do not have space diversity measurements available for climate P at similar elevation and frequency in order to make a comparison.

Fig. 11: Time Diversity Improvement for 180s Delay

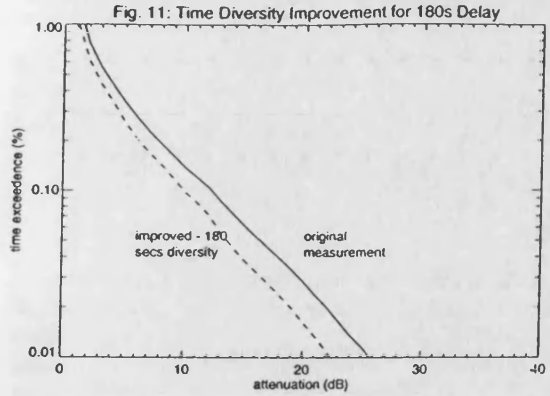

Fig. 12: Time Diversity Improvement for 300s Delay

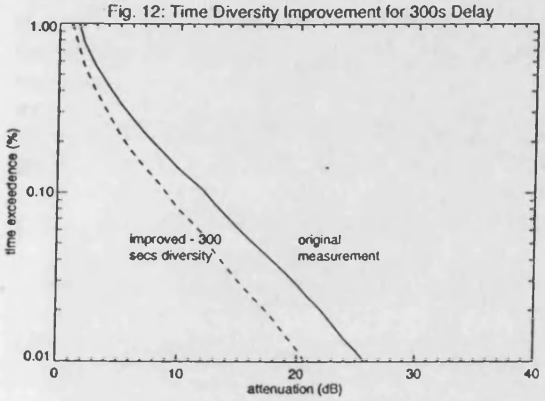

7. Conclusions

Preliminary studies relating to the prediction of attenuation by rainfall in tropical climates have been presented based on 1 year of attenuation and rain rate measurements in Malaysia, and 6 months radar data in PNG.

While it is too early to draw firm conclusion on such a small sample of data, evidence has been presented on the seasonal and diurnal variation of attenuation in Malaysia and on the rain height in PNG. Also the improvement from the use of time diversity at 12 GHz over the 12 month period has been measured for a number of diversity spacings and at 10 dB attenuation with 5 minutes delay we see a factor of 2 reduction in outage probability.

References

1. J.D. Eastment, M. Thurai, D.N. Ladd and I.N. Moore, "A Vertically-Pointing Dopler Radar to Measure Precipitation Characteristics in the Tropics", *IEE Trans. on Geosc. and Remote Sensing*, Vol. 33, No. 6, November 1995, 33, 960, pp 1336-1340
2. R.K. Crane, "Modelling Attenuation by Rain in Tropical Climates", *Int. J. Satell. Commun.*, Vol.8, No.3, May-June 1990, pp 197-210
3. J.P.V. Poiares Baptiste and E. Salonen, "Review of rainfall rate modelling and mapping", *URSI CLIMPARA '98*, Ottawa, Canada, April 1998, Proceedings, pp 35-44
4. J.T. Ong. and C.N. Zhu, "Rain Rate Measurements by a Rain Gauge Network in Singapore", *Elec. Letts.*, Vol. 33, No. 3, 1997, pp 240 - 242
5. R. Lekkla, P. Prapinmongkolkarn and K.S. McConnick, "Analysis of Rain Intensity in Southeast Asia Over 3-Years", *ibid*, pp 223-226
6. Allnutt, J.E. and Haidara, F. " Ku -Band Diurnal Rain Fade Statistics from Three, Two-Year, Earth-Space Experiments in Equatorial Africa", *ibid* pp 159 - 162
7. Assis, M.S. "On the accuracy of raingauge measurements", *CLIMPARA '94*, Moscow, June 1994, Proceedings, pp 2.5.1-2.5.3
8. Moupfouma, F., " More about rainfall rates and their prediction for radio systems engineering", *Proc. IEE*, Pt. H. Vol. 134, No. 6, Dec. 1987, pp 524 - 537
9. G.H. Bryant, "The Structure of Tropical Rain from Attenuation and Rain Exceedences", *Proceeding of ISAP, Sapporo*, Japan, 1992, pp.524-537
10. E. Couto de Miranda, M.S. Pontes, and L.A.R. da Silva Mello, "Statistical modelling of the cumulative probability distribution function of rainfall rate in Brazil", *URSI CLIMPARA '98*, Ottawa, Canada, April 1998, Proc. pp77-80
11. J.D. Eastment, M. Thurai, D.N. Ladd, D and I.N. Moore, "Radiowave propagation research in the tropics using a transportable multiparameter radar system", *Elect. and Comm. Eng. Jour.*, Feb. 1998, pp 4 - 16
12. L. Watai, Q.W. Pan, and G.H. Bryant, "Model for Tropical Rain", *URSI CLIMPARA '94*, Moscow, June 1994, Proc. pp 3.1.1 - 3.1.3
13. B.J. Bowthorpe, F.B. Andrews, C.J. Kikkert, and P.L. Arlett, "Elevation Angle Dependence in Tropical Regions" *Int. J. Satell. Commun.* Vol. 8, No. 3, May/June 1990, pp 211 - 221
14. Rec.ITU-R PN618-5, "Propagation Data and Prediction Method Required for the Design of Earth-space Telecommunication Systems", 1997
15. Rec.ITU-R PN618-4, "Propagation Data and Prediction Method Required for the Design of Earth-space Telecommunication Systems", 1995
16. K. Okamoto, T. Iguchi, T. Kozu, H. Kumagai, J. Awaka and R. Meneghim, "Early Resuts from the Precipitation Radar on the Tropical Rainfall Measuring Mission", *URSI CLIMPARA '98*, Ottawa, Canada, April 1998, Proc. pp 45 - 52
17. G. Brussaard and P.A. Watson, " Atmospheric Modelling and Millimetre Wave Propagation" Chapman and Hall, 1995, ISBN 0 412 56230 8

distribution of attenuation at two sites $p(A_1,A_2)$ is obtained according to the procedure in [4], the effective cumulative distribution of attenuation at site-2, a_{2e}, can be derived from the following equation when the satellite power is controlled according to the attenuation at site-1:

$$P(a_{2e} \geq X) = \int_0^{\infty} \int_{A1+X}^{\infty} p(A_1, A_2)\, dA_2\, dA_1 \qquad (1)$$

In the probability distribution, p, correlation coefficient of attenuations at 2-sites is needed. As an example of the correlation properties, Fig.5 shows those analyzed with long-term rain data in UK(PEPR data) and Japan(AMeDAS data). In Japanese data, there is little difference between northern and southern part in contrast to the large difference in rain cumulative distributions. Fig.6 shows an example of power control effect analysis using (1). In this figure, effective attenuation statistics with no power control situation is shown by a solid line, and those in power control situations are shown by dotted lines with correlation parameter rho. This figure shows that there is little improvement at the place with no rain-correlation (rho=0) with the monitor station. As a correlation coefficient larger than 0.5 corresponds to the mutual distance about less than 10km, the benefit of the method may be confined to the area near the monitor station.

REFERENCES

[1] H. Fukuchi, "Slant path attenuation analysis at 20 GHz for time diversity reception of future satellite broadcasting" *URSI-F Open Symposium, Ravenscar, UK*, Proc. pp 6.5.1- 6.5.4, June, 1992

[2] P.A. Watson, A.F. Ismail , P.K. Seng, Y.Y. Ja , H.S. Kamaruddin, J.D. Eastment and M. Thurai, "Investigation of rain fading and possible countermeasures on satellite-Earth links in tropical climates" *URSI-F Open Symposium, Aveiro, Portugal,* pp 3 – 7, Sept. 1998

[3] ITU-R *Handbook on Radiowave Propagation Information for Predictions for Earth-to-Space Path Communications* Radiocommunications Bureau, Geneva, 1996

[4]H.Fukuchi, "Correlation properties of rainfall rates in th 88, 1988.

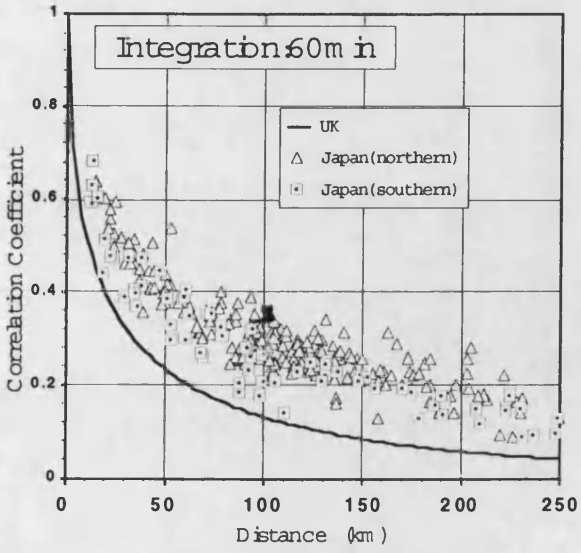

Fig.5 Spatial correlation properties of rain

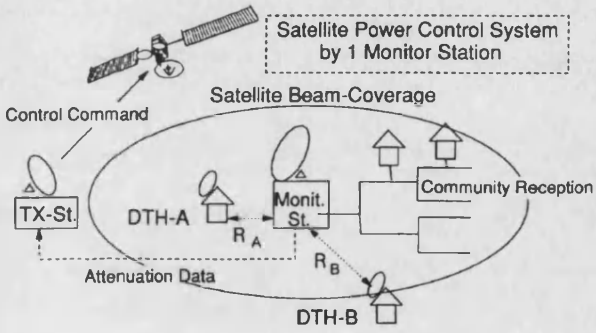

Fig.4 1-Moniter-station model for satellite power control

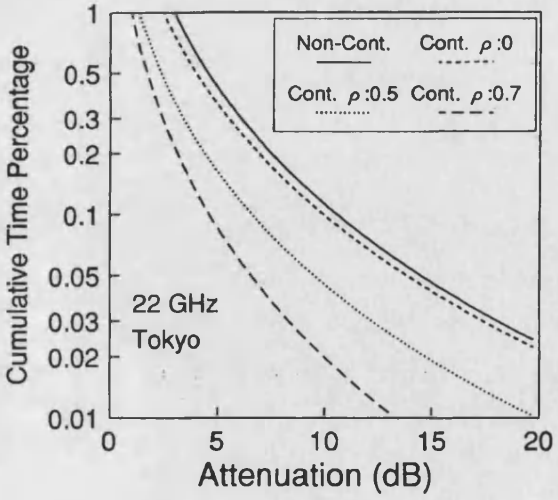

Fig.6 Effective attenuation statistics with satellite power control method

Investigation of Rain Fading and Possible Countermeasures on Satellite-Earth Links in Tropical Climates

P.A. Watson[1] and A.F. Ismail[2]
University of York, Department of Electronics, Heslington, York, YO1 5DD United Kingdom

P.K. Seng[3], Y.Y. Ja[4] and H.S. Kamaruddin[5]
All Asia Broadcast Centre, Technology Park Malaysia
Lebuhraya Puchong - Sungai Besi, Bukit Jalil, 57000 Kuala Lumpur, Malaysia

J.D. Eastment[6]
Rutherford Appleton Laboratory, Chilton, Didcot, Oxon OX11 0QX, United Kingdom

M. Thurai[7]
Radiocommunications Agency, New King's Beam House, 22 Upper Ground, London, SE1 9SA, United Kingdom
(on leave from: Rutherford Appleton Laboratory, Chilton, Didcot, Oxon OX11 0QX, United Kingdom)

1: Tel: +44-1904-432338, Fax: +44-1904-432335, email: paw@ohm.york.ac.uk
2: Tel: +44-1904-432415, Fax: +44-1904-432335, email: afi100@ohm.york.ac.uk
3: Tel: +60-3-5836688 Ext 6818, Fax: +60-3-5838009, email: kee-seng_poh@astro.com.my
4: Tel: +60-3-5836688 Ext 6811, Fax: +60-3-5836868, email: hafi_kamarudin@astro.com.my
5: Tel: +60-3-5836688 Ext 6811, Fax: +60-3-5836868, email: yap-ja_yan@astro.com.my
6: Tel: +44-1235-446546, Fax: +44-1235-446140, email: J.D.Eastment@rl.ac.uk
7: Tel: +44-0171-2110038, Fax: +44-0171-2110053, email: thuraim@ra.gtnet.gov.uk

Abstract

This paper is concerned with the prediction of attenuation caused by rainfall in tropical climates, and the possible use of time diversity as a fade countermeasure. Data from two regions are examined namely Malaysia and Papua New Guinea. In Malaysia we are able to compare measured attenuation data against predictions from rain and can draw conclusions on the possible performance of time-diversity as a fade countermeasure. In PNG we have direct evidence from a radar on rain height in conjunction with a beacon receiver and can thus also attempt to draw conclusions on the efficacy of the current prediction models, especially in relation to rain height.

Keywords: tropical climates; rainfall rates; attenuation

1. Introduction

The intensity of tropical rain climates and the vertical extent of rain in tropical climates ensure that quite significant fading is present on satellite radio links operating in the 11 - 14 GHz bands. The demand for radio spectrum in tropical regions, will no doubt increase in future, as it will in other regions, but in the tropics there may be fundamental limitations on the exploitation of bands above 20 GHz, making the accurate modelling and prediction of attenuation from rainfall an important issue. In addition, the seasonal and diurnal variations of attenuation from rain may have an important bearing on particular applications. (For example, a satellite broadcast system may find greatest viewer demand during the late afternoon and evening hours, times in some climates when the highest rainfalls occur.)

One year of observations of attenuation during rainfall from a 12 GHz satellite beacon measurement associated with the Malaysian MEASAT broadcasting satellite are used firstly with simultaneously gathered raingauge data to enable comparisons to be made with predicted models for annual cumulative statistics. We then investigate seasonal and diurnal variability, considering their importance for the prediction of annual statistics and for systems design.

Further evidence on the modelling of rain attenuation in tropical regions will be drawn from the RAL zenith pointing radar system which has been operated in Papua New Guinea [1] and the potential contribution of further studies using this and other radars will be assessed. Finally, in view of the extreme rainfall climates experienced in tropical regions, the possible use of time-diversity fade countermeasure techniques will be investigated using the MEASAT beacon data. Such techniques are relevant to messaging, retrieval and distribution applications, including broadcasting.

2. Attenuation in Tropical Rainfall: A Brief Overview

2.1 Rain climates and cumulative distributions of rain intensity

The variety of tropical rain types arises from the effects of the inter-tropical convergence zone, its north-south migration with season, combined with a secondary circulation overland, influenced by topography and surface heating (which results in the monsoons). The scarcity of long-record rain intensity data for the tropics has, in the past, lead to the association of climatically similar regions into rain climate zones [2] permitting (with some success, as will be seen later) the pooling of data, to overcome problems of year-to-year variability. More recently, global rain intensity mapping has been developed using 15 years of assimilated precipitation forecast data [3]. Both of these approaches require testing and development against high quality "ground truth" data.

A striking variety of diurnal and seasonal characteristics is evident in tropical rain, linked to the generation mechanisms (for example see [4,5 and 6]). Such variations can have a profound effect on the performance of communications systems and are not visible either in the ITU-R rain climates or (as yet) have not been extracted from the precipitation forecast data. A number of authors [7,8,9] have commented on the occurrence of "breakpoints" in tropical annual cumulative distributions of rain intensity and attenuation, near the 0.01% exceedance value. Explanations have been given in terms of the occurrence of various rain types and rain structures.

As a result the cumulative statistics often do not follow a simple lognormal distribution particularly well, though more generalised forms such as the gamma and Weibull distributions can be used [10]. The exponential distribution (a special case of the Weibull distribution} has been seen to fit quite well to data from 4 locations in Southeast Asia [5]. However, the importance of using long data records is emphasised before drawing conclusions in this context. As tools for investigation of the "breakpoint" phenomenon, we consider the classification and separate investigation of rain types occurring with season and time of day to be of value, and also the study of rain structure using radar. These are two of the main interests for our study.

2.2 Attenuation prediction models

Here the complications relate to rain type, rain height, vertical and horizontal structure and drop-size distribution. In many tropical climates, convective rain dominates, but radar evidence clearly indicates that in some tropical regions stratiform rain exists on a significant scale [11].

Also of significance is the fact that many tropical sites operating to GEO satellites do so at relatively high elevations, possibly giving more importance to rain structure models such as those proposed from observations in Papua New Guinea [12]. Studies on the use of the simple cosecant law for elevation scaling in rain has also pointed to the inadequacy of this approach at high elevations [13]. Until we have better knowledge of rain structures occurring in the various tropical climates, we continue to use the ITU-R "reduction factor" approach, despite its potential shortcomings.

The current ITU-R rain height model, though appropriate in certain regions is, one suspects, too simple and should in some regions take seasonal effects into account. The convective and stratiform rain types observed for example in Papua New Guinea [11] show quite different rain heights, which, for convective rains, can reach at least 7 km.

Further evidence on tropical rain structures and heights should emerge from the TRMM mission [16] especially if such observations can be combined with ground based measurements [1,11].

Some reports have been given on the rain drop-size distributions in tropical regions, however attenuation in the frequency range 10 to 30 GHz shows minimal variation with drop-size [17].

3. Measurement and Prediction of Annual Attenuation Cumulative Distributions

The MEASAT beacon receiving station, operated by the All Asia Broadcast Centre, is located at Bukit Jalil, Kuala Lumpur (101.42° E and 3.08° N) giving an elevation angle of 77.43°. A 13 m diameter, Cassegrain mounted paraboloidal antenna (vertically polarised) was used. A comparison of time-series of attenuation and rainfall rate for the 15 most significant events (see Fig. 1 for a typical example) especially in the tails of events, illustrated that problems with rain water falling on the antenna were minimal.

Fig. 1: Event on July 04, 1997; 17:37:34

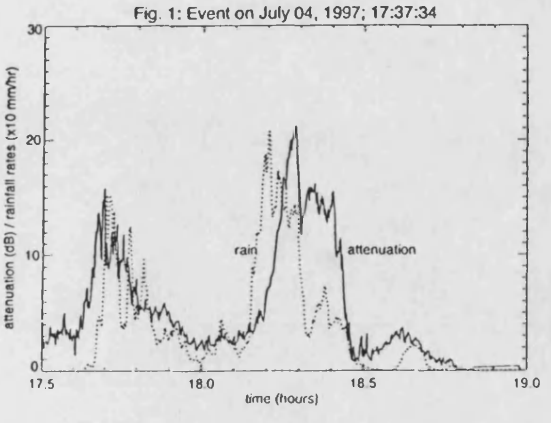

Measured annual cumulative distributions of attenuation are compared with predicted values using the latest ITU-R method [14] using (a) local rain data and (b) ITU-R climate P. Fig. 2 shows the results. It is

noted in particular that much better agreement between predicted and measured data is found with the new rain height model given in reference [14] than with that given in ITU-R 618-4 [15]. By implication the effective rain height for much of the time for in Malaysia is ~ 5km.

Fig. 2: Measured and Predicted Attenuation by Rain (a)

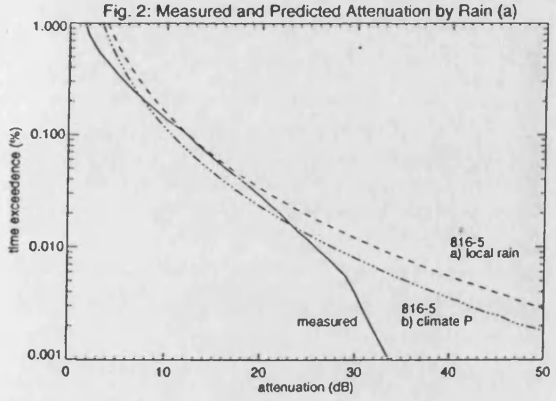

We note additionally the presence of a change of slope or "breakpoint" in the rain intensity statistics near 150 mm/hr (see Fig. 3). Any questions that the effect might relate to the performance of the raingauge seem to be answered by the knowledge that an optical "scintillation" type of raingauge was used. However, the question of the year-to-year variability of the cumulative distribution in the tail below 0.01% of time needs to be resolved by examining further annual data. It should be noted that fitting an exponential line of the form given in [6] gives a curve close to ITU-R climate P.

Fig. 3: Rainfall Rate Distribution

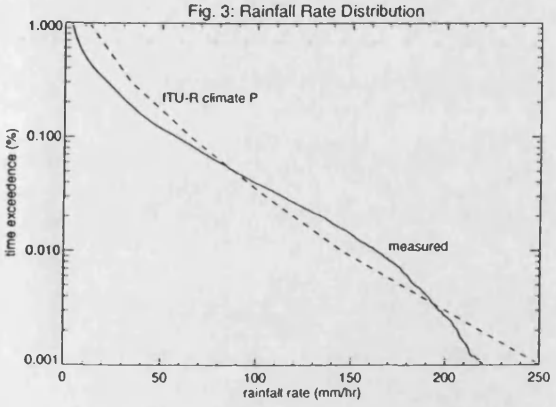

The breakpoint effect (whether a feature of this year's data alone or a longer term effect) leads inevitably to an overestimate of attenuation at the higher rain rates when using the simple ITU-R method, which extrapolates from the 0.01% value. A possible simple improvement to the model might be to use local rain data for all points above 150 mm/hr together with the ITU-R reduction factor (it is fixed above 100 mm/hr). Fig. 4 illustrates the application of this technique, which is seen to give a slight improvement, but still leaves an overestimation. An adequate physical explanation here is sought, but the occurrence of rain in high intensity narrow shafts (as observed by Bryant, [9]) may have a bearing. The radar data from PNG should be relevant here. Also the question of the limited spatial sampling of raingauge in relation to the radio link must be born in mind. For that reason we prefer to wait for at least another year's data before drawing any conclusions

Fig. 4: Measured and Predicted Attenuation by Rain (b)

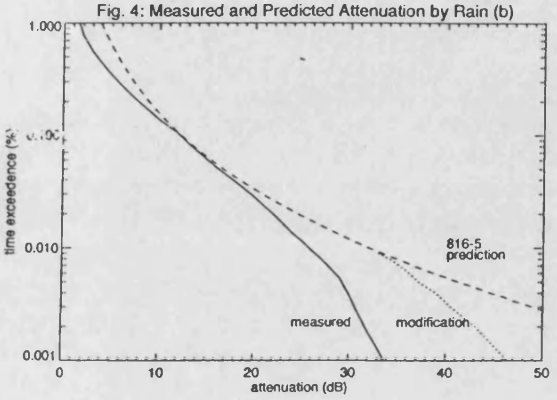

4. Seasonal and Diurnal Effects Observed in Malaysia

Fig. 5 illustrates the diurnal variation of attenuation throughout a year. Evidently there is a pronounced tendency at this location for severe fades to occur in the afternoon and evening, which has implications on the availability required for broadcast systems.

Fig.5: Distributions of Attenuation; Annual C.D. (solid line) Compared to Annual C.Ds. for Specific Hour of Day

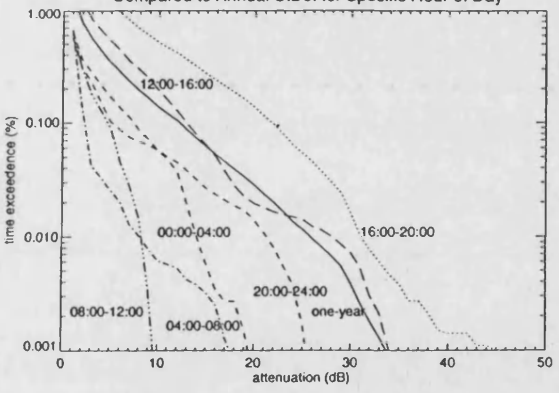

From one year's data we cannot yet comment on the long-term seasonal effects, nevertheless the monthly distributions are shown in Fig 6 and Fig 7. Most locations in Malaysia will show some seasonality from the effects of the south-west monsoon seen in the higher rainfall intensities in March/April. This type of seasonal behaviour has also been reported for Singapore [4]. The seasonal and diurnal patterns we observed indicate strong convective activity in the late afternoons, throughout the year, plus the influence of a relatively weak monsoon during March and April.

Fig 6: Monthly Distributions of Attenuation (Aug 96-Jan 97)

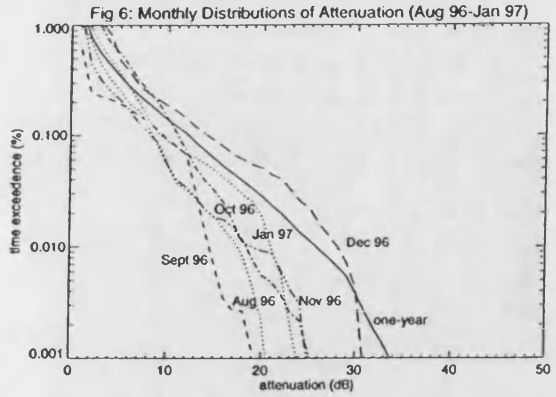

Fig. 7: Monthly Distributions of Attenuation (Feb 97-July 97)

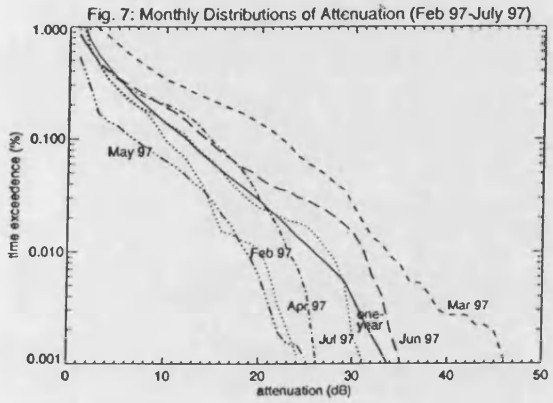

5. Radar Observations of Rain Height in Papua New Guinea

The vertically pointing Z/LDR radar with Doppler capability was operated in PNG for 6 months, during which time more than 50 rain events were recorded. These data have only been subject to preliminary analysis, but particularly pertinent to rain attenuation modelling are initial findings on rain height. Linear depolarisation ratio (LDR) is an excellent indicator of the boundary between rain and ice populations, evidence for the presence of which is clearly seen in both stratiform and convective structures (see Figs 8 and 9).

Fig. 8: PNG Stratiform Event 9/12/95, Start time; 14:28:24

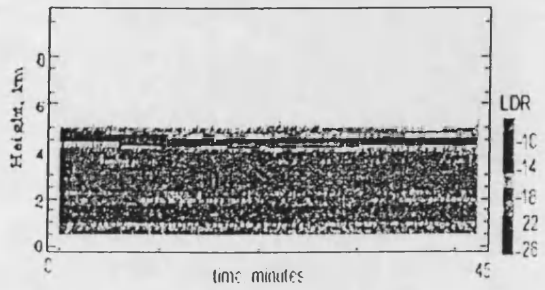

Fig. 9: PNG Convective Event 1/12/95 Start time; 10:35:57

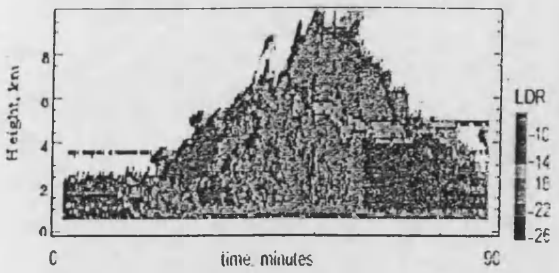

The typical convective event (Fig. 9) shows clear evidence of melting in the LDR returns from about minute 40, when a melting layer develops at approximately 7 km altitude and gradually descends to about 4 km over the next 20 minutes.Quite clearly, different rain heights apply for the two examples shown. The variation of melting layer height for all events over the 6 month period is shown in Fig. 10.

Fig.10: Melting Layer Distribution For Stratiform and Convective Events, over 6 month period

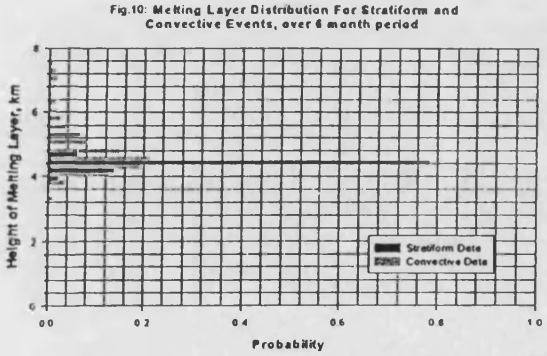

6. Investigation of Performance of Time Diversity as Fade Countermeasure

Uplink fading on satellite broadcast systems can be counteracted by the use of space diversity or uplink power control. The MEASAT earth station uses the latter. Time diversity represents a technique that might have potential for the use on the downlink, building in memory and switches into domestic receivers. Here we investigate the time diversity spacing necessary to achieve a significant improvement in availability.

Plots with and without time diversity gain are shown in Fig. 11 and Fig. 12 for diversity interval of 3 and 5 minutes. For 5 minutes interval we note from Fig. 12, diversity gains of 3.5 dB and 5.3 dB for 99.9% and 99.99% availabilities. At 10 dB attenuation the diversity improvement is a factor of 2. At present, we do not have space diversity measurements available for climate P at similar elevation and frequency in order to make a comparison.

Fig. 11: Time Diversity Improvement for 180s Delay

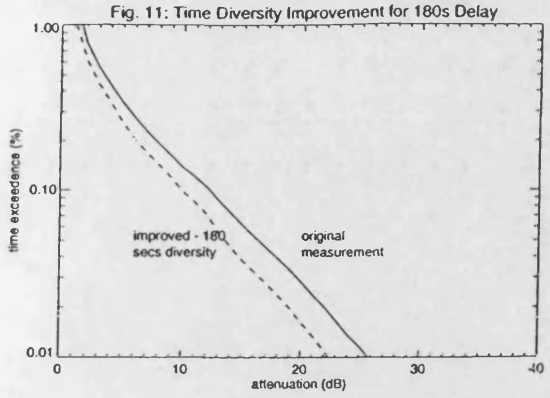

Fig. 12: Time Diversity Improvement for 300s Delay

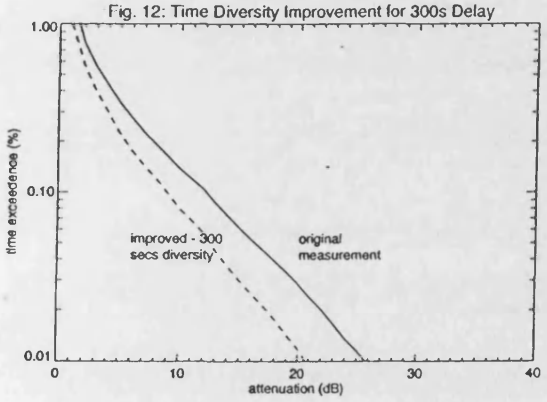

7. Conclusions

Preliminary studies relating to the prediction of attenuation by rainfall in tropical climates have been presented based on 1 year of attenuation and rain rate measurements in Malaysia, and 6 months radar data in PNG.

While it is too early to draw firm conclusion on such a small sample of data, evidence has been presented on the seasonal and diurnal variation of attenuation in Malaysia and on the rain height in PNG. Also the improvement from the use of time diversity at 12 GHz over the 12 month period has been measured for a number of diversity spacings and at 10 dB attenuation with 5 minutes delay we see a factor of 2 reduction in outage probability.

References

1. J.D. Eastment, M. Thurai, D.N. Ladd and I.N. Moore, "A Vertically-Pointing Dopler Radar to Measure Precipitation Characteristics in the Tropics", *IEE Trans. on Geosc. and Remote Sensing*, Vol. 33, No. 6, November 1995, 33, 960, pp 1336-1340
2. R.K. Crane, "Modelling Attenuation by Rain in Tropical Climates", *Int. J. Satell. Commun.*, Vol.8, No.3, May-June 1990, pp 197-210
3. J.P.V. Poiares Baptiste and E. Salonen, "Review of rainfall rate modelling and mapping", *URSI CLIMPARA '98*, Ottawa, Canada, April 1998, Proceedings, pp 35-44
4. J.T. Ong. and C.N. Zhu, "Rain Rate Measurements by a Rain Gauge Network in Singapore", *Elec. Letts.*, Vol. 33, No. 3, 1997, pp 240 - 242
5. R. Lekkla, P. Prapinmongkolkarn and K.S. McConnick, "Analysis of Rain Intensity in Southeast Asia Over 3-Years", *ibid*, pp 223-226
6. Allnutt, J.E. and Haidara, F. " Ku -Band Diurnal Rain Fade Statistics from Three, Two-Year, Earth-Space Experiments in Equatorial Africa", *ibid* pp 159 - 162
7. Assis, M.S. "On the accuracy of raingauge measurements", *CLIMPARA '94*, Moscow, June 1994, Proceedings, pp 2.5.1-2.5.3
8. Moupfouma, F., " More about rainfall rates and their prediction for radio systems engineering", *Proc. IEE*, Pt. H, Vol. 134, No. 6, Dec. 1987, pp 524 - 537
9. G.H. Bryant, "The Structure of Tropical Rain from Attenuation and Rain Exceedences", *Proceeding of ISAP, Sapporo*, Japan, 1992, pp.524-537
10. E. Couto de Miranda, M.S. Pontes, and L.A.R. da Silva Mello, "Statistical modelling of the cumulative probability distribution function of rainfall rate in Brazil", *URSI CLIMPARA '98*, Ottawa, Canada, April 1998, Proc. pp77-80
11. J.D. Eastment, M. Thurai, D.N. Ladd, D and I.N. Moore, "Radiowave propagation research in the tropics using a transportable multiparameter radar system", *Elect. and Comm. Eng. Jour.*, Feb. 1998, pp 4 - 16
12. L. Watai, Q.W. Pan, and G.H. Bryant, "Model for Tropical Rain", *URSI CLIMPARA '94*, Moscow, June 1994, Proc. pp 3.1.1 - 3.1.3
13. B.J. Bowthorpe, F.B. Andrews, C.J. Kikkert, and P.L. Arlett, "Elevation Angle Dependence in Tropical Regions" *Int. J. Satell. Commun.* Vol. 8, No. 3, May/June 1990, pp 211 - 221
14. Rec.ITU-R PN618-5, "Propagation Data and Prediction Method Required for the Design of Earth-space Telecommunication Systems", 1997
15. Rec.ITU-R PN618-4, "Propagation Data and Prediction Method Required for the Design of Earth-space Telecommunication Systems", 1995
16. K. Okamoto, T. Iguchi, T. Kozu, H. Kumagai, J. Awaka and R. Meneghim, "Early Resuts from the Precipitation Radar on the Tropical Rainfall Measuring Mission", *URSI CLIMPARA '98*, Ottawa, Canada, April 1998, Proc. pp 45 - 52
17. G. Brussaard and P.A. Watson, " Atmospheric Modelling and Millimetre Wave Propagation" Chapman and Hall, 1995, ISBN 0 412 56230 8